

Doctoral theses at NTNU, 2023:339

Eirik Svendsen

# Implantable sensing technologies for monitoring of behavioural and physiological dynamics in farmed Atlantic salmon

Doctoral thesis

**NTNU**  
Norwegian University of Science and Technology  
Thesis for the Degree of  
Philosophiae Doctor  
Faculty of Information Technology and Electrical  
Engineering  
Department of Engineering Cybernetics



Norwegian University of  
Science and Technology





Eirik Svendsen

# **Implantable sensing technologies for monitoring of behavioural and physiological dynamics in farmed Atlantic salmon**

Thesis for the Degree of Philosophiae Doctor

Trondheim, October 2023

Norwegian University of Science and Technology  
Faculty of Information Technology and Electrical Engineering  
Department of Engineering Cybernetics



Norwegian University of  
Science and Technology

**NTNU**

Norwegian University of Science and Technology

Thesis for the Degree of Philosophiae Doctor

Faculty of Information Technology and Electrical Engineering  
Department of Engineering Cybernetics

© Eirik Svendsen

ISBN 978-82-326-7378-0 (printed ver.)

ISBN 978-82-326-7377-3 (electronic ver.)

ISSN 1503-8181 (printed ver.)

ISSN 2703-8084 (online ver.)

Doctoral theses at NTNU, 2023:339

ITK report: 2023-22-W

Printed by NTNU Grafisk senter

# Abstract

Atlantic salmon aquaculture is a major food industry with 1.5 million tonnes produced for worldwide consumption in 2022. However, in Norway during the same year, current farming methods resulted in a 17.1% mortality rate (56.7 million individuals). Not only does this reduce profitability, it also leaves room for considerable improvement with respect to responsible marine aquaculture. Part of the losses in Atlantic salmon farming can be attributed to lack of objective data for the fish's behavioural and physiological responses and how they are related to health and welfare in different farming contexts. The main objective of this PhD project has therefore been to enable real-time data collection of fish parameters during full scale farming operations by creating technologies for behavioural and physiological monitoring to uncover their relation to stress and, by extension, welfare.

To this end, it was first shown that the connection between measured behavioural and physiological responses and stress could be made using existing off-the-shelf implants measuring heart rate and motion and blood sample analysis. The sensing principle of pulse oximetry was then selected because it would add to the suite of physiological parameters possible to obtain in real-time during full scale farming operations. The sensing principle was validated by measurement of the optical properties of Atlantic salmon blood. These measurements showed that its optical properties were such that pulse oximeters intended for humans can be used for this species. This was further verified by *in vitro* measurements of oxygenated and deoxygenated whole blood samples using an off the shelf miniaturized pulse oximeter and Monte Carlo simulations. Because welfare considerations indicated that sensors should be implanted in fish, eight different locations within the peritoneal cavity of live, anesthetized Atlantic salmon were tested. The location giving the best signals across individuals in terms of signal quality index was then used as input to hardware design. An implant simultaneously logging acceleration, rotation rates, compass heading, magnetic field strength, temperature, electrocardiogram and photoplethysmogram was then realized

using standard electronic components. The implant was then tested using live, free swimming fish under normoxic and hypoxic conditions. Using the collected data correction parameters were calculated and  $SpO_2$  estimated.

Based on this research it was concluded that the implant successfully enabled simultaneous logging of data to connect behaviour and physiological responses with the novel addition of pulse oximetry. This work, thus, added to the toolbox for measurement and evaluation of behaviour and physiological responses in terms of stress and animal welfare in both research and full scale Atlantic salmon farming.

# Preface

This thesis is submitted in partial fulfilment of the requirements for the degree of Philosophiae Doctor (PhD) at the Norwegian University of Science and Technology (NTNU). The research has been carried out at the Department of Engineering Cybernetics (ITK) under supervision of Professor Jo Arve Alfredsen (ITK), Associate Professor Martin Føre (ITK) and Professor Rolf Erik Olsen (Department of Biology). Through close collaboration, decisive contributions to the work has been provided by Professor Lise Lynsnes Randeberg (Department of Electronic Systems) and Professor Bengt Finstad (Department of Biology).

The focus of this thesis was directed towards development and verification, and experimental validation of technological solutions for logging of physiological and behavioural parameters from individual Atlantic salmon so the connection between behavioural and physiological responses and stress can be better understood. The research was undertaken from August 2018 to April 2023 as part of the 'SalmonInsight' project funded by the Research Council of Norway (RCN, project number 280864) and in kind by SINTEF Ocean AS.

## Acknowledgments

A multitude of people have contributed to this work to stitch together the fields of embedded computing systems and biology. First and foremost, I would like to thank my supervisors at NTNU Professor Jo Arve Alfredsen, Associate Professor Martin Føre and Professor Rolf Erik Olsen for their continuous support and direction. My gratitude extends to Professor Lise Lynsnes Randeberg and Professor Bengt Finstad for their invaluable contributions to discussions and experimental activities.

I also thank my colleagues in SINTEF Ocean AS as well as everyone involved from NINA, the Swedish University of Agricultural Sciences and

Gothenburg University for training, discussions, tips, tricks, fish carrying, water supply fixing, administrative assistance and everything else.

A special thanks goes to Marius Lind Volstad for assisting with the design and realization of the implant, without whom this may not have gone as smoothly.

Finally, I would like to thank Hannah, Brage and Eivor, my nearest and dearest, as well as brothers, sisters, parents, grandparents and other family for their presence, patience and continued support.

## **Outline**

This thesis is organized into four chapters. Chapter 1, Introduction, provides context by presenting general aquaculture facts, the motivation behind this work as well as a description of its belonging project. Finally the objectives and contributions of this work are summarized. Chapter 2 presents important background theory and principles required to understand the technologies and approaches used for feasibility testing, technology design and experimental work. Chapter 3 goes into the details of the testing, design and experimental activities. Because each activity is written as a continuation of the former, each section contains results as well as a discussion and concluding remarks per activity. Chapter 4 contains a synthesis of the results, presents concluding remarks and topics for further work.

# Contents

<b>Abstract</b>	<b>i</b>
<b>Preface</b>	<b>iii</b>
Acknowledgments . . . . .	iii
Outline . . . . .	iv
<b>1 Introduction</b>	<b>1</b>
1.1 Atlantic salmon aquaculture . . . . .	1
1.2 Scope and objectives . . . . .	4
1.3 Contributions - Implant development . . . . .	6
<b>2 Background</b>	<b>9</b>
2.1 Electronic tagging and tracking tools . . . . .	9
2.2 Sensing principle candidates . . . . .	11
2.3 Pulse oximetry . . . . .	12
2.4 Optical properties of tissue . . . . .	18
2.5 Monte Carlo simulations . . . . .	21
<b>3 Experimental work</b>	<b>25</b>
3.1 Ethical statement . . . . .	25
3.2 Linking physiology to tag data . . . . .	27
3.3 Testing pulse oximetry for Atlantic salmon . . . . .	29
3.4 Designing the implant . . . . .	40
3.5 Implant testing . . . . .	45
3.6 Monte Carlo simulations with multiple tissues . . . . .	51
<b>4 Concluding remarks</b>	<b>59</b>
4.1 Synthesis . . . . .	59
4.2 Further work . . . . .	60

References	65
Publications	75
Paper A	
Heart rate and swimming activity as stress indicators for Atlantic salmon ( <i>Salmo salar</i> )	77
Paper B	
Heart rate and swimming activity as indicators of post-surgical recovery time of Atlantic salmon ( <i>Salmo salar</i> )	89
Paper C	
Optical measurement of tissue perfusion changes as an alternative to electrocardiography for heart rate monitoring in Atlantic salmon ( <i>Salmo salar</i> )	105
Paper D	
Design of a novel biosensor implant for farmed Atlantic salmon ( <i>Salmo salar</i> )	119
Paper E	
Data for Characterization of the Optical Properties of Atlantic Salmon ( <i>Salmo salar</i> ) Blood	125
Paper F	
ECG Augmented Pulse Oximetry in Atlantic Salmon ( <i>Salmo salar</i> ) - a Pilot Study	141



# Chapter 1

## Introduction

### 1.1 Atlantic salmon aquaculture

Marine aquaculture is a growing worldwide industry creating economic opportunity and advancing technology (FAO, 2020). Norway has a large countrywide aquaculture industry with Atlantic salmon (*Salmo salar*) as the most important species with 1.5 million tonnes produced for worldwide consumption in 2022 (Directorate of Fisheries, 2023). Production is expected to increase by 50% towards 2050 (Almås and Ratvik, 2017) provided the growth can be realized in a responsible and sustainable manner (Ministry of Trade, Industry and Fisheries, 2021).

Atlantic salmon farming consists of two main stages: an on-shore freshwater stage followed by a seawater stage. In the freshwater stage, roe from brood stock fish farms is delivered to smolt producers and hatched into alevins. After the alevins have consumed their yolk sac they become fry and are moved to growth tanks with either flow-through or recirculated water. Over the course of a few months the fish develop scales and fins and turn into parr (Jobling et al., 2010). Using artificial lighting and functional feed, the fish are then transitioned into seawater tolerant smolts and transferred by wellboat to production cages in sea after approximately 18 months (Sjømat Norge, 2023).

The following seawater stage is a growth stage so the smolts can reach an appropriate weight before slaughter as adults. In this period, fish are typically contained in  $\approx 50$  m diameter cages. A widespread cage design consists of a floating collar suspending a vertical net section reaching  $\approx 20$  m depth where a rigid, circular sinker tube is attached so the net retains a roughly cylindrical shape. The volume is enclosed by a conical net section



Figure 1.1: Example of a salmon production site with 10 cages (Tristeinen, Tarva municipality, Norway). The frame mooring system is outlined by the yellow buoys, and the feed barge is seen in the background. Image credit: SINTEF ACE (SINTEF ACE, 2023).

with a weighted down apex at  $\approx 40$  m depth. A single cage can contain up to 200000 individuals (Lovdata, 2023). Most existing production sites are located in nearshore, sheltered waters and typically consists of 8-10 cages chained by a frame mooring system anchored to the seabed. A site also consists of a feed barge including a housing unit for personnel (figure 1.1).

In the sea stage, salmon husbandry consists of a broad range of farming operations including general farm logistics and inspection, feeding, crowding and pumping (for e.g., de-lousing or slaughter), equipment cleaning (e.g., nets and floating collars) and biomass monitoring (hereunder welfare evaluations). Atlantic salmon farming is therefore a complex affair and current farming practices may have negative impacts on fish health and welfare (Santurtun et al., 2018). To reduce such impacts, the mandatory manual daily farm inspection is supplemented by different monitoring technologies to harvest data fish farmers can use in their decision making. Such technologies may be based on sonar, passive hydro acoustic sensing and different types of cameras and environmental sensors. Additionally, fish health and welfare (e.g., behaviour, prevalence of injuries, lice count) are evaluated using guidelines/score cards (Noble et al., 2018) as part of inspection routines. Interpretation of such data for decision making largely relies on the farmer's

subjective experience. Despite these efforts, current farming methods resulted in a 17.1% country wide mortality rate (56.7 million individuals) in 2022 (Somerset et al., 2023; Grefsrud et al., 2022). Additionally, in 2020, the 'biological' production costs (e.g., negative welfare effects, disease and their treatments) exceeded that of feed, thus, constituting  $\geq 41\%$  of the total production cost (Misund, 2022; Directorate of fisheries, 2023). Not only does this reduce profitability, it also calls the industry's farming practices into question. In combination with exhaustive use of suitable farming areas and conflicting interests with, e.g., fisheries, fairways and preservation of nature diversity, the industry's desired expansion using existing production methods and sites is limited.

To address this limitation, novel containment systems have in recent years been developed for Atlantic salmon farming in more exposed locations further from land (Føre et al., 2022). It is postulated that this approach can improve welfare, accelerate growth, while giving access to additional locations (Misund and Thorvaldsen, 2022; Morro et al., 2022). Novel containment systems in exposed locations, however, come with their own set of challenges because larger containment volumes make the biomass harder to observe, while the effects of exposed environments on animal health and welfare remain uncertain (Hvas et al., 2021; Morro et al., 2022).

A supplementary contribution to increase yield besides expanding production to exposed locations can be to ensure that more fish survive for slaughter. Irrespective of whether production is increased by adapting new locations and containment systems or by reducing mortality (or both), our understanding of aquaculture operations effect on animal welfare must be improved to succeed, both in terms of profitability and ethical, sustainable Atlantic salmon production.

To this end, the 'Precision Fish Farming' (PFF) framework was coined in 2017 by Føre et al., to improve production control and animal health and welfare in aquaculture. The framework advocates using a feedback loop consisting of four steps: observe, interpret, decide and act. By re-iterating these steps using objective inputs and model-based data interpretation methods, farming operations can be continuously adapted to the present farming states. To realize this framework, it must first be made possible to collect relevant data in different farming contexts so operations do not negatively impact fish beyond their tolerances. Thus, suitable technologies must be developed to collect objective data for behavioural and physiological responses, and knowledge obtained on how such data relate to stress and, by extension, animal health and welfare. To obtain such data individual fish can

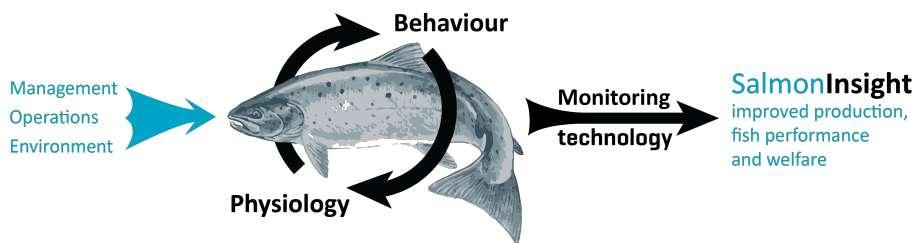


Figure 1.2: Relation between behaviour, physiology and technology in SalmonInsight. Ill: Hans Vanhauwaert Bjelland, SINTEF Ocean AS.

be equipped with a miniaturized, electronic sensor package (i.e., a 'tag') which may require surgery for attachment or implantation (Adams et al., 2012; Thorstad et al., 2013). If novel sensing principles (e.g., pulse oximetry) can be successfully adapted for Atlantic salmon, such solutions can support the industry's increasing focus on animal health and welfare while making production more profitable, sustainable and responsible.

## 1.2 Scope and objectives

### 1.2.1 SalmonInsight

The SalmonInsight project<sup>1</sup> was established in 2018 as an effort to realize PFF in Atlantic salmon farming. The project's main objective was to enable real-time data collection of fish parameters during full scale farming operations by creating technologies for behavioural and physiological monitoring to uncover their relation to stress and, by extension, welfare (figure 1.2). This is important because current methods to quantify stress as a proxy for welfare involves handling fish to obtain blood samples for stress hormone analysis. This limits the contexts in which stress can be evaluated. A blood sampling approach also introduces handling and sampling stress and it may be difficult to determine if stress hormones present in the sampled blood are caused by the (experiment) stressor or as a consequence of handling and sampling. If behavioural and physiological stress proxies can be measured using sensors, new possibilities to investigate stress responses open which, in turn, may improve animal welfare.

The project consisted of three interrelated work packages (WP) (figure 1.3). WP1 was aimed at identifying the relationship between the physiological condition and stress levels of Atlantic salmon and swimming ac-

---

<sup>1</sup>The Research Council of Norway project number 280864

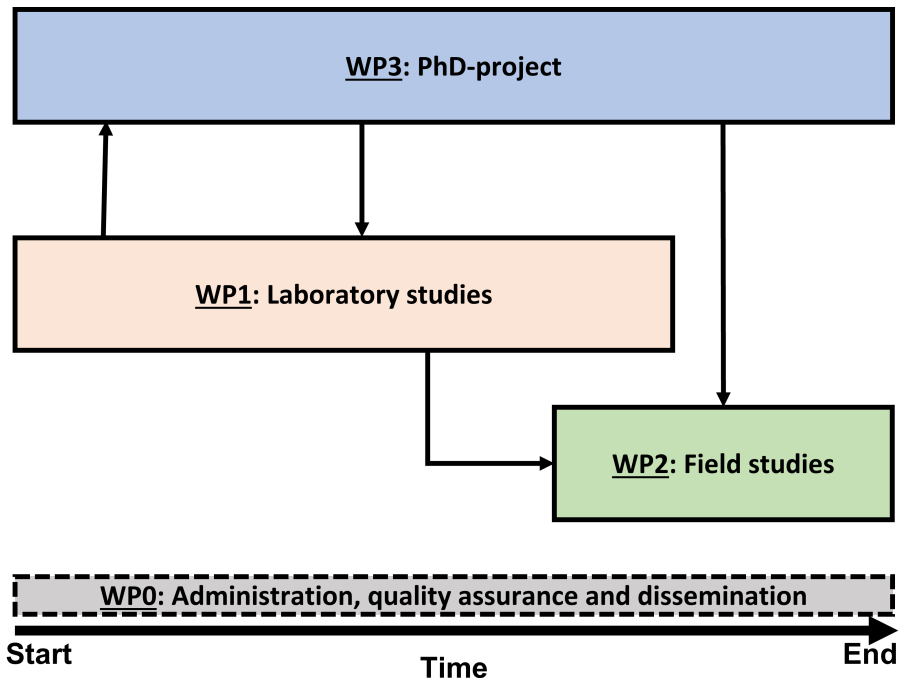


Figure 1.3: SalmonInsight work packages and their relationships.

tivity/behavioural parameters observable with state-of-the art logging and telemetry sensors. This was realised by swim tunnel trials and a controlled, experimental crowding event using fish in tanks where crowding was simulated by increasing fish density to induce crowding stress. In both trials, fish were equipped with sensors, and blood samples obtained analysed to investigate links between data sets. This was used as input to WP3.

WP2 sought to apply the knowledge from WP1 by demonstrating a telemetry solution for commercial production settings, and verify the approach in a mesoscale field trial with crowding induced stress. Individual physiology and behavioural data was collected using loggers to demonstrate the ability to measure and, thus, link and monitor indicators for physiological condition (i.e., stress) quantified using blood samples.

WP3 was the project's PhD activity specifically focusing on technology development to achieve SalmonInsight's main objective.

### 1.2.2 PhD work package objectives

The main objective for the PhD project (section 1.2.1) was to develop novel technologies to measure behavioural and physiological responses for individual fish. This was addressed by sub objectives defined as:

**O.1** - Investigate if physiological and behavioural data can be linked to stress in Atlantic salmon.

**O.2** - Select and test an appropriate sensing technique to add to the list of (physiological) parameters possible to measure in full scale Atlantic salmon production settings.

**O.3** - Design and implement a new multi sensor solution to enable concurrent measurement of behavioural and physiological responses for Atlantic salmon.

**O.4** - Test the sensor solutions in relevant (experimental) settings and evaluate its performance.

### 1.3 Contributions - Implant development

This thesis addresses the SalmonInsight PhD work package objectives (section 1.2.2) by developing a novel implant for concurrent logging of behavioural and physiological parameters from individual Atlantic salmon. To this end it was first demonstrated that behavioural and physiological parameters can be linked to stress using existing off-the-shelf implants. Then, pulse oximetry was selected as a novel sensing principle and tested for Atlantic salmon. Based on these tests, a pulse oximetry implant simultaneously logging other common behavioural and physiological parameters was designed and tested using both anesthetized and free-swimming Atlantic salmon. These contributions are detailed in the following included papers:

#### **Paper A (published)**

Svendsen, E., Føre, M., Økland, F., Gräns, A., Hedger, R. D., Alfredsen, J. A., Uglem, I., Rosten, C. M., Frank K., Erikson, U., Finstad, B., 2021. Heart rate and swimming activity as stress indicators for Atlantic salmon (*Salmo salar*). *Aquaculture*, 531, p.735804.

#### **Paper B (published)**

Føre, M., Svendsen, E., Økland, F., Gräns, A., Alfredsen, J. A., Finstad, B., Hedger, R. D. and Uglem, I., 2021. Heart rate and swimming activity as indicators of post-surgical recovery time of Atlantic salmon (*Salmo salar*). *Animal Biotelemetry*, 9, pp.1-13.

**Paper C (published)**

Svendsen, E., Økland, F., Føre, M., Randeberg, L. L., Finstad, B., Olsen, R. E. and Alfredsen, J. A., 2021. Optical measurement of tissue perfusion changes as an alternative to electrocardiography for heart rate monitoring in Atlantic salmon (*Salmo salar*). *Animal Biotelemetry*, 9(1), pp.1-12.

**Paper D (published)**

Svendsen, E., Føre, M., Randeberg, L. L. and Alfredsen, J. A., 2021. Design of a novel biosensor implant for farmed Atlantic salmon (*Salmo salar*). *IEEE Sensors 2021*, pp. 1-4.

**Paper E (published)**

Svendsen, E., Randeberg, L.L., Føre, M., Finstad, B., Olsen, R.E., Bloecher, N. and Alfredsen, J.A., Data for Characterization of the Optical Properties of Atlantic Salmon (*Salmo salar*) Blood. *Journal of Biophotonics*, p.e202300073.

**Paper F (published)**

Svendsen, E., Føre, M., Randeberg L. L., Olsen R. E., Finstad, B., Remen, M., Bloecher, N., Alfredsen, J. A., 2023. ECG Augmented Pulse Oximetry in Atlantic Salmon *Salmo salar* - A Pilot Study. *Computers and Electronics in Agriculture*, 212, p.108081.

During the course of this research, contributions to related work have been made with respect to data processing for experiments aiming to connect physiological and behavioural data to stress responses in larger scale, as well as tail beat frequency extraction using acceleration data. These contributions are detailed in the following papers (not included in this thesis):

**Paper R.A (in review)**

Bloecher, N., Finstad, B., Føre, M., Hedger, R., Olsen, R. E., Rosten, C., Svendsen, E., 2023. Assessment of activity and heart rate as stress indicators for Atlantic salmon in field tests. *Aquaculture*. In review.

**Paper R.B (accepted)**

Morgenroth, D., Kvaestad, B., Økland, F., Finstad, B., Olsen, R. E., Svendsen, E., Rosten, C., Axelsson, M., Bloecher, N., Føre, M., Gräns, A., 2023. Under the Sea: How can we use heart rate and accelerometers to remotely assess fish welfare in aquaculture? *Aquaculture*. Accepted.

**Paper R.C (published)**

Warren-Myers, F., Svendsen, E., Føre, M., Folkedal, O., Oppedal, F. and

Hvas, M., 2023. Novel tag-based method for measuring tailbeat frequency and variations in amplitude in fish. *Animal Biotelemetry*, 11(1), pp.1-13.

The scientific papers and how they relate to technology, behaviour and physiology within the context of SalmonInsight is illustrated in figure 1.4.

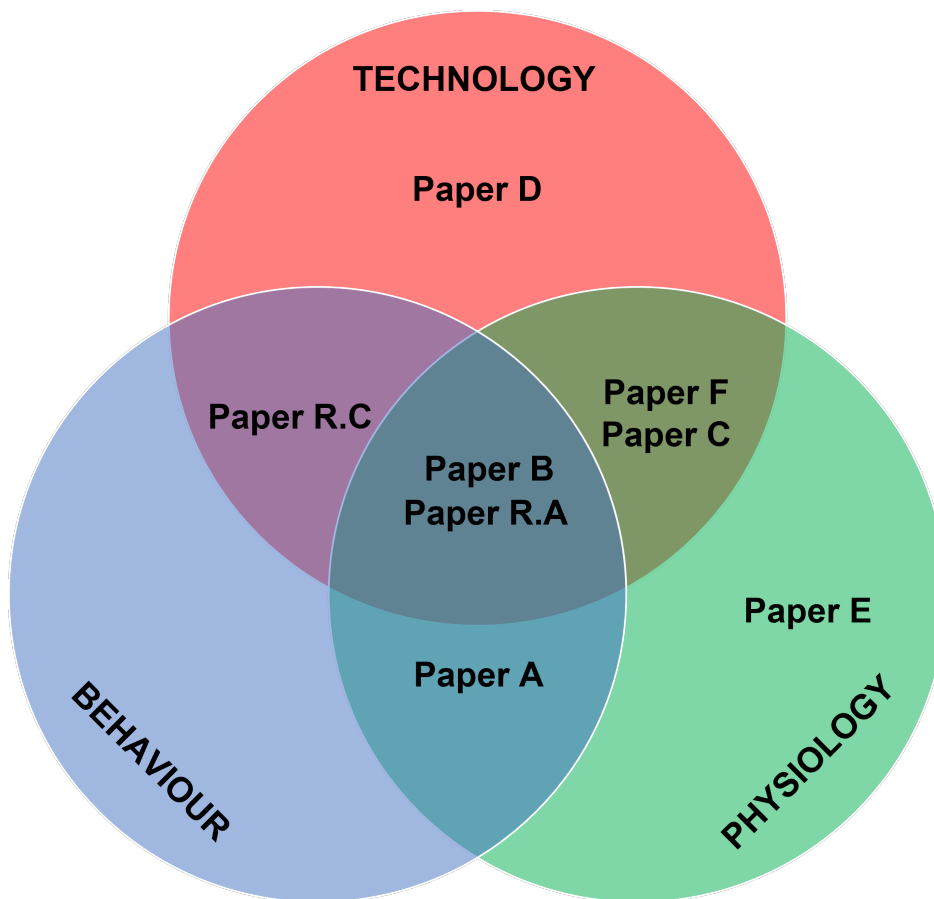


Figure 1.4: Scientific papers and their relation to technology, behaviour and physiology in SalmonInsight (section 1.2.1).



# Chapter 2

## Background

### 2.1 Electronic tagging and tracking tools

Electronic tagging and tracking tools (E3Ts) is a common denominator for biologging and biotelemetric approaches to obtain behavioural and physiological parameters from roaming animals (Cooke et al., 2021). E3Ts come in two main varieties: Archival (data storage) and transmitter tags. The former stores raw or processed data in an internal memory. Such tags generally offer high sampling rates but must be retrieved for data download and further processing. Transmission tags on the other hand, process measured data and transmit the result to receivers thereby providing near real-time access to data. In fresh water, data can be transmitted by radio or acoustic signalling. In sea water, however, data transfer is limited to acoustics due to sea water's impermeability to radio signals.

Several manufacturers of archival and transmitter tags considered suitable for full scale aquaculture operations exist and offer measurement of several behavioural, physiological and environmental parameters (table 2.1). The majority of available parameters are currently related to behaviour and the environment, while physiological parameters are limited to electrocardiogram (ECG) for heart rate estimation. Additional physiological parameters, e.g., electroencephalogram (Robb et al., 2000), electromyogram (EMG) (Thorstad et al., 2000), blood pressure (Morgenroth et al., 2019), cardiac output (Brodeur et al., 1999) and a range of blood parameters using dorsal aorta cannulation (Eliason et al., 2013) are possible to measure in fishes. Obtaining such parameters, however, requires advanced and invasive surgical procedures and are therefore not well suited for contexts outside the laboratory.

## 2. Background

Manufacturer	Acc.	Gyr.	Comp.	Press	Temp.	ECG	Pos.	Other
ATS	-	-	-	-	-	-	X	-
Biologging Solutions	-	-	-	-	X	-	X	Video, sound
Cefas	X	-	-	X	X	-	-	-
Innovasea	X	-	-	X	X	-	X	Predation
Lotek	X	-	-	X	X	-	X	-
Sonotronics	X	-	-	-	-	-	X	-
Star-Oddi	X	-	X	X	X	X	-	Salinity
Technosmart	X	X	X	X	X	-	X	Light
Thelma Biotel	X	-	-	X	X	-	X	Salinity

Table 2.1: A non-exhaustive overview of implant / tag manufacturers and parameters on offer. Acc. - Acceleration (multi purpose, e.g., activity, tilt, tailbeat activity (and frequency), mortality etc.), Gyr. - gyroscope (i.e., rotation rates), Comp. - Compass, Press. - Pressure (for depth estimation), Temp. - temperature, ECG - Electrocardiogram, Pos - Position/acoustic tracking.

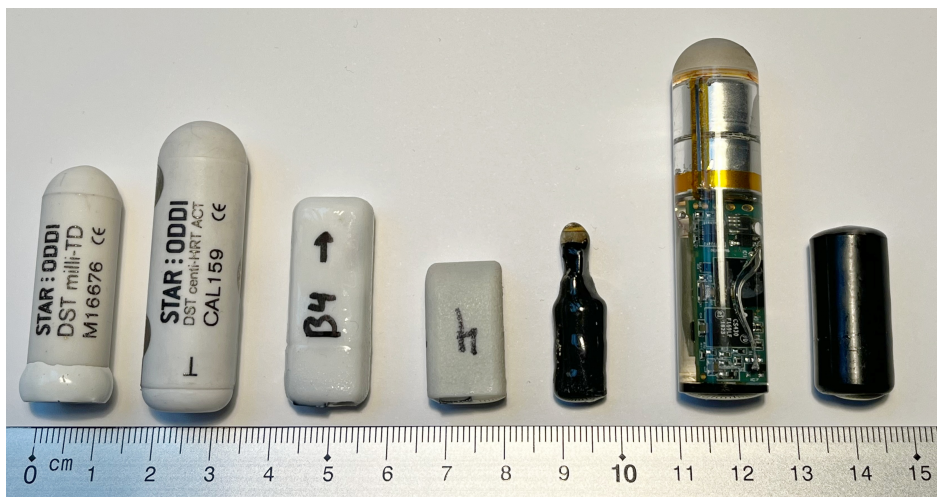


Figure 2.1: Examples of archival and transmission tags. From left to right: Star-Oddi Milli temperature and depth archival tag, Star-Oddi Centi heart rate and activity archival tag, Technosmart AGM acceleration, magnetometer, gyro and temperature archival tag, Technosmart Axy 5 XS acceleration, magnetometer and temperature archival tag, Innovasea HTI-LD acoustic transmitter, Cefas C7 acceleration archival tag, Thelma Biotel ID-MP13 activity acoustic transmitter tag

Existing tags come in a variety of implementations depending on their use and capability. To reduce the risk of tag loss and to avoid negative welfare impacts associated with external tagging methods (e.g., chafing and tag loss) (Jepsen et al., 2015), E3Ts for fish usually come in the form of intraperitoneal implants (figure 2.1).

Tags have seen extensive use in research (Adams et al., 2012; Thorstad et al., 2013), and have repeatedly been demonstrated in different aquaculture production contexts for measurement of, e.g., activity, swimming depth, temperature and swimming speed (Føre et al., 2011, 2017a; Hassan et al., 2022), position (Hassan et al., 2019; Muñoz et al., 2020) and heart rate (Brijs et al., 2018). Such studies provide interesting information on the behaviour and environmental preferences within the production environment for individual fish. However, due to the parameters possible to measure, such studies offer limited insight into connection with stress and welfare. The need to measure additional physiological parameters is therefore evident and is underscored by on-going research to realize, e.g., online glucose and cortisol measurements (Wu et al., 2019; Zimmer, 2023) and EMG (Yang et al., 2021). Additional sensing principles to further expand the growing list of physiological parameters which can be measured in aquaculture production contexts were therefore evaluated for inclusion in an implant for deployment in such contexts.

## **2.2 Sensing principle candidates**

As described in section 2.1, several implants already exist which offer a range of parameters (table 2.1). With this in mind, technology readiness level for new sensing principles was reviewed with respect to miniaturization level and power efficiency. These considerations limited the number of sufficiently mature technologies lending themselves to tag integration and simple deployment. Candidate technologies for physiological parameters were e.g., photonic hydrogel (Yetisen et al., 2016; Tavakoli and Tang, 2017) and electrochemical sensors.

Photonic hydrogels change measurable properties when interacting with an analyte. This interaction depends on the possibility to synthesize a polymer network sensitive to the desired analyte. Because this research aimed to use off the shelf electronic components and sensors, realizing a photonic hydrogel sensitive to some selected analyte simultaneously suited for integration in an implant was considered outside the scope of SalmonInsight (section 1.2.1).

Within the domain of electrochemical sensors applicable to fishes, ongoing research efforts aim to develop implantable electrochemical glucose and cortisol sensors (Wu et al., 2019; Zimmer, 2023). Such efforts were, thus, left to these research groups.

Because heart rate (ECG), already existed as an implantable data storage tag supplied by Star-Oddi (Star-Oddi, 2023), a remaining candidate was pulse oximetry, an optical sensing technique providing a measure of arterial blood oxygen saturation ( $SpO_2$ ) as well as a heart rate estimate. Development of miniaturized pulse oximetry sensors has in recent years been driven by the emergence of mobile medical equipment, smart phones and exercise watches (Steinhubl et al., 2015; Fahlman et al., 2021). This sensing technique was therefore considered the best candidate and was, thus, selected for further testing, not only due to its technology readiness level, but also because heart rate is likely linked to stress. Arterial blood oxygen saturation dynamics was also expected to increase insight into the physiological responses of Atlantic salmon in farming contexts with variations in dissolved oxygen (Alver et al., 2022) and, potentially, hypoxic conditions (Oldham et al., 2017).

### 2.3 Pulse oximetry

The ultimate goal of pulse oximetry (PO) is to determine the oxygen saturation in arterial blood ( $SpO_2$ ), i.e., the percentage of oxygen carrying hemoglobin in arterial blood given by

$$SpO_2 = \frac{(C_{HbO})}{(C_{Hb} + C_{HbO})} \cdot 100\%, \quad (2.1)$$

where  $C_{HbO}$  and  $C_{Hb}$  are the concentrations of oxyhemoglobin (oxygen carrying hemoglobin,  $HbO$ ) and deoxyhemoglobin (non oxygen carrying hemoglobin,  $Hb$ ), respectively. PO is divided into two main approaches, i.e., 'transmission' or 'reflection' PO. In transmission PO, the light emitters are placed so they shine through tissue towards the photo detector. In reflection PO, the light emitters are co-located with the photo detectors on the same side of the illuminated tissue (figure 2.2).

PO is based on the Beer-Lambert law (BLL) (Swinehart, 1962) stating that the intensity,  $I$  of light with a wavelength,  $\lambda$ , decays exponentially with absorption,  $A$ , and travel length,  $l$ , so

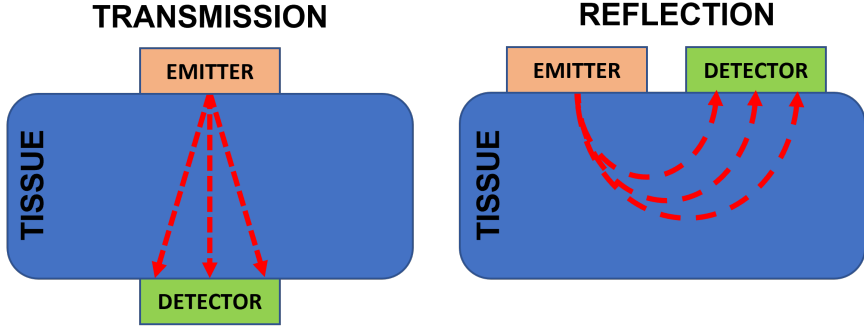


Figure 2.2: Illustration of transmission and reflection oximetry. In the case of reflection oximetry, photons travel from emitter to detector along a curved path referred to as the 'photon banana'.

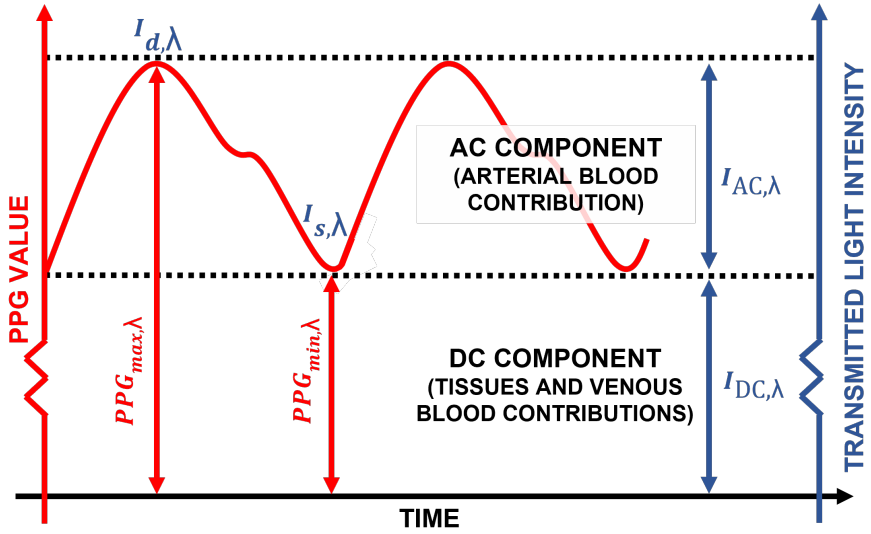


Figure 2.3: Illustration of the (measured) PPG value (red) and transmitted light intensity (blue), and their relationship with the cardiac cycle for a given wavelength,  $\lambda$ .

$$I_{\lambda} = I_{0,\lambda}e^{-A_{\lambda}} = I_{0,\lambda}e^{\varepsilon_{\lambda}Cl_{\lambda}} = I_{0,\lambda}e^{\mu_{a,\lambda}l_{\lambda}}, \quad (2.2)$$

where  $I_{0,\lambda}$  is the emitter intensity,  $\varepsilon_{\lambda}$  the wavelength and chromophore-dependent molar extinction coefficient,  $C$  the concentration of the chromophore and  $\mu_{a,\lambda} = \varepsilon_{\lambda}C$  the absorption coefficient.

PO is based on the assumption that absorption changes with the cardiac cycle due to changes in perfusion (i.e., the blood volume fraction) (figure 2.3). During diastole (heart relaxation), perfusion is low. Thus, less light is absorbed and detected light intensity reaches its maximum value,  $I_{d,\lambda}$ . During systole (heart contraction) arterioles and capillaries expand and perfusion increases. Thus, more light is absorbed and detected light intensity reaches its minimum value,  $I_{s,\lambda}$ . This creates a pulsatile 'AC' component in the measurement synchronous with the heart beat and uniquely associated with arterial blood. Because light is not only absorbed by arterial blood but also by other tissues, the PO measurement includes a near constant 'DC' component. The resulting curve is referred to as a 'photoplethysmogram' (PPG).

In real-world applications,  $I_{0,\lambda}$  and  $l_\lambda$  are unknown but the dependence upon these quantities can fortunately be removed.  $I_{0,\lambda}$  is eliminated by first applying (2.2) to the measured light intensities for the AC and DC components to obtain

$$I_{DC,\lambda} = I_{0,\lambda} \cdot e^{-\mu_{a,DC,\lambda} \cdot l_{DC,\lambda}} \quad (2.3)$$

and

$$I_{AC,\lambda} = I_{DC,\lambda} \cdot e^{-\mu_{a,AC,\lambda} \cdot l_{AC,\lambda}}. \quad (2.4)$$

The concept of transmittance defined by

$$T_\lambda = \frac{I_\lambda}{I_{0,\lambda}}, \quad (2.5)$$

i.e., the ratio between emitted and received light intensities, must now be introduced. By solely considering the AC component (figure 2.3), its transmittance is defined by

$$T_{AC,\lambda} = \frac{I_{AC,\lambda}}{I_{DC,\lambda}} \quad (2.6)$$

Now, substitution of (2.3) for  $I_{DC,\lambda}$  in (2.4) gives

$$I_{AC,\lambda} = I_{0,\lambda} \cdot e^{-\mu_{a,DC,\lambda} \cdot l_{DC,\lambda}} \cdot e^{-\mu_{a,AC,\lambda} \cdot l_{AC,\lambda}}. \quad (2.7)$$

Inserting (2.7) for  $I_{AC,\lambda}$  and (2.3) for  $I_{DC,\lambda}$  in (2.6), we get

$$T_{AC,\lambda} = \frac{I_{0,\lambda} \cdot e^{-\mu_{a,DC,\lambda} \cdot l_{DC,\lambda}} \cdot e^{-\mu_{a,AC,\lambda} \cdot l_{AC,\lambda}}}{I_{0,\lambda} \cdot e^{-\mu_{a,DC,\lambda} \cdot l_{DC,\lambda}}}. \quad (2.8)$$

The term  $I_{0,\lambda} \cdot e^{-\mu_{a,DC,\lambda} \cdot l}$  can then be cancelled giving

$$T_{AC,\lambda} = e^{-\mu_{a,AC,\lambda} \cdot l_{AC,\lambda}}. \quad (2.9)$$

Thus,  $T_{AC,\lambda}$  can be described independently from light source intensity.

The optical path length,  $l_{AC,\lambda}$  in (2.9), can now be eliminated by taking the logarithm of both sides giving

$$\ln(T_{AC,\lambda}) = \ln(e^{-\mu_{a,AC,\lambda} \cdot l_{AC,\lambda}}) = -\mu_{a,AC,\lambda} l_{AC,\lambda}. \quad (2.10)$$

Measuring  $T_{AC,\lambda}$  using two wavelengths,  $\lambda_1$  and  $\lambda_2$ , results in

$$\ln(T_{AC,\lambda_1}) = -\mu_{a,AC,\lambda_1} l_{AC,\lambda} \quad (2.11)$$

and

$$\ln(T_{AC,\lambda_2}) = -\mu_{a,AC,\lambda_2} l_{AC,\lambda}. \quad (2.12)$$

Solving for  $l_{AC,\lambda}$  in (2.12) and substituting in (2.11), gives

$$\ln(T_{AC,\lambda_1}) = -\mu_{a,AC,\lambda_1} \frac{\ln(T_{AC,\lambda_2})}{-\mu_{a,AC,\lambda_2}}. \quad (2.13)$$

Thus, the transmittance ratio, which equals the absorption coefficient ratio for the AC PPG component is obtained as

$$\frac{\ln(T_{AC,\lambda_1})}{\ln(T_{AC,\lambda_2})} = \frac{\mu_{a,AC,\lambda_1}}{\mu_{a,AC,\lambda_2}}. \quad (2.14)$$

Now that both  $I_{0,\lambda}$  and  $l_\lambda$  have been eliminated, (2.14) must be written in terms of the measured PPG signal. This is necessary because pulse oximeters do not measure transmitted light intensity per se, but rather a coincident digitized voltage (i.e., 'PPG value' in figure 2.3). Figure 2.3 shows that the PPG AC component can be written as the transmitted intensities so  $I_{AC,\lambda} = \Delta I_\lambda = I_{d,\lambda} - I_{s,\lambda}$ , and  $I_{DC,\lambda} = I_{s,\lambda}$ . Substituting for  $T_{AC,\lambda}$  in the nominator or denominator in (2.14) gives

$$\ln(T_{AC,\lambda}) = \ln\left(\frac{I_{AC,\lambda}}{I_{DC,\lambda}}\right) = \ln\left(\frac{I_{s,\lambda} - \Delta I_\lambda}{I_{s,\lambda}}\right) = \ln\left(1 - \frac{\Delta I_\lambda}{I_{s,\lambda}}\right). \quad (2.15)$$

Approximating (2.15) by a Maclaurin series expansion (Kreyszig, 2011) and ignoring higher order terms, (2.15) becomes

$$\begin{aligned} \ln(T_{AC,\lambda}) &= \ln\left(1 - \frac{\Delta I_\lambda}{I_{s,\lambda}}\right) \\ &= -\frac{\Delta I_\lambda}{I_{s,\lambda}} - \frac{(\Delta I_\lambda/I_{s,\lambda})^2}{2} - \frac{(\Delta I_\lambda/I_{s,\lambda})^3}{3} - \frac{(\Delta I_\lambda/I_{s,\lambda})^4}{4} \dots \quad (2.16) \\ &\approx -\frac{\Delta I_\lambda}{I_{s,\lambda}}. \end{aligned}$$

Ignoring the higher order terms of the Maclaurin series expansion is justified by the fact that in PO,  $I_{s,\lambda} \gg \Delta I_\lambda$  (figure 2.3). Thus,  $\Delta I_\lambda/I_{s,\lambda} \ll 1$  and becomes negligible when raised to the power of two and above in (2.16). Substituting (2.16) for both wavelengths in (2.14), the equation known as the 'ratio of ratios' is obtained as

$$R = \frac{\ln(T_{AC,\lambda_1})}{\ln(T_{AC,\lambda_2})} \approx \frac{(-\Delta I_{\lambda_1}/I_{s,\lambda_1})}{(-\Delta I_{\lambda_2}/I_{s,\lambda_2})} = \frac{\Delta I_{\lambda_1}/I_{s,\lambda_1}}{\Delta I_{\lambda_2}/I_{s,\lambda_2}}. \quad (2.17)$$

Normalizing the PPG for both wavelengths by their DC components, (2.17) becomes

$$\begin{aligned} R &\approx \frac{\frac{\Delta I_{\lambda_1}/I_{s,\lambda_1}}{I_{s,\lambda_1}}}{\frac{\Delta I_{\lambda_2}/I_{s,\lambda_2}}{I_{s,\lambda_2}}} = \frac{\Delta I_{\lambda_1}}{\Delta I_{\lambda_2}} = \frac{I_{d,\lambda_1} - I_{s,\lambda_1}}{I_{d,\lambda_2} - I_{s,\lambda_2}} \\ &= \frac{PPG_{max,\lambda_1} - PPG_{min,\lambda_1}}{PPG_{max,\lambda_2} - PPG_{min,\lambda_2}}, \end{aligned} \quad (2.18)$$

which is known as the 'modulation ratio' and is mapped to  $SpO_2$ .

In human PO, (2.18) is mapped to  $SpO_2$  via empirical calibration by having volunteers breathe a desaturated gas mixture while equipped with both a reference oximeter and the oximeter for calibration. The modulation ratio, (2.18), can then be mapped to the reference's  $SpO_2$  estimate. This



is to account for tissue inhomogeneity and light scattering which must be dealt with in real world PO applications.

Because PO in fishes was an unexplored area, no reference oximeter was available for empirical mapping. As an alternative, (2.2) was modified to account for scattering. In the scattering case for reflection oximetry, photons travel from the emitter to the detector along an optical path referred to as the 'photon banana' (figure 2.2) (Bigio and Fantini, 2016; Bhatt et al., 2016), given by

$$\bar{l}_\lambda = DPF_\lambda \cdot \rho, \quad (2.19)$$

where  $DPF_\lambda$  is a wavelength dependent constant known as the 'differential path length factor', and  $\rho$  the emitter-detector distance. Because the measured PPG (i.e., 'PPG value' in figure 2.3) is subject to scattering, the relationship between the modulation ratio, (2.18), and the absorption coefficient ratio, (2.14), can be written as

$$\frac{PPG_{max,\lambda 1} - PPG_{min,\lambda 1}}{PPG_{max,\lambda 2} - PPG_{min,\lambda 2}} = \frac{\mu_{a,AC,\lambda 1} \bar{l}_{\lambda 1}}{\mu_{a,AC,\lambda 2} \bar{l}_{\lambda 2}}. \quad (2.20)$$

By inserting (2.19) into the nominator or denominator in (2.20) we obtain

$$PPG_{max,\lambda} - PPG_{min,\lambda} = \mu_{a,AC,\lambda} DPF_\lambda \rho. \quad (2.21)$$

For  $i$  chromophores, we then get

$$\begin{aligned} PPG_{max,\lambda} - PPG_{min,\lambda} &= \\ &= \sum_i \mu_{a,i,\lambda} \cdot DPF_\lambda \cdot \rho = \\ &= \sum_i \varepsilon_{i,\lambda} C_i \cdot DPF_\lambda \cdot \rho, \end{aligned} \quad (2.22)$$

which is known as the modified Beer-Lambert law. Expanding (2.22) for two chromophores (oxyhemoglobin,  $HbO$ , and hemoglobin,  $Hb$ ) results in

$$PPG_{max,\lambda} - PPG_{min,\lambda} = (\varepsilon_{\lambda,HbO} \cdot C_{HbO} + \varepsilon_{\lambda,Hb} \cdot C_{Hb}) DPF_\lambda \cdot \rho. \quad (2.23)$$

Equation (2.23) can now be related to  $SpO_2$  by first solving (2.1) for  $C_{Hb}$  which gives

$$C_{Hb} = (1 - SpO_2) \cdot (C_{Hb} + C_{HbO}). \quad (2.24)$$

By substituting (2.24) for  $C_{Hb}$  in (2.23) we obtain

$$PPG_{max,\lambda} - PPG_{min,\lambda} = [\varepsilon_{HbO,\lambda} \cdot C_{HbO} + \varepsilon_{Hb,\lambda} \cdot (1 - SpO_2) \cdot (C_{Hb} + C_{HbO})] \cdot DPF_{\lambda} \cdot \rho. \quad (2.25)$$

Inserting (2.25) into (2.20) we get

$$R = \frac{PPG_{max,\lambda_1} - PPG_{min,\lambda_1}}{PPG_{max,\lambda_2} - PPG_{min,\lambda_2}} = \frac{[\varepsilon_{HbO,\lambda_1} \cdot C_{HbO} + \varepsilon_{Hb,\lambda_1}(1 - SpO_2)(C_{Hb} + C_{HbO})] \cdot DPF_{\lambda_1} \cdot \rho}{[\varepsilon_{HbO,\lambda_2} \cdot C_{HbO} + \varepsilon_{Hb,\lambda_2}(1 - SpO_2)(C_{Hb} + C_{HbO})] \cdot DPF_{\lambda_2} \cdot \rho}. \quad (2.26)$$

Solving (2.26) for  $SpO_2$  results in

$$SpO_2 = \frac{R \cdot \Gamma \cdot \varepsilon_{Hb,\lambda_2} - \varepsilon_{Hb,\lambda_1}}{R \cdot \Gamma \cdot (\varepsilon_{Hb,\lambda_2} - \varepsilon_{HbO,\lambda_2}) + (\varepsilon_{HbO,\lambda_1} - \varepsilon_{Hb,\lambda_1})} \cdot 100\%, \quad (2.27)$$

where  $\Gamma = DPF_{\lambda_2}/DPF_{\lambda_1}$ . Thus, if a value for  $\Gamma$  can be obtained,  $SpO_2$  compensated for scattering can be calculated.

## 2.4 Optical properties of tissue

Before attempting to obtain a value for the tissue inhomogeneity and light scattering compensation parameter,  $\Gamma$  in (2.27), it is useful to consider the optical properties of the tissues which may be present within the PO sensing volume. Adult Atlantic salmon relevant for implantation in this work, are torpedo shaped fish with an anterior center of gravity offset to improve directional stability when migrating large distances. They have a dark dorsal side, a light ventral side and spotted mirror right and left sides. Atlantic salmon have paired pectoral and pelvic fins, one anal fin, one dorsal fin, a homocercal (i.e., equal lobed) caudal fin and a fleshy adipose fin between the dorsal and caudal fins unless clipped for identification purposes. Other characterizing features are the mouth, nostrils, eyes and opercula on the head and the lateral line along both sides (figure 2.4).

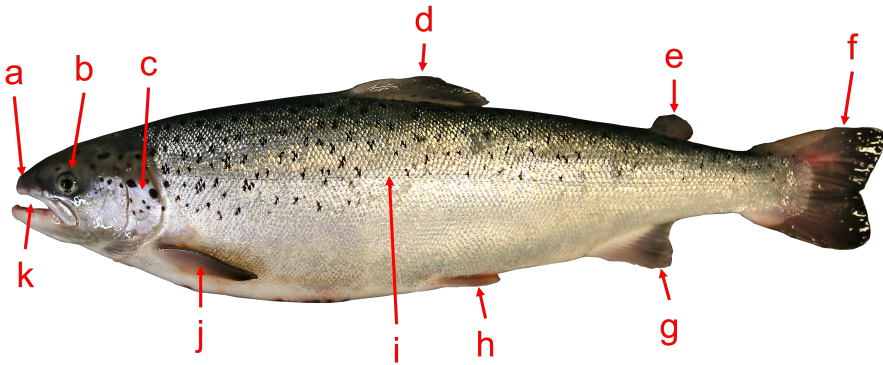


Figure 2.4: Atlantic salmon external gross anatomy. Arrow a - nostrils, b - eyes, c - opercula, d - dorsal fin, e - adipose fin, f - caudal fin, g - anal fin, h - pelvic fins, i - lateral line, j - pectoral fins and k - mouth.

In the context of implants for physiological measurements the internal anatomy is of greater interest. Starting anteriorly, the head contains the buccal cavity, brain and gills. Posterior from the buccal cavity is the pericardial cavity containing the heart. The peritoneal cavity is located posterior from the pericardial cavity and contains the viscera, the major parts of which are the liver, stomach, intestines, pyloric caeca, gall bladder, spleen, kidney, swim bladder and gonads. Some of these parts can be seen in figure 2.5.

The circulatory system is distributed throughout the entire body of the fish and consists of a primary system supplying e.g., the brain, viscera and muscles, and a secondary circulation system with high volumes but low exchange rates supplying e.g., the skin, scales and the fish's internal surfaces (Bone and Moore, 2008).

Atlantic salmon has three types of muscle, i.e., smooth, heart and skeletal. Smooth muscle is found in, e.g., the intestines, blood vessels and the eyes. Heart muscle is only found in the heart, while muscles for, e.g., swimming, fin and opercular movement consist of skeletal muscle. The majority of muscles is the lateral swim muscles arranged along both sides as W-shaped segments (myotomes) (Bone and Moore, 2008; Kryvi and Poppe, 2016).

The skeleton provides mechanical strength, consists mainly of bone and can be divided into the cranium, fin and axial skeleton. The cranium makes out the skull, opercula, jaws and gill arches. The fin skeleton consists of external rays and internal knuckles, while the axial skeleton consists of a series of connected vertebrae to make the spine (Kryvi and Poppe, 2016).

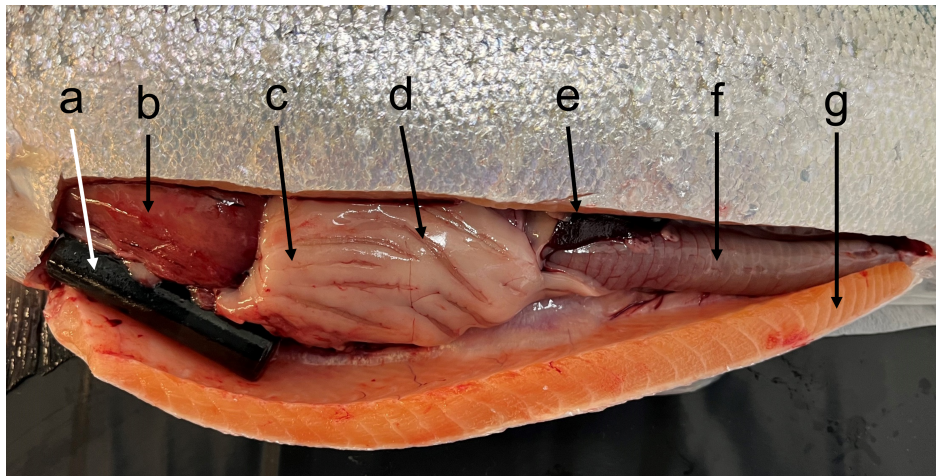


Figure 2.5: Atlantic salmon internal anatomy. Arrow a - PO tag as implanted using the techniques described herein, b - liver, c - visceral fat, d - pylorus caeca, e - spleen, f - intestine and g - myotomes.

Because tissues are unequally distributed, perfusion and the (tissue dependent) optical properties within a PO sensing volume will vary depending on the sensor's placement. In the case of intraperitoneal implantation, the sensing volume will be inhomogeneous and likely dominated by highly scattering tissues such as blood, fat, muscle and bone.

In terms of optical properties, blood is a highly scattering tissue consisting of white blood cells (e.g., neutrophils, monocytes and lymphocytes), platelets (thrombocytes) and red blood cells (RBC) (erythrocytes and reticulocytes) suspended in plasma [Härdig and Höglund \(1983\)](#); [Sandnes et al. \(1988\)](#). With respect to gross composition, Atlantic salmon blood shares commonalities with mammalian blood. There are, however, significant differences related to the number and ratio of the different cell types as well as their sizes. For the latter, Atlantic salmon RBCs are large ovoids with nuclei compared to the smaller, doughnut shaped mammalian RBCs without nuclei. RBCs completely dominate in terms of the number of cells per litre and will therefore be the dominating optical scatterer in whole blood, and a major contributor to scattering in a PO sensing volume containing several tissues. The optical absorption of blood is mainly due to hemoglobin, which absorbs light in the visible and near infrared wavelength range. The scattering of light by blood cells decreases as wavelength increases ([Friebel et al., 2009](#)).

Fat is a relatively transparent tissue in the visible and near-infrared regions of the electromagnetic spectrum. This is due to the low absorption coefficient of fat in these regions (Jacques, 2013). Fat does scatter light, however, with scattering decreasing as wavelength increases.

Muscle tissue has relatively high absorption in the visible and near-infrared regions of the electromagnetic spectrum due to the presence of myoglobin. The degree of absorption depends on the oxygenation of the muscle tissue. Muscle tissue scatters light, with the degree of scattering decreasing with increasing wavelength (Jacques, 2013).

Bone is a highly scattering tissue due to the presence of mineralized collagen. Absorption in bone is relatively low with near constant scattering in the visible and near-infrared regions of the electromagnetic spectrum (Ugryumova et al., 2004).

These absorption and scattering considerations are general and largely based on published data for human tissues due to the scarcity of such data for fishes. Care should therefore be exercised when assigning optical properties to fish tissues. To reduce these uncertainties, light propagation in scattering tissues can be modeled mathematically and simulated using a Monte Carlo approach. When combined with measurements, the optical properties of the sensing volume can be evaluated.

## 2.5 Monte Carlo simulations

The Monte Carlo (MC) method is an extensive class of algorithms for simulation of physical systems which can be represented by randomized changes in each simulation step (Bigio and Fantini, 2016; Prahl, 1989; Chatterjee et al., 2018; Reuss, 2005).

An MC simulation environment for light propagation in tissue is commonly defined in terms of a finite or infinite layered (slab) geometry where each layer is characterized by its absorption and scattering coefficients, its refractive index and thickness (Reuss, 2005). Super individuals referred to as 'photon packets' are initialized with a starting point, initial propagation angles (azimuth,  $\psi$ , and pitch,  $\theta$ ) from which direction cosines are calculated, an initial layer designation, a weight,  $w = 1$ , and a number of photons. The packet is then launched into the environment. For each simulation step, the packet propagation distance,  $\Delta_s$ , is determined by

$$\Delta_s = \frac{-\ln(\xi_1)}{\mu'_t} = \frac{-\ln(\xi_1)}{(\mu_a + \mu_s(1 - g))}, \quad (2.28)$$

where  $\xi_1 \in [0, 1]$  is a random number,  $\mu'_t$  the current layer's reduced total scattering coefficient,  $\mu_a$  the attenuation coefficient,  $\mu_s$  the scattering coefficient and  $g$  the anisotropy coefficient. The photon packet is then propagated to its new coordinates using

$$x' = x + \mu_x \Delta s, \quad (2.29)$$

$$y' = y + \mu_y \Delta s, \quad (2.30)$$

and

$$z' = x + \mu_z \Delta s, \quad (2.31)$$

where  $\mu_x$ ,  $\mu_y$  and  $\mu_z$  are the direction cosines. The incremental change in propagation angles are then updated by

$$\theta = \arccos(G) \quad (2.32)$$

$$\psi = 2\pi\xi_2, \quad (2.33)$$

where  $\xi_2 \in [0, 1]$  is a random variable. The (randomized), tissue-dependent, scattering angle cosine  $G$ , in (2.32) is determined by the Henyey-Greenstein phase function given by

$$G = \cos(\theta) = \frac{1}{2g} \left\{ 1 + g^2 - \left[ \frac{1 - g^2}{1 - g + 2g\xi_3} \right]^2 \right\}, \quad (2.34)$$

where,  $\xi_3 \in [0, 1]$  is a random variable and  $g$  the anisotropy coefficient for the (tissue) layer in which the photon packet is currently within (Binzoni et al., 2006). The next-step (new) direction cosines are given by

$$\mu'_x = \frac{\sin(\theta)}{\sqrt{1 - \mu_z^2}} (\mu_x \mu_z \cos(\phi) - \mu_y \sin(\phi)) + \mu_x \cos(\phi), \quad (2.35)$$

$$\mu'_y = \frac{\sin(\theta)}{\sqrt{1 - \mu_z^2}} (\mu_y \mu_z \cos(\phi) - \mu_x \sin(\phi)) + \mu_y \cos(\phi), \quad (2.36)$$

and

$$\mu'_z = -\sin(\theta)\cos(\phi)\sqrt{1 - \mu_z^2} + \mu_z\cos(\theta). \quad (2.37)$$

If the photon packet travels close to the vertical (e.g.,  $|\mu_z| > 0.99999$ ) the next-step direction cosines are given by

$$\mu'_x = \sin(\theta)\cos(\phi) \quad (2.38)$$

$$\mu'_y = \sin(\theta)\sin(\phi) \quad (2.39)$$

and

$$\mu'_z = \frac{\mu_z}{|\mu_z|}\cos(\phi). \quad (2.40)$$

In each simulation step, a fraction of the photons,  $F_a$ , in a photon packet is absorbed according to

$$F_a = \frac{\mu_a}{\mu'_t} = 1 - \frac{\mu_s(1 - g)}{\mu_a + \mu_s(1 - g)} = 1 - a, \quad (2.41)$$

where  $a$  is referred to as the photon packet's albedo. The new packet weight,  $w'$  is calculated as

$$w' = w \cdot a. \quad (2.42)$$

A photon packet is terminated when its number of photons reaches 0 or its weight falls below a preset threshold,  $\alpha$  (e.g., 0.001, [Prahl, 1989](#)). The motivation for the latter is evident when reviewing (2.42) for calculation of the photon packet weight which will never reach 0. To avoid violation of energy conservation, a roulette approach is employed by which a random number  $\xi_4 \in [0, 1]$  is generated and compared to the threshold  $\alpha$ . If  $\xi_4 < \alpha$  the photon packet is terminated, otherwise it is propagated.

Whether a packet is transmitted or reflected when crossing a boundary is determined by first calculating the Fresnel reflection coefficient [Jacques \(2010\)](#) given by

$$R(\theta_i) = \frac{1}{2} \left[ \frac{\sin^2(\theta_i - \theta_t)}{\sin^2(\theta_i + \theta_t)} + \frac{\tan^2(\theta_i - \theta_t)}{\tan^2(\theta_i + \theta_t)} \right], \quad (2.43)$$

where  $\theta_i$  and  $\theta_t$  are the photon packet's incident angle to the vertical (i.e., z-direction) and transmission angles, respectively. The incident and transmission angles are related by Snell's law as

$$n_1 \sin(\theta_i) = n_2 \sin(\theta_t), \quad (2.44)$$

where  $\theta_i$  is given by the z-direction cosine, i.e.,  $\theta_i = \arccos(\mu_z)$ .

A random number  $\xi_5 \in [0, 1]$  is then sampled. If  $\xi_5 < R(\theta_i)$  the packet is reflected at an angle  $\theta = \arccos(-\mu_z)$ , otherwise it is transmitted into the next layer at an angle  $\theta_t$  obtained directly from (2.44). If  $n_1 > n_2$  (2.44) cannot be solved for  $\theta_i \geq \theta_{crit}$ , where

$$\theta_{crit} = \arcsin\left(\frac{n_2}{n_1}\right). \quad (2.45)$$

In this case, total internal reflection occurs and the photon package is reflected back into the originating layer at an angle defined by  $\theta = \arccos(-\mu_z)$ .

By defining an appropriate simulation environment in terms of geometry and optical properties, light propagation in tissues can be simulated and analyzed.



## Chapter 3

# Experimental work

To realize a PO implant for Atlantic salmon, a series of experiments were conducted. First, the optical properties of Atlantic salmon blood were investigated by spectral analysis to evaluate if PO sensors were likely to be sensitive to changes in  $SpO_2$ . This was then supported by in vitro measurements of oxygenated and deoxygenated blood samples using a commercially available PO sensor. Results from the in vitro measurements were then reproduced in MC simulations, thus supporting the measured optical properties for Atlantic salmon blood. Confident that PO would be sensitive to changes in  $SpO_2$ , principal tests were conducted to see if PPGs could be obtained from live fish at all and where they should be recorded in this species. With this information, a PO implant was realized and tested in vivo using both anesthetized and free-swimming fish under normoxic and hypoxic conditions. The in vitro MC simulation was then expanded to represent the in vivo sensing case to support synthesis of all results.

### 3.1 Ethical statement

All animal experiments were approved by the Norwegian Animal Research Authorities (NARA) and explicitly linked to the thesis objectives (table 3.1). The experiments were conducted either at NINA's research facilities in Ims, Sandnes municipality, Rogaland, Norway (Norwegian Institute for Nature Research, 2023) or at NTNU / SINTEF SeaLab in Trondheim municipality, Trøndelag, Norway (NTNU, 2023; SINTEF Ocean AS, 2023). Both facilities had approved holding tanks suitable for Atlantic salmon.

Tanks at Ims were outdoors, square with rounded corners with approximate volume of 5.6 m<sup>3</sup> (figure 3.1). All tanks had adjustable water inlets

Table 3.1: Overview of NARA permits issued for the animal experiments.

<b>Description / title</b>	<b>NARA ID</b>	<b>Objective</b>	<b>Paper</b>
SalmonInsight Mesocosm	18431	O.1	A, B
Test av pulsoksimetri for oppdrettslaks (Test of pulse oximetry for farmed salmon)	20129	O.2, O.3	C, D
Stressforsøk til undervisningsformål (Stress trials for teaching purposes)	26085	O.2	E
Pilotforsøk for test av pulsoksimetri for oppdrettslaks (Pilot experiment for test of pulse oximetry for farmed salmon)	19909	O.2, O.3	F
Videreføring - Pilotforsøk for test av pulsoksymetri for oppdrettslaks (Continuation - Pilot study for test of pulse oximetry for farmed salmon)	24907	O.3, O.4	F
Pilotforsøk til test av implantat til sanntidsberegning og logging av haleslagsrate for oppdrettslaks (Pilot study for implant testing for real-time calculation and logging of tail beat frequency for farmed salmon)	27675	O.4	F



Figure 3.1: Experimental facilities at Ims showing the outdoor tanks.

(flow and direction) from a shared manifold and were equipped with sensors for temperature measurement and an oxygenation system to control dissolved oxygen.

Tanks at NTNU / SINTEF SeaLab were indoors, square with cut corners and an approximate volume of  $6\text{ m}^3$  (figure 3.2). Tanks were supplied with filtered seawater and were equipped with a Sterner Oxyguard oxygenation system maintaining oxygen saturation. A water circulation pump (EMAUX Super-Power) was mounted to the tanks to achieve and maintain a current speed up to approximately  $40\text{ cm} \cdot \text{s}^{-1}$  at the tank periphery.

Both locations had all necessary auxiliary infrastructure required for surgery (i.e., anesthesia and tag implantation) and euthanasia compliant with applicable regulations (Lovdata, 2015).

## 3.2 Linking physiology to tag data

(Objective O.1, paper A, B)

The main purpose of SalmonInsight was to investigate the link between behavioural and physiological responses and stress (section 1.2.1). Because activity (behaviour) and heart rate (physiology) could be measured using existing implants, an experiment was conducted at NINA's research facilities



Figure 3.2: Experimental facilities at NTNU / SINTEF SeaLab showing the indoor tanks.

in Ims to this end. This particular connection is relevant for PO because the measured change in perfusion coincides with the cardiac cycle. The PPG can, thus, be used to estimate heart rate and then stress based on their mutual relationship.

#### 3.2.1 Heart rate and activity as stress proxies

To identify the mutual relationship between heart rate, activity and stress, heart rate and activity tags from Star-Oddi and Thelma Biotel were implanted into twelve fish divided between four tanks including four untagged co inhabitants. Two additional tanks contained sixteen untagged individuals each for control.

After a recovery period of 14 days following surgery, stress was inflicted on all fish by simultaneously and repeatedly lowering the water level in the tanks. Using fish from the control groups as proxies, blood was sampled before, during and after stressing and analysed to obtain parameters associated with stress (cortisol, lactate, glucose and osmolality). These parameters were then co evaluated with tag data to identify if activity (behaviour) and/or heart rate (physiology) correlated with stress (paper A). Using the same tag data set, evaluations were made to evaluate the recovery time for the fish by assuming that trends in heart rate and activity would diminish over time

as the fish recovered (paper B).

The results from these studies revealed that heart rate increased with stress markers in the blood samples. The same applied to activity although delayed in time compared to the stressing events. One explanation for this result was that the activity proxy was tail beat dominated. Thus, when a tank's water level was reduced to its minimum, the fish may not have been able to express its stress in the form of movement (i.e., behaviour) encapsulated by the activity proxy. An additional explanation may have been that the repeated stressing events drove the fish to exhaustion. The fish may therefore have needed some time to recover before they started moving in a way which resulted in quantifiable changes in activity.

The results, however, led to the conclusion that heart rate and activity were both related to stress but that heart rate may be a more reliable proxy in this regard. With respect to recovery time, it was concluded that observed trends in the tag data subsided after an average of four days. Although this gave an indication that the fish had recovered from surgery, the recovery time very much depends on, e.g., the surgical procedure and the skill of the surgeon, the physiological state of the fish and water temperature. The four day recovery time for the fish in question should therefore not be thought of as a generalized recovery time after surgery for Atlantic salmon. The details for both studies can be found in paper A (linking behaviour and physiology) and B (recovery time).

## 3.3 Testing pulse oximetry for Atlantic salmon

(Objective O.2, paper C, D and E)

PO relies on the sensor's ability to respond to change in blood oxygenation level. Because pulse oximeters are designed with human blood in mind, it had to be validated that Atlantic salmon was sufficiently similar to that in humans for PO to work for this species. In the following sections efforts made to obtain this validation are described to justify that PO was an applicable sensing principle for Atlantic salmon and that pulse oximeters designed for humans can be used for this purpose.

### 3.3.1 Optical properties of Atlantic salmon blood constituents

As an initial step towards PO in Atlantic salmon, spectral analysis of blood constituents was done to quantify and compare their optical properties in terms of absorption and scattering to those published for human blood. Ob-

taining the optical properties of Atlantic salmon blood was initially thought to be a straightforward task. By using blood samples from fish kept at NTNU / SINTEF SeaLab, blood cells could be separated from plasma by centrifuging. Blood cells could then be hemolyzed to get hemoglobin. Thus, cell suspensions, plasma and hemoglobin dilutions could be obtained. By exposing the different samples to air, close to 100% oxygenation was expected to be achieved. 0% oxygenation was expected to be achieved by adding sodium dithionite. Different blood constituents in different dilutions at these extreme levels of oxygenation could then be measured using a photo spectrometer. It was soon realized, however, that Atlantic salmon blood was difficult to work with for this purpose.

From a blood sampling point of view, using the most practical blood sampling method (i.e., Vacutainers pre dosed with anti coagulant) could not be used reliably due to haemolysis (i.e., cell rupturing) turning plasma red. An alternative method using heparin coated syringes had to be used to minimise this phenomenon.

Batch processing of multiple samples was effectively ruled out due to sample coagulation and haemolysis over time. Coagulation likely occurred because the coagulation cascade was triggered when samples slowly haemolyzed so the amount of anti coagulant eventually became insufficient. Simply adding more anti coagulant was not a good option because it would have diluted the samples. This was also observed when diluting washed blood cells. The solution to these challenges was to add a calcium blocker (K2EDTA) to stop the coagulation cascade and to process each consecutive sample immediately. It was also discovered that using common centrifuge speeds ( $\geq 1500g$ ) resulted in a cell pellet too dense for consistent pipetting. Speed, thus, had to be reduced at the cost of time and increased risk of haemolysis.

Furthermore, the assumptions that 100% and 0% oxygenation levels could be reliably achieved by air exposure and sodium dithionite addition, respectively, were inaccurate. Air exposure for oxygenation did not give consistent results, while adding sodium dithionite made hemoglobin dilutions oxidize into methemoglobin judging the samples by their colour (brown as opposed to the expected deep red). This was addressed by making a system for oxygen and nitrogen bubbling.

After five repeated attempts, a method giving consistent results was achieved, and optical properties were measured using a FLAME-T-VIS-NIR-ES (350 nm to 1000 nm) photo spectrometer with a 360-2000 nm HL-2000-LL tungsten-halogen light source, both from Ocean Insight, Duiven, The

Netherlands. The measurements were supported by cell size measurements using a Coulter counter (Multisizer 4, Beckman Coulter, South Kraemer Boulevard, Brea, California 92821-6232) with a 100  $\mu\text{m}$  aperture.

The measurements showed that Atlantic salmon hemoglobin was similar to human hemoglobin with respect to its optical absorption properties. Thus, sensors originally intended for human PO could be adapted for this species. Measurements also showed that Atlantic salmon blood cells are highly scattering, while plasma contributes little in terms of absorption and scattering for wavelengths relevant for PO. Details on the final blood sampling and processing results can be found in paper E.

#### 3.3.2 In vitro whole blood measurements

The optical properties of Atlantic salmon blood constituents (section 3.3.1), indicated that PO using sensors intended for humans could be used. To investigate if a likely sensor candidate (MAX86150, [Analog Devices, 2018b](#)) was sensitive to different  $SpO_2$  levels in Atlantic salmon whole blood, in vitro tests were conducted to support further development.

Because only whole blood was needed for these measurements, samples from five fish kept at NTNU / SINTEF SeaLab were obtained using purple cap Vacutainers with K2EDTA anti coagulant (i.e., a calcium blocker) and a 21G (0.8 mm  $\times$  38 mm) needle (figure 3.3) for practical reasons. All Vacutainers were turned eight to ten times by hand for mixing with the anti coagulant (K2EDTA) before being placed on a rocker (Molek MiniMix XL) for continuous agitation inside a Styrofoam container with cooling elements for temperature control. After blood sampling the fish was euthanized.

Blood samples were oxygenated by extracting approximately 3 mL from a Vacutainer using a 10 mL syringe equipped with a 21G needle (0.8 mm  $\times$  50 mm). Using a gas sample bag with a needle diaphragm, 5 mL of oxygen (purity  $\geq 99\%$ ) was drawn into the syringe containing the sample. Following removal of the used needle and capping, the syringe was placed on the rocker for agitation/mixing for  $\geq 10$  min.

Because whole blood was used for these measurements, the samples could be consistently deoxygenated by pipetting 3 mL blood into a test tube containing 7.5 mg sodium dithionite and then mixed using the rocker (Molek MiniMix XL) for  $\geq 30$  min ([Briely-Sabo and Bjornerud, 2000](#)). Then in turn, 2 mL oxygenated or de-oxygenated whole blood was pipetted onto a hardwired MAX86150 biosensor glued into a cylindrical 15 mL test tube covered with opaque tape (figure 3.4). This resulted in a sample thickness





Figure 3.3: Blood sampling from caudal vein/artery using vacutainer.

of 1.2 cm on top of the sensor.

Emitter (660 nm and 880 nm) output power was set to 10 mA (10 mA to 100 mA allowed) to minimise light interaction with the test tube. The biosensor's sampling rate was set to 200 Hz. Software was written using Anaconda's Python 3.8 distribution (Anaconda Inc., Austin, Texas, USA) to accept and store the biosensor's raw data stream, and  $\approx 2$  min data stored for each oxygenated and de-oxygenated blood sample. Using the raw data, the first minute mean was calculated and used as the measurement result. Note that these values represent 'extinction', i.e., the combined effect of absorption and scattering.

The results (table 3.2) showed that the standard deviations for the deoxygenated samples were smaller compared to those for the oxygenated samples. This suggested that for whole blood, deoxygenation using sodium dithionite gave more consistent results compared to oxygenation by oxygen mixing. An alternative oxygenation approach for whole blood, e.g., by oxygen bubbling, should therefore be considered. Oxygen bubbling was attempted during one of the (failed) attempts to measure the optical properties of Atlantic salmon blood constituents (section 3.3.1) but the approach was abandoned due to challenges with making a closed system for small sam-



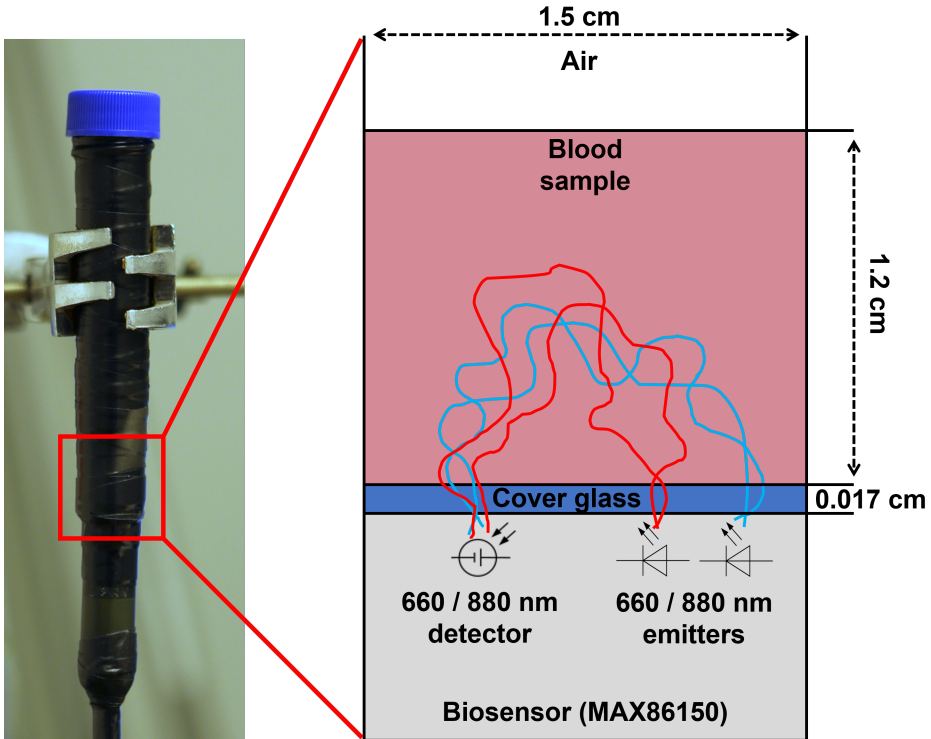


Figure 3.4: In vitro whole blood measurement set up.

Table 3.2: In vitro extinction measurement results for oxygenated ( $HbO$ ) and deoxygenated ( $Hb$ ) whole blood.

Sensing case	S1	S2	S3	S4	S5	$mean \pm sd$
660 nm $HbO$	33535	35080	29836	31382	44474	$34861 \pm 5130$
660 nm $Hb$	9768	11762	11905	10344	9962	$10748 \pm 906$
880 nm $HbO$	26625	25871	27020	23948	37610	$28215 \pm 4815$
880 nm $Hb$	28879	32424	31740	28395	29379	$30163 \pm 1612$

ple volumes using available equipment and materials. This approach should nevertheless be tested if an appropriate oxygen bubbling set up for whole blood can be made for such tests in the future.

When reviewing the mean extinction values in the context of human hemoglobin absorption (figure 3.5), they changed as expected. For 660 nm,  $HbO$  absorption was low while  $Hb$  absorption was high. Thus, the lower  $HbO$  absorption means more light reached the detector compared to the

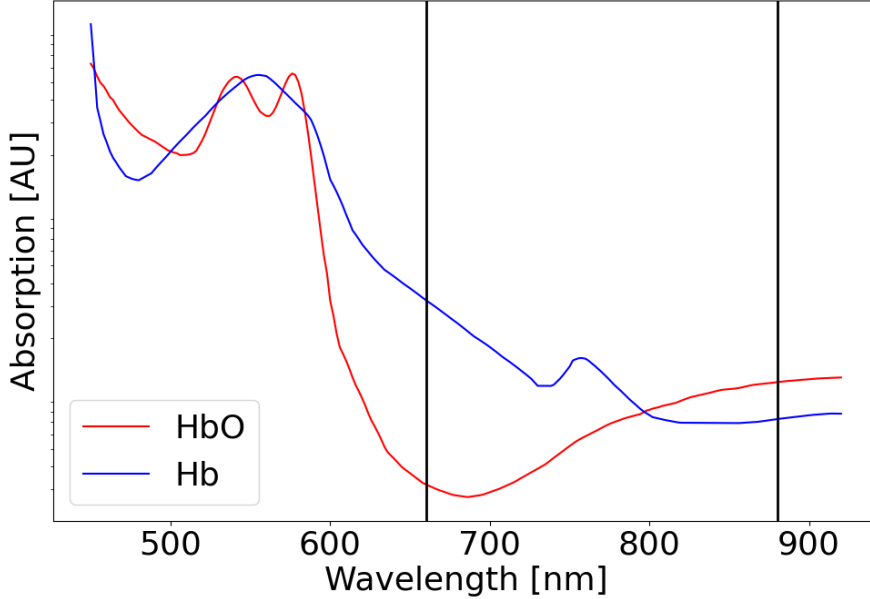


Figure 3.5: Human hemoglobin absorption spectra. Data adapted from [Prahl \(1998\)](#). The black vertical lines indicate 660 nm and 880 nm wavelengths.

opposite for *Hb*. For 880 nm, the situation was reversed resulting in higher measured values for *Hb* compared to *HbO*. It was, thus, concluded that the MAX86150 was sensitive to changes in oxygenation level in Atlantic salmon whole blood.

### 3.3.3 In vitro Monte Carlo simulations

Monte Carlo simulations (section 2.5) were now implemented to support and better understand the optical properties of Atlantic salmon whole blood. Using an iterative approach, simulation results were matched to the in vitro extinction measurements. This matching made it possible to assign a value to the attenuation scaling factor,  $Q_a$  ([Flock et al., 1989](#)), to obtain the effective attenuation given by

$$\mu_{a,eff} = \mu_a \cdot Q_a, \quad (3.1)$$

for Atlantic salmon blood. In (3.1),  $Q_a > 0$  is a scaling factor depending on several real-world uncertainties, e.g., the (actual) oxygenation level,

Table 3.3: Simulation geometry parameters for the in vitro simulation case.

Parameter	Cover glass	Blood	Air
$x_{min}$	-0.75	-0.75	-0.75
$x_{max}$	0.75	0.75	0.75
$y_{min}$	-0.75	-0.75	-0.75
$y_{max}$	0.75	0.75	0.75
$z_{min}$	0.0	0.017	1.217
$z_{max}$	0.017	1.217	$\infty$

hemoglobin concentration (i.e., hematocrit), the wavelength-dependent interaction between light and blood cells and the effect of other absorbers in the sample being simulated.  $Q_a$  was selected so the average of ten simulations matched the average in vitro measurement results (table 3.2) within one standard deviation.

The simulations duplicated the in vitro case geometry (figure 3.4) by defining a cylindrical three layer stack model geometry with a with radial limit of 7.5 mm consisting of the sensor’s cover glass followed whole blood and then air (table 3.3). The sensor was simulated with a point emitter source with a 60° opening angle and a emitter detector distance of 2.65 mm. The detector area was set to 2.5 mm × 3.3 mm as per the MAX86150 package outline.

Because Atlantic salmon hemoglobin was shown to be similar to human hemoglobin (section 3.3.1) the molar extinction coefficients,  $\epsilon$ , for  $Hb$  and  $HbO$  for 660 nm and 880 nm, were obtained from published, tabulated data for hemoglobin (Prahl, 1998). The hemoglobin concentration,  $C$ , was calculated using the published average amount of hemoglobin per litre,  $Q_{hb}$ , for Atlantic salmon blood (Sandnes et al., 1988) divided by hemoglobin’s molar mass,  $M = 64500$  (Prahl, 1998), so

$$C = \frac{Q_{hb}}{M} = \frac{96}{64500} = 1.49 \cdot 10^{-3}. \quad (3.2)$$

The absorption coefficient,  $\mu_a$ , was then calculated according to (2.2), so

$$\mu_a = \epsilon_\lambda \cdot C \quad (3.3)$$

The effective attenuation could then be calculated as in (3.1). The scattering parameter,  $\mu_s$ , for  $Hb$  and  $HbO$  was estimated using blood samples

and a Mie scattering calculator (Prahl, 2018) as described in paper E. The anisotropy coefficient,  $g$ , and refractive index,  $n$ , were assumed to be similar to values published for human tissues (Meinke et al., 2007; Liu et al., 2019).

The MAX86150 biosensor had a PPG resolution of  $2^{19}$  bit. For the MC simulations it was assumed that detection of a photon packet using 100% emitter output power (100 mA) without any transmission loss would result in a detected value of  $2^{19} = 524288$  (i.e., emitter-detector matching, Pintauro et al., 2021). During the in vitro measurements the emitter output power was set to 10 mA (section 3.3.2), i.e., 10% of the maximum value. The highest possible value for photon packet detection without transmission loss was therefore  $524288 \cdot 0.1 = 52429$ . Photon packets were, thus, initialized using this value and a randomized injection angle  $\pm 60^\circ$  from the vertical to emulate the emitter's light cone. Using these parameters, cases were simulated for 660 nm and 880 nm *HbO* and *Hb*, respectively. The simulations were terminated when the standard error of a simulation's mean was less than a predetermined percentage of the mean (Flegal et al., 2008), in this case 1%. Simulations were repeated ten times and their mean and standard deviation used as the final result.

Results from the simulations (table 3.5) showed that the model came close to duplicating the results from the in vitro blood measurements (table 3.2). Because MC models are designed to mimic light propagation, the matching results for extinction between simulations and measurements indicated that the MC model parameters were reasonable. This supported the conclusions from the in vitro measurements (section 3.3.2) that Atlantic salmon and human hemoglobin was similar and that the scattering coefficients identified using Coulter counter measurements (section 3.3.1, paper E) were reasonable.

The simulations resulted in a measure for the photon banana (figure 2.2). The accuracy of this result strongly depended on the sensor geometry obtained from the package outline schematic for the sensor which was scarce in detail. Even though the photon banana values seemed reasonable they could not be validated experimentally and was, thus, assumed to be inaccurate.

#### 3.3.4 External PPG measurements

Although the optical properties of Atlantic salmon blood (section 3.3.1), in vitro whole blood measurements (section 3.3.2) and their corresponding Monte Carlo simulations (section 3.3.3) implied that PPG measurements could be possible for Atlantic salmon, a necessary next step was to investi-

Table 3.4: Layer parameters for the in vitro simulation cases.  $WB_O$  - oxygenated whole blood,  $WB_{DO}$  - deoxygenated whole blood.

Layer	Parameter	660 nm	880 nm	Comment / ref.
Cover glass	$\varepsilon$	0.0	0.0	-
	$C_i$	0.0	0.0	-
	$\mu_a$	0.0	0.0	-
	$Q_a$	0.0	0.0	-
	$\mu_{a,eff}$	0.0	0.0	-
	$\mu_s$	0.0	0.0	-
	g	1.0	1.0	-
	n	1.52	1.52	Agar Scientific (2022)
$WB_O$	$\varepsilon$	320	1154	Prahl (1998)
	$C_i$	$1.49 \cdot 10^{-3}$	$1.49 \cdot 10^{-3}$	(3.2)
	$\mu_a$	0.47	1.72	(3.3)
	$Q_a$	1.118	0.55	-
	$\mu_{a,eff}$	0.53	0.95	(3.1)
	$\mu_s$	1887	2207	paper E
	g	0.95	0.95	Meinke et al. (2007)
	n	1.34	1.34	Liu et al. (2019)
$WB_{DO}$	$\varepsilon$	3227	726	Prahl (1998)
	$C_i$	$1.49 \cdot 10^{-3}$	$1.49 \cdot 10^{-3}$	(3.2)
	$\mu_a$	4.80	1.08	(3.3)
	$Q_a$	1.0	0.74	-
	$\mu_{a,eff}$	4.80	0.80	(3.1)
	$\mu_s$	1887	2207	paper E
	g	0.95	0.95	Meinke et al. (2007)
	n	1.34	1.34	Liu et al. (2019)
Air	$\varepsilon$	0.0	0.0	-
	$C_i$	0.0	0.0	-
	$\mu_a$	0.0	0.0	-
	$Q_a$	0.0	0.0	-
	$\mu_{a,eff}$	0.0	0.0	-
	$\mu_s$	0.0	0.0	-
	g	1.0	1.0	-
	n	1.0	1.0	-

### 3. Experimental work

---

Table 3.5: Aggregated results for all ten in vitro Monte Carlo simulations. 'Simulated extinction' is the average number of photons in the detected packets, 'Packets detected' is the average number of detected photon packets, 'Packets launched' is the number of photon packets launched before the simulation stop criterion was reached and 'Photon banana' is the average photon packet travel distance in cm.

Simulation case	Simulated extinction	Packets detected	Packets launched	Photon banana
660 nm <i>HbO</i>	$34899 \pm 284$	$745 \pm 209$	$30978 \pm 2059$	$0.91 \pm 0.02$
660 nm <i>Hb</i>	$10721 \pm 111$	$2859 \pm 604$	$294706 \pm 9870$	$0.41 \pm 0.003$
880 nm <i>HbO</i>	$28156 \pm 178$	$1380 \pm 37$	$49072 \pm 1478$	$0.80 \pm 0.01$
880 nm <i>Hb</i>	$30078 \pm 287$	$1253 \pm 59$	$43577 \pm 2229$	$0.85 \pm 0.02$

gate if such measurements could be obtained from live fish. This was done by a set of simple external measurements where a PPG sensor was held against the skin on several sensing locations.

Based on the assumption that light could penetrate the skin so perfusion changes could be detected, a proof of concept test was performed using a MAX30102 ([Analog Devices, 2018a](#)), the predecessor of the MAX86150 using identical wavelengths. The MAX30102 was preassembled on a printed circuit board containing all the peripheral circuitry required for control and communication. The circuitry was protected against fluid ingress using conformal coating and self vulcanizing tape.

Using real time logging software by Maxim Integrated, data were logged from seven fish by holding the sensor against the fish's skin at different locations where perfusion changes were expected to be high, i.e., the posterior wall of the buccal cavity, gill filaments and branchial arches, thorax area and red muscles along the lateral line.

The PPGs obtained by this exploratory approach were generally noisy and intermittent and could only be obtained from the thorax area (figure 3.6), likely due to challenges related to keeping the sensor in place and sufficiently still at other locations. Although no further signal processing was done using these data, the tests were encouraging and indicated that PPGs could be obtained from live Atlantic salmon.

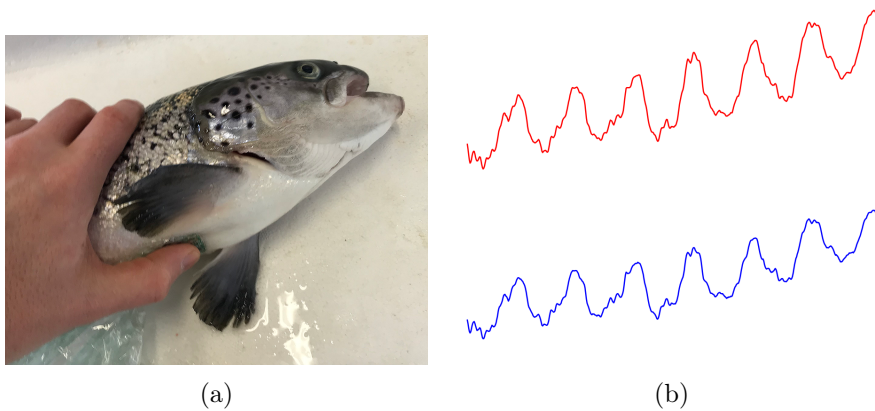


Figure 3.6: External measurements in the thorax area, (a), and example PPG data, (b), where red is 660 nm and blue is 880 nm.

### 3.3.5 In vivo PPG measurements - Sensing volume

At this point it was clear that pulse oximeters intended for human use were sensitive to  $SpO_2$  changes in Atlantic salmon blood and that PPGs could be obtained from live fish. Because animal welfare considerations (section 2.1) indicated that an implant had to be designed, an experiment was conducted to identify sensing volumes where perfusion changes could be reliably measured inside the fish.

For this purpose, a MAX86150 biosensor was cast in epoxy and mounted to the end of a metal rod with orientation marks. Electrical wires penetrated the cast for power and data streaming. Using anesthetized fish placed ventral side up in a surgery tray, ECG electrodes were placed close to the fish's heart. An incision was then made along the saggital line in the posterior part of the peritoneal wall. Using a holder attached to the metal rod, the MAX86150 was inserted horizontally into the peritoneal cavity and fixed in place. With the aid of the orientation marks on the metal rod, PPG and ECG were simultaneously collected for four sensor orientations with a  $90^\circ$  orientation interval. After data were collected in the horizontal orientation, a second incision was made along the saggital line in the anterior part of the peritoneal wall and the MAX86150 inserted vertically. Data were then collected from four orientations  $90^\circ$  apart. PPG data from the different orientations were then analyzed with respect to the signal quality index (SQI) (Elgendi, 2016) and PPG heart rate compared to that obtained using ECG. This procedure was repeated for eight fish.

This experiment demonstrated that PPGs could be obtained from all of the tested sensing volumes but with differences in SQI between them. Based on these data it was concluded that PPG was correlated with heart rate (i.e., changes in perfusion) and that such signals should be collected using a sensing volume in the anterior part of the peritoneal cavity and a sensing direction parallel with the sagittal line towards the head (i.e., not towards the sides or the intestines). Full details and results from this experiment are found in paper C.

## 3.4 Designing the implant

(Objective O.3, paper D)

Based on the PO tests (section 3.3) it was considered likely that PO could work for Atlantic salmon. An implant to measure PPGs from the sensing volume anterior in the peritoneal cavity (section 3.3.5) was, thus, designed and implemented. In addition to the novelty of PO, the implant was designed for simultaneous logging of acceleration, rotation rates, compass heading, temperature, magnetic field strength and ECG, thereby combining the capabilities of several existing implants (table 2.1) into one. When designing the implant, use cases and functional descriptions were first defined followed by hardware selection and realization, firmware implementation and, finally, testing.

### 3.4.1 Use cases and requirements

The main intended use cases for the implant were laboratory scale data collection experiments (i.e., tank or swim tunnel experiments). In such settings the environment can be controlled allowing shorter tests with higher data sampling rates and more accurate time control both of which are important for subsequent data evaluations and processing.

Motivated by the typical duration of swim tunnel trials where rapidly changing signals such as ECG must be accurately captured, the battery was required to last at least 30 minutes when continuously storing raw data with a minimum sampling frequency of 200 Hz. Moreover, to enable longer lasting trials in tanks, a requirement was that it should be possible to log data for at least 5 days (120 hours) by duty cycling data capture and storage. This would also facilitate future testing in meso and full scales (i.e., Atlantic salmon production settings).

To minimize (future) unit cost and facilitate design flexibility, it was required that the implant consisted of standard electronic components (i.e.



not application specific integrated circuits). Since the implant had to be placed inside fish with minimum impact on its behaviour and performance, it needed to be as small and lightweight as possible. Memory had to be non-volatile to retain data should the battery become exhausted. Furthermore, the implant was required to be re-programmable and the battery replaceable for implant re-use.

The implant encapsulation was required be biologically inert (i.e., non-toxic) and as smooth as possible to prevent chafing or irritation/damage to surrounding tissues. It was also required to have a suture canal so it could be fixed in place during surgery both to obtain as stable sensing conditions as possible, and to enable data collection from comparable PPG sensing volumes between different fish.

### 3.4.2 Hardware

The implant's main components (figure 3.8 a)) were the micro controller (EFM32TG11, Silicon Labs, Austin, Texas, USA), the non-volatile memory (MX25R64F, Macronix Internatinal, Hsinchu, Taiwan), temperature sensor (TMP117, Texas Instruments, Dallas, Texas, USA), the hall-effect sensor (SI7210, Silicon Labs, Austin, Texas, USA) and inertial motion unit (IMU) (ICM-20948, TDK InvenSense, San Jose, California, USA). These components were selected based on their intrinsic processing capacities, market availability, package size, ease of integration and favourable power consumption.

Due to the novelty of PO for Atlantic salmon, particular attention was devoted to selection of this component. The PPG sensor should be as small as possible with the lowest possible power consumption. The sensor should be configurable to optimize signal quality. A non-exhaustive overview of sensors available at the time (2019) is given in table 3.6.

When comparing alternatives from Maxim Integrated and Osram, it was clear that only Maxim Integrated offered a highly integrated package which included on-board signal processing and a communications interface. The sensors from Osram only contained the LEDs and a photo detector which had to be completely controlled by external circuitry, thus requiring a larger printed circuit board (PCB) footprint. Other solutions also existed such as the MIKROE-3102 by Mikroelektronika. This was also a pulse oximeter but far less integrated compared to the alternatives. The same applied to the products from Texas Instruments which were mainly analog front ends (e.g., TI AFE4410) facilitating implementation of pulse oximeters.

Table 3.6: Comparison of typical available off-the-shelf pulse oximeters (2019).

Manufacturer	Type	L[mm]	W[mm]	H[mm]	$\lambda_{red}$ [nm]	$\lambda_{IR}$ [nm]	$V_{supp}$ [V]	$I_{typ}$ [ $\mu A$ ]	ECG
Maxim Integrated	MAXX30100	5.6	2.8	1.2	660	880	1.8	600	-
Maxim Integrated	MAXX30101	5.6	3.3	1.55	660	880	1.8	600	-
Maxim Integrated	MAXX30102	5.6	3.3	1.55	660	880	1.8	600	-
Maxim Integrated	MAXX86140	2.048	2.048	1.848	$N/A^{1)}$	$N/A^{1)}$	1.8	600	-
Maxim Integrated	MAXX86141	2.048	2.048	1.848	$N/A^{1)}$	$N/A^{1)}$	1.8	600	-
Maxim Integrated	MAXX86150	5.6	3.3	1.3	660	880	1.8	750	X
MediaTek	MT6381	6.8	4.9	1.2	$UNK^{2)}$	$UNK^{2)}$	$UNK^{2)}$	$UNK^{2)}$	X
Osrain	SFH 7050	4.7	2.5	0.9	530 and 660	940	1.8	5000	-
Osrain	SFH 7051	4.7	2.5	0.9	530 and 660	940	1.8	5000	-
Osrain	SFH 7060	7.2	2.5	0.9	530 and 660	940	1.8	5000	-

1) Requires external LEDs.

2) Unknown - Not provided by supplier.

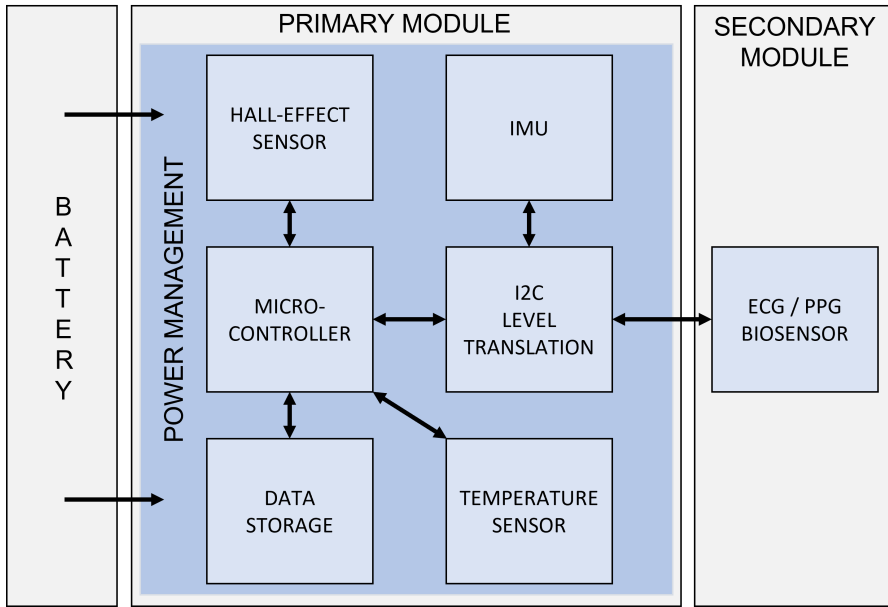


Figure 3.7: Hardware block diagram.

Because of their availability and favourable capabilities, the MAX30102 and MAX86150 were selected. The former was initially used for external PPG measurements (section 3.3.4), and replaced upon release of the MAX86150. This was motivated by the fact that the MAX86150 could provide ECG in addition to PPG, an advantage when combined for  $SpO_2$  estimation.

In addition to the main components, the electrical design included peripheral circuitry (i.e., voltage regulators, communication level translators and connectors) as specified by the main component’s reference circuits (figure 3.8 a)). The electronic components were divided between two PCBs with all components except the MAX86150 placed on a ‘primary module’. The latter was placed on a ‘secondary module’ for proper (physical) orientation with respect to sensing direction, but also to facilitate future replacement by a different pulse oximeter or, perhaps, a different biosensor if relevant (figure 3.7).

To enable data download and battery replacement a flexible PCB with exposed connection pads was soldered to the main component PCB (figure 3.8 b)). The battery could then be connected using a removable conductive adhesive. The encapsulation measured  $47\text{ mm} \times 13\text{ mm}$  and was made using a Prusa SL1 3D printer and 3Dresyn Biotough D80 MF ULWA Monomer Free Ultra Low Water Absorption resin. This resulted in a non toxic, bio

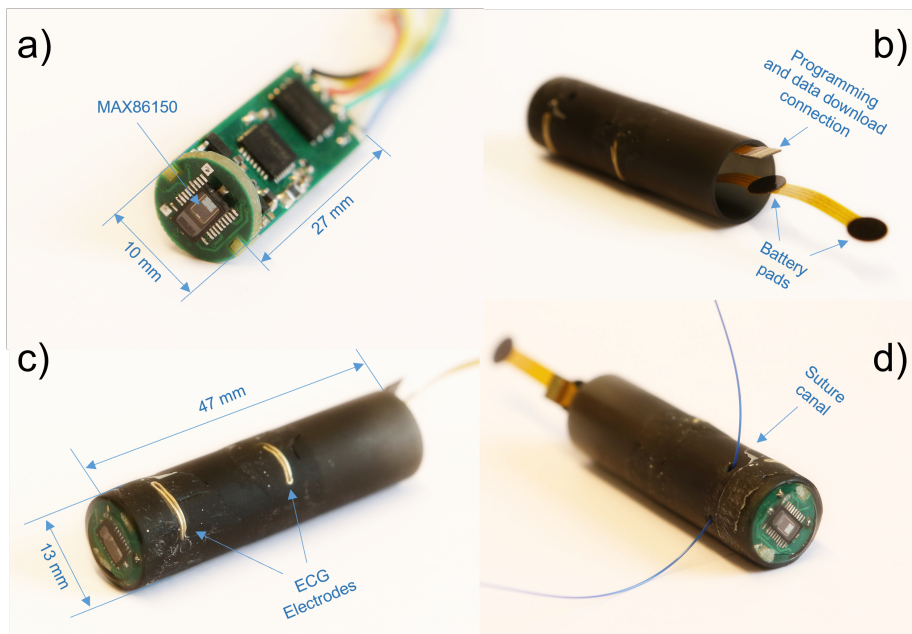


Figure 3.8: a) Implant internal PCB, b) flexible PCB for programming/data download and battery connection, c) encapsulation and ECG electrodes and, d), encapsulation with suture canal.

compatible design with sufficiently high spatial accuracy to accommodate openings for 14 ct gold ECG wire electrodes (figure 3.8 c)) and a suture canal (3.8 d)). Fully assembled, the implant weighed 9.4 g in air including battery.

Two different versions of the implant was made. One with an electrical wire interface for continuous data streaming for in vivo data collection using anesthetized fish, and a battery powered stand alone version for implantation in free swimming, conscious fish. Of the former, 2 pieces were made, and 5 of the latter.

#### 3.4.3 Firmware

Because the implant could be reprogrammed, different firmware versions with functionality to cover different use cases were developed. With the C programming language (Kernighan and Ritchie, 1988) and Simplicity Studio (V. 4.1.14, Silicon Labs) firmware to cover use cases for

1. Continuous data streaming for in vivo operation (section 3.5.1).

2. Duty cycled data capture and storage with long start delay for tank operation (section 3.5.2).
3. Continuous data capture and storage with short start delay for swim tunnel operation (section 3.5.3).

was written. A notable difference between the data streaming and data logging firmware versions was that the latter had automatic gain control functionality which adjusted emitter output to prevent PPG saturation. This was not required for the data streaming version because raw data could not be continuously inspected and emitter output manually adjusted. Following download, data were post processed and analyzed using Anaconda's Python 3.8 distribution (Anaconda Inc., Austin, Texas, USA).

## 3.5 Implant testing

(Objective O.4, paper F)

An implant was now available and had to be tested to evaluate its ability to capture data of sufficient quality using live fish with focus on capture of PPGs to estimate  $SpO_2$ . To validate the implant's intended function, three experiments were conducted at NTNU / SINTEF SeaLab. The first experiment used anesthetized fish under hypoxic conditions and the wired implant version, while the second and third experiments used implanted, free swimming fish under normoxic and hypoxic conditions. Based on these experiments a motion artifact (MA, i.e., signal noise caused by motion) reduction approach was developed, and a light scattering compensation parameter calculated for use in (2.27) to obtain  $SpO_2$ .

### 3.5.1 In vivo oxygen challenge test

The purpose of the in vivo oxygen challenge test test was to validate that PPGs obtained by the MAX86150 could be used to estimate changes in  $SpO_2$ . Three fish were subsequently captured from their holding tank and transferred to a tub containing knock-out anesthetic (70 mg/L, Benzoak Vet). When the fish was judged to have reached level 3 anesthesia (Coyle et al., 2004), the fish was placed ventral side up in a surgical tray. A tube was inserted into the fish's buccal cavity to circulate water with maintenance anesthetic (35 mg/L, Benzoak Vet) over its gills. A 2 cm incision was made in line with the sagittal plane anterior from the pelvic fins. The wired implant version was then inserted into the peritoneal cavity of the fish and placed towards the sensing volume expected to give the best signal quality (paper C) (figure 3.9).

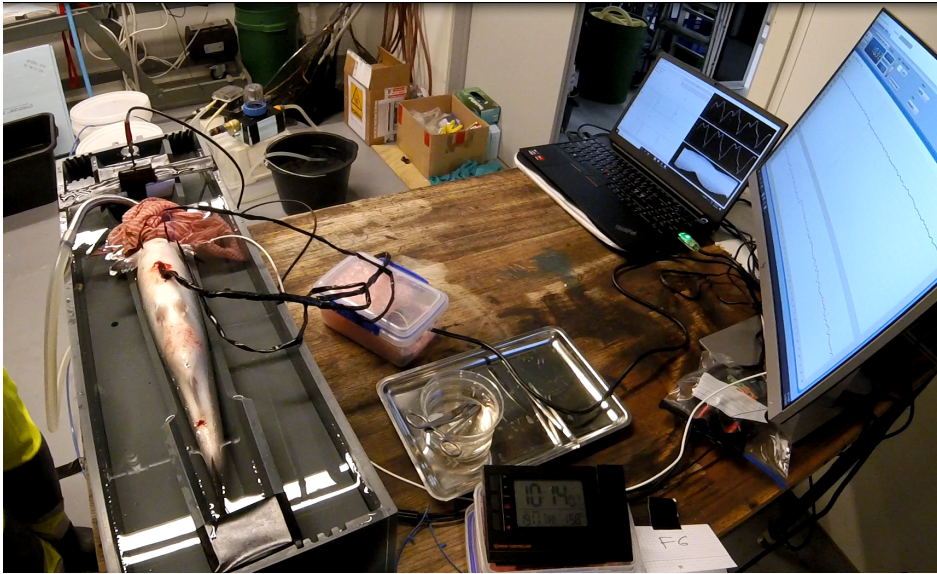


Figure 3.9: In vivo data collection. Note the black cable bundle entering the fish's peritoneal cavity where the biosensor was placed anterior in the peritoneal cavity.

Data collection was then started, and the water supplied to the buccal cavity switched to deoxygenated water ( $\leq 2$  mg/L, nitrogen purged) with maintenance anesthetic (35 mg/L, Benzoak Vet). Dissolved oxygen in the water presented to the fish was measured using a temperature compensated Neofox optical probe kit (OceanInsight, Diuven, The Netherlands). The deoxygenated water supply was maintained for approximately 10 min before being switched back to aerated water for 5 minutes. This cycle was repeated 3 times per fish to see if concurrent changes in  $SpO_2$  could be observed. Because the fish was anesthetized, no motion artifacts were expected. Therefore, high-pass filtered raw data were used to obtain calculate the modulation ratio. (2.18). When this experiment was conducted, scattering compensation was not yet investigated. Thus, only changes in the modulation ratio,  $R$  was plotted since any change in  $R$  would be directly associated with change in  $SpO_2$

During this experiment, live PPG data were streamed to a monitor for evaluation. PPGs should consist of a salient pulsatile component. This was not always the case for these fish, where PPGs were sometimes distorted and generally diminished in amplitude over time. These phenomena may have been the result of the prolonged exposure to the anesthetic which may

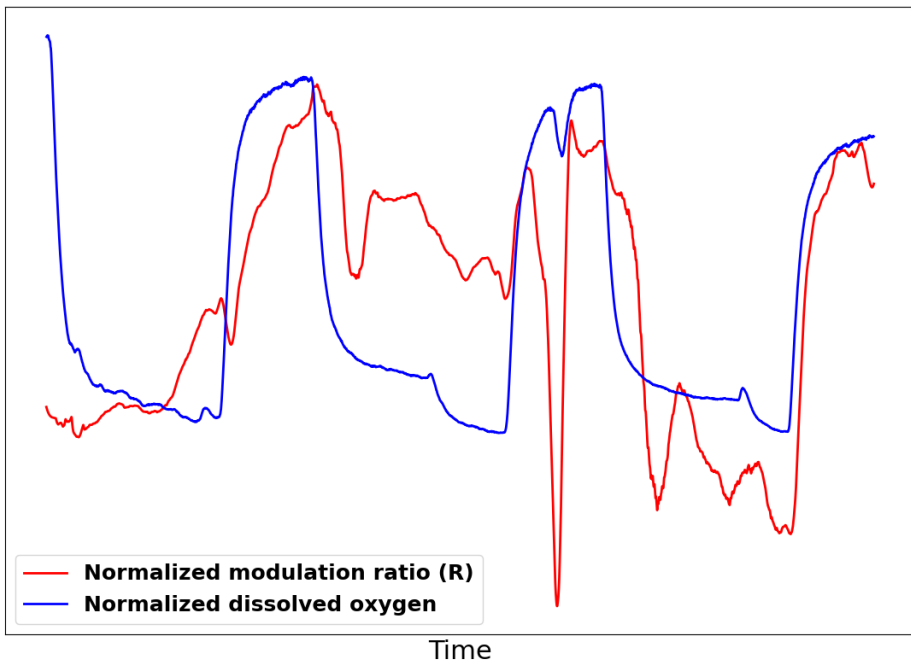


Figure 3.10: Co-variation of modulation ratio,  $R$ , (normalized to  $[0, 1]$ , arbitrary units) with dissolved oxygen in water (normalized to  $[0, 1]$ , arbitrary units).

have affected the circulatory system and blood pressure. To adhere to 3R principles (Norecopa, 2023), this experiment was abandoned after three fish since data quality was judged to be low. Out of these, a single data set was obtained where PPGs remained relatively stable throughout the test so the modulation ratio,  $R$ , could be reliably calculated (figure 3.10).

Although this experiment was not as successful as initially hoped, all results combined confirmed that the implant was able to collect data. The results also indicated that the modulation ratio,  $R$  changed with  $SpO_2$  and, thus, that PO could be possible. It was concluded, however, that such tests should be conducted using conscious, free-swimming fish. This would introduce the additional challenge of PPG motion artifacts (MA) which could prevent  $SpO_2$  estimation. The next step therefore became to investigate the influence of motion on PPGs obtained from the sensing volume anterior in the peritoneal cavity using live, free swimming fish.



#### 3.5.2 Tank experiment

Motion artifacts are a persistent challenge in PO (Chan et al., 2013). Such artifacts are generally caused by motion induced perfusion changes and distort the PPG shape. Because PO assumes a salient pulsatile PPG component solely contributed by arterial blood, such distortions will negatively affect, and potentially inhibit,  $SpO_2$  estimation. To investigate the influence of motion on Atlantic salmon PPGs, an experiment using live, free swimming fish in a tank setup was implemented. The experiment was conducted under the assumption that  $SpO_2$  was 95 % to 100 % for healthy individuals under normoxic conditions. This assumption allowed testing of an MA compensation approach and estimation of a light scattering compensation parameter for use in (2.27).

During this experiment, five randomly captured fish were implanted and placed in a test tank at SeaLab (section 3.1) on day one. Implantation first involved anesthesia (Benzoak Vet, 70 mg/L knock-out solution until level 3 anesthesia (Coyle et al., 2004) was reached, and 35 mg L maintenance anesthetic during surgery) followed by making an incision along the sagittal plane slightly more than one tag length posterior from the septum transversum. A plastic spatula was then inserted through the incision until it reached the septum. With the spatula in place, a needle was inserted through the peritoneal wall until it hit the spatula. By simultaneously pushing the needle and withdrawing the spatula the needle point was brought to the incision. A sterile monofilament was then threaded through the implant's suture canal (figure 3.8 d) and inserted into the tip of the needle (figure 3.11). The needle was then withdrawn to pull the monofilament out through the needle's penetration point in the peritoneal wall while using the spatula to protect the viscera. This procedure was then repeated on the other side of the sagittal plane. The implant was then inserted through the incision, pulled into position using both ends of the monofilament and then anchored in place by an (external) surgical knot. The incision was then closed using 3 - 4 interrupted sutures. On average, surgery lasted 14 min and 35 s. Following surgery, the fish was placed in a recovery tank with circulating seawater where it was kept until it regained consciousness and then transferred to the test tank.

After a recovery period of 18 h to 20 h at  $\approx 15$  cm/s water current, all implants simultaneously started logging PPG, ECG and motion data at 09:00 on day two. Data were logged with a duty cycle of 1:2 and a sampling rate of 200 Hz. After 30 min, water current was increased to  $\approx 40$  cm/s at the tank periphery. Data logging continued for another 36 min before the implant memories were full, the experiment terminated, and the fish removed from





Figure 3.11: Tag implantation surgery. Note the yellow spatula exiting the incision protecting the viscera from the needle used to extract the monofilament through the peritoneal wall.

the tank for euthanization. The implants were then retrieved and their data downloaded for processing.

To suppress MA, a synthetic PPG reference was constructed using ECG. Using the synthetic reference, PPGs were filtered using a least mean squares adaptive filter. Using the motion artifact compensated PPGs, an average scattering compensation parameter,  $\Gamma_{avg}$ , was calculated by assuming  $SpO_2 = 100\%$  and solving (2.27) for  $\Gamma$  to obtain a correction factor of 0.35 (paper F).  $SpO_2$  was then estimated using (2.27) including the value for  $\Gamma_{avg}$  and compared to the expected range of 95% to 100% for both water current speeds. With this approach, average  $SpO_2$  was estimated to  $96.98 \pm 0.08$  and  $96.44 \pm 0.09$  for low and high water current speeds, respectively. The full details and discussion for this experiment can be seen in paper F.

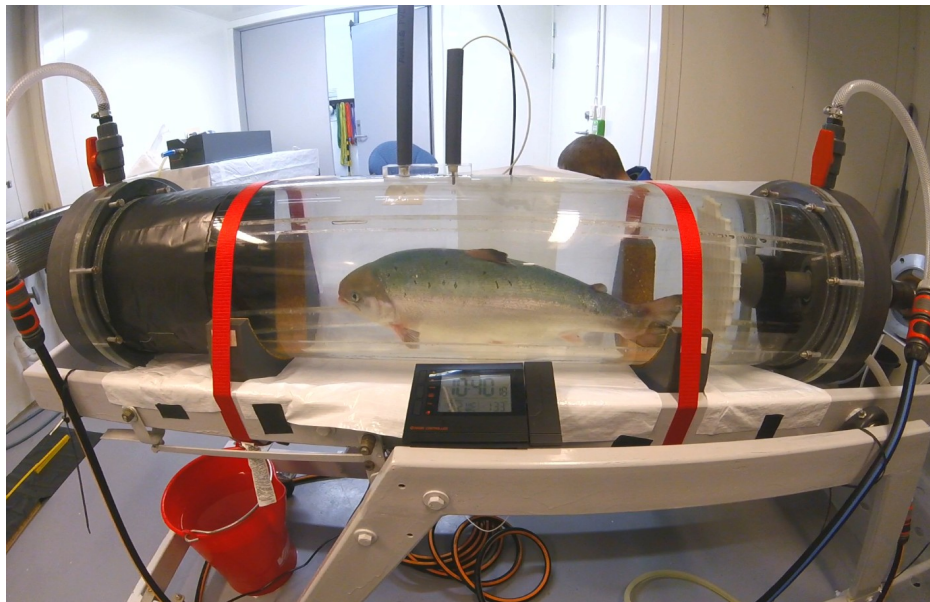


Figure 3.12: Blazka swim tunnel during the swim tunnel oxygen challenge experiment. Note that the cylindrical shape of the tunnel distorted the shape of the fish as seen from outside the tunnel.

#### 3.5.3 Swim tunnel oxygen challenge experiment

Due to the challenges encountered during the *in vivo* oxygen challenge test (section 3.5.1), a similar but more comprehensive oxygen challenge experiment was conducted using conscious, free swimming fish. This was possible because viable approaches for motion artifact and light scattering compensation were obtained using data from the tank experiment (section 3.5.2).

In this experiment, eight fish were subsequently implanted using the method described in section 3.5.2, and placed in a Blazka type swim tunnel (116 cm length X 24 cm diameter, 55 L volume) instrumented with a temperature compensated dissolved oxygen sensor (NEOFOX, Ocean Insight, Duiven, The Netherlands), and connected to a sea water supply (figure 3.12). After a short recovery time (30 min to 40 min depending on the time required for surgery and anesthesia), data logging (ECG, PPG and IMU at 200 Hz sampling rate) started automatically and lasted for 33 min.

The first fish was unchallenged (i.e., no hypoxia) for the entire duration of the data logging period to act as control. For the other seven fish, sea water exchange was temporarily closed after 3 min (pre hypoxia period), and a

portion of the water inside the tunnel replaced with sea water de-oxygenated using instrument nitrogen. This effectively created hypoxic conditions under which the fish remained for the next 25 min (hypoxia period) before sea water circulation was resumed. After another 5 min (post hypoxia period), data logging stopped. The fish was then extracted from the swim tunnel, euthanized, and the implant retrieved for data download. Using the motion artifact reduction approach and light scattering compensation parameter from the tank experiment (section 3.5.2),  $SpO_2$  was estimated using (2.27) and relative changes in  $SpO_2$  evaluated.

The control fish had a median  $SpO_2$  of 100.7% and a min-max variation of 4.53%. The average median / min-max variation for the seven test fish were 97.18% / 2.41%, 97.27% / 4.75% and 97.43% / 2.25% for the pre hypoxia, hypoxia and post hypoxia periods, respectively. Results from the test fish, thus, showed greater variation during the hypoxia period compared to the pre and post hypoxia periods and were similar to the values estimated using data from the control fish. Fitting a linear curve (figure 3.13) to the (compensated) modulation ratios,  $R$ , used to estimate  $SpO_2$  (2.27) resulted in a mapping of

$$SpO_2 = -10.0R + 107.4. \quad (3.4)$$

It was, thus, concluded that changes in  $SpO_2$  could be detected using a pulse oximeter implanted in Atlantic salmon. The full details and discussion for this experiment can be seen in paper F.

## 3.6 Monte Carlo simulations with multiple tissues

(Objective O.4)

In the actual sensing situation it was expected that multiple tissues would be present within the sensing volume. Because animal welfare motivated designing an implant (section 2.1), an in vivo simulation case building on the in vitro simulation case (section 3.3.3) was implemented to support the data from the tank (section 3.5.2) and swim tunnel (section 3.5.3) experiments.

### 3.6.1 In vivo Monte Carlo simulations

For the in vivo case it was assumed that the sensing volume could be approximated by a cylindrical slab (table 3.7) of a generalized high-fat tissue (Jacques, 2013). A post mortem inspection (figure 2.5) of the sensing vol-

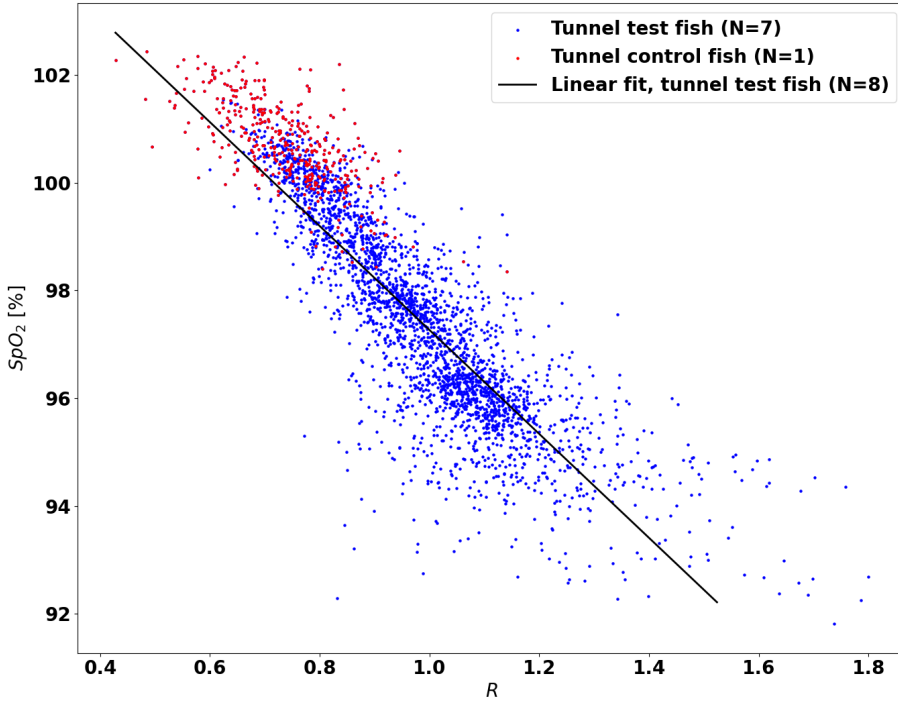


Figure 3.13: Linear fit to all swim tunnel data.

Table 3.7: Simulation geometry parameters for the in vivo simulation case.

Parameter	Cover glass	Perfused fat
$x_{min}$	-0.75	-0.75
$x_{max}$	0.75	0.75
$y_{min}$	-0.75	-0.75
$y_{max}$	0.75	0.75
$z_{min}$	0.0	0.017
$z_{max}$	0.017	$\infty$

ume with the highest SQI (paper C) using an endoscope supported using this approximation (figure 3.14).

The generalized tissue added to both absorption and scattering. Values for total attenuation ( $\mu_{a,tot}$ ) and scattering ( $\mu_{s,tot}$ ) were obtained by adding the corresponding values for the generalized tissue to those in table 3.3. The anisotropy factor,  $g$ , was assumed to be close to reported values for human

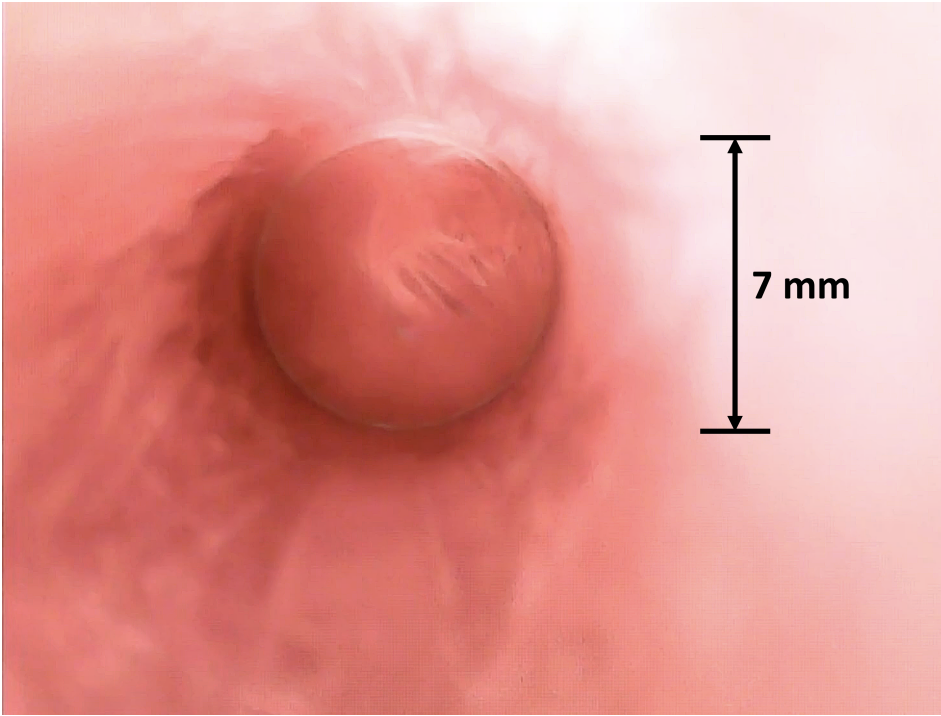


Figure 3.14: Internal view of sensing volume as captured using an endoscope showing a sensing volume consisting of perfused fat.

adipose tissue (i.e., fat) (Jacques, 2010), while the refractive index,  $n$  was increased to account for the increase in density compared to blood only (Yanina et al., 2018). Similarly, the anisotropy factor,  $g$  was reduced to account for the expected increase in back scattering. Maximum and minimum PPG values (figure 2.3) to use in (2.18) were determined by simulating cases using concentrations (i.e., perfusion) of 2% and 10%. Using these settings (table 3.8) cases for 660 nm and 880 nm HbO and Hb, were simulated. The simulations were terminated when the standard error of a simulation's mean was less than a predetermined percentage of the mean (Flegal et al., 2008), in this case 1%. Simulations were repeated ten times and their mean and standard deviation used as the final result.

Using the simulated results (table 3.9), the modulation ratios for  $HbO$  and  $Hb$  were calculated using (2.18) to obtain

$$R_{HbO} = \frac{PPG_{lc,660} - PPG_{hc,660}}{PPG_{lc,880} - PPG_{hc,880}} \Bigg|_{HbO} = \frac{44566 - 42933}{43478 - 41498} = 0.82, \quad (3.5)$$

### 3. Experimental work

---

Table 3.8: Layer parameters for the low concentration (lc) and high concentration (hc) in vivo simulation cases.

Layer	Parameter	660 nm	880 nm	Comment / ref.
Cover glass	$\mu_a$	0.0	0.0	-
	$\mu_s$	0.0	0.0	-
	g	1.0	1.0	-
	n	1.52	1.52	Agar Scientific (2022)
Perfused fat / HbO	$\varepsilon$	320	1154	Prahl (1998)
	$\mu_{a,eff}$	0.53	0.95	table 3.4
	$C_{lc}$	$0.02 \cdot C_i$	$0.02 \cdot C_i$	table 3.4
	$\mu_{a,gt,lc}$	0.18	0.20	Jacques (2013)
	$\mu_{a,tot,lc}$	0.19	0.22	-
	$C_{hc}$	$0.1 \cdot C_i$	$0.1 \cdot C_i$	table 3.4
	$\mu_{a,gt,hc}$	0.18	0.1767	Jacques (2013)
	$\mu_{a,tot,hc}$	0.23	0.27	-
	$\mu_s$	$1187 \cdot C_i$	$2207 \cdot C_i$	table 3.4
	$\mu_{s,gt}$	800	600	Jacques (2013)
	$\mu_{s,tot}$	838	644	-
	g	0.95	0.95	Jacques (2013)
	n	1.45	1.45	Yanina et al. (2018)
Perfused fat / Hb	$\varepsilon$	3227	726	Prahl (1998)
	$\mu_{a,eff}$	4.80	1.08	table 3.4
	$C_{lc}$	$0.02 \cdot C_i$	$0.02 \cdot C_i$	table 3.4
	$\mu_{a,gt,lc}$	0.18	0.20	Jacques (2013)
	$\mu_{a,tot,lc}$	0.28	0.22	-
	$C_{hc}$	$0.1 \cdot C_i$	$0.1 \cdot C_i$	table 3.4
	$\mu_{a,gt,hc}$	0.18	0.166	Jacques (2013)
	$\mu_{a,tot,hc}$	0.66	0.25	-
	$\mu_s$	$1187 \cdot C_i$	$2207 \cdot C_i$	table 3.4
	$\mu_{s,gt}$	2687	2807	Jacques (2013)
	$\mu_{s,tot}$	1927	2237	table 3.4
	g	0.95	0.95	Jacques (2013)
	n	1.45	1.45	Yanina et al. (2018)



Table 3.9: Aggregated results for all ten in vivo Monte Carlo simulations. 'Simulated extinction' is the average number of photons in the detected packets, 'Packets detected' is the average number of detected photon packets, 'Packets launched' is the number of photon packets launched before the simulation stop criterion was reached, 'Photon banana' is the average photon packet travel distance in cm, 'LC' denotes low concentration, and 'HC' high concentration.

	<b>Simulation case</b>	<b>Simulated extinction</b>	<b>Packets detected</b>	<b>Packets launched</b>	<b>Photon banana</b>
LC	660 nm <i>HbO</i>	44566 ± 288	150 ± 19	11952 ± 2207	0.92 ± 0.04
	660 nm <i>Hb</i>	41667 ± 259	275 ± 34	22796 ± 2910	0.91 ± 0.03
	880 nm <i>HbO</i>	43478 ± 322	191 ± 33	21814 ± 3897	0.92 ± 0.04
	880 nm <i>Hb</i>	43341 ± 257	194 ± 16	21029 ± 1880	0.94 ± 0.03
HC	660 nm <i>HbO</i>	42933 ± 229	238 ± 28	16399 ± 2392	0.95 ± 0.06
	660 nm <i>Hb</i>	31722 ± 266	1073 ± 55	73112 ± 3854	0.90 ± 0.02
	880 nm <i>HbO</i>	41498 ± 339	302 ± 31	24697 ± 3192	0.95 ± 0.04
	880 nm <i>Hb</i>	42560 ± 204	234 ± 17	19597 ± 2507	0.92 ± 0.02

and

$$R_{Hb} = \frac{PPG_{lc,660} - PPG_{hc,660}}{PPG_{lc,880} - PPG_{hc,880}} \Bigg|_{Hb} = \frac{41667 - 31722}{43341 - 42457} = 11.25. \quad (3.6)$$

The slope and intersect were then calculated as

$$slope = \frac{100}{R_{Hb} - R_{HbO}} = \frac{100}{11.25 - 0.82} = -9.6, \quad (3.7)$$

and

$$intersect = 100 - slope \cdot R_{HbO} = 100 - (-9.6) \cdot 0.82 = 107.9. \quad (3.8)$$

The average simulated function mapping  $R$  to  $SpO_2$ , thus, became

$$SpO_2 = -9.6R + 107.9. \quad (3.9)$$

An estimate for the correction parameter,  $\Gamma$  in (2.27) could now be obtained as described in paper F so

$$\Gamma_{avg} = \frac{\varepsilon_{HbO,660}}{R_{HbO} \cdot \varepsilon_{HbO,880}} = \frac{320}{0.82 \cdot 1154} = 0.34. \quad (3.10)$$

For these simulations, parameters were chosen so the mean of 10 simulations matched the in vivo measurements (section 3.5.2 and 3.5.3) within one standard deviation. Although several of the simulation parameters were considered relatively certain (e.g., the hemoglobin extinction coefficients), some were not. For instance, the lowest perfusion (and, by extension, the change in concentration) was based on a general value for fatty tissues (Bigio and Fantini, 2016) which may be inaccurate for fish. This assumption should therefore be validated in future activities by in vivo spectral measurements for the sensing volume. The highest perfusion value of 10 % resulted from trial and error, and other values resulted in a mismatch with the in vivo measurements.

Similarly, there was uncertainty related to the effect of the generalized fatty tissue with respect to absorption and scattering. By assuming Mie dominant scattering, values for scattering were obtained from Jacques (2013) (table 3.4). The uncertainty related to scattering would have had limited effect on the final simulation result because the reduced scattering coefficient was used in the MC model. Thus, the scattering coefficient was multiplied by  $1 - g = 0.05$  before being used to calculate step length (2.28) and the fraction of photons absorbed in each simulation step (2.41).

The effect on absorption ( $\mu_{a,gt,lc}$  and  $\mu_{a,gt,lc}$ ), however, was a different matter. In practice these values were treated as tuning parameters similar to effective attenuation in the in vitro simulation case (section 3.3.3). It was noted, however, that all values for  $\mu_{a,gt}$  were within the range for Mie scattering dominated tissues (Jacques, 2013). Thus, the values for added absorption were considered reasonable.

As expected, the simulated photon bananas were similar across simulation cases because (blood) concentration was low. Because the low and high concentration cases were used to represent maximum and minimum PPG values, respectively, (2.19) was used to calculate the DPF for 100 %  $SpO_2$ . With an emitter-detector distance of 0.265 cm, the DPF ratio, i.e.,  $\Gamma$ , in (2.27) was then obtained as 0.99, while  $\Gamma$  obtained experimentally was 0.35 (section 3.5.3). This deviation supports the assumption that the best available information for the sensor geometry given in its package outline was too scarce for accurate simulation of the photon bananas (section 3.3.3) and suggests that simulations should be repeated if accurate data for the sensor geometry can be obtained.



The simulations were, however, successful with respect to absorption and indicated that light propagation using a perfused, fatty, generalized tissue could be simulated to resemble the sensing volume for the implant location which gave the best SQI in paper C. When matched to data measured in vivo, the simulations indicated that this location had an average change in perfusion between individuals of 8%, and that the mapping between  $SpO_2$  and  $R$  could be expressed as in (3.9).



# Chapter 4

## Concluding remarks

### 4.1 Synthesis

In this work it has been demonstrated that physiological and behavioural data can be linked to stress (objective O.1) in Atlantic salmon by comparing an activity proxy and heart rate to changes in blood chemistry. Based on this demonstration an appropriate sensing technique was selected and tested to expand the scope of this possibility (objective O.2). Using the selected sensing technique, an implantable multi sensor solution for simultaneous logging of both common (ECG, acceleration, temperature) and new (PPG, rotation rates, compass direction, magnetic field strength) data types was designed and implemented (objective O.3) to further facilitate the possibility to uncover the relationships between behaviour and physiology. The implant was then tested in relevant experimental settings (objective O.4) in the form of in vivo, tank and swim tunnel experiments (sections 3.5.1, 3.5.2 and 3.5.3) to develop motion artifact and light scattering compensation strategies so a mapping between the PPG modulation ratio (2.18) and  $SpO_2$  (3.4) could be obtained. This result was supported by Monte Carlo simulations which resulted in a similar mapping (3.9). With all experimental and simulation results available, a linear fit to both tank and swim tunnel data was made resulting in a mapping of

$$SpO_2 = -9.6R + 106.9. \quad (4.1)$$

A composite representation of all results was then made for comparison (figure 4.1) showing that both experimental and simulated results align. Furthermore, the tank experiment (section 3.5.2) and in vivo MC simulations (section 3.6) independently resulted in light scattering compensation param-

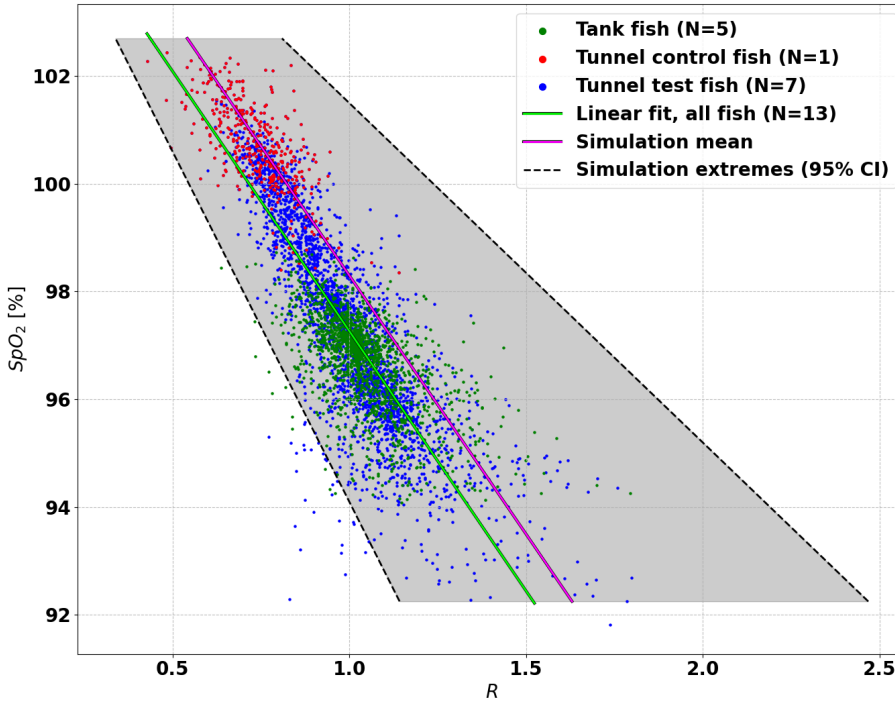


Figure 4.1: Composite representation of experimental and simulated results.

eters,  $\Gamma_{avg}$  of 0.35 (paper F) and 0.34 (3.10) using experimental data and simulated values, respectively. This makes it probable that PO is possible using PPGs obtained from Atlantic salmon. It is, thus, concluded that by successfully addressing the objectives (section 1.2.2), the developed implant enables concurrent logging of data to connect behaviour and physiological responses with the novel addition of PO.

## 4.2 Further work

### 4.2.1 Improving pulse oximetry accuracy

Although a mapping between the modulation ratio,  $R$ , and  $SpO_2$  was identified (4.1), further experimentation to confirm this mapping should be considered. The in vivo oxygen challenge experiment (section 3.5.3) could be refined using dorsal aorta cannulated fish. An oxygen sensor can then be inserted through the cannula (Lennox et al., 2018) for an independently measured baseline under hypoxic conditions for comparison and calibration.

Alternatively, an independent baseline can be obtained using blood sampled from the cannula for blood gas analysis (paper R.B). An empirical mapping between  $R$  (2.18) and  $SpO_2$  can then be made. During such an experiment obtaining an empirical mapping for a greater induced change in  $SpO_2$  should be attempted provided such a trial can be sanctioned by the Norwegian Animal Research Administration.

### 4.2.2 Implant design improvements

During the course of this work, five stand alone implants were made (section 3.4.2). Although well suited for the purposes of this work, future implementations should implement several design improvements.

When in use, the implants were sealed using cast silicone plugs friction fit to the inner wall of the 3D printed encapsulation. Despite fitting snugly, these plugs had a tendency to move outwards during data collection, possibly due to being in tension with the battery and/or because the small amount air inside the implant was compressed when the plug was installed. The resulting gap between the plug and encapsulation sometimes led to fluid ingress (but not tag failure). At most, the implants were placed inside fish for 18 h to 20 h, and longer implantation times must be expected in future experiments. Therefore, an improved seal to reduce the risk of fluid ingress causing tag failure should be prioritized. One way to address this may be to implement a spring loaded bayonet style end cap with integrated battery connection similar to that found in flashlights.

The flexible PCB for battery connection and programming / data download (figure 3.8 b)) was designed to wrap around the edge of the PCB for soldering. This puts the wrap in tension and it was suspected that this caused power connection issues in one of the implants. This solution should be made more robust by, e.g., designing two separate flexible PCBs and soldering these to each side of the PCB thereby eliminating the wrap.

The ECG electrodes were implemented as 14 ct gold wires coiled and glued to the outside of the encapsulation. Excess glue was sanded down to make the surface as smooth and conform as possible with the encapsulation profile. This solution should be changed to make the electrodes even smoother and completely flush with the surrounding surface by using e.g., low profile gold foil or graphene electrodes.

Although the anterior part of the peritoneal cavity provided the best data in terms of signal quality index, valid PPG data were obtained from all tested sensing volumes (paper C). Other sensing volumes may, perhaps,

require more power during data collection, but offer less variation in sensing volume tissue composition across individuals. This may result in more consistent PPGs and, thus, more robust signal processing and analysis. The sensing volume considered most relevant in this respect is the large muscles on each side of the peritoneal cavity. The pulse oximeter could then be placed in contact with the peritoneal wall level with the lateral line. This placement can be achieved by implementing the electronics on a flexible PCB cast in bio compatible silicone. The resulting wafer-shaped circuit can then be slid into position along the peritoneal wall. This be combined with a modular approach with larger components such as the battery and acoustic transmitter being in interconnected separate modules. Although this approach has not been tested, it is thought to have several benefits such as requiring a smaller incision during surgery and, perhaps, being less obstructive compared to rigid, cylindrical implants, thereby reducing the potential negative impact of implantation (Virtanen et al., 2023).

Irrespective of the future physical implementation, on-board data processing for extended operation and acoustic wireless data communication should be part of future designs to facilitate experiments in tanks or sea cages. For swim tunnel / raceway experiments the short distance to the tagged fish can make it possible to inductively power an implant and continuously stream data via radio. The latter, however, will likely take some development, but create room for swim tunnel studies of indefinite duration with high data resolution.

As a final note, it is mentioned that multispectral pulse oximeters are expected to become commercially available in the future. Replacing the MAX86150 with such sensors may enable more advanced compensations based on the additional wavelengths to further improve accuracy (Von Chong et al., 2019).

#### 4.2.3 Data analysis

In paper F a least mean squares adaptive filter was used to suppress motion artifacts before  $SpO_2$  estimation. This approach only works if ECG is available to generate the filter's synthetic reference. To increase knowledge about the characteristics of motion artifacts in Atlantic salmon PPGs, developing a method that does not require ECG should be considered. Because motion data (i.e., IMU) are measured by the implant, preliminary tests using such data for motion artifact reduction were conducted using methods developed for motion corrupted PPG data obtained from human test subjects (e.g., Zhang et al., 2014). The efficacy of such IMU based motion artifact meth-

ods rest upon the assumption that motion artifacts are separate from the PPG in either the time and/or frequency domain (i.e., they must be distinguishable from the PPG in either time and/or frequency). This is generally the case for humans running or swimming. Inspecting PPG and IMU data from the tank (section 3.5.2) and swim tunnel (section 3.5.3) experiments, it was clear that motion artifacts were difficult to suppress using such methods as they were sometimes weak and not easily distinguishable in time or frequency. This was likely caused by the oscillatory movements of the fish's tail or opercula. Future work should therefore explore, adapt and evaluate such methods to improve motion artifact suppression in Atlantic salmon PPGs.

Provided motion artifacts can be effectively reduced in future data processing approaches, more accurate knowledge of the PPG shape for Atlantic salmon can be obtained. In humans, different PPG parts and their morphology are associated with various physiological responses. For instance, PPG amplitude and baseline wandering are associated with perfusion, blood pressure and stroke volume (Park et al., 2022), while the pulse transit time (i.e., the time difference between ECG and PPG peaks) is associated with arterial stiffness (Safavi et al., 2020). If accurate knowledge of the Atlantic salmon PPG shape can be obtained, similar associations can be investigated to further our understanding of the physiological responses (e.g., how Atlantic salmon adjusts stroke volume by the Frank-Starling mechanism) of this species in different contexts.

3D acceleration data obtained from fish can be used to derive the fish's tail beat frequency and activity. This is traditionally achieved by band pass filtering motion signals to suppress gravity effects followed by frequency analysis to obtain tail beats, and by applying a 30s rolling window to the 3D  $L_2$  acceleration norm to represent activity. These approaches have the downside that they can filter out information associated with body motion other than the tail beat.

In a recent attempt to avoid this (paper R.C), tail beat frequency and relative changes in tail beat amplitude were calculated by first levelling the accelerometer axes by mathematical rotation before subtracting gravity instead of filtering the gravity component based on assumed filtering criteria. The resulting (rotated) signal contained not only the tail beat contributions but also other motion contributions by the fish. Because the implant not only measures acceleration but also rotation rates, an additional parameter to analyze motion (i.e., behaviour) is available. As opposed to acceleration, rotation rates are not affected by the same disturbances such as gravity. It is expected that rotation rates contain tail beat frequency data and can be

used for this purpose. The rotated acceleration data containing all motion contributions from the fish can then be used to represent activity. Accelerations and rotation rates measured during the tank experiment (section 3.5.2) should therefore be used to investigate these options for comparison.

#### 4.2.4 The future of E3Ts in Atlantic salmon farming

In recent years, the scope and performance of E3Ts have expanded to include smaller devices with ever improving performance and ability to measure new data types. E3Ts, thus, have potential to provide Atlantic salmon farmers with objective data for animal welfare related decision making. This can only happen if the data can be interpreted to accurately represent the animal's physiological status and their tolerance limits are known. Currently there is no replacement when it comes to measuring the responses of an animal as a 'whole'. Thus, animal experiments are currently unavoidable. As should be the case, such research is strictly regulated (Lovdata, 2015) to enforce ethical compliance and adherence to the principles of reduction, replacement and refinement (3R, Smith, 2021). However, because all animal tagging falls under the animal experiment regulations, its restrictive enforcement, stalls introduction of E3Ts in Atlantic salmon farming, thus, upholding the extent of animal mortality currently taking place (Sommerset et al., 2023; Grefsrud et al., 2022) and is accepted under different regulations existing to ensure animal welfare (Lovdata, 2010, 2023).

In the future, this admittedly complex topic, should be the subject of a discussion including e.g., researchers, technology developers, fish farmers, animal rights representatives and authorities with the aim to establish an accepted practice for the use of E3Ts in Atlantic salmon farming. Provided such a practice can be established, E3Ts, could become an integrated part of intensive fish farming (Brijs et al., 2021), for instance in the form of tagged 'sentinel fish' (Føre et al., 2017a) acting as representatives for the biomass as a whole. Even further into the future when a more refined understanding of which crucial data types to measure to ensure animal welfare becomes available, it can be envisioned that specialized sub miniature sensors for this purpose can be injected in a large number of fish, e.g., during vaccination.

Irrespective of how behavioural and physiological data are obtained, the opportunities offered by the increasing number of tools for this purpose should be welcomed both to uncover the link between behavioural and physiological parameters and stress, and as tools to support the Atlantic salmon farming industry's increasing focus on animal health and welfare thereby making production more profitable and responsible.



# References

- Adams, N.S., Beeman, J.W., Eiler, J.H., 2012. Telemetry techniques: a user guide for fisheries research. American Fisheries Society Bethesda, Maryland.
- Agar Scientific, 2022. Circular coverglasses - 10mm diameter. URL: <https://www.agarscientific.com/circular-coverglasses-12065>. Accessed 03.04.2023.
- Almås, K.A., Ratvik, I., 2017. Sjøkart mot 2050. SINTEF Ocean AS OC2017 A-092.
- Alver, M.O., Føre, M., Alfredsen, J.A., 2022. Predicting oxygen levels in atlantic salmon (*salmo salar*) sea cages. *Aquaculture* 548, 737720.
- Analog Devices, 2018a. High-sensitivity pulse oximeter and heart-rate sensor for wearable health. URL: <https://www.analog.com/media/en/technical-documentation/data-sheets/MAX30102.pdf>. Accessed: 30.03.2023.
- Analog Devices, 2018b. Max86150 integrated photoplethysmogram and electrocardiogram bio-sensor module for mobile health, rev. 2. URL: <https://www.analog.com/media/en/technical-documentation/data-sheets/max86150.pdf>. Accessed: 10.03.2023.
- Bhatt, M., Ayyalasomayajula, K.R., Yalavarthy, P.K., 2016. Generalized beer–lambert model for near-infrared light propagation in thick biological tissues. *Journal of biomedical optics* 21, 076012.
- Bigio, I.J., Fantini, S., 2016. Quantitative biomedical optics: theory, methods, and applications. Cambridge University Press.
- Binzoni, T., Leung, T.S., Gandjbakhche, A.H., Rüfenacht, D., Delpy, D.T., 2006. The use of the henye–greenstein phase function in monte carlo

- simulations in biomedical optics. *Physics in Medicine and Biology* 51, N313–N322. doi:[10.1088/0031-9155/51/17/n04](https://doi.org/10.1088/0031-9155/51/17/n04).
- Bone, Q., Moore, R., 2008. *Biology of fishes*. Taylor & Francis.
- Briely-Sabo, K., Bjornerud, A., 2000. Accurate de-oxygenation of ex vivo whole blood using sodium dithionite, in: *Proc. Intl. Sot. Mag. Reson. Med.*, p. 2025.
- Brijs, J., Føre, M., Gräns, A., Clark, T., Axelsson, M., Johansen, J., 2021. Bio-sensing technologies in aquaculture: how remote monitoring can bring us closer to our farm animals. *Philosophical Transactions of the Royal Society B* 376, 20200218.
- Brijs, J., Sandblom, E., Axelsson, M., Sundell, K., Sundh, H., Huyben, D., Broström, R., Kiessling, A., Berg, C., Gräns, A., 2018. The final countdown: Continuous physiological welfare evaluation of farmed fish during common aquaculture practices before and during harvest. *Aquaculture* 495, 903–911. URL: <https://www.sciencedirect.com/science/article/pii/S004484861830125X>, doi:<https://doi.org/10.1016/j.aquaculture.2018.06.081>.
- Brodeur, J.C., Ytrestøyl, T., Finstad, B., McKinley, R.S., 1999. Increase of heart rate without elevation of cardiac output in adult atlantic salmon (*salmo salar*) exposed to acidic water and aluminium. *Canadian Journal of Fisheries and Aquatic Sciences* 56, 184–190.
- Chan, E.D., Chan, M.M., Chan, M.M., 2013. Pulse oximetry: understanding its basic principles facilitates appreciation of its limitations. *Respiratory medicine* 107, 789–799.
- Chatterjee, S., Abay, T.Y., Phillips, J.P., Kyriacou, P.A., 2018. Investigating optical path and differential pathlength factor in reflectance photoplethysmography for the assessment of perfusion. *Journal of biomedical optics* 23, 075005.
- Cooke, S.J., Lennox, R.J., Brownscombe, J.W., Iverson, S.J., Whoriskey, F.G., Millspaugh, J.J., Hussey, N.E., Crossin, G.T., Godley, B.J., Harcourt, R., 2021. A case for restoring unity between biotelemetry and bio-logging to enhance animal tracking research. *Facets* 6, 1260–1265.
- Coyle, S.D., Durborow, R.M., Tidwell, J.H., et al., 2004. *Anesthetics in aquaculture*. volume 3900. Southern Regional Aquaculture Center Stoneville.

- Directorate of Fisheries, 2023. Biomassestatistikk etter fylke. URL: <https://www.fiskeridir.no/Akvakultur/Tall-og-analyse/Biomassestatistikk/Biomassestatistikk-etter-fylke>. Accessed: 09.02.2023.
- Directorate of fisheries, 2023. Lønnsomhetsundersøkelse for laks og regnbueørret: matfiskproduksjon. URL: <https://www.fiskeridir.no/Akvakultur/Tall-og-analyse/Loennsomhetsundersoekelse-for-laks-og-regnbueoerret/Matfiskproduksjon-laks-og-regnbueoerret>. Accessed: 10.03.2023.
- Elgendi, M., 2016. Optimal signal quality index for photoplethysmogram signals. *Bioengineering* 3, 21.
- Eliason, E.J., Clark, T.D., Hinch, S.G., Farrell, A.P., 2013. Cardiorespiratory performance and blood chemistry during swimming and recovery in three populations of elite swimmers: adult sockeye salmon. *Comparative Biochemistry and Physiology Part A: Molecular & Integrative Physiology* 166, 385–397.
- Fahlman, A., Aoki, K., Bale, G., Brijs, J., Chon, K., Drummond, C., Føre, M., Manteca, X., McDonald, B., McKnight, J., et al., 2021. The new era of physio-logging and their grand challenges. *front physiol* 12: 669158.
- FAO, 2020. The State of World Fisheries and Aquaculture 2020. URL: <https://www.fao.org/3/ca9229en/CA9229EN.pdf>. Accessed: 09.02.2023.
- Flegal, J.M., Haran, M., Jones, G.L., 2008. Markov chain monte carlo: Can we trust the third significant figure? *Statistical Science* , 250–260.
- Flock, S.T., Wilson, B.C., Patterson, M.S., 1989. Monte carlo modeling of light propagation in highly scattering tissues. ii. comparison with measurements in phantoms. *IEEE Transactions on Biomedical Engineering* 36, 1169–1173.
- Føre, H.M., Thorvaldsen, T., Osmundsen, T.C., Asche, F., Tveterås, R., Fagertun, J.T., Bjelland, H.V., 2022. Technological innovations promoting sustainable salmon (*salmo salar*) aquaculture in norway. *Aquaculture Reports* 24, 101115.
- Føre, M., Alfredsen, J.A., Gronningsater, A., 2011. Development of two telemetry-based systems for monitoring the feeding behaviour of Atlantic salmon (*Salmo salar* L.) in aquaculture sea-cages. *Computers and electronics in agriculture* 76, 240–251. URL: <https://doi.org/10.1016/j.compelecag.2011.05.008>

[//www.sciencedirect.com/science/article/pii/S0168169911000536](http://www.sciencedirect.com/science/article/pii/S0168169911000536),  
doi:<https://doi.org/10.1016/j.compag.2011.02.003>.

- Føre, M., Frank, K., Dempster, T., Alfredsen, J.A., Høy, E., 2017a. Biomonitoring using tagged sentinel fish and acoustic telemetry in commercial salmon aquaculture: a feasibility study. *Aquacultural Engineering* 78, 163–172.
- Føre, M., Frank, K., Norton, T., Svendsen, E., Alfredsen, J.A., Dempster, T., Eguiraun, H., Watson, W., Stahl, A., Sunde, L.M., et al., 2017b. Precision fish farming: A new framework to improve production in aquaculture. *Biosystems Engineering* URL: <https://www.sciencedirect.com/science/article/pii/S1537511017304488>, doi:<https://doi.org/10.1016/j.biosystemseng.2017.10.014>.
- Friebel, M., Helfmann, J., Netz, U., Meinke, M., 2009. Influence of oxygen saturation on the optical scattering properties of human red blood cells in the spectral range 250 to 2000 nm. *Journal of biomedical optics* 14, 034001–034001.
- Grefsrud, E.S., Andersen, L.B., Bjørn, P.A., Grøsvik, B.E., Hansen, P.K., Husa, V., Karlsen, Ø., Kvamme, B.O., Samuelsen, O.B., Sandlund, N., et al., 2022. Risikoreport norsk fiskeoppdrett 2022-risikovurdering—effekter på miljø og dyrevelferd i norsk fiskeoppdrett. Rapport fra havforskningen URL: <https://www.hi.no/hi/nettrapporter/rapport-fra-havforskningen-2022-13>. Accessed: 08.02.2023.
- Härdig, J., Höglund, L.B., 1983. On accuracy in estimating fish blood variables. *Comparative Biochemistry and Physiology Part A: Physiology* 75, 35–40.
- Hassan, W., Føre, M., Urke, H.A., Kristensen, T., Ulvund, J.B., Alfredsen, J.A., 2019. System for real-time positioning and monitoring of fish in commercial marine farms based on acoustic telemetry and internet of fish (iof), in: *The 29th International Ocean and Polar Engineering Conference, ISOPE*.
- Hassan, W., Føre, M., Urke, H.A., Ulvund, J.B., Bendiksen, E., Alfredsen, J.A., 2022. New concept for measuring swimming speed of free-ranging fish using acoustic telemetry and doppler analysis. *Biosystems Engineering* 220, 103–113.

- Hvas, M., Folkedal, O., Oppedal, F., 2021. Fish welfare in offshore salmon aquaculture. *Reviews in Aquaculture* 13, 836–852.
- Jacques, S.L., 2010. Monte carlo modeling of light transport in tissue (steady state and time of flight), in: *Optical-thermal response of laser-irradiated tissue*. Springer, pp. 109–144.
- Jacques, S.L., 2013. Optical properties of biological tissues: a review. *Physics in Medicine & Biology* 58, R37.
- Jepsen, N., Thorstad, E.B., Havn, T., Lucas, M.C., 2015. The use of external electronic tags on fish: an evaluation of tag retention and tagging effects. *Animal Biotelemetry* 3, 1–23.
- Jobling, M., Arnesen, A.M., Benfey, T., Carter, C., Hardy, R., François, N.L., O’Keefe, R., Koskela, J., Lamarre, S.G., 2010. The salmonids (family: Salmonidae)., in: *Finfish aquaculture diversification*. CABI Wallingford UK, pp. 234–289.
- Kernighan, B.W., Ritchie, D.M., 1988. *The C Programming Language*. Prentice-Hall, Inc.
- Kreyszig, E., 2011. *Advanced Engineering Mathematics 10th Edition*. John Wiley & Sons.
- Kryvi, H., Poppe, T., 2016. *Fiskeanatomi*. Fagbokforlaget.
- Lennox, R.J., Eliason, E.J., Havn, T.B., Johansen, M.R., Thorstad, E.B., Cooke, S.J., Diserud, O.H., Whoriskey, F.G., Farrell, A.P., Uglem, I., 2018. Bioenergetic consequences of warming rivers to adult atlantic salmon *salmo salar* during their spawning migration. *Freshwater Biology* 63, 1381–1393.
- Liu, S., Deng, Z., Li, J., Wang, J., Huang, N., Cui, R., Zhang, Q., Mei, J., Zhou, W., Zhang, C., et al., 2019. Measurement of the refractive index of whole blood and its components for a continuous spectral region. *Journal of biomedical optics* 24, 035003–035003.
- Lovdata, 2010. Lov om dyrevelferd. URL: <https://lovdata.no/dokument/NL/lov/2009-06-19-97?q=dyrevelferdsloven>. Accessed: 04.05.2023.
- Lovdata, 2015. Forskrift om bruk av dyr i forsøk. URL: <https://lovdata.no/dokument/SF/forskrift/2015-06-18-761>. Accessed: 09.02.2023.

- Lovdata, 2023. Forskrift om drift av akvakulturanlegg (akvakulturdriftsforskriften). URL: <https://lovdata.no/dokument/SF/forskrift/2008-06-17-822>. Accessed: 09.02.2023.
- Meinke, M., Müller, G., Helfmann, J., Friebel, M., 2007. Optical properties of platelets and blood plasma and their influence on the optical behavior of whole blood in the visible to near infrared wavelength range. *Journal of Biomedical Optics* 12, 014024–014024.
- Ministry of Trade, Industry and Fisheries, 2021. Havbruksstrategien - et hav av muligheter. URL: <https://www.regjeringen.no/no/dokumenter/havbruksstrategien-et-hav-av-muligheter/id2864482/>. Accessed 22.05.2023.
- Misund, A.U., Thorvaldsen, T., 2022. Nye produksjonssystemer i havbruk-utfordringer og muligheter. SINTEF Ocean AS 2022:01019 A.
- Misund, B., 2022. Kostnadsutvikling i oppdrett av laks og ørret: Hva koster biologisk risiko? NORCE Norwegian Research Centre 41-2022.
- Morgenroth, D., Ekström, A., Hjelmstedt, P., Gräns, A., Axelsson, M., Sandblom, E., 2019. Hemodynamic responses to warming in euryhaline rainbow trout: implications of the osmo-respiratory compromise. *Journal of Experimental Biology* 222, jeb207522.
- Morro, B., Davidson, K., Adams, T.P., Falconer, L., Holloway, M., Dale, A., Aleynik, D., Thies, P.R., Khalid, F., Hardwick, J., et al., 2022. Offshore aquaculture of finfish: Big expectations at sea. *Reviews in Aquaculture* 14, 791–815.
- Muñoz, L., Aspillaga, E., Palmer, M., Saraiva, J.L., Arechavala-Lopez, P., 2020. Acoustic telemetry: a tool to monitor fish swimming behavior in sea-cage aquaculture. *Frontiers in Marine Science* 7, 645.
- Noble, C., Nilsson, J., Stien, L.H., Iversen, M.H., Kolarevic, J., Gismervik, K., 2018. Velferdsindikatorer for oppdrettlaks: Hvordan vurdere og dokumentere fiskevelferd. 2. utgave URL: <https://brage.bibsys.no/xmlui/bitstream/handle/11250/2493926/Velferdsindikatorer-for-oppdrettlaks-2018+-+2+utgave.pdf?sequence=1>.
- Norecopa, 2023. Norecopa. URL: <https://norecopa.no/>. Accessed 12.04.2023.

- Norwegian Institute for Nature Research, 2023. Nina forskningsstasjon ims. URL: <https://www.nina.no/Om-NINA/Kompetanse-og-tjenester/NINA-Forskningsstasjon>. Accessed: 23.03.2023.
- NTNU, 2023. Sealab research infrastructure. URL: <https://www.ntnu.edu/sealab>. Accessed: 23.03.2023.
- Oldham, T., Dempster, T., Fosse, J.O., Oppedal, F., 2017. Oxygen gradients affect behaviour of caged atlantic salmon *salmo salar*. *Aquaculture Environment Interactions* 9, 145–153.
- Park, J., Seok, H.S., Kim, S.S., Shin, H., 2022. Photoplethysmogram analysis and applications: An integrative review. *Frontiers in Physiology* 12, 2511.
- Pintavirooj, C., Ni, B., Chatkobkool, C., Piniijkij, K., 2021. Noninvasive portable hemoglobin concentration monitoring system using optical sensor for anemia disease, in: *Healthcare*, MDPI. p. 647.
- Prahl, S., 1998. Tabulated molar extinction coefficients for hemoglobin in water. URL: <https://omlc.org/spectra/hemoglobin/summary.html>. Accessed 08.11.2022.
- Prahl, S., 2018. Mie scattering calculator. URL: [https://omlc.org/calc/mie\\_calc.html](https://omlc.org/calc/mie_calc.html). Accessed 03.04.2023.
- Prahl, S.A., 1989. A monte carlo model of light propagation in tissue, in: *Dosimetry of laser radiation in medicine and biology*, International Society for Optics and Photonics. p. 1030509.
- Reuss, J.L., 2005. Multilayer modeling of reflectance pulse oximetry. *IEEE transactions on biomedical engineering* 52, 153–159.
- Robb, D., Wotton, S., McKinstry, J., Sørensen, N., Kestin, S., Sørensen, N., 2000. Commercial slaughter methods used on atlantic salmon: determination of the onset of brain failure by electroencephalography. *Veterinary Record* 147, 298–303.
- Safavi, S.M., Valisharifabad, N., Sabino, R.C., Tran, D., Lin, J., Lopour, B., Chou, P.H., 2020. Investigation of morphological variations of photoplethysmography signal in human epilepsy, in: *2020 42nd Annual International Conference of the IEEE Engineering in Medicine & Biology Society (EMBC)*, IEEE. pp. 2687–2690.

- Sandnes, K., Lie, Ø., Waagbø, R., 1988. Normal ranges of some blood chemistry parameters in adult farmed atlantic salmon, *salmo salar*. *Journal of Fish Biology* 32, 129–136.
- Santurtun, E., Broom, D., Phillips, C., 2018. A review of factors affecting the welfare of atlantic salmon (*salmo salar*). *Animal Welfare* 27, 193–204.
- SINTEF ACE, 2023. SINTEF ACE full-scale laboratory facility. URL: <https://www.sintef.no/en/all-laboratories/ace/>. Accessed: 08.02.2023.
- SINTEF Ocean AS, 2023. Sintef sealab. URL: <https://www.sintef.no/en/all-laboratories/sintef-sealab/>. Accessed: 23.03.2023.
- Sjømat Norge, 2023. Norsk laks fra fjord til bord. URL: <https://laks.no/lakseproduksjon/>. Accessed: 09.02.2023.
- Smith, A.J., 2021. Norecopa: A database of global 3r resources for better science. *Biomedical Science and Engineering* 4.
- Sommerset, I., Walde, C., Bang Jensen, B., Wiik-Nielsen, J., Bornø, B., Oliveira, V., Brun, E., 2023. Fiskehelserapporten 2022, veterinærinstituttets rapportserie nr 5a/2023. URL: [https://www.vetinst.no/rapporter-og-publikasjoner/rapporter/2023/fiskehelserapporten-2022/\\_/attachment/download/164c2980-d87f-4ac9-a11d-bff201c7ed10:34fc4f3e776b896d8a6eb321b98e510ff9cd80c6/FHR%202022.pdf](https://www.vetinst.no/rapporter-og-publikasjoner/rapporter/2023/fiskehelserapporten-2022/_/attachment/download/164c2980-d87f-4ac9-a11d-bff201c7ed10:34fc4f3e776b896d8a6eb321b98e510ff9cd80c6/FHR%202022.pdf). Accessed: 08.02.2023.
- Star-Oddi, 2023. Star-oddi - logging life science. URL: <https://www.star-oddi.com/>. Accessed: 17.01.2023.
- Steinhubl, S.R., Muse, E.D., Topol, E.J., 2015. The emerging field of mobile health. *Science translational medicine* 7, 283rv3–283rv3.
- Swinehart, D.F., 1962. The beer-lambert law. *Journal of chemical education* 39, 333.
- Tavakoli, J., Tang, Y., 2017. Hydrogel based sensors for biomedical applications: An updated review. *Polymers* 9, 364.
- Thorstad, E., Økland, F., Koed, A., McKinley, R., 2000. Radio-transmitted electromyogram signals as indicators of swimming speed in lake trout and brown trout. *Journal of Fish Biology* 57, 547–561.



- Thorstad, E.B., Rikardsen, A.H., Alp, A., Økland, F., 2013. The use of electronic tags in fish research—an overview of fish telemetry methods. *Turkish Journal of Fisheries and Aquatic Sciences* 13, 881–896.
- Ugryumova, N., Matcher, S.J., Attenburrow, D.P., 2004. Measurement of bone mineral density via light scattering. *Physics in Medicine & Biology* 49, 469.
- Virtanen, M.I., Brinchmann, M.F., Patel, D.M., Iversen, M.H., 2023. Chronic stress negatively impacts wound healing, welfare, and stress regulation in internally tagged atlantic salmon (*salmo salar*). *Frontiers in Physiology* 14, 459.
- Von Chong, A., Terosiet, M., Histace, A., Romain, O., 2019. Towards a novel single-led pulse oximeter based on a multispectral sensor for iot applications. *Microelectronics Journal* 88, 128–136.
- Wu, H., Shinoda, R., Murata, M., Matsumoto, H., Ohnuki, H., Endo, H., 2019. Development of a novel led color-switching type biosensor system for the visualization of fish stress responses. *Analytical Methods* 11, 5623–5628.
- Yang, Y., Lu, J., Pflugrath, B.D., Li, H., Martinez, J.J., Regmi, S., Wu, B., Xiao, J., Deng, Z.D., 2021. Lab-on-a-fish: Wireless, miniaturized, fully integrated, implantable biotelemetric tag for real-time in vivo monitoring of aquatic animals. *IEEE Internet of Things Journal* 9, 10751–10762.
- Yanina, I.Y., Lazareva, E.N., Tuchin, V.V., 2018. Refractive index of adipose tissue and lipid droplet measured in wide spectral and temperature ranges. *Applied optics* 57, 4839–4848.
- Yetisen, A.K., Butt, H., Volpatti, L.R., Pavlichenko, I., Humar, M., Kwok, S.J., Koo, H., Kim, K.S., Naydenova, I., Khademhosseini, A., et al., 2016. Photonic hydrogel sensors. *Biotechnology advances* 34, 250–271.
- Zhang, Z., Pi, Z., Liu, B., 2014. Troika: A general framework for heart rate monitoring using wrist-type photoplethysmographic signals during intensive physical exercise. *IEEE Transactions on biomedical engineering* 62, 522–531.
- Zimmer, E., 2023. Biosensory implants for in vivo real-time measurement of stress indicators. URL: <https://prosjektbanken.forskningsradet.no/project/FORISS/309881>. Accessed: 08.02.2023.



# Publications



Paper A  
Heart rate and swimming  
activity as stress indicators for  
Atlantic salmon (*Salmo salar*)

Paper A

*Heart rate and swimming activity as stress indicators for Atlantic salmon  
(Salmo salar)*

---



ELSEVIER

Contents lists available at ScienceDirect

Aquaculture

journal homepage: [www.elsevier.com/locate/aquaculture](http://www.elsevier.com/locate/aquaculture)

## Heart rate and swimming activity as stress indicators for Atlantic salmon (*Salmo salar*)



E. Svendsen<sup>a,b,\*</sup>, M. Føre<sup>b,a</sup>, F. Økland<sup>c</sup>, A. Gräns<sup>d</sup>, R.D. Hedger<sup>c</sup>, J.A. Alfredsen<sup>b</sup>, I. Uglem<sup>c</sup>, C.M. Rosten<sup>c</sup>, K. Frank<sup>a</sup>, U. Erikson<sup>a</sup>, B. Finstad<sup>c,e</sup>

<sup>a</sup> SINTEF Ocean, 7465 Trondheim, Norway

<sup>b</sup> NTNU Department of Engineering Cybernetics, 7491 Trondheim, Norway

<sup>c</sup> Norwegian Institute for Nature Research, 7485 Trondheim, Norway

<sup>d</sup> Department of Animal Environment and Health, Swedish University of Agricultural Sciences, Skara SE-532 31, Sweden

<sup>e</sup> NTNU Department of Biology, 7491 Trondheim, Norway

### ARTICLE INFO

#### Keywords:

Plasma cortisol  
Lactate  
Glucose  
Osmolality  
Implants

### ABSTRACT

We investigated the relationship between telemetry measurements of heart rate and swimming activity and the physiological status in farmed Atlantic salmon (*Salmo salar*) to assess the potential to use telemetry measurements as proxies for stress. Sensor tags measuring heart rate and swimming activity were surgically implanted into the peritoneal cavity of Atlantic salmon individuals kept in tanks. Four tanks were stocked with three tagged fish and four untagged cohabitants, while two additional tanks containing 16 untagged fish were used as reference groups. Following surgery, tagged fish were kept undisturbed for 14 days as acclimation period. All fish were then subjected to physical stress by reducing the tank water level in 4 consecutive rounds, after which they were left undisturbed for another ten days before the experiment ended. Plasma cortisol, glucose, lactate and osmolality were measured to assess stress levels from fish in the reference groups before and after being subjected to stressing and from all fish at the end of the experiment. Both heart rate and swimming activity rose after the stress treatment, remaining elevated for 24.5 and 16.2 Hrs respectively. Glucose, plasma cortisol, lactate and osmolality levels were significantly greater when measured immediately after stress. Results from the experiment indicate that heart rate and swimming activity can be used as proxies for fish stress, thus opening the possibility for on-line stress monitoring in full scale production.

### 1. Introduction

Atlantic salmon (*Salmo salar*) farming is a growing global industry (Directorate of Fisheries, 2019) responding to increased global need for ocean-based protein production (Olafsen et al., 2012). The industry faces challenges regarding fish welfare and is under pressure to improve production methods and farm operations. Operations involving fish handling (e.g. crowding using sweep-nets followed by pumping and treatment against sea lice (*Lepeophtheirus salmonis*) or disease) are common in Norwegian aquaculture and detrimental to fish welfare (Hjeltnes et al., 2018). To increase production volumes efforts are made to develop larger, higher capacity production systems at more exposed locations (Bjelland et al., 2015) which will entail that such operations must handle fish in larger groups and under more challenging conditions. Handling related welfare hazards are believed to be major contributors to the annual mortality in salmon production (Bleie and

Skrudland, 2014). With a mortality of 14.7% for the sea stage in 2018 (Norwegian Food Safety Authority, 2018), this highlights the need for better control of how operations are conducted and their impact on fish welfare.

Monitoring fish welfare during aquaculture operations is a challenge and extensive resources and research efforts have been allocated over the last decades to developing new methods to monitor and reduce negative welfare effects of common aquaculture practices on fish. Existing tools to evaluate fish welfare are typically referred to as Operational Welfare Indicators (OWIs) derived from an extensive literature review (Noble et al., 2018). Most state-of-the-art methods fish farmers employ to evaluate fish welfare and quantify OWIs in an industrial production setting are based on visual observations from e.g. sampling of fish or various camera feeds. However, the outcomes of these may rely on the personal experience of the observer and can thus be influenced by subjective observation bias. In addition, with each sea

\* Corresponding author at: SINTEF Ocean, 7465 Trondheim, Norway.

E-mail address: [eirik.svendsen@sintef.no](mailto:eirik.svendsen@sintef.no) (E. Svendsen).

<https://doi.org/10.1016/j.aquaculture.2020.735804>

Received 27 January 2020; Received in revised form 3 August 2020; Accepted 3 August 2020

Available online 09 August 2020

0044-8486/ © 2020 The Authors. Published by Elsevier B.V. This is an open access article under the CC BY license

(<http://creativecommons.org/licenses/by/4.0/>).

cage being up to 50 m deep and containing up to 200,000 fish, only a fraction of the individuals can be observed from the surface at any given time making the total population difficult to monitor through surface observations. Underwater cameras are therefore often used to supplement such methods as they enable data collection from a larger part of the cage volume, essentially making more of the total population observable. However, placing cameras within sea-cages may conflict with cage operations and be of limited use because low visibility and high biomass densities (e.g. during crowding) may prevent a sufficiently wide field of view to extract useful information (Shieh and Petrell, 1998). Other instruments such as active hydroacoustic instruments (e.g. sonars and echo sounders) may provide additional insight into the distribution and behaviour of the fish but are of limited use when biomass density exceeds a certain threshold as signal saturation makes fish density estimates uncertain. Because of these technological limitations, visual inspection and subjective evaluation of relevant welfare indicators remain the most common fish welfare monitoring methods (Føre et al., 2018a).

The observability of the fish in aquaculture can be improved by equipping individual fish with electronic devices ("tags") containing sensors that can measure various parameters in or near the fish (Thorstad et al., 2013). Using tags will result in individual data histories for the tagged fish, which is complementary information to that obtained through e.g. cameras, echo sounders and direct observations. Acoustic telemetry is a type of biotelemetry where tags contain a transmitter and data are transferred wirelessly to the user in real time using acoustic signals. This method has recently been shown to be viable for individual based data collection in commercial salmon cages (e.g. Føre et al., 2017; Stehfest et al., 2017). Data Storage Tags (DSTs) represent a different branch in biosensing where the tags store data internally and thus must be retrieved for the user to access the data. This method has been employed to log e.g. swimming depth and temperature for individual salmon in aquaculture production cages (Johansson et al., 2009). Since DSTs are not limited by acoustic bandwidth, this method may result in higher data density than the acoustic counterpart but faces challenges related to tag retrieval in commercial size fish populations in addition to data being available only for retrospective analysis.

Recent studies have used acoustic telemetry to study the swimming activity of salmon during crowding and delousing (Føre et al., 2018) and DSTs to study the effects of crowding and transport on heart rate in rainbow trout (*Oncorhynchus mykiss*) (Brijs et al., 2018). These studies imply that swimming activity and heart rate may be useful indicators of welfare during such operations and demonstrate that these parameters can be measured in industrially relevant situations. If the characteristics in these parameters during welfare critical operations in fish farms could be detected and linked to stress, they can potentially serve as OWI's.

Stress as defined within the context of biology is the non-specific bodily response to demands for change (Selye, 1973). The first step in identifying the link between stress and measurable physiological parameters is to conduct laboratory studies through which it is possible to collect detailed data under controlled conditions. In this study we investigate the links between variables that can be measured using existing sensor tags (heart rate, swimming activity) and the stress level of the fish quantified by blood analysis. This included a laboratory study where off-the-shelf sensors measuring heart rate and swimming activity were implanted into fish which were then subject to stress. Blood was sampled and analysed at different times during the experiment to determine the actual stress level of the fish and to evaluate if the data from the implants provided valid proxies for stress based on the hypothesis that heart rate and swimming activity are affected by and linked to stress.

## 2. Materials and methods

### 2.1. Ethical statement

All fish handling and surgery was done in compliance with the Norwegian Animal Welfare Act (2009). The experiment was approved by the local responsible laboratory animal science specialist under the surveillance and approval of the Norwegian Animal Research Authority (NARA) (ID 18/18431). The fish were allowed to habituate to the experimental tanks for a month before surgery. During this period, inspection and feeding operations were limited to once per day to minimize the potential stress induced upon the fish. Several experimental refinement strategies were applied in the trials, including fish sampling using a knotless dip net, immediately transferring sampled fish to an anaesthetic bath to minimize stress, and continuously irrigating the gills with aerated water containing maintenance anaesthetic and covering the heads of all fish with a moist cloth during surgery. Mortality after surgery was 0%.

### 2.2. Experimental animals, housing and husbandry

The experiment was conducted between January 1st and March 3rd, 2019, at the Norwegian Institute for Nature Research's (NINA) Aquatic Research Station, Ims (Sandnes municipality, Norway). Sixty Atlantic salmon ( $55.5 \pm 5.7$  cm fork length) of the Aqua Gen genetic strain were randomly selected from a holding tank and distributed between the six experimental tanks (hereafter denoted Tank 1 - Tank 6). The tanks were square with rounded corners, had a volume of approximately  $5.6 \text{ m}^3$ , and were equipped with adjustable (flow and direction) seawater inlets from a shared manifold, overflow outlets, sensors for temperature and dissolved  $\text{O}_2$  (DO) and oxygenation equipment to ensure a stable and controlled environment. Water temperatures and DO levels registered during the experimental period were  $4.2 \pm 0.2$  °C and  $97.7 \pm 0.2\%$  respectively. Husbandry was carried out by on-site personnel trained in handling experimental fish and entailed daily feeding and general supervision.

### 2.3. Study design and timeline

The experiment animals were distributed such that Tanks 1–4 each contained three tagged fish and four untagged fish. Tanks 5 and 6 each contained a reference group of 16 untagged fish. All tagged fish were equipped with DSTs (Centi HRT, Centi HRT ACT and Milli HRT, Star Oddi LTD, Gardabaer, Iceland) all of which registered heart rate, and some also registered tri-axial acceleration at 1 Hz (Centi HRT ACT). These are the same tags employed by Brijs et al. (2018), ensuring comparability with that study. The Centi HRT and Centi HRT ACT tags logged data with a sampling interval of 2 min for 25 days. Due to a lower internal storage capacity, the Milli HRT tags were set with a longer sampling interval of 10 min, which was reduced to 2 min between March 3rd 08:00 and March 6th 08:00 to achieve higher data resolution during and after stressing. Two fish in both Tanks 1 and 2 were also equipped with acoustic telemetry tags of the type A-MP 9 (Thelma Biotel AS, Trondheim, Norway) containing a three-axis accelerometer with a range of  $0\text{--}2.1 \text{ m/s}^2$  sampling at 5 Hz. The tags were set to sample accelerations in consecutive 30 s windows from which the average Euclidean norm was calculated as in Føre et al. (2018), but with a lower maximum value for swimming activity ( $2.1 \text{ m/s}^2$ ) to obtain higher output resolution. The resulting swimming activity indicator was transmitted every 40s, providing a higher data density for this parameter than in Føre et al. (2018). Two acoustic receivers (Thelma Biotel TBR700 and TBR700-RT) were installed in each of the tanks containing acoustic telemetry tags (Tanks 1 and 2) for redundant data capture and storage. The distribution of fish and tags between tanks is illustrated in Fig. 1.

Tags were surgically implanted into the peritoneal cavity while the



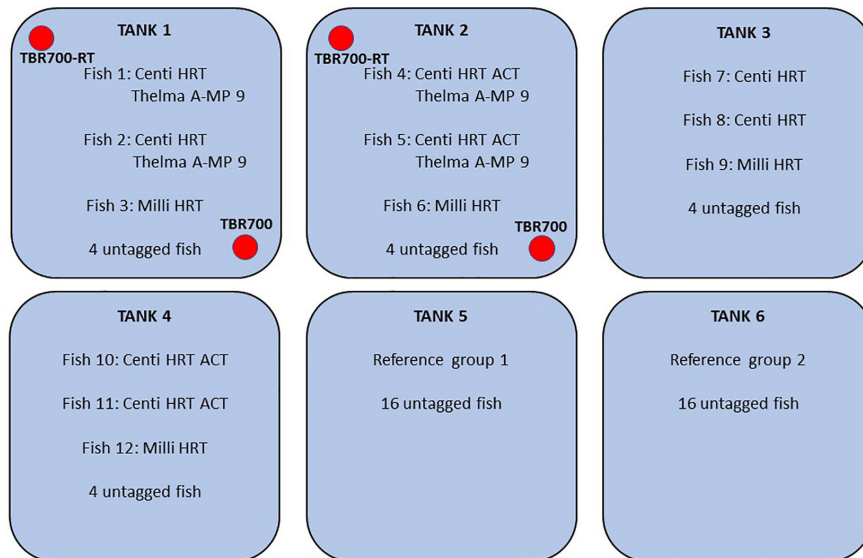


Fig. 1. Study design: Fish and tag distribution between experiment tanks. The red circles for tanks 1 and 2 denote the location of the hydroacoustic receivers. (For interpretation of the references to colour in this figure legend, the reader is referred to the web version of this article.)

fish were anaesthetised using Benzoak Vet (70 mg/L knock-out solution and 35 mg/L maintenance dosage during surgery). The DSTs were implanted using a procedure similar to that of Brijs et al. (2018), where the tag was inserted through an incision in the abdomen. An extra step was taken in this study to prevent tag movement relative to the heart by anchoring the heart rate tags to the peritoneal wall using an anterior suture close to the peritoneal septum. For fish equipped with two tags, both were inserted through the same incision. After tag implantation, the incision was closed with 3–4 interrupted sutures. The tagged fish was then transferred to a recovery tank with circulating sea water where it was kept until it had regained full consciousness, upon which it was transferred back to the tank it had been collected from. These procedures and their potential impact on the fish are described and discussed in greater detail in Føre et al. (2019).

Surgery was conducted on February 18th and was followed by a fourteen-day recovery period until March 3rd, when the fish were subjected to stress by repeated draining of the water levels in all tanks simultaneously. Following this, the fish recovered for ten days until March 14th, when the experiment was concluded by euthanising all fish. Tag data were collected throughout the entire experimental period and blood samples were taken after surgery (February 18th), before and after stressing (March 4th), and prior to euthanasia (March 14th). In the periods between the main experimental events the fish were kept undisturbed in their tanks except for daily hand feeding and visual welfare evaluations. After conclusion of the study, data from the DSTs was downloaded using the proprietary base stations and software (Mercury v5.20) from Star Oddi, while data from the Thelma tags were downloaded from the TBR700-units using a native Bluetooth interface and software (ComPort v3.0.0).

## 2.4. Experimental procedures

Stressing of the fish was done by reducing tank water levels until the dorsal region of the fish was exposed to air (Fig. 2) in four iterations with different durations. For all iterations, lowering the water level took approximately 1 min. For the first iteration, the water level was restored immediately. For the second iteration the water level was kept

low for 1 min. For the third and fourth iterations, the water level was kept low for 5 min. During the last iteration, the stressing also included chasing the fish around the tank with a dip net until fish exhaustion. For all iterations, re-filling the tanks took approximately 10 min. Each iteration was started on the hour, so the time between iteration was 49 min, 47 min, 42 min and 35 min respectively. The stress procedure was conducted simultaneously for all tanks so that all fish were subject to the same treatment. Four people participated when stressing the fish to ensure similar operations on all tanks.

Blood was sampled from fish in the reference groups and involved opening the tank lid, netting a random fish from the tank as quickly as possible using a knotless dip net, and placing it in an anaesthetic knock-out solution (Aqui-S, > 80 mg isoeugenol/L water). Blood was sampled from the caudal artery using heparinized syringes immediately after loss of consciousness. The fish was thereafter euthanized by a powerful blow to the head. Blood samples were centrifuged, and plasma was collected for analysis.

## 2.5. Data processing

### 2.5.1. Heart rate

Heart rates were derived from on-board, proprietary signal processing methods and stored in the DSTs. Outliers due to measurement errors were removed using the Median Absolute Deviation (MAD) approach (Huber, 1981; Leys et al., 2013). The MAD decision criterion was set to 3 (very conservative according to Miller (1991)) to exclude heart rate values outside published heart rate ranges ( $15 < HR < 80$ ) for Atlantic salmon (Lucas, 1994) and comparable species (Brijs et al., 2019). Heart rate periodicity was evaluated by calculating the real, one-sided Fast Fourier Transform of the average of all heart rate time series collected in the 7 days before stressing.

### 2.5.2. Swimming activity

When using accelerometers to measure fish swimming activity, the gravity vector will introduce a slow varying gravity component convolved with both the low frequency fish attitude component and the high frequency motion component induced by fish motion. The impact



Fig. 2. Photograph of low-water stress imposed on the fish. Water level was lowered until the dorsal fins remained in air for up to 5 min (photo: Bengt Finstad).

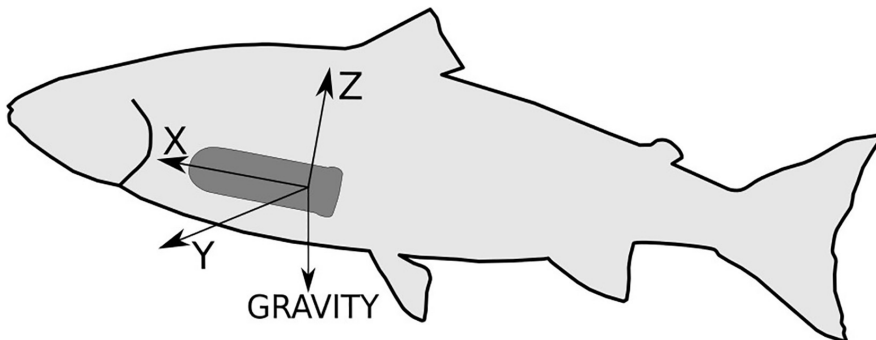


Fig. 3. DST and fish orientation relative to gravity vector. The gravity vector always points towards the centre of the earth. Hence the contribution from the gravity vector will depend on the orientation of the tag and the fish. The X, Y and Z axes denote the alignment of the accelerometer's sensing axes.

of this effect on the three sensing axes depends on the relative orientation between the tag and the fish's orientation relative to the earth's gravity vector (Fig. 3). In the Thelma Biotel tags, this effect is countermanded by low pass filtering the raw data and subtracting the resulting low frequency (LF) component from the raw signal, resulting in a high frequency (HF) component representing the swimming activity of the fish. A swimming activity proxy is achieved by calculating the magnitude (Zwillinger, 2007) of the HF signal and applying a moving average with a 30 s time window. To ensure that swimming activity values measured using the Centi HRT ACT could be compared to data collected by Thelma tags, a similar signal processing approach was applied to the raw acceleration data measured by the Centi HRT ACT tags. Low pass filtering was achieved using a Butterworth low pass filter with a cutoff frequency of 0.2 Hz. The resulting LF component was subtracted from the raw values for each axis, and the magnitude of the HF signal (swimming activity) was calculated as given in Eq. (1).

$$activity = \sqrt{|X|^2 + |Y|^2 + |Z|^2} \quad (1)$$

The result was then smoothed by calculating the moving average over a 30 s time window. Although this results in swimming activity

proxies with the same unit ( $m/s^2$ ), measured accelerations differed between the Thelma and the Star-Oddi tags due to differences in accelerometer properties and intraperitoneal placement. To reduce the impact of these effects, swimming activity data were normalized to a mean of zero and a standard deviation of one (the effect of this procedure is demonstrated for Fish 2 in tank 2 during the first six days of the experiment in Fig. 4).

#### 2.5.3. Blood sample analysis

Sampled blood was centrifuged at 3250 g for 5 min and plasma was removed and stored in cryo tubes at  $-36^\circ\text{C}$  until analyses were performed. A Freestyle Freedom Lite™ (Abbott Diabetes Care Inc.) handheld blood glucose measuring device for people with diabetes which registers concentrations from 1,1–27,8 mmol/L (mM) and uses a dosage of 0.3  $\mu\text{L}$  per reading was used. A study by Wells and Pankhurst (1999), confirms that the use of such a device in animal glucose evaluation is adequate. A Lactate Scout +™ (EKF Diagnostics for life) handheld blood lactate measuring device was used which registers concentrations of 0.5–25,0 mmol/L (mM) and uses a dosage of 0.2  $\mu\text{L}$  per reading. A study by Wells and Pankhurst (1999) as well as EKF Diagnostics for life

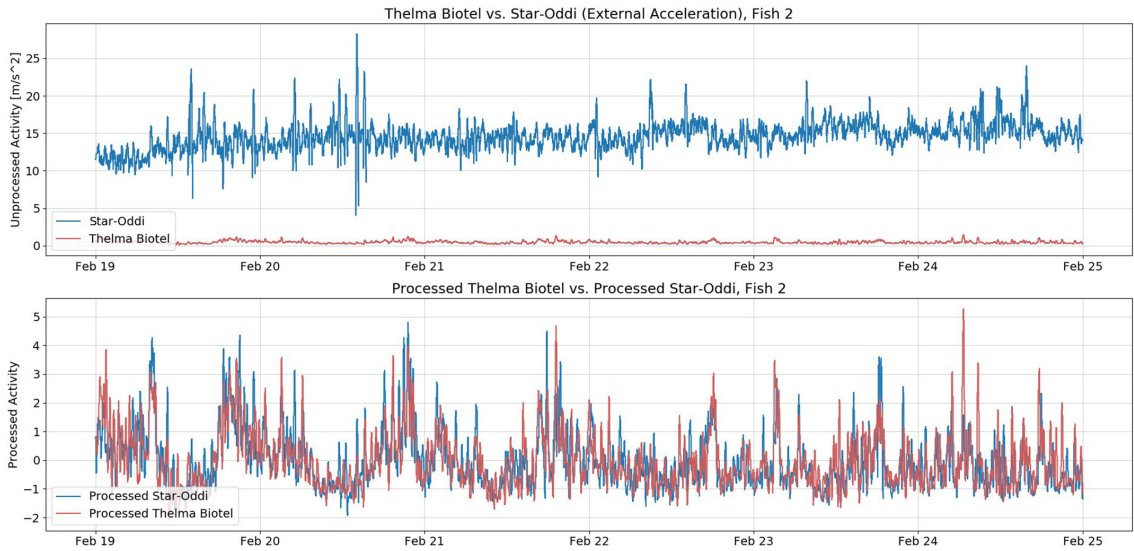


Fig. 4. Before (top) and after (bottom) Star-Oddi data processing.

confirm that the use of such a device in animal lactate evaluation is adequate. A radioimmunoassay technique was used to measure plasma cortisol concentrations as described by Iversen et al. (1998). Plasma osmolality was analysed using a Wescor 5500 osmometer (Wescor™, Elitech Goup, Salon-de-Provence, France).

## 2.6. Statistical methods

A binary recursive partitioning approach (Vignon, 2015) was employed to identify systemic changes in heart rate and swimming activity that could result from stressing. This approach recursively splits the explanatory variable (time in this case) into distinct segments such that the response variable values (heart rate or swimming activity) in each segment are maximally different from one another. The recursive approach means that the most significant split (in terms of deviance between the two segments) is identified first, and splits of lesser significance are subsequently identified in a recursive procedure. Binary recursive partitioning may overfit data, so some smoothing of the input data and/or simplification of the fitted model may be required. The procedure used was therefore as follows:

- 1) Time-series were processed to remove features that were not evident of systematic trends in physiometry related to stress. For heart rate, circadian trends in time-series were removed. For swimming activity, the scaled (mean = 0; SD = 1) time-series were smoothed using a kernel smoother (using the *ksmooth* function in R; bandwidth = 1 h, kernel type = "box") to remove short-peaks in swimming activity.
- 2) Time-series were then partitioned using the *rpart* function of the *rpart* library in R. After an initial partitioning, fitted models were simplified using cost-complexity pruning (using the *prune.rpart* function). The optimal model was that with the largest number of partition breaks where the cross-validated error was at least one SD greater than the minimum cross validated error of the full model. Differences in mean rank blood parameters (plasma cortisol, glucose, lactate and osmolality) between the start, pre-stressing, post-stressing and recovery samples were determined using Kruskal-Wallis tests. Post-hoc analysis was done using pairwise Wilcoxon tests.

## 3. Results

The FFT analysis revealed a dominating variation in heart rate with a period of 24.0 h, showing a circadian variation with a peak to peak difference in heart rate of 4.53 beats per min (BPM) between day and night in the 7 days preceding stressing (Fig. 5). A similar circadian pattern was identified for the 7-day period before the end of the experiment, with a period of 24.0 h and a peak to peak day/night heart rate difference of 5.19 BPM.

The average baseline heart rate for all fish equipped with heart rate DSTs ( $N = 12$ ) in the 48 h prior to stressing was 24.2 BPM (SD = 2.3 BPM), while the average baseline swimming activity for all fish equipped with swimming activity DSTs ( $N = 4$ ) before normalization was  $0.48 \text{ m/s}^2$  (SD =  $0.12 \text{ m/s}^2$ ). Binary recursive partitioning showed that there were systematic changes in the average heart rate and swimming activity of the tagged fish throughout the study (Fig. 6). An immediate increase in heart rate occurred on initiation of the stressing period. From there, heart rate remained at an elevated level for 24.5 h, before returning to a level similar to that pre-stressing. There was not, however, a systematic increase in mean swimming activity immediately on commencement of the stressing period. Rather, mean swimming activity remained low for 2.4 h before showing a systematic increase. Mean swimming activity remained high for 16.2 h, before returning to a level similar to that pre-stressing. Heart rate remained at a systematically elevated level for 1.9 h after swimming activity has returned to a level similar to that pre-stressing. During the stress period four peaks in swimming activity corresponding to the points in time when stressing was initiated could be seen in the raw data for all fish equipped with activity tags as shown in Fig. 7.

Significant differences in blood parameter levels (Kruskal-Wallis test,  $p < 0.05$ ) existed according to when they were measured (Fig. 8). All measured blood parameters (plasma cortisol, lactate, glucose and osmolality) rose from initial low levels at the start of the experiment (Feb 18th) and pre-stressing (10:54 Hrs March 4th) to reach maximum levels immediately post-stressing (15:38 Hrs March 4th) (Table 1). Significant differences between pre- and post-stressing samples were observed for all parameters (Wilcoxon-test  $p < 0.05$ ), indicating a physiological response to treatment. Blood parameter levels sampled at the end of the experiment in the recovery period (March 14th) had

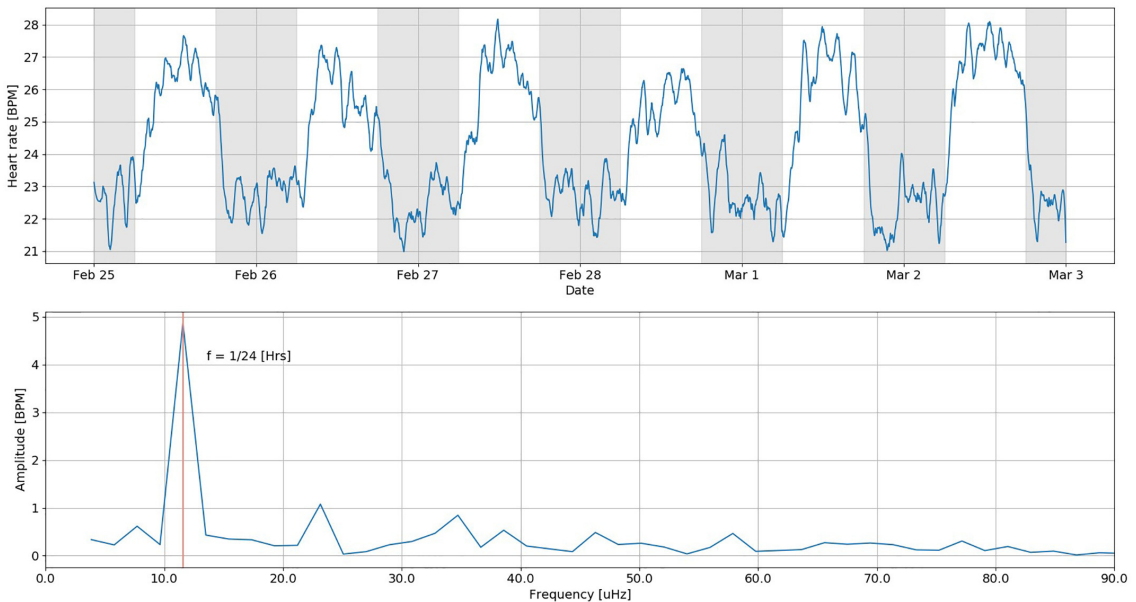


**Fig. 5.** Average heart rate (top) and the corresponding real, one-sided Fourier transform (bottom). For the average heart rate, night (18:00–06:00) is shaded grey. For the Fourier transform, frequency along the x-axis given in micro-Hertz ( $\mu\text{Hz}$ ). The highest peak (indicated by the vertical red line) resulting from the Fourier transform places the dominating variation in heart rate at 24.0 h (i.e. circadian). (For interpretation of the references to colour in this figure legend, the reader is referred to the web version of this article.)

fallen to levels similar to those at the start and pre-stressing samples (Table 1), indicating a physiological recovery.

#### 4. Discussion

The results from this experiment demonstrate that there are changes in heart rate and swimming activity in response to stress events that are consistent with blood proxies for stress levels in Atlantic salmon. The physiological responses of plasma cortisol, lactate, glucose and osmolality followed the treatment timeline by increasing post-stress and levelling off during recovery. The data types measured in this study are therefore candidates for indirect stress monitoring in free-swimming salmon. Since both tag types applied in the experiment have been used in industrial settings (Føre et al., 2018; Brijs et al., 2018), their application in commercial facilities might be considered a more objective and operational tool for monitoring fish stress than conventional approaches involving manual observation and blood sampling.

Several blood parameters were included in the analysis both to evaluate stress levels and how they can be related to heart rate and swimming activity.

Plasma cortisol measurements can provide useful information on the primary stress response in fish. Studies carried out by Iversen and Eliassen (2012) reported a link between high resting levels of plasma cortisol during commercial smolt production and mortality at plasma cortisol levels above 50 nM after transfer to seawater. Similar studies have shown that the normal resting levels of plasma cortisol in fish can be as low as 13.8 nM, while fish with a chronically activated stress response can have a resting level  $> 27.5$  nM (Maule et al., 1987; Pickering and Pottinger, 1989; Van Zwol et al., 2012; Noble et al., 2018). Similar to glucocorticoids (mainly cortisol), catecholamines (i.e. adrenalin and noradrenalin) also play a role in the primary stress response. But due to the difficulties associated with interpretation of catecholamines caused by their short half-life in circulation, they are of limited use as indicators of the primary stress response (Bonga, 1997,

2011) and have therefore been omitted from this study.

Lactate is produced by anaerobic ATP production (glycolysis) when oxygen is not available in sufficient amounts for the cells to utilise aerobic metabolism. The drivers behind this could be decreased oxygen levels in the water (Remen et al., 2012) or heavy physical exercise (Milligan and Girard, 1993). As lactate is primarily produced in muscle cells, it takes some time before it appears in blood and the response is delayed by a few hours after the event. In most cases the animal will recover after 6–12 h (Hatloy, 2015). The peak of plasma lactate during stressors such as transport and handling ranges from 6.4 to 13.3 mM (Hatloy, 2015; Iversen et al., 2003; Noble et al., 2018). Pre-stress levels of plasma lactate are normally between 3 and 5 mM (Carey and McCormick, 1998; Iversen et al., 2005). Elevations in plasma cortisol stimulate glycogenolysis which is the conversion of glycogen stored in the tissue to glucose released into the blood (Barton and Iwama, 1991).

Increased plasma glucose in the blood is a relatively slow response to a stressor and peaks after around 3–6 h in salmon (Olsen et al., 2003). In salmon, plasma glucose levels can increase to twice that of baseline levels 4 h after acute stress but can return to baseline levels much faster (2 h) in fasted fish than in fed fish. Pre-stress levels of plasma glucose are normally between 3.7 and 4.6 mM (Carey and McCormick, 1998; Skjervold et al., 2001).

In general, teleosts attempt to keep an osmolality of between 290 and 340 mOsm regardless of the surrounding salinity. Deviations from these levels for prolonged periods will result in mortality (McCormick et al., 2013). Arnesen et al. (1998) reported that typical osmolality in freshwater was approximately 320 mOsm, while osmolality ranged from 325 to 345 mOsm in seawater adapted Atlantic salmon. The selected blood parameters are therefore relevant when evaluating stress levels in fish.

Heart rate data showed an immediate response to induced stress through a significant increase that coincided with the stressing period implying that heart rate could serve as a sensitive and immediate stress indicator for salmon. In contrast, the swimming activity derived from

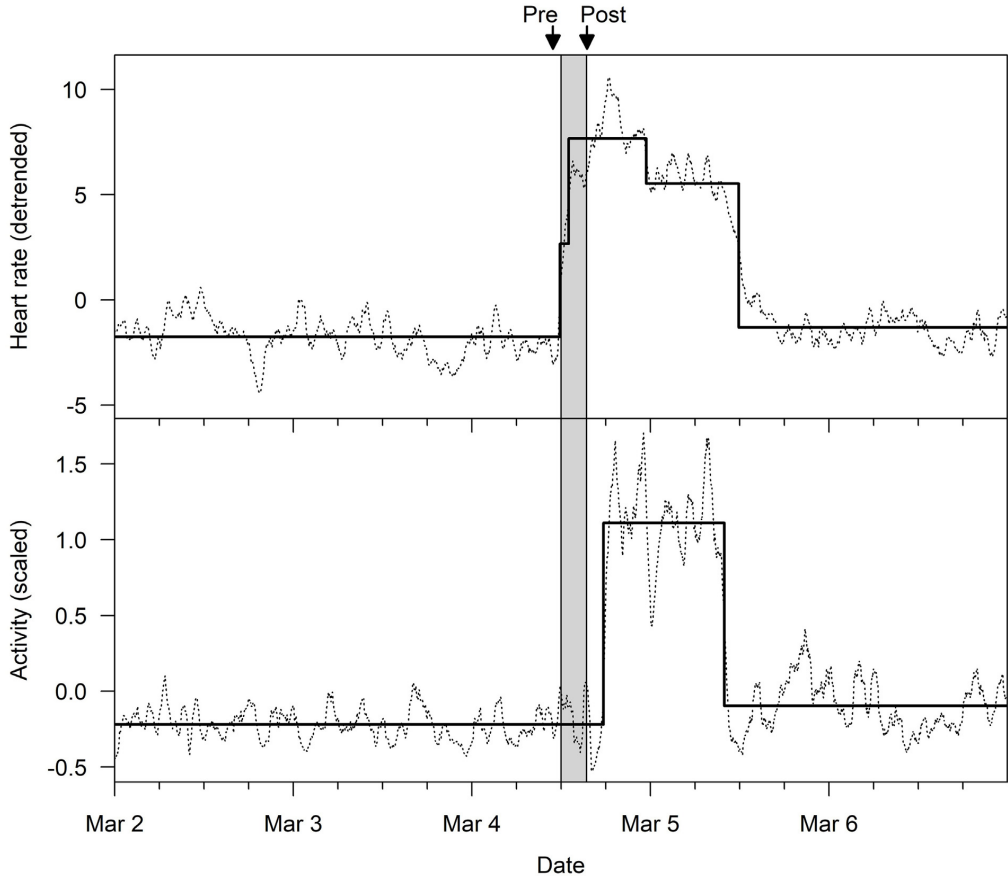


Fig. 6. Mean heart rate and mean activity partitions. Time-series are shown by dotted lines; partitions are shown by thick lines; the stress period is shown by the grey bar; the times of pre- and post-stressing blood samples in the reference group tanks are shown by dashed vertical lines. Time-series of heart rate have had circadian trends removed; time-series of activity have been smoothed and scaled.; time-series of heart rate have had circadian trends removed.

the accelerometers was low immediately after water levels were restored after stressing, a situation that lasted 2.4 h before swimming activity increased significantly to levels higher than before the stress period (Fig. 6). This was an unexpected result, as a previous study where salmon were subjected to crowding and delousing in a commercial cage found a gradual increase in swimming activity while the

fish were subjected to the stressor, and an immediate drop to lower levels as soon as they were released (Føre et al., 2018). A possible explanation for these dissimilar results could be that the four consecutive stress events in the present study drove the fish to a more complete state of exhaustion than the earlier cage-trials. The low swimming activity period could therefore represent a restitution period where the fish had

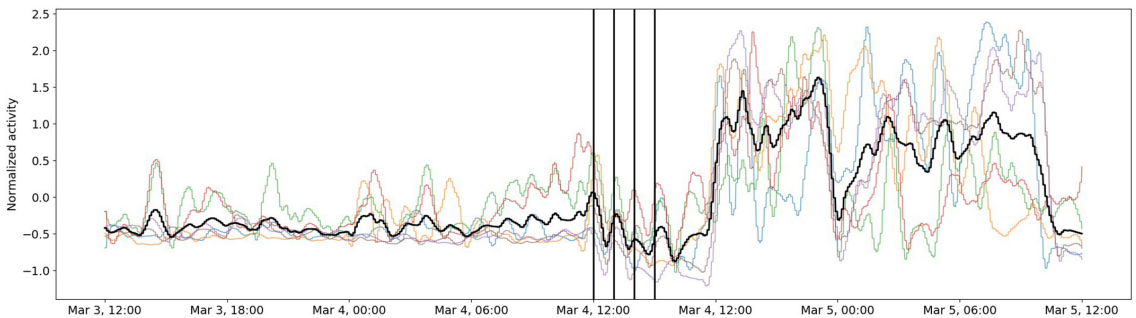
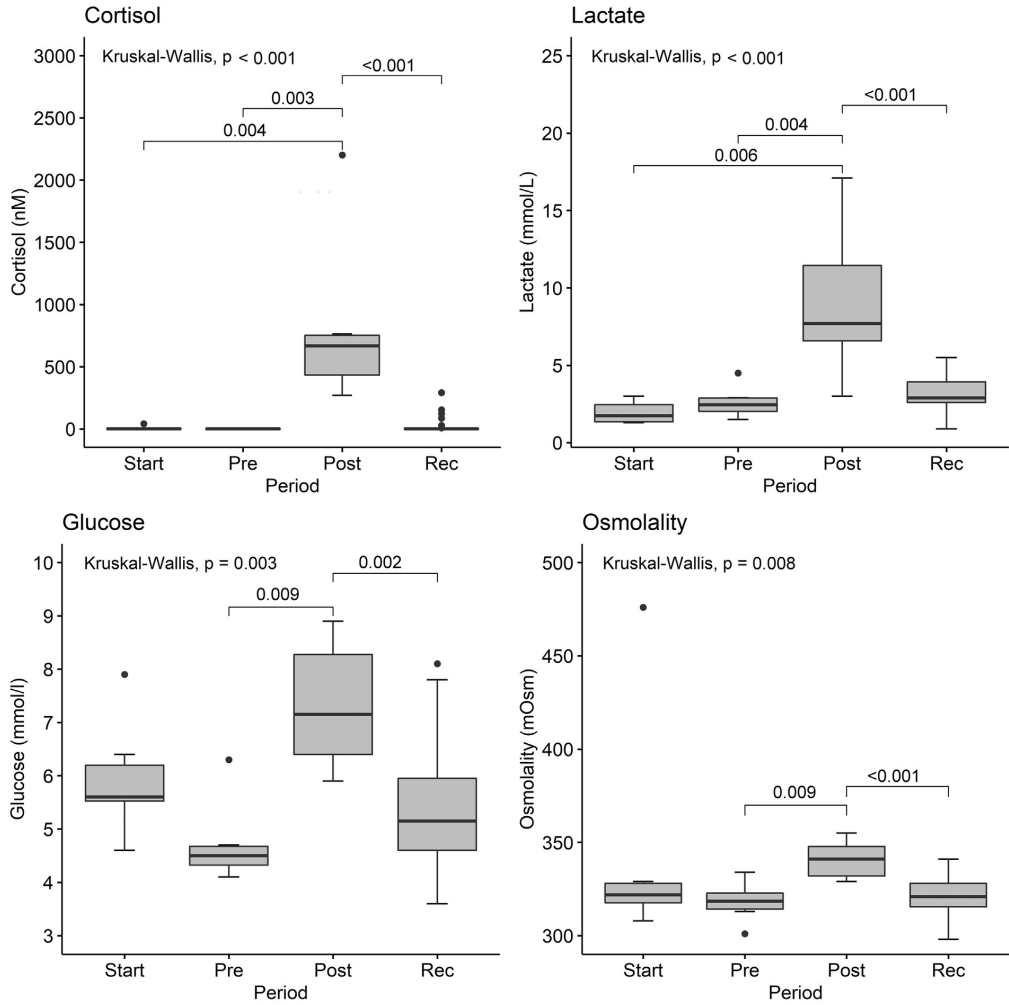


Fig. 7. Activity data for all fish during and post stressing with average activity shown by the solid black line. The vertical lines indicate the start time for each stressing.





**Fig. 8.** Blood properties (cortisol, lactate, glucose and osmolality) measured from fish at the start of the experiment (Start,  $N = 6$ ), pre-stressing (Pre,  $N = 6$ ), post-stressing (Post,  $N = 6$ ) and in recovery (Rec,  $N = 40$ ). Note that the total number of blood samples are 58 and not 60 as in the total number of fish due to the two males with agonistic behaviour dying the day before the conclusion of the experiment.

to recover physiologically before being able to express their behavioural/flight response to the stressors.

Results from this experiment were robust because all attempts were made to remove extraneous factors that could influence the results. The experimental tanks were located outdoors, meaning that external disturbances such as noise from local traffic, fauna and weather could be suspected to influence the data in inducing responses in the fish. However, it is unlikely that this had a strong effect on stress levels since

all fish used in these experiments had been reared in outdoor tanks at the same site from fry to adult fish and thus were likely accustomed to local ambient sounds. Furthermore, the crew on site ensured that regular tasks such as feeding and daily husbandry were conducted at approximately the same times each day and with the same duration thereby reducing the chance that they could affect the stress levels. Furthermore, the homogeneity in the diurnal cycle throughout the experiment (outside the stress period), indicates that the fish were well

**Table 1**  
Blood property values.

Date	Handling	Fish length (cm)	Plasma cortisol (nM)	Lactate (mM)	Glucose (mM)	Osmolality (mOsm)
February 2nd	Start	56.1 ± 5.9 (6)	8.5 ± 16.7	2.0 ± 1.0	5.9 ± 1.1	345.7 ± 64.3
March 4th	Pre-stressing	58.3 ± 4.3 (6)	1.7 ± 0.0	2.6 ± 1.1	4.7 ± 0.8	318.2 ± 11.0
March 4th	Post-stressing	58.9 ± 4.4 (6)	824.4 ± 702.1	9.1 ± 5.0	7.3 ± 1.2	340.8 ± 10.6
March 15th	Recovery	56.4 ± 3.1 (6)	27.0 ± 62.0	1.9 ± 0.7	5.4 ± 1.4	318.5 ± 11.2

habituated to their environment.

About half of the experimental fish reached sexual maturity during the trials. Two male fish kept in tank 3 (one tagged and one untagged individual) exhibited agonistic behaviour throughout the experimental period until they died the day before the conclusion of the experiment. Apart from this, the response patterns in the sensor measurements were similar across tanks, suggesting that the chosen data types are robust indicators of stress in salmon.

An approved anaesthetic was used for surgery and used in the recommended dosage by experienced personnel. As shown by Føre et al. (2019), the heart rate and swimming activity levels for fish having undergone surgery stabilises after 6 days. It is therefore likely that no adverse effects were introduced by either anaesthesia or surgery.

Due to the low temperature during the study ( $4.2 \pm 0.2$  °C), it was expected that all biological processes were slower than they would have been compared to higher temperatures. This may have had an impact on e.g. the fish's timely response to the stressors. Blood properties (Table 1), however, show the expected changes to stress. Posthumous examination and dissection revealed no signs of poor wound healing or infection. Hence, the impact of water temperature on the overall results could be negligible.

The carefully controlled conditions caused similar responses among tagged individuals, such that it was possible to identify the effect of stress despite the small sample size. Heart rate and activity responses were consistent across most tags, involving an immediate increase in heart rate and a delayed increase in activity, followed by a period of high heart rate and activity, after which levels declined to those pre-stress. This pattern was absent in only one heart rate tag (Fish 7, 1CHL0310; Fig. 11 in supplementary material) and one activity tag (Fish 11, 1CAL0165, Fig. 15 in supplementary material). Likewise, the controlled conditions allowed for identification of significant differences in blood parameter levels according to sample period. It is possible that an increased sample size will have provided a better indication of changes in blood parameters. For example, no significant difference in either glucose or osmolality was identified between the blood samples taken at the start of the experiment and those taken post-stressing. This lack of a significant difference was caused by a single outlier value for each of glucose and osmolality, and a greater sample size would have helped identify whether there was a systematic difference in parameter values between these sample periods.

The main reason for the slight variations in the swimming activity results between co-located Thelma Biotel and Star-Oddi tags (Fig. 7) was probably that the tags were located in different positions within the peritoneal cavity and would thus have experienced different accelerations due to fish movements. For the Thelma tags, which were not anchored using a suture (Føre et al., 2019), shifts in the tag's position within the peritoneal cavity could also result in transients not seen in Star-Oddi data. An additional source for these differences between tag types may also lie in that key components in the tags (e.g. the accelerometer) were not identical between types.

To further investigate the links between heart rate, swimming activity and stress response, at least two options for further work are considered. One is to gain a more detailed understanding of the responses by doing swim respirometer trials with cannulated fish in controlled laboratory conditions. The other is to increase scale and repeat the experiment in meso- or full scale to approach an industrial setting and application.

Supplementary data to this article can be found online at <https://doi.org/10.1016/j.aquaculture.2020.735804>.

## Funding

This study was funded by the Research Council of Norway (RCN) through the project SalmonInsight (RCN project number 280864).

## Declaration of Competing Interest

No competing interests are declared.

## Acknowledgements

We would like to thank the crew at NINA's research station at Ims, particularly Knut Bergesen. We would also like to thank Erik Høy at Thelma Biotel AS and Asgeir Bjarnason at Star Oddi LTD for collaboration in specifying the acoustic tags and DSTs used in the study.

## References

- Animal Welfare Act, 2009. Available at: <https://www.regjeringen.no/en/dokumenter/animal-welfare-act/id571188/> (Accessed 10.12.2019).
- Arnesen, A.M., Johnsen, H.K., Mortensen, A., Jobling, M., 1998. Acclimation of Atlantic salmon (*Salmo salar* L.) smolts to 'cold' sea water following direct transfer from fresh water. *Aquaculture* 168, 351–367. [https://doi.org/10.1016/S0044-8486\(98\)00361-5](https://doi.org/10.1016/S0044-8486(98)00361-5).
- Barton, B.A., Iwama, G.K., 1991. Physiological changes in fish from stress in aquaculture with emphasis on the response and effects of corticosteroids. *Annu. Rev. Fish Dis.* 1, 3–26. [https://doi.org/10.1016/0959-8030\(91\)90019-G](https://doi.org/10.1016/0959-8030(91)90019-G).
- Bjelland, H.V., Føre, M., Lader, P., Kristiansen, D., Holmen, I.M., Fredheim, A., Grøtli, E.I., Fathi, D.E., Oppedal, F., Utne, I.B., Schjølberg, I., 2015. Exposed aquaculture in Norway. In: OCEANS 2015-MTS/IEEE Washington, pp. 1–10. <https://doi.org/10.23919/OCEANS.2015.7404486>.
- Bleie, H., Skrudland, A., 2014. Tap av Laksefisk i sjø. (Report from the Norwegian Food Safety Authority). Available at: [https://www.mattilsynet.no/fisk\\_og\\_akvakultur/fiskevelferd/tap\\_av\\_laksefisk\\_i\\_sjo.2014.15430/binary/Tap%20av%20laksefisk%20i%20sj%C3%B8%20](https://www.mattilsynet.no/fisk_og_akvakultur/fiskevelferd/tap_av_laksefisk_i_sjo.2014.15430/binary/Tap%20av%20laksefisk%20i%20sj%C3%B8%20) (Accessed 04.05.2020).
- Bonga, S.W., 1997. The stress response in fish. *Physiol. Rev.* 77 (3), 591–625. <https://doi.org/10.1152/physrev.1997.77.3.591>.
- Bonga, S.W., 2011. Hormonal responses to stress. In: Anthony, P.F. (Ed.), *Encyclopaedia of Fish Physiology*. Academic Press, San Diego, USA, pp. 1515–1523.
- Brijs, J., Sandblom, E., Axelsson, M., Sundell, K., Sundh, H., Huyben, D., Broström, R., Kiessling, A., Berg, C., Gräns, A., 2018. The final countdown: continuous physiological welfare evaluation of farmed fish during common aquaculture practices before and during harvest. *Aquaculture* 495, 903–911. <https://doi.org/10.1016/j.aquaculture.2018.06.081>.
- Brijs, J., Sandblom, E., Rosengren, M., Sundell, K., Berg, C., Axelsson, M., Gräns, A., 2019. Prospects and pitfalls of using heart rate bio-loggers to assess the welfare of rainbow trout (*Oncorhynchus mykiss*) in aquaculture. *Aquaculture* 509, 188–197. <https://doi.org/10.1016/j.aquaculture.2019.05.007>.
- Carey, J.B., McCormick, S.D., 1998. Atlantic salmon smolts are more responsive to an acute handling and confinement stress than parr. *Aquaculture* 168, 237–253. [https://doi.org/10.1016/S0044-8486\(98\)00352-4](https://doi.org/10.1016/S0044-8486(98)00352-4).
- Directorate of Fisheries, 2019. Uttak av slaktet fisk fordelt på art 2005–2019 (Fylke). Available at: <https://www.fiskeridir.no/content/download/8957/109341/version/183/file/biostat-uttak01-flk-20190516.xlsx> (Accessed 27.05.2019).
- Føre, M., Frank, K., Dempster, T., Alfreidsen, J.A., Høy, E., 2017. Biomonitoring using tagged sentinel fish and acoustic telemetry in commercial salmon aquaculture: a feasibility study. *Aquac. Eng.* 78, 163–172. <https://doi.org/10.1016/j.aquaeng.2017.07.004>.
- Føre, M., Svendsen, E., Alfreidsen, J.A., Uglem, I., Bloecher, N., Sveier, H., Sunde, L.M., Frank, K., 2018. Using acoustic telemetry to monitor the effects of crowding and delousing procedures on farmed Atlantic salmon (*Salmo salar*). *Aquaculture* 495, 757–765. <https://doi.org/10.1016/j.aquaculture.2018.06.060>.
- Føre, M., Frank, K., Norton, T., Svendsen, E., Alfreidsen, J.A., Dempster, T., Eguiraun, H., Watson, W., Stahl, A., Sunde, L.M., Schellewale, C., 2018a. Precision fish farming: a new framework to improve production in aquaculture. *Biosyst. Eng.* 173, 176–193. <https://doi.org/10.1016/j.biosystemseng.2017.10.014>.
- Føre, M., Svendsen, E., Økland, F., Gräns, A., Alfreidsen, J.A., Finstad, B., Uglem, I., 2019. Heart rate as an Indicator of post-surgical recovery time of Atlantic Salmon (*Salmo Salar*). *An. Biotelemet.* <https://doi.org/10.21203/rs.3.rs-23506/v1>. In review.
- Hatloy, T., 2015. Effekten av akutt allostatisk belastning på hypothalamus –hypofyse – interrenal akselen, og dets betydning på dyrevelferden hos diploid og triploid atlantisk laksesmolt (*Salmo salar* L.). M.sc thesis. Nord University, Bodo, Norway.
- Hjeltnes, B., Bang Jensen, B., Bornø, G., Haukaas, A., Walde, C.S., 2018. Fiskehelsesrapporten 2018. Norwegian Veterinary Institute report no. 6a-2019 Available at: <https://www.vetinst.no/rapporter-og-publikasjoner/rapporter/2019/fiskehelsesrapporten-2018> (accessed 04.05.2020).
- Huber, P.J., 1981. *Robust Statistics*. John Wiley and Sons, Inc, New York.
- Iversen, M., Eliassen, R., 2012. Stressovervåking av settefiskproduksjonen i Mainstream Norway AS 2009–2011. Stresskartlegging av laksesmolt (Salmo salar L.), og effekten av stressreducerende tiltak på stressnivå, dyrevelferd og produksjonsresultatet. (UIN-report no. 05/2012).
- Iversen, M., Finstad, B., Nilssen, K.J., 1998. Recovery from loading and transport stress in Atlantic salmon (*Salmo salar* L.) smolts. *Aquaculture* 168, 387–394. [https://doi.org/10.1016/S0044-8486\(98\)00364-0](https://doi.org/10.1016/S0044-8486(98)00364-0).
- Iversen, M., Finstad, B., McKinley, R.S., Eliassen, R.A., 2003. The efficacy of metomidate, clove oil, AQUI-S (TM) and Benzocain (R) as anaesthetics in Atlantic salmon (*Salmo*

- salar* L.) smolts, and their potential stress-reducing capacity. *Aquaculture* 221, 549–566. [https://doi.org/10.1016/S0044-8486\(03\)00111-X](https://doi.org/10.1016/S0044-8486(03)00111-X).
- Iversen, M., Finstad, B., McKinley, R.S., Eliassen, R.A., Carlsen, K.T., Evjen, T., 2005. Stress responses in Atlantic salmon (*Salmo salar* L.) smolts during commercial well boat transports, and effects on survival after transfer to sea. *Aquaculture* 243, 373–382. <https://doi.org/10.1016/j.aquaculture.2004.10.019>.
- Johansson, D., Ruohonen, K., Juell, J.E., Oppedal, F., 2009. Swimming depth and thermal history of individual Atlantic salmon (*Salmo salar* L.) in production cages under different ambient temperature conditions. *Aquaculture* 290 (3–4), 296–303. <https://doi.org/10.1016/j.aquaculture.2009.02.022>.
- Leys, C., Ley, C., Klein, O., Bernard, P., Licata, L., 2013. Detecting outliers: do not use standard deviation around the mean, use absolute deviation around the median. *J. Exp. Soc. Psychol.* 49 (4), 764–766. <https://doi.org/10.1016/j.jesp.2013.03.013>.
- Lucas, M.C., 1994. Heart rate as an indicator of metabolic rate and activity in adult Atlantic salmon, *Salmo salar*. *J. Fish Biol.* 44 (5), 889–903. <https://doi.org/10.1111/j.1095-8649.1994.tb01262.x>.
- Maule, A.G., Schreck, C.B., Kaattari, S.L., 1987. Changes in the immune system of coho salmon (*Oncorhynchus kisutch*) during the parr-to-smolt transformation and after implantation of cortisol. *Can. J. Fish. Aquat. Sci.* 44, 161–166. <https://doi.org/10.1139/f87-021>.
- McCormick, S.D., Farrell, A.P., Brauner, C.J. (Eds.), 2013. *Fish Physiology: Euryhaline Fishes*. Vol. 32 Academic Press.
- Miller, J., 1991. Reaction time analysis with outlier exclusion: Bias varies with sample size. *Q. J. Exp. Psychol.* 43 (4), 907–912. <https://doi.org/10.1080/14640749108400962>.
- Milligan, C.L., Girard, S.S., 1993. Lactate metabolism in rainbow trout. *J. Exp. Biol.* 180, 175–193.
- Noble, C., Gismervik, K., Iversen, M.H., Kolarevic, J., Nilsson, J., Stien, L.H., Turnbull, J.F., 2018. Welfare Indicators for farmed Atlantic salmon: tools for assessing fish welfare. (NOFIMA report, ISBN 978–82–8296–556–9). Available at: <https://nofima.no/wp-content/uploads/2018/11/FISHWELL-Welfare-indicators-for-farmed-Atlantic-salmon-November-2018.pdf> (Accessed 04.05.2020).
- Norwegian Food Safety Authority, 2018. Årsrapport. pp. 2018. Available at: [https://www.mattilsynet.no/om\\_mattilsynet/mattilsynets\\_aarsrapport\\_2018.34249](https://www.mattilsynet.no/om_mattilsynet/mattilsynets_aarsrapport_2018.34249) Accessed 04.05.2020.
- Olafsen, T., Winther, U., Olsen, Y., Skjermo, J., 2012. Verdiskaping basert på produktive hav i 2050. (Report published by Det Kongelige Norske Videnskabers selskab). Available at: [https://www.sintef.no/globalassets/upload/fiskeri\\_og\\_havbruk/publikasjoner/verdiskaping-basert-pa-produktive-hav-i-2050.pdf](https://www.sintef.no/globalassets/upload/fiskeri_og_havbruk/publikasjoner/verdiskaping-basert-pa-produktive-hav-i-2050.pdf) (Accessed 04.05.2020).
- Olsen, R.E., Sundell, K., Hansen, T., Hemre, G.-I., Myklebust, R., Mayhew, T.M., Ringø, E., 2003. Acute stress alters the intestinal lining of Atlantic salmon, *Salmo salar* L.: an electron microscopical study. *Fish Physiol. Biochem.* 26, 211–221.
- Pickering, A.D., Pottinger, T.G., 1989. Stress responses and disease resistance in salmonid fish: effects of chronic elevation of plasma cortisol. *Fish Physiol. Biochem.* 7, 253–258.
- Remen, M., Oppedal, F., Torgersen, T., Innsland, A.K., Olsen, R.E., 2012. Effects of cyclic environmental hypoxia on physiology and feed intake of post-smolt Atlantic salmon: initial responses and acclimation. *Aquaculture* 326, 148–155. <https://doi.org/10.1016/j.aquaculture.2011.11.036>.
- Selye, H., 1973. The evolution of the stress concept: the originator of the concept traces its development from the discovery in 1936 of the alarm reaction to modern therapeutic applications of syntoxic and catatoxic hormones. *Am. Sci.* 61 (6), 692–699.
- Shieh, A.C.R., Petrell, R.J., 1998. Measurement of fish size in Atlantic salmon (*Salmo salar* L.) cages using stereographic video techniques. *Aquac. Eng.* 17 (1), 29–43. [https://doi.org/10.1016/S0144-8609\(97\)00012-5](https://doi.org/10.1016/S0144-8609(97)00012-5).
- Skjervold, P.O., Fjæra, S.O., Østby, P.B., Einen, O., 2001. Live-chilling and crowding stress before slaughter of Atlantic salmon (*Salmo salar*). *Aquaculture* 192, 265–280. [https://doi.org/10.1016/S0044-8486\(00\)00447-6](https://doi.org/10.1016/S0044-8486(00)00447-6).
- Stehfest, K.M., Carter, C.G., McAllister, J.D., Ross, J.D., Semmens, J.M., 2017. Response of Atlantic salmon *Salmo salar* to temperature and dissolved oxygen extremes established using animal-borne environmental sensors. *Sci. Rep.* 7 (1), 4545.
- Thorstad, E.B., Rikardsen, A.H., Alp, A., Økland, F., 2013. The use of electronic tags in fish research—an overview of fish telemetry methods. *Turk. J. Fish. Aquat. Sci.* 13 (5), 881–896. [https://doi.org/10.4194/1303-2712-v13\\_5\\_13](https://doi.org/10.4194/1303-2712-v13_5_13).
- Van Zwol, J.A., Neff, B.D., Wilson, C.C., 2012. The influence of non-native salmonids on circulating hormone concentrations in juvenile Atlantic salmon. *Anim. Behav.* 83 (1), 119–129. <https://doi.org/10.1016/j.anbehav.2011.10.015>.
- Vignon, M., 2015. Extracting environmental histories from sclerochronological structures - recursive partitioning as a mean to explore multi-elemental composition of fish otolith. *Ecol. Informatics* 30, 159–169. <https://doi.org/10.1016/j.ecoinf.2015.10.002>.
- Wells, R.M.G., Pankhurst, N.W., 1999. Evaluation of simple instruments for the measurement of blood glucose and lactate, and plasma protein as stress indicators in fish. *J. World Aquacult. Soc.* (2), 276–284. <https://doi.org/10.1111/j.1749-7345.1999.tb00876.x>.
- Zwillinger, D. (Ed.), 2007. *Table of Integrals, Series, and Products*. Academic Press, Inc, New York.



## Paper B

Heart rate and swimming activity as indicators of post-surgical recovery time of Atlantic salmon (*Salmo salar*)

Paper B

*Heart rate and swimming activity as indicators of post-surgical recovery  
time of Atlantic salmon (*Salmo salar*)*

---

TELEMETRY CASE REPORT

Open Access



# Heart rate and swimming activity as indicators of post-surgical recovery time of Atlantic salmon (*Salmo salar*)

M. Føre<sup>1,2\*</sup> , E. Svendsen<sup>1,2</sup>, F. Økland<sup>3</sup>, A. Gräns<sup>4</sup>, J. A. Alfredsen<sup>2</sup>, B. Finstad<sup>3,5</sup>, R. D. Hedger<sup>3</sup> and I. Uglem<sup>3</sup>

## Abstract

**Background:** Fish telemetry using electronic transmitter or data storage tags has become a common method for studying free-swimming fish both in the wild and in aquaculture. However, fish used in telemetry studies must be handled, anaesthetised and often subjected to surgical procedures to be equipped with tags, processes that will shift the fish from their normal physiological and behavioural states. In many projects, information is needed on when the fish has recovered after handling and tagging so that only the data recorded after the fish has fully recovered are used in analyses. We aimed to establish recovery times of adult Atlantic salmon (*Salmo salar*) after an intraperitoneal tagging procedure featuring handling, anaesthesia and surgery.

**Results:** Based on ECG and accelerometer data collected with telemetry from nine individual Atlantic salmon during the first period after tagging, we found that heart rate was initially elevated in all fish and that it took an average of  $\approx 4$  days and a maximum of 6 days for heart rate to return to an assumed baseline level. One activity tag showed no consistent decline in activity, and two others did not show strong evidence of complete recovery by the end of the experiment: baseline levels of the remaining tags were on average reached after  $\approx 3.3$  days.

**Conclusion:** Our findings showed that the Atlantic salmon used in this study required an average of  $\approx 4$  days, with a maximum interval of 6 days, of recovery after tagging before tag data could be considered valid. Moreover, the differences between recovery times for heart rate and activity imply that recovery time recommendations should be developed based on a combination of indicators and not just on e.g. behavioural observations.

**Keywords:** Fish telemetry/biologging, Atlantic salmon, Post-tagging recovery, Heart rate, Swimming activity

## Background

Fish telemetry/biologging is a method of monitoring free-swimming fish where individual animals are equipped with electronic tags that often contain sensors for collecting data on the conditions within or near the fish [1, 2]. Such tags may either be transmitter tags transferring data wirelessly to the user (see [3] for details on the structure of an electronic transmitter tag) or data storage/archival

tags (DSTs) that store data in internal storage mediums accessible only after the fish (and tag) has been recaptured [2]. Irrespective of tag type, most studies using such methods aim to assess the status of wild fish in ecological settings (e.g. [4, 5]), to evaluate how fish communities respond to man-made structures (e.g. [6]), or as a tool to provide knowledge for fisheries management (reviewed by [7]). The interest in using this approach in aquaculture is also increasing, both because ongoing technological advances are rapidly expanding the possibilities [8], and because new production philosophies such as Precision Fish Farming promote monitoring at an individual level [9]. Example uses of telemetry/biologging in aquaculture

\*Correspondence: martin.fore@ntnu.no

<sup>1</sup> Department of Engineering Cybernetics, Norwegian University of Science and Technology, 7491 Trondheim, Norway

Full list of author information is available at the end of the article



© The Author(s) 2021. This article is licensed under a Creative Commons Attribution 4.0 International License, which permits use, sharing, adaptation, distribution and reproduction in any medium or format, as long as you give appropriate credit to the original author(s) and the source, provide a link to the Creative Commons licence, and indicate if changes were made. The images or other third party material in this article are included in the article's Creative Commons licence, unless indicated otherwise in a credit line to the material. If material is not included in the article's Creative Commons licence and your intended use is not permitted by statutory regulation or exceeds the permitted use, you will need to obtain permission directly from the copyright holder. To view a copy of this licence, visit <http://creativecommons.org/licenses/by/4.0/>. The Creative Commons Public Domain Dedication waiver (<http://creativecommons.org/publicdomain/zero/1.0/>) applies to the data made available in this article, unless otherwise stated in a credit line to the data.

include studies to assess fish responses during welfare-critical operations such as crowding (e.g. [10]) and transport (e.g. [11]), and responses to environmental variability such as temperature variations (e.g. [12]).

In animal monitoring, it is essential to ensure that the observed animals are representative of the targeted population. When using telemetry, the fish selected for tagging must therefore be representative both before and after the tags are deployed. Ideally, this means that the selection of fish should be truly random and representative and that the tags do not influence physiology or behaviour in such a way that the tagged fish differ significantly from untagged fish (e.g. [13]). In addition, tagging procedures include several steps (e.g. handling, anaesthesia and surgical procedures) that may induce stress, that in turn may lead to physiological and/or behavioural changes in the fish [2, 14–17]. Acute (short term) followed by chronic (long term) stress in farmed fish may lead to undesirable effects such as reduced disease resistance, reduced growth rates, impaired health, and increased mortality [18–21]. Stress responses in fish are described by primary responses that include the release of stress hormones such as catecholamines and cortisol into the circulation system, followed by secondary responses such as changes in glucose levels, electrolyte balance and heart rate and, finally tertiary (whole animal) responses. If the fish is unable to acclimate to the stressor at this stage, effects such as behavioural changes, decreased reproductive capacity and growth may occur, sometimes even resulting in that the animal dies (see [22] and references therein). If such changes are chronic, the fish cannot be considered representative of the population and should be excluded from further analyses [1, 23]. Conversely, if the changes are transient, the fish may be considered fully recovered once the response patterns return to those expected from an untagged fish. This means that tagged fish can be used in analyses if the data from the period of recovery are excluded. However, this also raises the question: how can we define when a fish is properly recovered after a tagging procedure?

Jepsen et al. [16] sought to identify the duration of post-surgery recovery for Chinook salmon (*Oncorhynchus tshawytscha*) by studying changes in commonly used blood indicators of the primary (cortisol) and secondary (glucose and lactate) stress responses in teleosts. The authors found that all measured parameters decreased from initially elevated levels to within normal ranges within 7 days post-surgery, with glucose and lactate (substrate and by-product, respectively, of elevated anaerobic metabolism) normalising during the first 24 h, a recovery time resembling that seen in several studies (e.g. [24, 25]). Coping with stress is also an energy-demanding process [26] and one of the most

common indicators of metabolic effects due to stress is the increase in plasma glucose concentration [22]. Such changes have recently been shown to lead to increased heart rates also in fish [27]. Other studies have aimed to evaluate post-surgery recovery by comparing the behaviour of the tagged fish to their behaviour before surgery or in untagged cohabitant fish. This method has for instance been applied in laboratory experiments with tilapia (*Tilapia* sp.) who appeared fully recovered 24 h post-surgery after displaying loss of equilibrium and reduced swimming activity and feeding just after tagging [17]. Swimming activity was then assessed by measuring the posture of the fish, and presented as the percentage of the time the fish was resting (assuming an oblique angle with the snout towards the surface) or actively swimming (horizontal orientation or snout pointing toward the bottom).

Recovery after tagging may also be studied with sensor telemetry. The information conveyed by the tag must then reflect the state of the fish, and typical sensor values for unstressed fish should be available as a baseline for comparison. Previous studies using this approach include using heart rate tags to compare tagging methods for black cod (*Paranotothenia angustata*, [14]), and more recently to study post-surgery stress-responses [28] and potential effects of antibiotics on post-surgical recovery [29] in rainbow trout (*O. mykiss*). While Brijis et al. [28] implied a recovery from surgical implantation > 72 h, Hjelmstedt et al. [29] demonstrated a decrease in heart rate to within baseline levels 72–96 h after anaesthesia and surgery. Other sensor measurements that could potentially be used in this way include tri-axial accelerometers, as previous studies have identified links between accelerometer-based activity proxies that are particularly sensitive to tail beat frequency and amplitude and orientation changes, and stress in salmon [10, 30].

Although Atlantic salmon (*Salmo salar*) has been frequently studied using telemetry, there is still a lack of detailed quantitative information on the post-surgery recovery of this species. We, therefore, sought to identify the recovery time of Atlantic salmon after intraperitoneal tagging. This was done using heart rate and acceleration data collected using intraperitoneally implanted electronic tags, meaning that data could be collected without introducing the additional handling stress that would accompany other methods such as blood sampling. The parameters were chosen because they have previously been found to be linked with stress (e.g. [10, 28, 31]) and welfare [32] in salmonids and are commercially available in archival and telemetry tags. The data were collected in a controlled experiment in tanks studying how stress responses in Atlantic salmon can be measured using state-of-the-art technology. The stress response part of

this experiment is described in greater detail by Svendsen et al. [27].

**Materials and methods**

**Experimental site and fish**

The experiments were conducted at the NINA Ims Research Station near Stavanger, Norway, between January and March 2019, using 60 hatchery-reared adult Atlantic salmon of the Aqua Gen strain (mean  $55.5 \pm \text{stdev } 5.7$  cm fork length, mean weight 2100 g). The experiment started on January 28th by stocking four square tanks (tank 1–4, 215 cm side, 122 cm depth, 5600 L) with seven fish each. The fish were then allowed to habituate to the tanks for a period of 21 days until February 18th when three fish in each of tanks 1–4 were selected at random and equipped with tags, resulting in 12 tagged fish in total (Table 1).

The tanks were set up with flow-through configuration, with filtered fresh water from the nearby Imsa river mixed with small amounts (3–6 ppt, average 5 ppt) of seawater supplied from seawater inlets at 30 m depth to ensure a stable and homogeneous water quality and avoid the introduction of parasites and pathogens to the tanks. Consequently, tank water properties followed the ambient conditions in the river, temperatures increasing from 3.9 to 5.0 °C and with DO varying between 93.8 and 101.2% between the start and end of the experiment (March 15th). Oxygen sensors and oxygenation were also used to prevent unfavourable DO levels. The fish were fed once per day between 08:00 and 10:00 in the morning throughout the entire experimental period, with each meal consisting of 2 dL tank<sup>-1</sup> (Skretting Røye Vitalis

600-60A 7 mm pellets). The fish were not subjected to any fasting during the experiment period.

**Biotelemetry/logging systems and surgical procedures**

All 12 tagged fish (Table 1) were equipped with one of three different types of heart rate monitoring Data Storage Tags (DSTs, Star Oddi Ltd.): 4 × DST milli-HRT (39.5 × 13 mm, 11.8 g in air); 4 × DST centi-HRT (46 × 15 mm, 19 g); 4 × DST centi-HRT ACT (46 × 15 mm, 19 g). Using different DST types rather than equipping all fish with the same tag types allowed us to also investigate whether all three tag varieties would be suitable for experiments with Atlantic salmon, which is relevant because this is one of the first applications of this technology on this species. Furthermore, since all three tag types were from the same provider, contained the same type of heart rate sensor and comparable sampling frequencies (80 Hz over 7.5 s per HR sample point for the centi tags and 100 Hz over 15 s per HR sample point for the milli tags), and applied the same post-processing methods to the resulting data, they provided heart rate data sets that were comparable among tags. The milli-HRT type was set with a higher sample storage interval (10 min) than the others (5 min) as they used more of their internal storage medium for raw ECG traces. All data were timestamped using the tag internal clocks to facilitate comparison, and eventual clock drift between individual clocks was negligible compared to the time scale of the experiment. One tag type (DST centi-HRT ACT) also measured activity using an embedded tri-axial accelerometer (1 Hz sampling rate).

In addition to the DSTs that were applied, a total of 4 tagged fish (two fish each from tanks 1 and 2, Table 1)

**Table 1 Information about the tagged individuals used in the study**

Fish #	Body length (cm)	Est. body weight (kg)	Tank	DST type	Acoustic tag	Time anaesthesia (mm:ss)	Time surgery (mm:ss)	Sex	Mature
F1	59.5	2.3	1	centi HRT	X	08:00	08:03	F	
F2	52	1.6	1	centi HRT	X	08:20	08:12	F	
F3	57	2.1	1	milli HRT		08:45	06:31	F	
F4	63	2.8	2	centi HRT ACT	X	08:06	06:30	M	x
F5	53	1.7	2	centi HRT ACT	X	08:30	06:50	F	x
F6	53	1.7	2	milli HRT		07:30	06:00	M	
F7	74	4.5	4	centi HRT ACT		07:40	07:00	F	
F8	67	3.3	4	centi HRT ACT		08:00	06:30	M	x
F9	55	1.9	4	milli HRT		08:10	08:00	M	
F10	62.5	2.7	3	centi HRT		05:30	07:00	M	x
F11	61.5	2.6	3	centi HRT		07:00	06:30	F	
F12	55	1.9	3	milli HRT		07:00	06:50	F	x

Individual body weight was not measured and was hence estimated using an allometric model ( $W = aL^b$ ) with  $a = 0.0142$  and  $b = 2.9401$

were fitted with acoustic tags (A MP-9,  $24.4 \times 9$  mm, 3.6 g; Thelma Biotel AS) that contained tri-axial accelerometers (5 Hz sampling rate) and transmitted an activity proxy derived from the accelerometer measurements every 40 s. These tags compute the proxy by first high pass filtering the accelerations from all three axes using a cutoff frequency of 0.2 Hz to remove low-frequency acceleration components due to gravity and body orientation. The remaining high-frequency components then mainly contain accelerations caused by features related to bodily movement that are of interest when evaluating activity levels, such as tail beats (frequency and amplitude) and rapid changes in attitude/orientation. The Euclidian norm of the three high pass filtered accelerometer axes is then computed to yield the magnitude of the total high pass filtered 3D acceleration sensed by the accelerometer. Although Føre et al. [10] used the same activity proxy with a maximum value of  $3.465 \text{ m s}^{-2}$ , we chose to limit the proxy to  $0\text{--}2.1 \text{ m s}^{-2}$  in our study as this gave us a higher resolution and hence precision for the activity measures. Moreover, Føre et al. [10] observed very few activity values above  $2 \text{ m s}^{-2}$  in Atlantic salmon during stressing, implying that using a lower range would not compromise the ability to capture the dynamics associated with salmon swimming activity. To be comparable with the data from the acoustic tags, the activity data from the centi-HRT ACT DSTs were analysed similarly by applying filtering and computing the Euclidian norm as explained for the acoustic tags (see [27] for more details). Adding the acoustic tags thus allowed us to compare their activity proxies with those based on the acceleration data from the DSTs and resulted in that the

experiment produced 12 data sets on heart rate, and 8 data sets on swimming activity. With mean fish weight being 2100 g and a maximum total tag weight carried by an individual at 22.6 g (DST centi-HRT + A MP-9) the tag vs. fish weight ratio of all fish were well within the informal rule of thumb of 2% for maximum tag mass relative to fish mass [2].

Each tag implantation was started by capturing a random fish from an experiment tank using a knotless dip net and immediately transferring it to an anaesthetic bath (Benzoak Vet, 70 mg/L) where the fish was kept until it lost its equilibrium and stage III anaesthesia [33] was reached (average time 7.7 min). The fish was then carefully placed with its ventral side up on a specialised surgical table with a v-shaped mid-section designed such that the head of the fish was immersed in water throughout the whole procedure. A hose circulating anaesthetic (Benzoak Vet, 35 mg/L) through the orobranchial cavity of the fish was inserted into its mouth and the head was covered by a moist cloth (Fig. 1).

A 2–3 cm incision was made along the sagittal plane starting slightly more than one tag length (i.e. the length of the tag to be implanted) posterior from the transverse pericardial septum.

A finger was inserted through the incision to locate the transverse pericardial septum. While retaining the finger inside the peritoneal cavity for support, a needle was positioned in the skin just posterior to the transverse septum and slightly laterally from the sagittal plane. The finger was withdrawn, and a smooth plastic spoon inserted through the incision until it was just below the needle insertion point. The needle was then pushed



**Fig. 1** Fish in the surgical table with anaesthetic circulation tube and head cover, indicating approximate locations of DSTs (white tag) and acoustic tags (black tag) after implantation

through the peritoneal wall while simultaneously withdrawing the spoon to extract the needle out through the incision while protecting the viscera. One end of a suture threaded through the end of the tag was inserted into the tip of the needle. The needle was then withdrawn to pull the suture out through the needle's entry point. This procedure was then repeated on the other side of the sagittal plane. The tag was then inserted through the incision and anchored anteriorly in the peritoneal cavity using the suture and an (external) surgical knot. For the four fish also equipped with separate acoustic tags, the second tag was inserted into the peritoneal cavity through the same incision. Finally, the incision was closed using interrupted sutures. The fish was then transferred to a recovery tank with circulating seawater where it was kept until it regained consciousness, upon which it was transferred back into the tank it was collected from. See Table 1 for anaesthesia bath and surgery durations for all tagged fish.

#### Timeline and experimental design

Since the present study focused on investigating the post-tagging recovery, the analyses only included data from the 2 weeks following tagging. To avoid inducing other stress effects that could disturb their recovery, the fish were sheltered from all potential stress factors except those necessary to feed and provide for the fish in this period.

None of the fish exhibited signs of adverse health after tagging or during the trials, and all fish were euthanised after the conclusion of the experiment. Posthumous pathology of all remaining experimental fish at the end of the experiment (19 female, 23 male) revealed that about one-third of these fish (14 in total, 8 F, 6 M) exhibited signs of sexual maturation through the experimental period, including 5 of the tagged individuals (Table 1). Although this appeared to have a little direct impact on the fish in three of the tanks, the data from the fish in one of the tanks (tank 3) were excluded from the statistical data analyses due to perpetual inter-individual aggression between two matured males in that tank throughout the experimental period. This left nine fish tagged with DSTs measuring heart rate, six of which also measured activity. Since two of these fish contained both a DST and an acoustic tag measuring activity, this resulted in a total of eight time-series of activity.

#### Data processing and statistics

Heart rate data were used as downloaded from the DSTs. Outliers were removed using the Median Absolute Deviation (MAD) approach [34], using a MAD decision criterion of 3, which is a conservative value (see [35]). The MAD decision criterion denotes the standard deviation from the dataset's sample average

above which samples are rejected. The MAD decision criterion typically ranges from 2 (poorly conservative) to 3 (very conservative). In this study, the choice of 3 is justified by the measured heart ranges compared to typical heart rates published in the literature ( $15 < \text{HR} < 80$ ) for Atlantic salmon and comparable species [28, 36]. Activity data from the DST centi-HRT ACT tags were downloaded as raw acceleration values along all three axes and then subjected to similar post processing as that used to compute the activity proxy in the A MP-9 acoustic transmitter tags to yield a comparable measure of activity between the two tag types.

In a non-decomposed time-series, circadian variation (that between day and night) and irregular variation (that other than circadian of long-term) had the potential to obscure long-term trends in heart rate and activity. Time-series of heart rate and activity were therefore first decomposed into circadian, long-term trend, and irregular components. Decomposition, and subsequent removal of the circadian and irregular components of the time-series, leaving a long-term component (that showed the long-term growth or decline of the time-series values over the temporal extent of the series), allowed for the examination of the form of the long-term trends towards recovery. To decompose each time-series, it was first binned into 15 min intervals (each 15 min interval showing a mean heart rate or intensity over that interval) and then converted into a time-series object [R function *ts* {stats}; Becker et al. [37]]. Time-series objects were then decomposed using the Seasonal Decomposition of Time Series by Loess R function *stl* {stats} (B. D. Ripley; Fortran code by Cleveland et al. [38] from "netlib"). Long-term trend components were then analysed for a systematic change in heart rate or activity that could be indicative of a post-surgery recovery by first modelling the temporal relationship and then compartmentalising this into pre- and post-recovery phases.

The relationship between the long-term trend component of heart rate or activity ( $y$ ) and time post-tagging ( $t$ ) was modelled using an exponential decay model:

$$y(t) = y_p + (y_0 - y_p)e^{-\alpha t},$$

where  $\alpha$  defines the decay constant from  $y_0$  (at time zero) to  $y_p$ , the model plateau. Models were fitted with the *nls* {stats} R function (D. M. Bates and S. DebRoy; D. M. Gay for the Fortran code used by algorithm="port"), using the self-starting asymptotic regression function *SSasympt* {stats} (J. Pinheiro and D. M. Bates). Most trend components followed an exponentially decaying pattern, ensuring model convergence, but some included parts that were inconsistent



with an exponential decay. First, some tags (three heart-rate tags and four activity tags) showed a short initial post-surgery increase in registered values at the beginning of the experiment. Secondly, some tags (one heart rate and two activity tags) showed an increase in registered values after  $\approx 5\text{--}6$  days. This late increase in activity or heart-rate was likely a result of a separate, post-recovery change in behaviour of these individuals. To ensure model convergence, these parts of the long-term trend components were removed prior to model fitting. That is, the exponential model was only fitted to parts of the long-term trend component that were consistent with a post-surgery exponential decline. One activity tag (fish F4 in tank 8) did not show an exponential decline with time and was thus not fitted with a model.

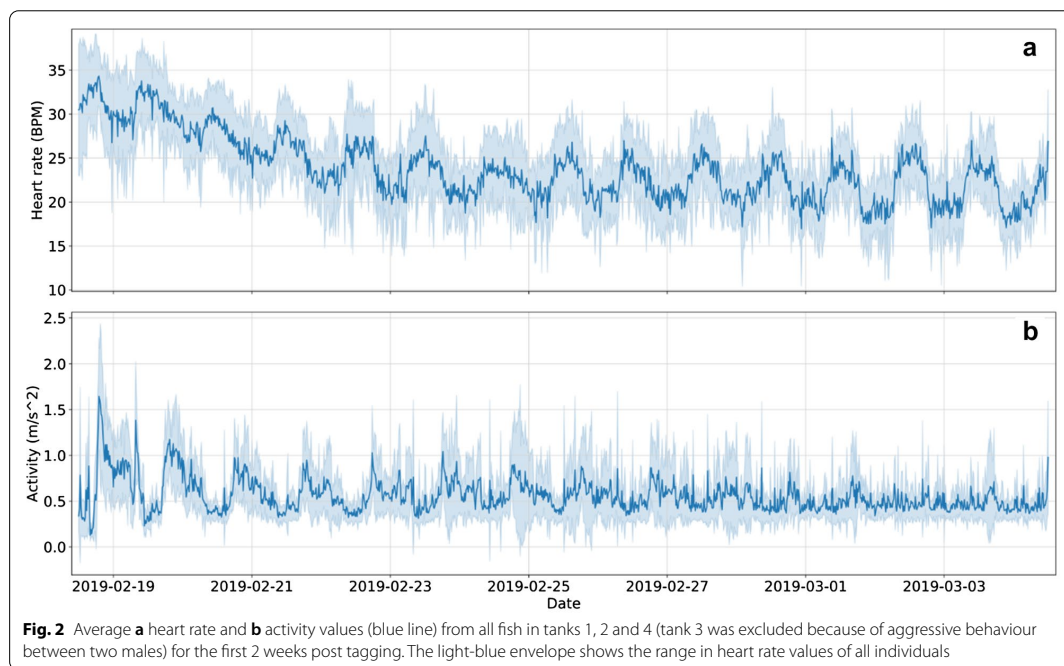
Identification of breakpoints between pre- and post-recovery phases was done on an individual basis. The breakpoint between pre- and post-recovery for each tag was set where the heart rate or activity reached a recovery threshold, defined as the heart rate or activity level delimiting those pre- and post-recovery. A recovery threshold was defined for each tag as the mean + 2SD of the long-term trend component values calculated from the final 3 days of the fitted series. Inspection of the tags showed that trend components were approaching

asymptotes in the final 3 days, so it was reasonable to assume that values from these days represented post-recovery signature. Thresholds were established on an individual basis to allow for post-recovery heart rate or activity to change according to individuals.

## Results

### Post-surgery recovery

Daily heart rate significantly declined from a mean of 36.0 bpm (range = 24.6–45.6, SD = 5.6,  $n=9$ ) on the day of surgery to a mean of 22.3 bpm (range = 17.5–26.6, SD = 2.6,  $n=9$ ) 13 days later (one-sided Wilcoxon's rank test,  $V=45$ ,  $p=0.002$ ) (Fig. 2a; raw data for all tags shown in). Daily activity significantly declined from a mean of 0.57  $\text{m s}^{-2}$  (range = 0.26–0.92, SD = 0.23,  $n=8$ ) on the day of surgery to a mean of 0.33  $\text{m s}^{-2}$  (range = 0.27–0.41, SD = 0.06,  $n=8$ ) 13 days later (one-sided Wilcoxon's rank test,  $V=45$ ,  $p=0.008$ ) (Fig. 2b). However, individual variation in activity was high (Fig. 2b). Both heart rate and activity displayed circadian variation. Heart rate was greater during daytime (mean = 25.8 bpm, range = 22.2–26.7, SD = 1.9,  $n=9$ ) than during night (mean = 22.7 bpm, range = 19.6–24.9, SD = 1.9,  $n=9$ ) (Fig. 2a; raw data for all tags shown in Additional file 1: Figures S1, S2). In contrast, activity was greater during night (mean = 0.47  $\text{m s}^{-2}$ , range = 0.32–0.60, SD = 0.11,

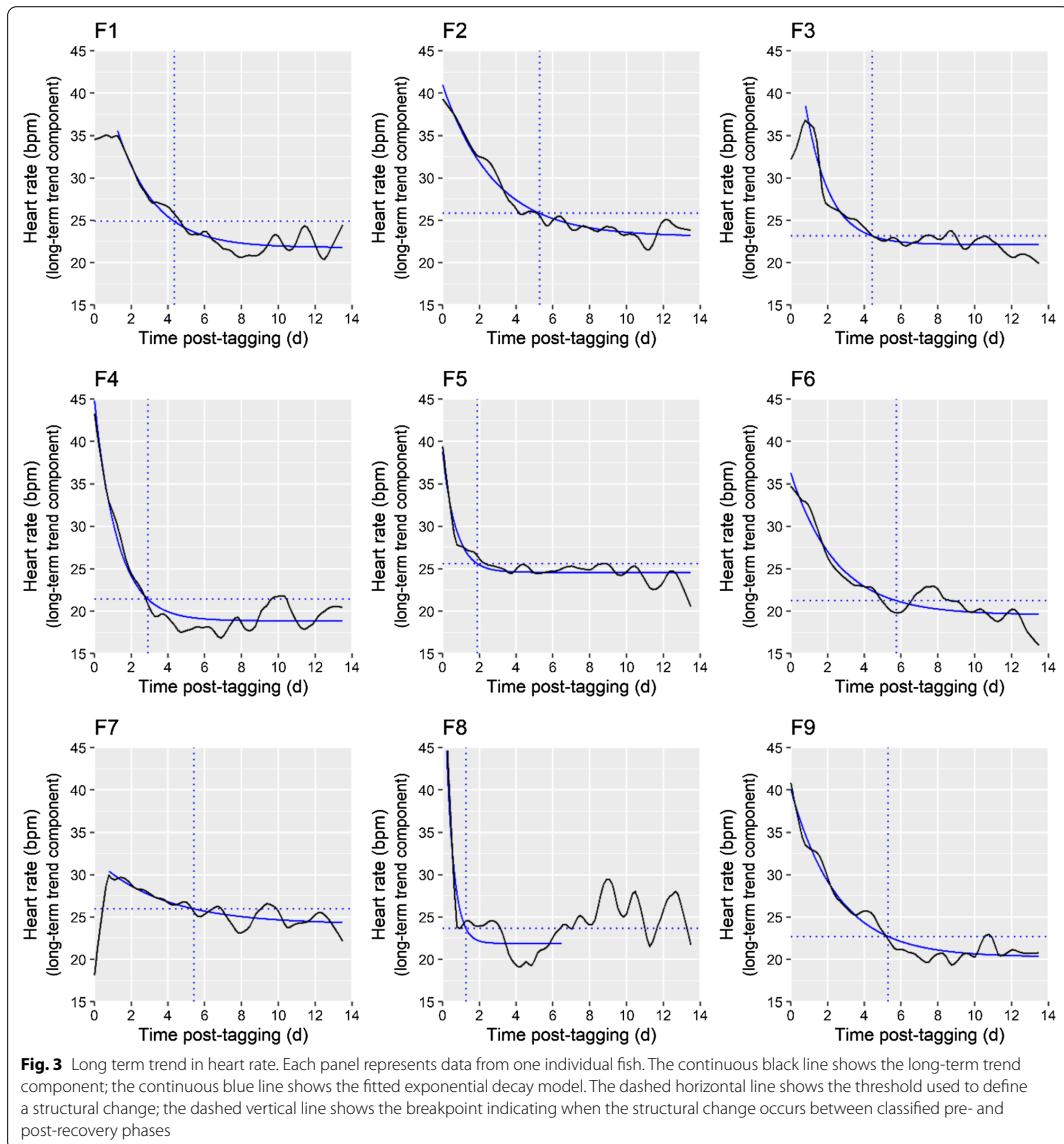




$n=8$ ) than during daytime (mean = 0.34  $m s^{-2}$ , range = 0.25–0.43, SD = 0.06,  $n=8$ ) (Fig. 2b; raw data for all tags shown in Additional file 1: Figures S3, S4). Circadian differences were present throughout the experiment. However, the circadian difference in activity declined throughout the experiment. This circadian variation was shown by all individuals, as revealed by the

circadian components from the time series (Additional file 1: Figures S5, S6). There was generally greater activity during the evening than during morning (Additional file 1: Figure S6).

The heart rate trend component showed a decline that could be modelled with an exponential decay function (Fig. 3). However, the trend component still



showed considerable temporal variation, depending on the tagged individual. For example, the trend component for fish F4 showed a sharp decline during the first day after tagging, but this then fluctuated for the remainder of the 2-week post-tagging period. The activity trend component also showed a pattern consistent

with an exponential decay (Fig. 4), except for one fish (fish F8) where an exponential decay model could not be fitted due to the activity trend component peaking  $\approx 7$  days after tagging. Two fish (fish F1 and F2) showed an exponential decline in activity but did not reach a

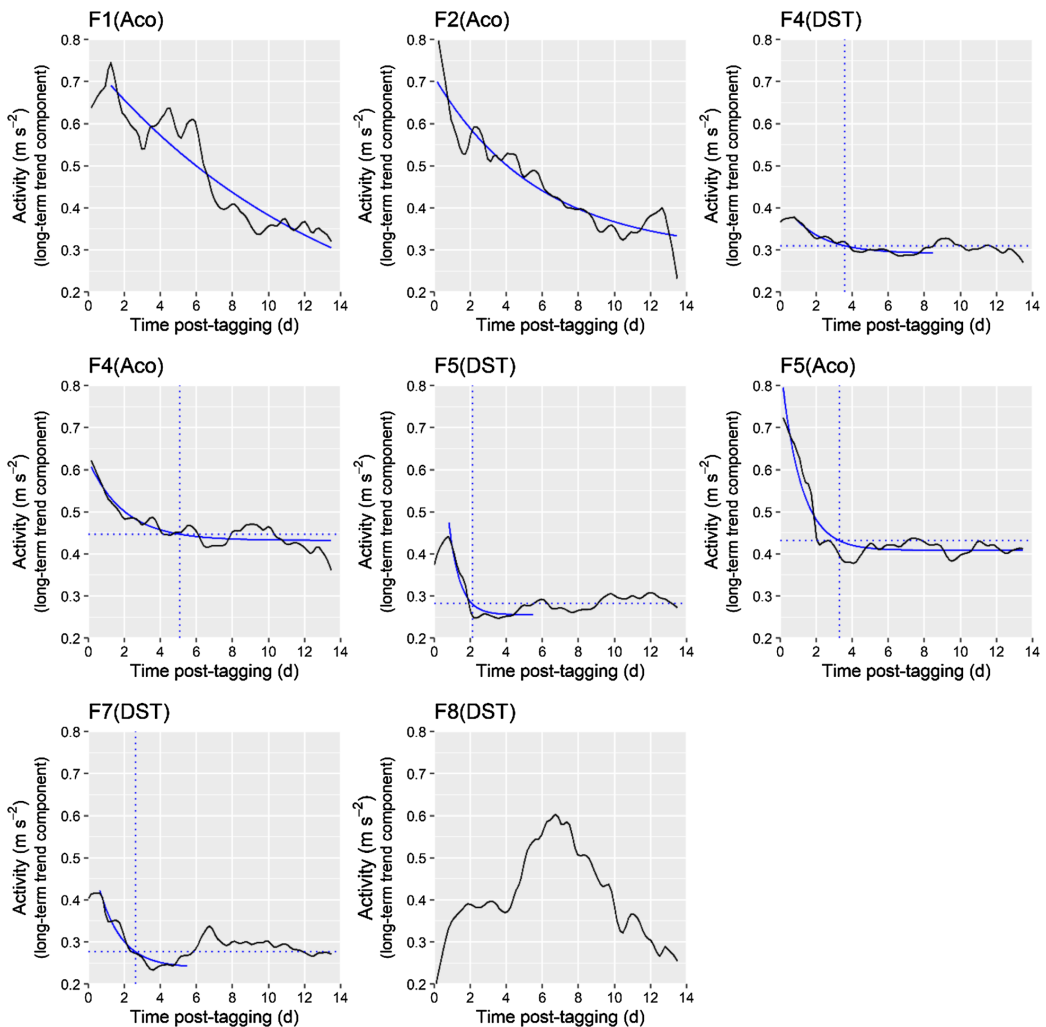


**Fig. 4** Long term trend in activity. Each panel represents data from one individual fish. The continuous black line shows the long-term trend component; the continuous blue line shows the fitted exponential decay model. The dashed horizontal line shows the threshold used to define a structural change; the dashed vertical line shows the breakpoint indicating when the structural change occurs between classified pre- and post-recovery phases. It was not possible to fit an exponential decay model to the long-term trend component of fish F8. Thresholds and breakpoints were not established for fish F1 and F2 where the exponential model did not plateau. Tag type (DST = Data Storage Tag; Aco = Acoustic tag) is shown in parentheses following the fish ID

plateau during the study period, suggesting that these fish has not fully recovered in terms of activity.

Time to recovery (as defined by the location of the breakpoint between pre- and post-recovery phases) varied between individuals, and the metric used (heart rate or activity, Figs. 3, 4, Table 2). The mean threshold value for heart rate in a ‘recovered’ individual was 23.8 bpm (range = 21.2–26.0, SD = 1.18,  $n=9$ ). The mean time to reach this threshold (i.e. breakpoint between pre-recovery and post-recovery) was 4.1 days (range = 1.3–5.8, SD = 1.7,  $n=9$ ). The threshold for activity recovery was greater for the acoustic tags (mean = 0.44  $m\ s^{-2}$ ,  $n=2$ ) than the DSTs (mean = 0.29  $m\ s^{-2}$ ,  $n=3$ ), reflecting the higher activity values registered by the acoustic tags. For the activity tags where there was evidence of recovery, the mean time taken to reach the threshold was similar to that for the heart rate tags (mean 3.3 days, range = 2.1–5.7, SD = 0.09). For the two individuals that were each tagged with two activity tags, the identified breakpoints between the parts of the time series classified as pre- and post-recovery depended on the tag: in both individuals, the threshold to reach post-recovery occurred later for the acoustic tag than the DST.

Although raw values of mean heart rate on the day of anaesthesia and surgery (mean = 36.0 bpm, range = 24.6–45.6, SD = 5.6,  $n=9$ ) varied more than the recovery threshold (mean = 23.8 bpm, range = 21.2–26.0, SD = 1.8,  $n=9$ , Table 2), there was a clear declining trend for all tagged individuals. With the exception of one

individual (F8, Fig. 4), there was a similar trend for activity: day of anaesthesia and surgery, mean = 0.64  $m\ s^{-2}$ , range = 0.39–0.92, SD = 0.20,  $n=7$ ; recovery threshold, mean = 0.36  $m\ s^{-2}$ , range = 0.28–0.43 SD = 0.07,  $n=7$ . For both heart rate and activity, raw values pre-recovery were significantly greater than those post-recovery (one-sided Wilcoxon’s signed-rank test: heart rate,  $V=45$ ,  $p=0.002$ ,  $n=9$ ; activity,  $V=28$ ,  $p=0.008$ ,  $n=7$ ).

### Discussion

The current study showed plateauing of most time-series, indicative of recovery, within the 14 days of the experiment. Two activity tags, F1(Aco) and F2(Aco), however, did not show plateauing, suggesting that the tagged fish had not fully recovered in terms of activity during this period. Other time-series showed gentle gradients even after the recovery breakpoint (for example, the F6 heart rate tag) so the definition of the point of recovery of some individuals as having fully recovered is less robust. However, identified breakpoints generally corresponded with systematic changes in the time-series. For example, the breakpoint on the F6 heart rate tag occurred in a trough separating the sharp initial decline over the first 5.75 days with the gentle gradient afterwards, so it is reasonable to infer that the identified breakpoint corresponded to the transition to post-recovery. The modelling approach used here allowed for a consistent method for establishing the time until recovery among a group of time-series. It should be noted, however, that estimated times until recovery is dependent on modelling approach used. For instance, fitting an exponential model to raw—rather than detrended timeseries, or using a different method to establish a breakpoint between pre- and post-recovery parts of the time-series, would yield different estimates. The exponential model used in this study is a well-validated method for modelling physiological recovery [39] but alternative approaches may also be considered (e.g. [27]). The sample size of fish in this study was small ( $N=9$ ); a larger sample size would allow a better quantification of the range of behaviour during recovery and allow better selection of the modelling approach.

The heart rate data suggest that the tagged Atlantic salmon in our study could only be considered fully recovered from the anaesthesia and surgical procedure of intraperitoneal tag implantation after an average of  $\approx 4$  and up to a maximum of 6 days post-surgery. While some studies have indicated longer recovery times post-tagging [32], our observations concur with several previous studies that have reported similar lengths of recovery post-tagging as our study [11, 16, 24, 25, 28]. Although some data series from the tagged fish in our study may visually appear to continue declining after fulfilling the recovery threshold criteria, these changes were not found to be

**Table 2 Recovery based on heart rate and activity sensors**

Tag ID	Heart rate recovery		Activity recovery	
	Threshold (bpm)	Time (days)	Threshold ( $m\ s^{-2}$ )	Time (days)
F1	24.90	4.33	No rec	No rec
F2	25.83	5.27	No rec	No rec
F3	23.17	4.42		
F4	21.43	2.92	0.31 0.45*	3.59 5.08*
F5	25.63	1.89	0.28 0.43*	2.10 3.30*
F6	21.24	5.75		
F7	25.97	5.41	0.28	2.60
F8	23.68	1.27	No fit	No fit
F9	22.71	5.29		
Mean	23.84	4.06	0.35	3.3

Activity sensors with a \* suffix indicate acoustic tags. “No fit” indicates that the long-term component of the time-series did not follow an exponential decline and that an exponential model could not be fitted; “No rec” indicates that it was possible to fit an exponential model to the time-series but that recovery thresholds and times were not assigned because the fitted exponential model did plateau

statistically significant. Recovery results based on activity data varied more in the recovery threshold criteria and time to recovery than heart rate, suggesting it might be a less consistent indicator of recovery between individuals. Moreover, both the temporal patterns and absolute values changed less for activity than heart rate between post-tagging and post-recovery periods, implying a lower ratio between the baseline pattern (i.e. circadian variations) and the changes in activity caused by the tagging procedure. Together, these factors suggest that activity may be a less consistent indicator of post-tagging recovery than heart rate, and that heart rate might be a generally more sensitive indicator than activity, especially for post-tagging recovery.

It is also important to note that there were individual variations in the recovery time assessed from heart rate. Although inter-individual variation in recovery time might be an inherent effect one should expect when tagging *A. salmon*, we did find that mature fish had a lower heart-rate recovery time than immature fish. However, the low sample size did not provide enough statistical power to robustly test influences on recovery time, so we recommend further studies with larger sample sizes to increase power in analyses of potential influences.

Based on these results, we urge caution on using telemetry data collected after anaesthesia and surgery without first ensuring that the fish are fully recovered [1, 23]. Biosensors that measure heart rate and/or activity can be potent tools in such evaluations, as they provide quantitative, high-resolution data that will be both more consistent, precise and objective in capturing the full post-anaesthesia/surgery effects than e.g. comparing behavioural observations of tagged vs. untagged fish.

Alternative parameters that could be used to assess post-tagging recovery in individual fish include blood glucose, lactate or pulse oximetry/ppg. These could provide a more direct assessment of stress levels in salmon, but we are not aware of any commercial electronic tags able to sense such parameters in live fish. Other techniques based on measuring cortisol in faecal matter [40] or bioelectric field monitoring akin to that used by sharks [41] could potentially result in future solutions that could be used evaluate recovery in a less invasive and independent manner, where the fish are monitored before, during and after the procedure. However, these methods are still to be developed to a stage where they can be applied to free-swimming fish, at least in large groups under commercial production conditions, and would only be able to provide information on a group level.

All three DST types tested in this experiment appeared to be suitable for applications on Atlantic salmon as all tagged fish provided valid heart rate data. Moreover, the activity proxy computed from the DSTs containing

accelerometers were found to be comparable to those measured by the acoustic tags (see [27] for details on this comparison). The lower absolute amplitude of the activity proxies computed from the DST data was probably caused by them sampling at a lower frequency (1 Hz) than the acoustic tags (5 Hz), thereby capturing fewer high-frequency components. The surgical procedure used to implant the heart rate tags was much simpler than the procedure needed for multivariate implants recently used in rainbow trout by Brijs et al. [31] but was more comprehensive and invasive than that used for conventional intraperitoneal tag placement. It is likely that less complex surgical procedures would lead to shorter recovery times in Atlantic salmon, as previously found for rainbow trout [42, 43]. However, it is probably reasonable to be conservative with respect to recovery times, especially if the data are to be used e.g. as a management tool in aquaculture applications or to evaluate stress effects on fish in conjunction with ecological studies. Using data from fish that are still recovering from post-anaesthesia/surgery effects in such applications could result in sub-optimal management decisions or erroneous conclusions that could have ramifications beyond the study itself.

The fish included in the analyses exhibited heart rates that gradually stabilised at daily means between 21 and 26 bpm (daily variations between 15 and 30 bpm, similar to that observed by for adult *A. salmon* of mean fork length of 62.3 cm at 4 °C by Lucas [36]). Due to the similarities across tanks and individuals, this range in heart rate may be typical for Atlantic salmon of this size and with the prevailing temperatures. Moreover, all individuals in tanks 1, 2 and 4 had similar circadian rhythms (higher heart rates during daytime than at night) and gradual post-surgery declines in mean daily heart rate (from more than 30 bpm after surgery to 21–26 bpm after up to 6 days). This implies a regularity across individuals that increases the likelihood that heart rate may function as a consistent stress indicator in Atlantic salmon that may be used to assess fish recovery after tagging. The tagged fish in tank 3 were excluded from the study due to inter-individual aggression. These individuals demonstrated measured heart rates that differed from the others both in individual and aggregate values. Although these fish also showed signs of circadian variation in heart rate, the mean value did not appear to decline over the days following tagging, an effect that was attributed to inter-individual aggression, all else being held equal. This may indicate that the stress induced by the aggression between the two males in this tank overrode the stress response due to recovery. A potential interpretation of this is that the aggressive encounters caused chronically elevated stress levels that masked the recovery stress caused by handling, anaesthesia and surgery. This could

further mean that recovery stress can be difficult to monitor if the fish are simultaneously influenced by independent external events, such as individual interactions due to dominance hierarchies [44, 45].

Based on established knowledge on how salmon swimming speeds are affected by variations in light intensity [46], as well as previous telemetry studies applying similar activity proxies on salmon in sea-cages (e.g. [10]), we expected to see a circadian rhythm in activity where activity was higher during the day than at night in the present study. In contrast to these expectations, the circadian trends in the activity of our fish were on average higher during night-time than during the day. A similar “inverse circadian” rhythm was observed in salmon reared in fish tanks during the period after tagging by Kolarevic et al. [30] and could imply that a “normal circadian” activity rhythm may arise only after the salmon have recovered after tagging in tanks. Conversely, the circadian rhythm in heart rate was more like expected (higher during daytime), meaning that the fish displayed generally higher heart rates when measured activity was low than when activity was high. This may seem counter-intuitive as one would expect more active fish to display higher heart rates since salmon tend to display increased heart rates with increased swimming activity [47]. However, it is possible that the higher heart rates during daytime were caused by effects such as feeding activity [48, 49] or perceived increased predation risk due to higher light levels [50]. These results are unexpected and very interesting, but further extrapolations and discussions on this matter would probably require further experiments with more data.

Although this study underlines the importance of critical evaluation with regards to recovery from anaesthesia and surgery when using telemetry, the data collected also highlight the importance of telemetry as a method for studying free-swimming fish. The heart rate and activity values for all tagged fish eventually plateaued, possibly indicating that they all recovered from the anaesthesia/surgery, and posthumous pathology revealed no inflammations or other apparent morphological signs of reduced welfare due to the surgical procedures. Even though the low water temperatures during the experiment may have led to handling and surgery having less impact on the fish, the tagging procedure used here was more complex than conventional intraperitoneal tagging. It is thus reasonable to conclude that fish carrying telemetry tags can be considered representative members of the group they were selected from once they are fully recovered from anaesthesia and surgery, provided that they were a representative selection to begin with. However, this also requires that the recommendations on ratio between tag size and fish size are not exceeded (e.g. “the

2% rule”, [2]). Since we worked with adult salmon with a mean weight of 2100 g, and the maximum tag weight carried by the fish was 22.6 g (around 1% of the fish body mass) this was not a challenge in our study.

#### **Future research and potential technological improvements**

Since this study only focused on Atlantic salmon exposed to one set of environmental conditions, it is difficult to assess if these concerns are also relevant for other species, and/or fish under different conditions. Similar studies on rainbow trout using the same tag type found that they recovered 72–96 h after surgery [28], which was shorter than the Atlantic salmon in the present study. Moreover, wounds in Atlantic salmon are known to heal faster in warmer temperatures than in cold water [51], suggesting that the low water temperatures in the present study may have contributed to longer recovery periods. These elements suggest that species-specific effects or differences in external environmental conditions are important to consider when studying recovery times. Future studies on the relationship between heart rate and post anaesthesia/surgery recovery time should therefore be conducted for other species of interest, across relevant temperature ranges, to obtain a more complete picture of this relationship.

In the present experiment, the fish were kept in groups in small tanks. To investigate how recovery time is affected by eventual scaling effects and social/inter-individual effects arising due to group dynamics, future studies addressing post-tagging effects should be done with a larger number of tagged fish at larger spatial scales. This would also enable a deeper scrutiny into individual variations in recovery, as a higher number of tagged fish would provide a good foundation for finding statistical relationships on the individual level. Although our present results imply that inter-individual variations are a prominent feature in the recovery time of tagged salmon, a larger sample number will be necessary to properly conclude upon the nature of such variations. To increase the relevance of a larger follow-up study, it could be done in fish cages in the marine environment, perhaps first by using meso-scale size cages containing fewer fish than a commercial cage but at similar densities, and then moving to full-scale studies to cover all steps in the transition from lab to industrial scale.

#### **Conclusion**

The main conclusion from this study is that the Atlantic salmon in these experiments required an average of  $\approx 4$  and up to a maximum interval of 6 days of recovery after anaesthesia and surgery before their heart rates returned to assumed baseline routine values. Moreover, although observation of behaviour and/or activity may

alone be insufficient to assess that the fish has physiologically recovered, activity measurements indicated similar recovery periods to those based on heart rate, although there was a longer maximum period of 10 days. We, therefore, urge caution when using data collected after surgery and anaesthesia in studies using biologging/telemetry tags. Assuming that we want all individuals to be recovered, our study thus implies that only data collected after 6 days recovery time should be used for further analyses. However, this recommendation would only be applicable to studies featuring Atlantic salmon reared in similar experimental conditions as we used. Since recovery time will vary with factors such as fish species, water temperature, invasiveness of the surgery, anaesthesia time, fish density and physical scale, it is difficult to make general recommendations on when one can assume the fish to be recovered from tagging, and the data to be safe for use in biological analyses. However, by conducting experiments similar to the present study where these parameters are varied, a more complete picture of how we need to account for fish recovery after tagging in telemetry studies may be obtained.

## Supplementary Information

The online version contains supplementary material available at <https://doi.org/10.1186/s40317-020-00226-8>.

**Additional file 1: Figure S1.** Measured heart rate for Tag IDs F1–F4. The y-axis upper limit has been constrained to 50 bpm. **Figure S2.** Measured heart rate for Tag IDs F5–F9. The y-axis upper limit has been constrained to 50 bpm. **Figure S3.** Measured activity for acoustic tags. **Figure S4.** Measured activity for DSTs. The y-axis upper limit has been constrained to  $5 \text{ m s}^{-2}$ . **Figure S5.** Circadian component of heart rate. Each panel represents data from one individual fish. **Figure S6.** Circadian component of the activity. Each panel represents data from one individual fish.

## Acknowledgements

In addition to thanking the Research Council of Norway for financial support (see "Funding"), we would like to thank the crew at NINA's research station at lms, particularly Knut Bergesen, for their effort in the experiments. We would also like to thank Asgeir Bjarnason at Star Oddi LTD and Erik Høy at Thelma Biotel AS for collaboration in specifying the loggers and transmitter tags used in the study. Bengt Finstad acknowledges the financial support obtained from DNV GL, while Martin Føre acknowledges the financial support from Salmar ASA/Salmar Ocean.

## Authors' contributions

MF manages the funding project, participated in the planning and execution of the experiments, and did the main job in preparing the manuscript. ES participated in the experiments, prepared the data, and was central in analysing the data. FØ was central in planning the experiments and conducted the surgery to equip the fish with the tags (together with AG). AG programmed the heart rate loggers, conducted the surgery to equip the fish with the tags (together with FØ) and contributed in the data analyses. JAA participated in the planning of the experiments and data analyses. BF was the main person behind the planning and execution of the experiment and participated in the experiment and data analyses. RH was responsible for the statistical analyses and contributed to the general processing of data. IU had a key role in planning the experiments and had the original idea behind the study resulting in this article. All authors have contributed to writing the manuscript. All authors read and approved the final manuscript.

## Funding

This study was funded by the Research Council of Norway (NFR Project Number 280864).

## Availability of data and materials

The datasets used and/or analysed during the current study are available from the corresponding author on reasonable request.

## Ethics approval and consent to participate

All fish handling and surgery were made in compliance with the Norwegian animal welfare act and were approved by the Norwegian Animal Research Authority (Permit No. 18/18431).

## Consent for publication

Not applicable.

## Competing interests

The authors declare that they have no competing interests.

## Author details

<sup>1</sup> Department of Engineering Cybernetics, Norwegian University of Science and Technology, 7491 Trondheim, Norway. <sup>2</sup> SINTEF Ocean, 7465 Trondheim, Norway. <sup>3</sup> Norwegian Institute for Nature Research, 7485 Trondheim, Norway. <sup>4</sup> Department of Animal Environment and Health, Swedish University of Agricultural Sciences, 532 31 Skara, Sweden. <sup>5</sup> Department of Biology, Norwegian University of Science and Technology, 7491 Trondheim, Norway.

Received: 16 April 2020 Accepted: 9 December 2020

Published online: 05 January 2021

## References

- Cooke SJ, Woodley CM, Eppard MB, Brown RS, Nielsen JL. Advancing the surgical implantation of electronic tags in fish: a gap analysis and research agenda based on a review of trends in intracoelomic tagging effects studies. *Rev Fish Biol Fish.* 2011;21(1):127–51.
- Thorstad EB, Rikardsen AH, Alp A, Økland F. The use of electronic tags in fish research—an overview of fish telemetry methods. *Turk J Fish Aquat Sci.* 2013;13(5):881–96.
- Føre M, Alfredsen JA, Gronningsater A. Development of two telemetry-based systems for monitoring the feeding behaviour of Atlantic salmon (*Salmo salar* L.) in aquaculture sea-cages. *Comput Electron Agric.* 2011;76(2):240–51.
- Taylor MD, Babcock RC, Simpfordorfer CA, Crook DA. Where technology meets ecology: acoustic telemetry in contemporary Australian aquatic research and management. *Mar Freshw Res.* 2017;68(8):1397–402.
- Welsh JQ, Bellwood DR. Spatial ecology of the steephead parrotfish (*Chlorurus microrhinos*): an evaluation using acoustic telemetry. *Coral Reefs.* 2012;31(1):55–65.
- Cooke SJ, Bunt CM, Schreier JF. Understanding fish behavior, distribution, and survival in thermal effluents using fixed telemetry arrays: a case study of smallmouth bass in a discharge canal during winter. *Environ Manag.* 2004;33(1):140–50.
- Crossin GT, Heupel MR, Holbrook CM, Hussey NE, Lowerre-Barbieri SK, Nguyen VM, Raby GD, Cooke SJ. Acoustic telemetry and fisheries management. *Ecol Appl.* 2017;27(4):1031–49.
- Hussey NE, Kessel ST, Aarestrup K, Cooke SJ, Cowley PD, Fisk AT, Harcourt RG, Holland KN, Iverson SJ, Kocik JF, Flemming JEM. Aquatic animal telemetry: a panoramic window into the underwater world. *Science.* 2015;348(6240):1255642.
- Føre M, Frank K, Norton T, Svendsen E, Alfredsen JA, Dempster T, Eguirau H, Watson W, Stahl A, Sunde LM, Schellewald C, Skoien KR, Alver MO, Berckmans D. Precision fish farming: a new framework to improve production in aquaculture. *Biosyst Eng.* 2018;173:176–93.
- Føre M, Svendsen E, Alfredsen JA, Uglem I, Bloecher N, Sveier H, Sunde LM, Frank K. Using acoustic telemetry to monitor the effects of crowding and delousing procedures on farmed Atlantic salmon (*Salmo salar*). *Aquaculture.* 2018;495:757–65.
- Brijs J, Sandblom E, Axelsson M, Sundell K, Sundh H, Huyben D, Broström R, Kiessling A, Berg C, Gräns A. The final countdown: continuous



- physiological welfare evaluation of farmed fish during common aquaculture practices before and during harvest. *Aquaculture*. 2018;495:903–11.
12. Johansson D, Ruohonen K, Juell JE, Oppedal F. Swimming depth and thermal history of individual Atlantic salmon (*Salmo salar* L.) in production cages under different ambient temperature conditions. *Aquaculture*. 2009;290(3–4):296–303.
  13. Wright DW, Stien LH, Dempster T, Oppedal F. Differential effects of internal tagging depending on depth treatment in Atlantic salmon: a cautionary tale for aquatic animal tag use. *Curr Zool*. 2018;65:665–73.
  14. Campbell HA, Bishop CM, Davies DA, Egginton S. Recording long-term heart rate in *Paranotothenia angustata* using an electronic datalogger. *J Fish Biol*. 2005;67(4):1150–6.
  15. Connors KB, Scruton D, Brown JA, McKinley RS. The effects of surgically implanted dummy radio transmitters on the behaviour of wild Atlantic salmon smolts. In: *Aquatic telemetry*. Dordrecht: Springer; 2002. p. 231–7.
  16. Jepsen N, Davis LE, Schreck CB, Siddens B. The physiological response of Chinook salmon smolts to two methods of radio-tagging. *Trans Am Fish Soc*. 2001;130(3):495–500.
  17. Thoreau X, Baras E. Evaluation of surgery procedures for implanting telemetry transmitters into the body cavity of tilapia *Oreochromis aureus*. *Aquat Living Resour*. 1997;10(4):207–11.
  18. Ellis T, North B, Scott AP, Bromage NR, Porter M, Gadd D. The relationship between stocking density and welfare in farmed rainbow trout. *J Fish Biol*. 2002;61:493–531.
  19. Pickering AD. Stress responses of farmed fish. *Biology of Farmed Fish*. Sheffield: Sheffield Academic Press; 1998. p. 222–55.
  20. Schreck CB. Accumulation and long-term effects of stress in fish. In: Moberg GP, Mench JA, editors. *The biology of animal stress*. Wallingford: CAB International; 2000. p. 147–58.
  21. Wedemeyer GA. Effect of rearing conditions on the health and physiological quality of fish in intensive fish culture. In: Iwama GK, Pickering AD, Sumpter JP, Schreck CB, editors. *Fish stress and health in aquaculture*, vol. 62. Society for Experimental Biology Seminar Series. Cambridge: Cambridge University Press; 1997. p. 35–72.
  22. Iwama GK, Afonso LOB, Vijayan MM, Iwama GK, Afonso LOB, Vijayan MM. Stress in fishes. In: Evans DE, Claiborne JB, editors. *The physiology of fishes*. Boca Raton: CRC Press; 2006. p. 319–42.
  23. Mulcahy DM. Surgical implantation of transmitters into fish. *ILAR J*. 2003;44(4):295–306.
  24. Bridger CJ, Booth RK. The effects of biotelemetry transmitter presence and attachment procedures on fish physiology and behavior. *Rev Fish Sci*. 2003;11(1):13–34.
  25. Martinelli TL, Hansel HC, Shively RS. Growth and physiological responses to surgical and gastric radio transmitter implantation techniques in subyearling chinook salmon (*Oncorhynchus tshawytscha*). In: *Advances in invertebrates and fish telemetry*. Dordrecht: Springer; 1998. p. 79–87.
  26. Barton BA, Schreck CB. Metabolic cost of acute physical stress in juvenile steelhead. *Trans Am Fish Soc*. 1987;116(2):257–63.
  27. Svendsen E, Føre M, Økland F, Gråns A, Hedger RD, Alfredsen JA, Uglem I, Rosten CM, Frank K, Erikson U, Finstad B. Heart rate and swimming activity as stress indicators for Atlantic salmon (*Salmo salar*). *Aquaculture*. 2020;531:735804.
  28. Brijs J, Sandblom E, Rosengren M, Sundell K, Berg C, Axelsson M, Gråns A. Prospects and pit-falls of using heart rate to the welfare of rainbow trout (*Oncorhynchus mykiss*) in aquaculture. *Aquaculture*. 2019;509:188–97.
  29. Hjelmsæd P, Sundh H, Brijs J, Ekström A, Sundell KS, Berg C, Sandblom E, Bowman J, Morgenroth D, Gråns A. Effects of prophylactic antibiotic-treatment on post-surgical recovery following intraperitoneal bio-logger implantation in rainbow trout. *Sci Rep*. 2020;10(1):1–9.
  30. Kolarevic J, Aas-Hansen Ø, Espmark Å, Baeverfjord G, Terjesen BF, Damsgård B. The use of acoustic acceleration transmitter tags for monitoring of Atlantic salmon swimming activity in recirculating aquaculture systems (RAS). *Aquacult Eng*. 2016;72–73:30–9.
  31. Brijs J, Sandblom E, Axelsson M, Sundell K, Sundh H, Kiessling A, Berg C, Gråns A. Remote physiological monitoring provides unique insights on the cardiovascular performance and stress responses of freely swimming rainbow trout in aquaculture. *Sci Rep*. 2019;9(1):9090.
  32. Hvas M, Folkedal O, Oppedal F. Heart rate bio-loggers as welfare indicators in Atlantic salmon (*Salmo salar*) aquaculture. *Aquaculture*. 2020;529:735630.
  33. Coyle SD, Durborow RM, Tidwell JH. *Anesthetics in aquaculture*, vol. 3900. Texas: Southern Regional Aquaculture Center; 2004.
  34. Leys C, Ley C, Klein O, Bernard P, Licata L. Detecting outliers: do not use standard deviation around the mean, use absolute deviation around the median. *J Exp Soc Psychol*. 2013;49(4):764–6.
  35. Miller J. Reaction time analysis with outlier exclusion: bias varies with sample size. *Q J Exp Psychol*. 1991;43(4):907–12.
  36. Lucas MC. Heart rate as an indicator of metabolic rate and activity in adult Atlantic salmon, *Salmo salar*. *J Fish Biol*. 1994;44(5):889–903.
  37. Becker R, Chambers JM, Wilks AR. 2018. *The new S language*. CRC Press.
  38. Cleveland RB, Cleveland WS, McRae JE, Terpenning I. STL: a seasonal-trend decomposition procedure based on loess. *J Off Stat*. 1990;6:3–73.
  39. Bartels-Ferreira R, de Sousa ED, Trevizani GA, Silva LP, Nakamura FY, Forjaz CLM, Lima JRP, Pecanha T. Can a first-order exponential decay model fit heart rate recovery after resistance exercise? *Clin Physiol Funct Imaging*. 2015;35(2):98–103.
  40. Cao Y, Tveten AK, Stene A. Establishment of a non-invasive method for stress evaluation in farmed salmon based on direct fecal corticoid metabolites measurement. *Fish Shellfish Immunol*. 2017;66:317–24.
  41. Kalmijn AJ. Bioelectric fields in sea water and the function of the ampullae of Lorenzini in elasmobranch fishes (No. SIO-REF-72-83). La Jolla: Scripps Institution of Oceanography; 1972.
  42. Altimiras J, Larsen E. Non-invasive recording of heart rate and ventilation rate in rainbow trout during rest and swimming. *Fish go wireless!* *J Fish Biol*. 2000;57(1):197–209.
  43. Gråns A, Sandblom E, Kiessling A, Axelsson M. Post-surgical analgesia in rainbow trout: is reduced cardioventilatory activity a sign of improved animal welfare or the adverse effects of an opioid drug? *PLoS ONE*. 2014;9(4):e95283.
  44. Cubitt KF, Winberg S, Huntingford FA, Kadri S, Crampton VO, Øverli Ø. Social hierarchies, growth and brain serotonin metabolism in Atlantic salmon (*Salmo salar*) kept under commercial rearing conditions. *Physiol Behav*. 2008;94(4):529–35.
  45. Sloman KA, Metcalfe NB, Taylor AC, Gilmour KM. Plasma cortisol concentrations before and after social stress in rainbow trout and brown trout. *Physiol Biochem Zool*. 2001;74(3):383–9.
  46. Oppedal F, Dempster T, Stien LH. Environmental drivers of Atlantic salmon behaviour in sea-cages: a review. *Aquaculture* 2011;311(1–4):1–18
  47. Hvas M, Folkedal O, Oppedal F. Heart rates of Atlantic salmon *Salmo salar* during a critical swim speed test and subsequent recovery. *J Fish Biol*. 2020. <https://doi.org/10.1111/jfb.14561>.
  48. Eliason EJ, Higgs DA, Farrell AP. Postprandial gastrointestinal blood flow, oxygen consumption and heart rate in rainbow trout (*Oncorhynchus mykiss*). *Comp Biochem Physiol A Mol Integr Physiol*. 2008;149(4):380–8.
  49. Gråns A, Albertsson F, Axelsson M, Olsson C. Postprandial changes in enteric electrical activity and gut blood flow in rainbow trout (*Oncorhynchus mykiss*) acclimated to different temperatures. *J Exp Biol*. 2009;212(16):2550–7.
  50. Johnsson JI, Höjesjö J, Fleming IA. Behavioural and heart rate responses to predation risk in wild and domesticated Atlantic salmon. *Can J Fish Aquat Sci*. 2001;58(4):788–94.
  51. Jensen LB, Wahli T, McGurk C, Eriksen TB, Obach A, Waagbø R, Handler A, Tafalla C. Effect of temperature and diet on wound healing in Atlantic salmon (*Salmo salar* L.). *Fish Physiol Biochem*. 2015;41(6):1527–43.

## Publisher's Note

Springer Nature remains neutral with regard to jurisdictional claims in published maps and institutional affiliations.





## Paper C

Optical measurement of tissue perfusion changes as an alternative to electrocardiography for heart rate monitoring in Atlantic salmon (*Salmo salar*)

*Paper C*

*Optical measurement of tissue perfusion changes as an alternative to electrocardiography for heart rate monitoring in Atlantic salmon (*Salmo salar*)*


---

METHODOLOGY

Open Access



# Optical measurement of tissue perfusion changes as an alternative to electrocardiography for heart rate monitoring in Atlantic salmon (*Salmo salar*)

Eirik Svendsen<sup>1,2\*</sup> , Finn Økland<sup>4</sup>, Martin Føre<sup>1</sup>, Lise L. Randeberg<sup>3</sup>, Bengt Finstad<sup>5</sup>, Rolf E. Olsen<sup>5</sup> and Jo A. Alfredsen<sup>1</sup>

## Abstract

**Background:** Welfare challenges in salmon farming highlights the need to improve understanding of the fish's response to its environment and rearing operations. This can be achieved by monitoring physiological responses such as heart rate (HR) for individual fish. Existing solutions for heart rate monitoring are typically based on Electrocardiography (ECG) which is sensitive to placement and electrode orientation. These factors are difficult to control and affects the reliability of the principle, prompting the desire to find an alternative to ECG for heart rate monitoring in fish. This study was aimed at adapting an optical photoplethysmography (PPG) sensor for this purpose. An embedded sensor unit measuring both PPG and ECG was developed and tested using anesthetized Atlantic salmon in a series of in-vivo experiments. HR was derived from PPG and compared to the ECG baseline to evaluate its efficacy in estimating heart rate.

**Results:** The results show that PPG HR was estimated with an accuracy of  $0.7 \pm 1.0\%$  for 660 nm and  $1.1 \pm 1.2\%$  for 880 nm wavelengths, respectively, relative to the ECG HR baseline. The results also indicate that PPG should be measured in the anterior part of the peritoneal cavity in the direction of the heart.

**Conclusion:** A PPG/ECG module was successfully adapted to measure both ECG and PPG in-vivo for anesthetized Atlantic salmon. Using ECG as baseline, PPG analysis results show that that HR can be accurately estimated from PPG. Thus, PPG has the potential to become an alternative to ECG HR measurements in fish.

**Keywords:** *Salmo salar*, Heart rate, Implant, Biosensors, Photoplethysmography

## Background

Atlantic salmon (*Salmo salar*) is one of the most important species in fish farming with more than 2.6 Mt produced globally in 2019 [1]. A typical salmon production site consists of 8–10 flexible sea cages usually 50 m in diameter that holds a volume of around 40,000 m<sup>3</sup>. The

management and operation of such salmon farms entails a broad range of interrelated operations exerting convoluted effects on the fish. To ensure acceptable fish health and welfare conditions during production, relevant data to describe these must be collected and evaluated in conjunction with operational data. Such evaluations are largely subjective and experience based, and are carried out as part of the daily inspection and feeding routines.

About 15% of all farmed salmon are lost during production, a loss partly attributed to the lack of objective input to production control [2]. To address this loss,

\*Correspondence: eirik.svendsen@ntnu.no

<sup>1</sup> Department of Engineering Cybernetics, NTNU, O.S. Bragstads Plass 2D, 7034 Trondheim, Norway

Full list of author information is available at the end of the article



© The Author(s) 2021. **Open Access** This article is licensed under a Creative Commons Attribution 4.0 International License, which permits use, sharing, adaptation, distribution and reproduction in any medium or format, as long as you give appropriate credit to the original author(s) and the source, provide a link to the Creative Commons licence, and indicate if changes were made. The images or other third party material in this article are included in the article's Creative Commons licence, unless indicated otherwise in a credit line to the material. If material is not included in the article's Creative Commons licence and your intended use is not permitted by statutory regulation or exceeds the permitted use, you will need to obtain permission directly from the copyright holder. To view a copy of this licence, visit <http://creativecommons.org/licenses/by/4.0/>. The Creative Commons Public Domain Dedication waiver (<http://creativecommons.org/publicdomain/zero/1.0/>) applies to the data made available in this article, unless otherwise stated in a credit line to the data.

recent research efforts have focused on determining what constitutes good fish welfare and which indicators one should quantify (i.e., measure) to obtain a more objective foundation for making welfare critical decisions [3], and safeguard ethically sound production. Sensing such indicators should be done using as unobtrusive measures as possible to avoid compromising safe and efficient operations. However, this is in conflict with the challenge of collecting data from a biomass contained in a volume of roughly 40,000 m<sup>3</sup> of water, as this calls for distributed or mobile data collection systems which are based on, e.g., environmental sensing networks, sonars/echo sounders, passive acoustic monitoring and different types of optical methods such as underwater cameras [4]. Such systems are likely to be intrusive on the production, and may thus have to be removed from the aquaculture cage before operations are carried out to reduce the likelihood of, e.g., equipment damage. Furthermore, such technologies provide data with different spatial and temporal resolution and provide data on a population level since the recorded data are obtained from a sub-volume in the sea cage rather than from a specific group of fish. Sonars and cameras can provide data on a group level if smaller parts of the biomass are present within the sensor's field of view, a feature that has been used to estimate, e.g., fish size and cage biomass [5]. Although group and population level data can provide a certain insight into the dynamics in animal husbandry operations, the sensing technologies' intrusiveness on operations and limited understanding of the measurements' link to welfare imply that alternative or supplemental solutions for welfare evaluations are needed.

Individual level data provides the highest possible data resolution with respect to biomass, a feature recognized in precision farming both on land [6] and at sea [4]. In aquaculture, the main method for obtaining individual level data is using miniaturized, encapsulated electronic systems commonly referred to as "tags". Typical parameters that can be measured in an operational setting today are activity and swimming depth [7], heart rate (HR) [8], swimming speed [9] and position [10, 11]. Tags are available in two main types: Data storage tags (DSTs) and telemetry transmitter tags [12], and are usually surgically implanted into the fish's peritoneal cavity.

Tagging has been used successfully to study fish in different situations ranging from tracking fish in rivers and sea [13–15] to shedding light on fish behaviour in sea cages during aquaculture operations [7, 16]. Thus, tagged individuals may act as representatives (i.e., "sentinel fish") for the rest of the biomass in an aquaculture cage [17] to facilitate safer and less operationally intrusive welfare evaluations.

Changes in treatment and/or living conditions challenges an animal's homeostasis and may be expressed as various stress responses [18]. Recently, heart rate measured using DSTs was demonstrated as being linked to welfare [19] and stress [20] in Atlantic salmon and in other salmonids such as rainbow trout [21]. Heart rate may, therefore, serve as a proxy for stress, thereby providing information on the fish's welfare in aquaculture provided that heart rate can be obtained in real time. Heart rate estimates for fish are most commonly derived from an electrocardiogram (ECG) measured by electrodes integrated in the tag's encapsulation. However, the reliability of this method has been shown to be sensitive to tag deployment as the derived heart rate depends on the lateral placement in the fish as well as the tag's orientation [21]. Exploring other potentially more robust measurement principles for their ability to sense heart rate is, therefore, desirable, as it might contribute to making heart rate data more reliable and feasible to obtain for free swimming fish in aquaculture.

Photoplethysmography is an optical sensing technique quantifying changes in tissue perfusion (i.e., blood volume) by optical absorption. The photoplethysmogram (PPG) is a convolution of many components. In humans, slow-varying components may arise from breathing [22], while the superimposed pulsatile component changes with the cardiac cycle [23]. Using the pulsatile component from several wavelengths of light enables estimation of arterial blood oxygen saturation (*SpO2*) provided a mapping function compensating for tissue scattering effects is known [24]. Independent from this, the pulsatile component can be used to obtain a heart rate estimate as shown for both humans and other mammals [25, 26]. Thus, PPG is considered a likely candidate to address the challenges associated with ECG obtained using implants provided a suitable sensing solution can be designed.

Implantable PPG solutions have been developed for, e.g., sheep [27] and other mammals [28]. Although potentially relevant, such solutions are proprietary and either require additional, external interfaces for power and data collection/processing, or depend on radio-based data transfer, making them infeasible for use in fish in seawater. Measurement of PPG has been demonstrated for aquatic animals such as zebrafish (*Danio rerio*) using imaging PPG [29]. This is a suitable technique when tissues with low opacity can be remotely imaged in a controlled environment. This is the case for zebrafish in the larval stage, but not for Atlantic salmon in a context where using implants is considered relevant. Correspondingly, obtaining heart rate from PPG has been demonstrated by drilling holes and inserting PPG sensors through the shell of the Mediterranean mussel (*Mytilus galloprovincialis*) [30]. This

approach requires stationary subjects as the sensors are wired to external hardware for power and data logging. These approaches are, thus, not directly suited for fish implants, but demonstrate the feasibility of applying PPG for heart rate sensing for different aquatic animal groups.

In recent years a market desire for mobile medical equipment and consumer products containing such sensors (e.g., smart phones and sports watches [31, 32]) has driven development and miniaturization of PPG sensors. Such innovations have increased the potential to include such off-the-shelf sensors in implants for fish, as this is an application with similar requirements with respect to size and power consumption. However, the anatomical and optical tissue property differences between mammals and fishes, raise the question of whether PPG captured in Atlantic salmon using the common intraperitoneal implantation approach results in useful data. The purpose of this study was, therefore, to adapt an off-the-shelf PPG/ECG biosensing module for in-vivo testing in Atlantic salmon to investigate its potential to provide an alternative heart rate estimate from Atlantic salmon that does not suffer from the same limitations as ECG, while facilitating a future low-cost implant based on standard electronic components.

## Methods

### Sensing and logging equipment

The MAX86150 optical biosensor module [33] from Maxim Integrated (San Jose, USA) that offers both PPG and ECG output in a miniature package ( $3.3 \times 5.6 \times \text{mm}$ ) with ultra-low power consumption, was selected for the measurements in this study. The physical and electrical properties of the module make it suitable for integration as the biosensor element of a prospective DST or acoustic tag with such sensing capability. A printed circuit board (PCB) was designed as a platform for miniaturizing the reference circuit design for the MAX86150. The PCB was subsequently cast in a cylindrical epoxy casing such that the sensing direction was perpendicular to the cylinder's longitudinal axis. Seven thin electrical wires protruded the rear of the cast and was used to extend the ECG electrode connections of the MAX86150, and to enable power connection and data transfer from the sensor. A battery powered MAX32630FTHR microcontroller board was used to relay data to a PC using Bluetooth. The cast also included a threaded aluminium end piece for attachment to a fixture rod. The fixture rod allowed horizontal and vertical sensor orientations as well as rotation of the sensor around its longitudinal axis. The complete assembly is shown in Fig. 1. Maxim DeviceStudio (V 5.3.03289.0) was installed on a Dell Latitude 7490

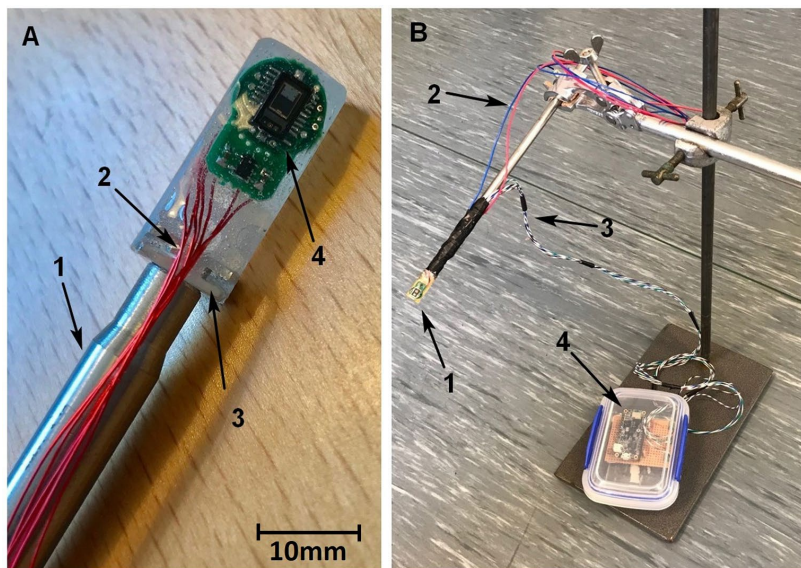


**Fig. 1** **A** (left): 1. Fixture rod, 2. Wire extensions for MAX86150 ECG electrodes, power connection and data transfer, 3. Threaded aluminium end piece, 4. MAX86150 biosensor module. **B** (right): 1. Epoxy cast with MAX86150 biosensor module, 2. ECG electrode extension leads, 3. Data and power supply extension leads, 4. MAX32630FTHR microcontroller board for wireless data transfer to PC

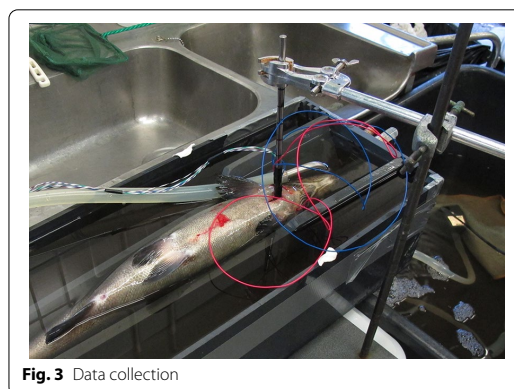
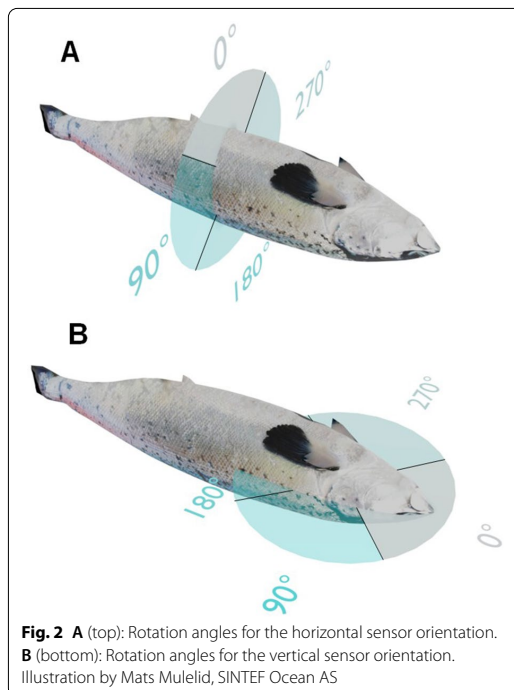
laptop computer and used for real-time data inspection and logging.

To determine the biosensor's feasibility when applied to Atlantic salmon, all sensor settings were kept the same for all data sets (sampling frequency  $f_s=200$  Hz, RED (660 nm) and IR (880 nm) LED pulse amplitudes  $A_{660}=A_{880}=20$  mA, LED pulse width  $PW=400$   $\mu$ s, and no sample averaging), thus enabling signal quality comparisons across data sets. Note that when using PPG to estimate heart rate only, no reference measurements apart from the ECG baseline used for HR comparisons are required.

### Experimental procedures

Individual fish were captured from a holding tank using a knotless dip net and immediately transferred to a tank containing water from the same water supply and anesthetic in a knock-out solution ( $70$  mg  $l^{-1}$  Benzoak Vet). The tank was covered using a Styrofoam plate after the fish was placed inside. Using a wheeled trolley, the tank was then moved to the indoor experimental location. When deemed to have reached level 3 anesthesia [34], the fish was placed in a specialized surgical table. By inserting a hose connected to a small pump into the fish' buccal cavity, continuously aerated water with maintenance anesthetic ( $35$  mg  $l^{-1}$  Benzoak Vet) was used to irrigate the gills and keep the fish sedated. The wire electrodes for ECG measurement attached to the MAX86150 were inserted into the muscle on the left and right lateral sides close to the heart. A 1–2 cm incision was made in the abdominal wall along the sagittal plane just anterior of the pelvic fins (position 1, Fig. 2A). For position 1, the sensor was inserted horizontally into the peritoneal cavity and one data set collected for orientations of  $0^\circ$  (ventral),  $90^\circ$  (right lateral),  $180^\circ$  (dorsal),  $270^\circ$  (left lateral) and  $0^\circ$  (ventral repeated) degrees rotation, respectively (Fig. 2A). Following data collection in position 1, a second 1 cm incision was made in the abdominal wall along the sagittal plane just posterior from the transverse septum (position 2, Fig. 2B). For position 2, the sensor was inserted vertically into the peritoneal cavity and one data set collected for orientations of  $0^\circ$  (anterior),  $90^\circ$  (right lateral),  $180^\circ$  (posterior),  $270^\circ$  (left lateral) and  $0^\circ$  (anterior repeated) degrees, respectively (see Figs. 2B and 3). Data was collected for 1 min for both positions and all orientations for each individual (10 data sets per fish / 50 data sets in total), after which the fish was euthanized by an anesthetic overdose ( $>70$  mg  $l^{-1}$  Benzoak Vet) and exsanguination.

A total of 7 fish were used for the experiment. No valid data was obtained for the first fish due to electrical interference likely caused by a nearby water pump



preventing valid ECG signals. Data collection was successful from the remaining 6 fish (from now on referred to as Fish 1 through 6), resulting in 10 data sets for fish 1, 2, 4, 5 and 6, and 6 data sets for fish 3 which suffered cardiac arrest after 6 data sets. The analyses were thus based on 56 data sets in total.



**Data processing**

Valid 20 s data subsets were manually selected and labelled based on the data evaluation criteria presented by Elgendi [35]:

- Salient ECG baseline.
- Salient PPG signal for one or both wavelengths.
- Similar PPG waveform morphology throughout the entire subset.

Data analysis using Python 3.8 (Anaconda Inc., Austin, Texas, USA) could then be conducted for valid data sets labelled “GOOD” (accept) or “FAIR” (accept). Data sets labelled “BAD” (reject) were judged to not contain the required information for signal quality calculations and were, therefore, omitted from further analysis. A complete overview of data sets and corresponding wavelengths considered valid based on these criteria is given in Table 1, while representative samples of PPG data sets labelled “GOOD”, “FAIR” and “BAD” can be seen in Fig. 4.

The default filtered ECG signal output from the MAX86150 was used to find HR by first scaling the filtered output to [0, 1] and then running a peak detection algorithm. Scaling was done so the same peak detection parameters for all ECG time series could be used. Peaks were identified using the “find peaks()” method in Python’s statistics module utilizing both a time window (i.e., the minimum required distance between peaks) and a prominence limit to identify the QRS peaks (i.e., ventricle depolarization) [36]. The time window was set to 160 samples (i.e., 0.8 s) based on a maximum expected HR of 80 BPM for Atlantic salmon [37] and comparable species [21]. Prominence was set to 0.4, thus demanding that the

QRS peaks were 40% higher than neighbouring peaks. HR was then determined by the average time difference ( $\Delta t_{avg}$ ) between peaks using:

$$HR_{BPM} = \left( \frac{1}{\Delta t_{avg}} \right) \cdot 60 \tag{1}$$

Because raw PPG data containing both a stochastic trend and measurement noise was logged, a preprocessing step to remove these was necessary. The slow-varying (i.e., low-frequency) trend was removed using a third order Butterworth highpass filter [38] with a cutoff frequency of 0.25 Hz. Measurement noise was reduced using a second-order Savitzky-Golay filter [39] with a 50 sample (i.e., 0.25 s) window. This window size was chosen to retain as much information in the signal as possible based on the lowest expected HR of 15 BPM for Atlantic Salmon [37] and comparable species [21]. An example illustrating the result of these processing steps is given in Fig. 5. HR from PPG was then calculated from the de-trended and noise suppressed signal using autocorrelation defined by:

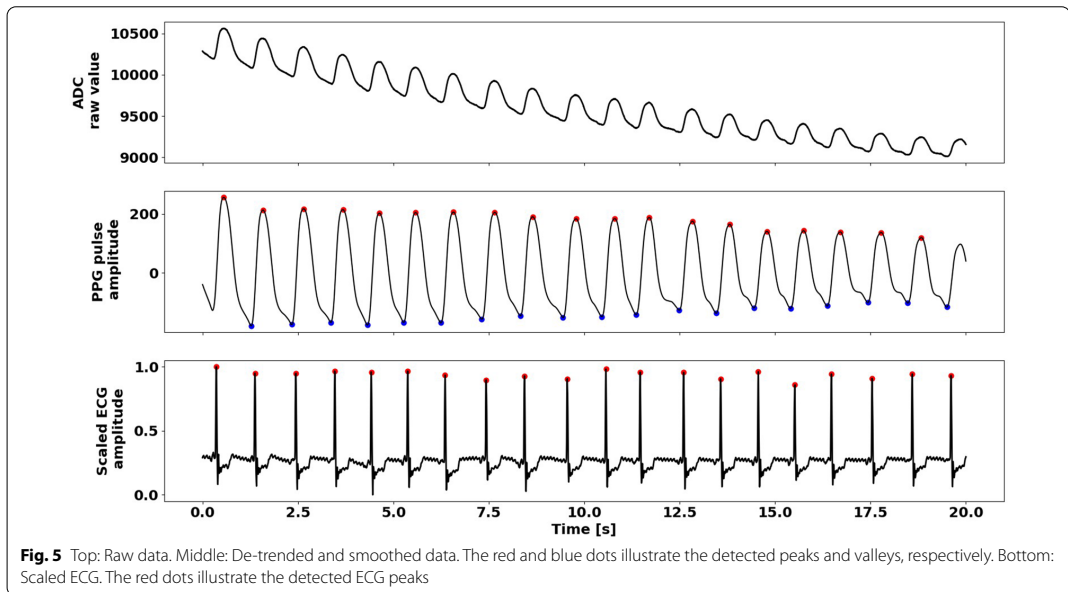
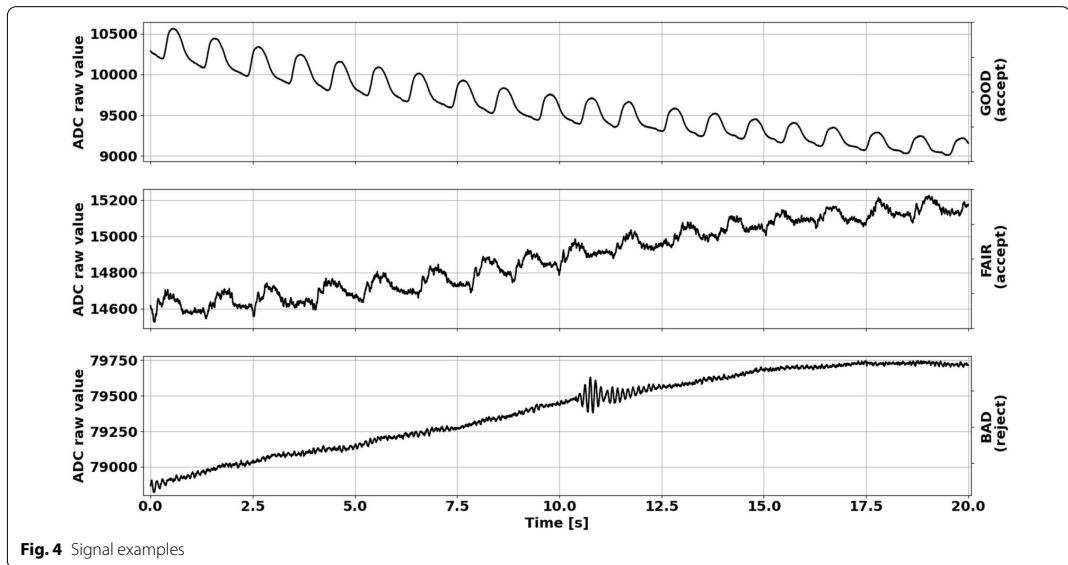
$$y(m) = \sum_{n=1}^N X(n)X(n+m) \tag{2}$$

where  $N$  is the number of samples in the signal  $X$ , and  $m \in [0, N-1]$ . By applying the same peak detection method as that used for ECG, the index of the dominating peak (i.e., the first peak) in the autocorrelation series was identified. Because the autocorrelation series featured softer (but not flat/diffuse) peaks compared to the ECG signal, the prominence setting in the peak detection algorithm was relaxed to 0.3 to avoid too

**Table 1** Summary of data set evaluations for both orientations, “Or.” (Hor = horizontal and Ver = vertical) and all rotations, “Rot.” (see Fig. 2) for all fish

Or.	Rot.	Fish1	Fish2	Fish3	Fish4	Fish5	Fish6
Hor 1	0	NVD	NVD	$\lambda_2$	NVD	$\lambda_2$	NVD
Hor	90	NVD	NVD	$\lambda_2$	NVD	NVD	NVD
Hor	180	NVD	NVD	$\lambda_1, \lambda_2$	NVD	$\lambda_2$	NVD
Hor	270	NVD	NVD	$\lambda_1, \lambda_2$	NVD	$\lambda_1, \lambda_2$	NVD
Hor 2	0	NVD	NVD	$\lambda_1, \lambda_2$	NVD	NVD	NVD
Ver 1	0	$\lambda_1, \lambda_2$	$\lambda_1, \lambda_2$	$\lambda_1, \lambda_2$	$\lambda_1, \lambda_2$	$\lambda_1, \lambda_2$	NVD
Ver	90	$\lambda_1, \lambda_2$	$\lambda_1, \lambda_2$	N/A	$\lambda_1, \lambda_2$	NVD	$\lambda_1, \lambda_2$
Ver	180	$\lambda_1, \lambda_2$	NVD	N/A	NVD	NVD	NVD
Ver	270	$\lambda_1, \lambda_2$	$\lambda_1, \lambda_2$	N/A	$\lambda_1, \lambda_2$	$\lambda_1, \lambda_2$	$\lambda_1, \lambda_2$
Ver 2	0	$\lambda_1, \lambda_2$	$\lambda_1, \lambda_2$	N/A	$\lambda_1, \lambda_2$	$\lambda_1, \lambda_2$	$\lambda_1, \lambda_2$

NVD signifies “No Valid Data”, i.e., no part of the time series fulfils all selection requirements.  $\lambda_1$  and  $\lambda_2$  represents valid data for 660 nm and 880 nm, respectively “N/A” (Not Applicable) denotes the data series which could not be collected for Fish 3 due to cardiac arrest. Note that the 0 degrees measurement has been repeated for both orientations

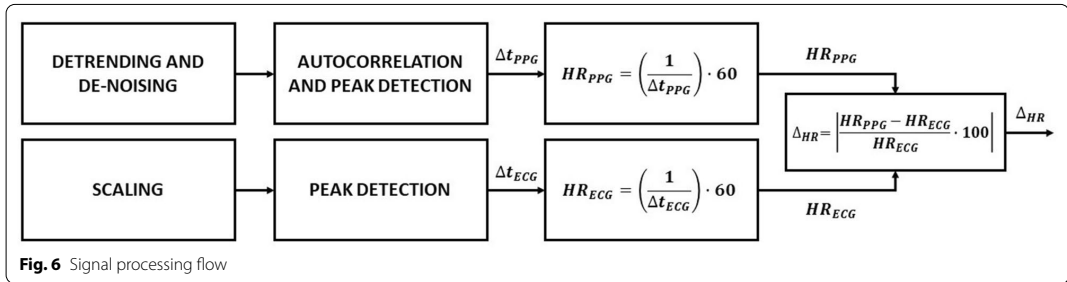


aggressive peak rejection. As for ECG HR, the time window was set to 160 samples. The index of the identified peak, therefore, represented the average time delay between peaks in the PPG time series, and was used to

calculate PPG HR in beats per minute (HRBPM) using Eq. 1.

To evaluate which sensor orientation and rotation gave the highest quality data, the signal quality index (SQI) for





the noise suppressed (but not de-trended) PPG signals, was calculated. SQI is defined for individual PPG pulses by [35]:

$$P_{SQI} = \frac{PPG_{pa}}{PPG_{avg}} \cdot 100 \quad (3)$$

where  $PPG_{pa}$  is the peak-to-peak PPG pulse amplitude and  $PPG_{avg}$  its mean value. The PPG signal where only noise suppression had been applied was used to retain access to the pulses' mean value which was removed during de-trending. A pulse was defined as the valley to valley noise suppressed data subsets. Valley indices (i.e., positions) were identified by inverting the de-trended (i.e., mean-centered) signal and reapplying the peak detection algorithm with the same window and prominence settings as those for autocorrelation peak detection. Using the valley indices, the pulses were extracted from the noise suppressed (but not de-trended) data sets, and the average SQI ( $SQI_{avg}$ ) for all pulses calculated to represent the subset SQI. An example illustrating the peak detection result is given in Fig. 5.

To evaluate the accuracy of the PPG HR estimates, the difference between the ECG baseline and both wavelengths separately were calculated in percent using:

$$\Delta_{HR} = \left| \frac{HR_{PPG} - HR_{ECG}}{HR_{ECG}} \cdot 100 \right| \quad (4)$$

The signal processing flow is illustrated in Fig. 6.

## Results

ECG was labeled “GOOD” in all data sets, while one or both PPG wavelengths were judged to qualify as “GOOD” or “FAIR” in 28 data sets. Thus, 28 (of 56) data sets were omitted from analysis. The results from the data processing are given in Table 2. The results show an average accuracy of  $0.7 \pm 1.0\%$  for 660 nm and  $1.1 \pm 1.2\%$  for 880 nm wavelengths relative to the ECG HR baseline. The average SQI ( $SQI_{avg}$  column in Table 2) indicates that the vertical orientation and 0 degrees rotation (i.e., measuring towards the heart) resulted in the best data quality.

## Discussion

The high accuracy for HR computed from PPG compared to the ECG baseline from our experiments indicates that PPG is a viable alternative sensor principle for monitoring heart rate in Atlantic salmon. Moreover, the MAX86150 unit appears to be a suitable sensor module for implementation in future DSTs or transmitter tags aiming to measure and report HR over time. Although the sensor is designed for integration in optical HR measurement applications for humans and, thus, with human tissues and blood in mind, the HR estimate relies solely on the time-varying tissue perfusion. While human and fish blood is different with respect to composition and cell morphology, the essential functionality is the same, as is the hemoglobin [40]. The wavelengths emitted by the MAX86150 sensor are chosen due to their absorption sensitivity to oxy- and deoxyhemoglobin which determines the blood's oxygenation and thus its colour. Because tissue colour is affected by perfusion, processing either or both wavelength will be a feasible approach to obtain HR in both humans and fishes.

The data used in this study originates from 6 different fish, yielding 28 data sets. Although up to 10 data sets were collected from each fish, the data sets are considered independent because each data set is separate in either time, relates to different tissues, or both. When reviewing Table 1, most data available for processing came from the anterior part of the fish. This is probably because the measurements in this region coincide with locations with a high blood supply such as the liver and gut (thus implying high perfusion) compared to the posterior region where tissues with lower perfusion (mostly white muscle tissue) are present. This is supported by that the average SQI (Table 2) was highest for locations and orientations associated with the anterior part of the fish, especially for the 0 degree rotation which is towards the heart. This indicates that future implementations of PPG sensors for Atlantic salmon should facilitate data collection in this area.

**Table 2** Results sorted by average SQI where the columns named Fish is the fish number, Or. is the orientation, Rot. is the rotation, HR<sub>ECG</sub> is the heart rate in BPM calculated from ECG, HR<sub>660</sub> is the calculated heart rate in BPM for the 660 nm time series, HR<sub>880</sub> is the calculated heart rate in BPM for the 880 nm time series,  $\Delta$ HR<sub>660</sub> is the difference in HR estimate between the 660 nm time series and ECG in percent,  $\Delta$ HR<sub>880</sub> is the difference in HR estimate between the 880 nm time series and ECG in percent, SQI<sub>660</sub> is the SQI for 660 nm, SQI<sub>880</sub> is the SQI for 880 nm and SQI<sub>avg</sub> is the average SQI, respectively

Fish	Or.	Rot.	HR <sub>ECG</sub>	HR <sub>660</sub>	HR <sub>880</sub>	$\Delta$ HR <sub>660</sub>	$\Delta$ HR <sub>880</sub>	SQI <sub>660</sub>	SQI <sub>880</sub>	SQI <sub>avg</sub>	Likely tissues
5	Ver	270	50.4	50.2	50.4	0.40	0.00	0.03	0.02	0.02	M, F
3	Hor 2	0	53.1	53.3	53.3	0.38	0.38	0.04	0.05	0.05	F
5	Hor	270	50.6	50.4	50.6	0.40	0.00	0.02	0.08	0.05	M, F
5	Hor 1	0	35.9	N/A	35.2	N/A	1.95	N/A	0.08	0.08	F
5	Hor	180	46.0	N/A	46.0	N/A	0.00	N/A	0.10	0.10	F, I
2	Ver	270	43.0	42.7	42.4	0.70	1.40	0.16	0.14	0.15	M, F
5	Ver 1	0	49.0	48.6	48.2	0.82	1.63	0.28	0.06	0.17	L, G
3	Hor	90	41.1	N/A	40.7	N/A	0.97	N/A	0.18	0.18	M, F
3	Hor 1	0	41.1	N/A	40.7	N/A	0.97	N/A	0.18	0.18	F
3	Hor	180	41.7	41.2	41.0	1.20	1.68	0.21	0.21	0.21	F, I
6	Ver	90	27.5	27.3	26.8	0.73	2.55	0.36	0.17	0.26	M, F
3	Hor	270	42.9	42.9	43.5	0.00	1.40	0.48	0.24	0.36	M, F
5	Ver 2	0	52.6	52.6	52.6	0.00	0.00	0.48	0.25	0.36	L, G
4	Ver	270	37.7	37.7	37.9	0.00	0.53	0.81	0.51	0.66	M, F
2	Ver	90	35.0	35.1	35.2	0.29	0.57	0.95	0.74	0.84	M, F
6	Ver	270	36.0	35.8	35.7	0.56	0.83	1.51	0.55	1.03	M, F
2	Ver 2	0	48.6	48.8	48.8	0.41	0.41	0.87	1.59	1.23	L, G
1	Ver	270	18.0	18.2	18.2	1.11	1.11	2.35	0.63	1.49	M, F
1	Ver	90	13.9	13.8	13.8	0.72	0.72	1.95	1.24	1.60	M, F
1	Ver	180	19.0	18.9	18.9	0.53	0.53	2.55	0.69	1.62	G, F
6	Ver 2	0	33.6	33.6	33.6	0.00	0.00	3.27	0.66	1.96	L, G
2	Ver 1	0	32.8	32.0	32.0	2.44	2.44	2.66	1.84	2.25	L, G
4	Ver 2	0	70.2	70.2	70.2	0.00	0.00	2.96	1.61	2.28	L, G
3	Ver 1	0	59.4	59.4	59.4	0.00	0.00	3.75	1.32	2.54	L, G
4	Ver 1	0	32.4	30.7	31.3	5.25	3.40	4.69	1.38	3.04	L, G
1	Ver 1	0	19.4	19.3	19.3	0.52	0.52	13.2	2.90	8.05	L, G
1	Ver 2	0	26.7	26.5	26.5	0.75	0.75	14.59	6.20	10.40	L, G
4	Ver	90	37.2	37.6	39.2	1.08	5.38	24.68	7.92	16.30	M, F

The table entry "N/A" (Not Applicable) is for the cases where no valid data could be identified for the respective wavelength in a particular data set. Entries in the Likely tissues column are: M: Muscle, F: Fat, I: Intestines, L: Liver and G: Gut, and denote tissues likely present in the sensing volume for the associated sensor orientation and rotation

The range between the lowest (13.9 BPM) and highest (70.2 BPM) heart rates may be explained by that different fish individuals would have had different physiological baselines (e.g., stress levels and health) prior to the experiments. These differences would, thus, have yielded different individual responses to handling and anesthesia. Differences in heart rates were, therefore, expected. Reported heart rates for Atlantic salmon and comparable species are between 15 and 80 BPM [21, 37]. With the exception of one individual (13.9 BPM) all measured heart rates fell within this expected range. The individual having a heart rate below 15 could have been more susceptible to sedation thus explaining this result, or the reported HR range is conservative.

In our results, HR was reported using one decimal because additional decimal points are likely inaccurate. This conclusion stems from considering the HR-dependent quantification error for our highest HR (70.2 BPM). When sampling at 200 Hz, the change in BPM resulting from what is considered the maximum timely offset from true peak position can be calculated. This is achieved by first finding beats per second (BPS) which in this case is  $70.2/60 = 1.17$  BPS. The time between HR peaks will in this case be  $\Delta t = 1/1.17 = 0.855$  s. A timely offset in true peak placement exceeding 50% of the sampling interval implies that a peak will be associated with the previous or next sampling point. Hence, for our quantification error we get  $E_q = 0.855 + (1/200) \cdot 0.5 = 0.8575$  s. This peak to

peak distance which includes the 50% offset, then gives a shifted BPM of  $\text{BPM} = 60/0.8575 = 69.995$ . The BPM difference can then be calculated as  $\Delta\text{BPM} = 70.2 - 69.995 \approx 0.2$  BPM. The corresponding number for our lowest baseline HR (13.9 BPM) is 0.008 BPM.

The quantification error considerations are closely related to our measurements' sensitivity. By first accepting that a peak cannot be placed "between" two sampling points, the sensitivity can then be evaluated in the same way as the quantification error, only using the whole sampling interval. Thus, the sensitivity can be considered to be twice that of the quantification error, i.e., 0.4 BPM per sample offset for 70.2 BPM, and 0.016 BPM per sample offset for 13.9 BPM.

The deviation from the baseline of  $0.7 \pm 1.0\%$  for 660 nm and  $1.1 \pm 1.2\%$  for 880 nm can be explained by different factors. One potentially important source of error is that PPG is sensitive to motion artefacts. Such artefacts can be divided into two types: Perfusion changes in tissue caused by motion and relative motion between the sensor and the sensing volume. The former is not considered relevant when evaluating the results because all fish were in level 3 anesthesia (surgical) and, thus, motionless. However, such artefacts are likely to be important when the method is applied to free-swimming non-sedated fish. A logical next step on the path towards an operational measurement method would, therefore, be to apply the sensor to fish exhibiting normal swimming behaviour, and collect concurrent PPG and motion data to assess the potential impact of specific motion patterns.

To minimize the effect of the latter, the setup was designed to be as rigid as possible to ensure a stable sensing environment during data collection (Figs. 1 and 3). However, although the setup was mechanically stable and the fish in level 3 anesthesia, motion artifacts caused by potential tissue movement such as peristalsis [40] may have caused transient changes in the trend and potential changes in the amplitude of the PPG's pulsatile

component. This is partly remedied using high pass filtering in the analyses, as this effectually reduces or removes long term trends and any changes therein. Moreover, an estimate of HR relies solely on the frequency content in the PPG signal measurement signal, and not the amplitude. Based on these observations, movement of tissues relative to the sensor during data collection were unlikely to have had impact on the results.

Motion artefacts may also have been caused by tissue contraction (e.g., the heart) if it was within the sensing volume during data collection. This is particularly relevant for the vertical orientation with  $0^\circ$  rotation (i.e., when the sensor was pointing towards the heart). Because this is of particular concern, a subsequent post mortem dissection of Atlantic salmon was done to assess the sensing volume for this orientation and rotation. The dissection revealed that the tissue observed with the present method was likely dominated by low-perfusion fatty tissues surrounding larger blood vessels such as the hepatic arteries and veins (Fig. 7) [40]. Fat has a high optical scattering [41] coefficient due to lipid droplets inside the fat cells. Due to the size of the scatters, this scattering is highly forward directed and almost independent of the wavelength of the light. This implies that the light from the sensor is strongly scattered by the tissue while the intensity decays exponentially with distance from the light source in accordance with the (modified) Beer–Lambert law [42], thus limiting the distance light travels. This is indicated by the fact that the SQI for both wavelengths was generally low due to the big difference between the pulsatile PPG component's amplitude and the signal mean. A large mean value implies that a lot of light is scattered back to the receiver without having penetrated far into the tissue. It is, therefore, likely that the data originates from tissues close to the light source and that the heart is not part of the sensing volume.

Accuracy may also have been affected by the physiological state of the fish. The fish used in the experiment were

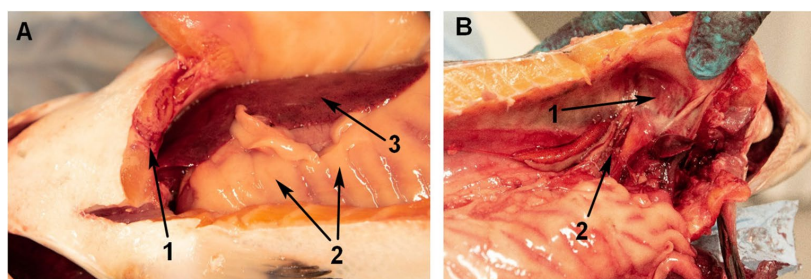


**Fig. 7** **A** (left): 1. Epigastric vein/artery, 2. Pylorus caeca/lipid deposits, 3. Liver. **B** (right) 1. Septum transversum, 2. Hepatic arteries/veins

lab grown and showed no signs of deteriorated health. The anesthesia had both an analgesic and a paralyzing effect. It must, therefore, be expected that the secondary circulation system driven by the caudal heart and movement was impaired during data collection. In addition, the fish underwent a surgical procedure and the incisions as well as the sensor insertion may have further disturbed parts of the circulation system. When reviewing Table 2 for fish where data for both iterations of the horizontal and vertical 0° are available, similar SQIs for both iterations appear to be the trend. Although this indicates that the physiological state of the fish remained stable during data collection, it is likely that this state differs from that a fully awake and moving fish would exhibit. This underlines the necessity of conducting further experiments with fish exhibiting more normal behaviours and physiological function.

The peak detection procedure may have affected the accuracy of the method because the detrended PPG signals consisted of an oscillating curve with wide peaks compared to the ECG peaks. The accuracy in PPG peak detection was, therefore, lower, thus resulting in slight differences in the intervals between the detected PPG peaks and their corresponding ECG peaks. For long time series containing many peaks, such differences are expected to cancel out, but this may not have been the case for 20 s data sets. This may have been further exacerbated by the fact that the various orientations and rotations would have illuminated tissues and capillary beds supplied by haemal arches connected to different points along the dorsal artery. The resulting differences in pulse transit times (PTT, i.e., times between the heart beat and when it is observable in the sensing volume), may have shifted the PPG in relation to the ECG [43]. Furthermore, if different capillary beds with different PTTs were present in the sensing volume it could have distorted the PPG pulses by dragging them out in time, thereby explaining the differences in morphology seen between the “GOOD” and “FAIR” pulse examples in Fig. 4.

The criteria used for the selection of valid data subsets for analyses are subject to interpretation as highlighted by Elgendi et al. [35], meaning that other evaluators could have included some rejected data sets and vice versa. Although this is an inherent weakness in this method for assessing data quality, it is of greatest importance when using PPG for determination of  $SpO_2$  where the PPG shape is paramount for the validity of the  $SpO_2$  estimate [24]. When estimating HR only, PPG morphology is of lesser concern since only the frequency content of the pulsatile PPG component is required. The PPG based HR estimate is, therefore, considered robust against variations in interpretation of the subset selection criteria.

Autocorrelation was chosen for PPG analysis because its low computational demand and robustness against potential transient motion artifacts makes it a likely candidate for implementation in a microcontroller suitable for integration in a size and energy constrained fish tag. However, it cannot be ruled out that other, more computationally demanding approaches such as singular spectrum analysis [44], wavelet analysis [45] or a fast Fourier transform [46] approach could have given better results.

The perfusion index (Eq. 3) was used to evaluate signal quality because this is considered the “gold standard” for PPG signal quality evaluation, even though alternative methods (e.g., skewness, kurtosis and entropy) [35] which might lead to better results, exist. Such methods, however, are derived using reference data readily available for humans. To the authors’ knowledge, no reference PPG data for fish exist for comparison. Such data would be a very useful resource in developing new methods for quality evaluations of PPG data from fish, particularly if aspiring to quantify  $SpO_2$ .

Overall, valid data was identified for all orientations and rotations. Although certain combinations of orientation and rotation yielded fewer data sets fulfilling the subset selection criteria than others, this does not necessarily mean that data are harder to obtain for these orientations and rotations. The same low-energy output settings were used for both orientations and all rotations, thus implying that more valid data could have been obtained if sensor settings, such as output power, had been increased. PPG, therefore, has the potential of being a robust alternative to ECG for HR measurement in fish.

## Conclusions

A PPG/ECG module has been successfully adapted to measure both ECG and PPG in-vivo for anesthetized Atlantic salmon. Using ECG as baseline, results from an analysis of the PPG signals show that HR can be accurately estimated from the PPG measurement, thus having the potential to become an alternative to ECG HR measurements in fish.

Based on the encouraging results from this experiment, the MAX86150 has been integrated with an inertial motion unit, a temperature and a magnetic field sensor in a stand-alone cylindrical implant measuring  $13 \times 40$  mm [47]. This implant will undergo testing in swim tunnel trials logging motion data, ECG and PPG. Data from both wavelengths will be logged to evaluate the possibility of deriving  $SpO_2$  from the data. These studies will enable the evaluation of how motion artefacts due to swimming motion impacts the data, and potentially how such artefacts can be remedied in post-processing.

Because this implant measures both ECG and PPG, co-processing of ECG and PPG for an even more robust HR estimate is made possible. This is already a topic in human medicine to improve accuracy and robustness for heart rate variability estimates beyond what is currently possible using ECG alone [48].

#### Acknowledgements

The authors thank the Research Council of Norway for funding the work (see “Funding”) as well as SINTEF Ocean AS for supporting the PhD project through their in-kind contribution. We also thank the personnel at NINA’s research station at Ims for facilitating the experiment.

#### Authors’ contributions

ES and JAA conceived the idea for the setup and testing the sensing principle in fish. ES is responsible for the completion of the PhD in the funding project, designed the required equipment, planned and executed the experiment, prepared and processed data, and did the main job in preparing the manuscript. FØ participated in the planning and execution of the experiments with emphasis on anesthesia and surgery. MF, JAA assisted in equipment design and planning of the experiment. LLR has participated in data processing, while BF and REO have contributed with the anatomical and physiological considerations. All authors have provided feedback and contributed to writing the manuscript. All authors read and approved the final manuscript.

#### Funding

This study was funded by the Research Council of Norway (RCN Project Number 280864) and through in-kind from SINTEF Ocean.

#### Availability of data and materials

The data sets used and/or analysed during the current study are available from the corresponding author on reasonable request.

#### Declarations

##### Ethics approval and consent to participate

The animal experiment described herein was conducted with permission given by the Norwegian Food Safety Authority (permit number 19/104024). Permission to use up to, but not exceeding, 15 individual Atlantic salmon was given under the condition that data collection was stopped when 5 complete data sets were obtained as a reduction measure (3R) [49], a point that was reached after 7 fish. The experiment was carried out at NINA Ims Research Station close to Stavanger, Norway, on August 28th, 2019.

##### Consent for publication

Not applicable.

##### Competing interests

The authors declare that they have no competing interests.

##### Author details

<sup>1</sup>Department of Engineering Cybernetics, NTNU, O.S. Bragstads Plass 2D, 7034 Trondheim, Norway. <sup>2</sup>Department of Aquaculture Technology, SINTEF Ocean, Brattørkaia 17C, 7010 Trondheim, Norway. <sup>3</sup>Department of Electronic Systems, O.S. Bragstads Plass 2B, 7034 Trondheim, Norway. <sup>4</sup>Norwegian Institute for Nature Research, Høgskoleringen 9, 7485 Trondheim, Norway. <sup>5</sup>Department of Biology, NTNU, Brattørkaia 17B, 7010 Trondheim, Norway.

Received: 6 May 2021 Accepted: 13 September 2021

Published online: 22 September 2021

#### References

1. FAO: Food and Agriculture Organization of the United Nations, Fisheries and Aquaculture department (2021). <http://www.fao.org/fishery/aquaculture/en> Accessed 2 May 2021

2. Sommerset I, Walde C, Bang Jensen B, Børnø B, Haukaas A, Brun E. Fiskehelse rapporten 2019. report 5a/2020 (Norwegian Veterinary Institute, Oslo, Norway, 2019) (2020)
3. Noble C, Nilsson J, Stien LH, Iversen MH, Kolarevic J, Gismervik K. Velferdsindikatorer for oppdrettslaks: Hvordan vurdere og dokumentere fiskevelferd. 2. utgave (2018)
4. Føre M, Frank K, Norton T, Svendsen E, Alfreidsen JA, Dempster T, Eguiraun H, Watson W, Stahl A, Sunde LM, et al. Precision fish farming: a new framework to improve production in aquaculture. *Biosys Eng.* 2017. <https://doi.org/10.1016/j.biosystemseng.2017.10.014>.
5. Knudsen F, Fosseidengen J, Oppedal F, Karlsen Ø, Ona E. Hydroacoustic monitoring of fish in sea cages: target strength (ts) measurements on Atlantic salmon (*Salmo salar*). *Fish Res.* 2004;69(2):205–9.
6. Berckmans D. General introduction to precision livestock farming. *Anim Front.* 2017;7(1):6–11.
7. Føre M, Svendsen E, Alfreidsen JA, Uglem I, Bloecher N, Sveier H, Sunde LM, Frank K. Using acoustic telemetry to monitor the effects of crowding and delousing procedures on farmed Atlantic salmon (*Salmo salar*). *Aquaculture.* 2018;495:757–65.
8. Brijis J, Sandblom E, Axelsson M, Sundell K, Sundh H, Huyben D, Broström R, Kiessling A, Berg C, Gråns A. The final countdown: continuous physiological welfare evaluation of farmed fish during common aquaculture practices before and during harvest. *Aquaculture.* 2018;495:903–911
9. Hassan W, Føre M, Pedersen, M.O., Alfreidsen, J.A.: A novel doppler based speed measurement technique for individual free-ranging fish. In: 2019 IEEE SENSORS, pp. 1–4 (2019). IEEE
10. Baktoft H, Gjelland KØ, Økland F, Thygesen UH. Positioning of aquatic animals based on time-of-arrival and random walk models using yaps (yet another positioning solver). *Sci Rep.* 2017;7(1):1–10.
11. Hassan W, Føre M, Urke HA, Kristensen T, Ulvund JB, Alfreidsen JA, et al. System for real-time positioning and monitoring of fish in commercial marine farms based on acoustic telemetry and internet of fish (iof). In: The 29th International Ocean and Polar Engineering Conference (2019). International Society of Offshore and Polar Engineers
12. Thorstad EB, Rikardsen AH, Alp A, Økland F. The use of electronic tags in fish research—an overview of fish telemetry methods. *Turk J Fish Aquat Sci.* 2013;13(5):881–96.
13. Deng ZD, Weiland MA, Fu T, Seim TA, LaMarche BL, Choi EY, Carlson TJ, Eppard MB. A cabled acoustic telemetry system for detecting and tracking juvenile salmon: Part 2. Three-dimensional tracking and passage outcomes. *Sensors.* 2011;11(6):5661–76. Doi: <https://doi.org/10.3390/s110605661>
14. Weiland MA, Deng ZD, Seim TA, LaMarche BL, Choi EY, Fu T, Carlson TJ, Thronas AI, Eppard MB. A cabled acoustic telemetry system for detecting and tracking juvenile salmon: Part 1. Engineering design and instrumentation. *Sensors.* 2011;11(6):5645–60. Doi: <https://doi.org/10.3390/s110605645>
15. Hussey NE, Kessel ST, Aarestrup K, Cooke SJ, Cowley PD, Fisk AT, Harcourt RG, Holland KN, Iverson SJ, Kocik JF et al. Aquatic animal telemetry: a panoramic window into the underwater world. *Science.* 2015;348(6240):1255642
16. Muñoz L, Aspillaga E, Palmer M, Saraiva JL, Arechavala-Lopez P. Acoustic telemetry: a tool to monitor fish swimming behavior in sea-cage aquaculture. *Front Marine Sci.* 2020;7: 645
17. Føre M, Frank K, Dempster T, Alfreidsen JA, Høy E. Biomonitoring using tagged sentinel fish and acoustic telemetry in commercial salmon aquaculture: a feasibility study. *Aquacult Eng.* 2017;78:163–72.
18. Wendelaar Bonga SE. The stress response in fish. *Physiol Rev.* 1997;77(3):591–625.
19. Hvas M, Folkedal O, Oppedal F. Heart rate bio-loggers as welfare indicators in Atlantic salmon (*Salmo salar*) aquaculture. *Aquaculture.* 2020;529:735630.
20. Svendsen E, Føre M, Økland F, Gråns A, Hedger RD, Alfreidsen JA, Uglem I, Rosten C, Frank K, Erikson U et al. Heart rate and swimming activity as stress indicators for Atlantic salmon (*Salmo salar*). *Aquaculture.* 2020;531: 735804
21. Brijis J, Sandblom E, Rosengren M, Sundell K, Berg C, Axelsson M, Gråns A. Prospects and pitfalls of using heart rate bio-loggers to assess the welfare of rainbow trout (*Oncorhynchus mykiss*) in aquaculture. *Aquaculture.* 2019;509:188–197

22. Charlton PH, Birrenkott DA, Bonnici T, Pimentel MA, Johnson AE, Alastruey J, Tarassenko L, Watkinson PJ, Beale R, Clifton DA. Breathing rate estimation from the electrocardiogram and photoplethysmogram: a review. *IEEE Rev Biomed Eng.* 2017;1:12–20.
23. Severinghaus JW. Takuo aoyagi: discovery of pulse oximetry. *Anesth Analg.* 2007;105(6):1–4.
24. Chan ED, Chan MM, Chan MM. Pulse oximetry: understanding its basic principles facilitates appreciation of its limitations. *Respir Med.* 2013;107(6):789–99.
25. Islam MT, Zahir I, Ahamed ST, Yasar MT, Shahnaz C, Fattah SA. A time-frequency domain approach of heart rate estimation from photoplethysmographic (ppg) signal. *Biomed Signal Process Control.* 2017;36:146–54.
26. Erhardt W, Lendl C, Hipp R, von Hegel G, Wiesner G, Wiesner H. The use of pulse oximetry in clinical veterinary anaesthesia. *J Assoc Vet Anaesth Great Br Irel.* 1990;17(1):30–1. <https://doi.org/10.1111/j.1467-2995.1990.tb00385.x>.
27. Theodor M, Ruh D, Subramanian S, Förster, K, Heilmann C, Beyersdorf F, Plachta D, Manoli Y, Zappe H, Seifert A. Implantable pulse oximetry on subcutaneous tissue. In: 2014 36th Annual International Conference of the IEEE Engineering in Medicine and Biology Society, pp. 2089–2092 (2014). IEEE
28. Reynolds J, Ahmmed P, Bozkurt A. An injectable system for subcutaneous photoplethysmography, accelerometry, and thermometry in animals. *IEEE Trans Biomed Circuits Syst.* 2019;13(5):825–34.
29. Machikhin AS, Burlakov AB, Volkov MV, Khokhlov DD. Imaging photoplethysmography and videoangiography enable noninvasive study of zebrafish cardiovascular system functioning. *J Biophotonics.* 2020;13(7):202000061.
30. Seo E, Sazi T, Togawa M, Nagata O, Murakami M, Kojima S, Seo Y. A portable infrared photoplethysmograph: heartbeat of *Mytilus galloprovincialis* analyzed by mri and application to bathymodiolus septemdemium. *Biol Open.* 2016;5(11):1752–7.
31. Tomlinson S, Behrmann S, Cranford J, Louie M, Hashikawa A. Accuracy of smartphone-based pulse oximetry compared with hospital-grade pulse oximetry in healthy children. *Telemed e-Health.* 2018;24(7):527–35. <https://doi.org/10.1089/tmj.2017.0166>.
32. Hahnen C, Freeman CG, Haldar N, Hamati JN, Bard DM, Murali V, Merli GJ, Joseph JJ, van Helmond N. Accuracy of vital signs measurements by a smartwatch and a portable health device: validation study. *JMIR Mhealth Uhealth.* 2020;8(2):16811.
33. Maxim Integrated: Maxim Integrated, Integrated Photoplethysmogram and Electrocardiogram Bio-sensor Module for Mobile Health (2021). <https://datasheets.maximintegrated.com/en/ds/MAX86150.pdf> Accessed 9 Aug 2021.
34. Coyle SD, Durborow RM, Tidwell JH, et al. Anesthetics in aquaculture vol. 3900. Southern Regional Aquaculture Center, Stoneville (2004)
35. Elgendi M. Optimal signal quality index for photoplethysmogram signals. *Bioengineering.* 2016;3(4):21. <https://doi.org/10.3390/bioengineering3040021>.
36. Doving K, Reimers E. *Fiskens Fysiologi*. Bergen: John Grieg; 1992
37. Lucas M. Heart rate as an indicator of metabolic rate and activity in adult Atlantic salmon, *Salmo salar*. *J Fish Biol.* 1994;44(5):889–903.
38. Butterworth C. Filter approximation theory. *Engineer.* 1930;7:536–41.
39. Savitzky A, Golay MJ. Smoothing and differentiation of data by simplified least squares procedures. *Anal Chem.* 1964;36(8):1627–39.
40. Farrell AP. *Encyclopedia of fish physiology: from genome to environment*. London: Academic press; 2011.
41. Johns M, Giller CA, German DC, Liu H. Determination of reduced scattering coefficient of biological tissue from a needle-like probe. *Opt Express.* 2005;13(13):4828–42.
42. Bigio, I.J., Fantini, S.: *Quantitative Biomedical Optics: Theory, Methods, and Applications*. Cambridge University Press, University Printing Press, Cambridge CB2 8BS, United Kingdom (2016)
43. Nitzan M, Khanokh B, Slovik Y. The difference in pulse transit time to the toe and finger measured by photoplethysmography. *Physiol Meas.* 2001;23(1):85.
44. Golyandina N, Zhigljavsky A. *Singular spectrum analysis for time series*, vol. 120. Heidelberg New York Dordrech London: Springer; 2013.
45. Meyer Y. *Wavelets: algorithms & applications*. Philadelphia: SIAM (Society for Industrial and Applied Mathematics; 1993.
46. Cooley JW, Tukey JW. An algorithm for the machine calculation of complex fourier series. *Math Comput.* 1965;19(90):297–301.
47. Svendsen E, Føre M, Randeberg L, JA., Design of a novel biosensor implant for farmed Atlantic salmon (*Salmo salar*). In: 2021 IEEE SENSORS, Accepted for Publication (2021). IEEE
48. Zaretskiy A, Mityagin K, Tarasov V, Moroz D, Kuraleva A. Robust heart rate estimation using combined ecg and ppg signal processing. In: IOP Conference Series: Materials Science and Engineering, vol. 537, p. 042077 (2019). IOP Publishing
49. Norecopa: Norecopa, Norway's National Consensus Platform (2021). <https://norecopa.no/> Accessed 10 Mar 2021

## Publisher's Note

Springer Nature remains neutral with regard to jurisdictional claims in published maps and institutional affiliations.

### Ready to submit your research? Choose BMC and benefit from:

- fast, convenient online submission
- thorough peer review by experienced researchers in your field
- rapid publication on acceptance
- support for research data, including large and complex data types
- gold Open Access which fosters wider collaboration and increased citations
- maximum visibility for your research: over 100M website views per year

At BMC, research is always in progress.

Learn more [biomedcentral.com/submissions](https://biomedcentral.com/submissions)



## Paper D

Design of a novel biosensor  
implant for farmed Atlantic  
salmon (*Salmo salar*)

*Paper D*

*Design of a novel biosensor implant for farmed Atlantic salmon (*Salmo salar*)*

---

This paper is not included due to IEEE restrictions  
available at <https://doi.org/10.1109/SENSORS47087.2021.9639671>



Paper E  
Data for Characterization of  
the Optical Properties of  
Atlantic Salmon (*Salmo salar*)  
Blood


Paper E

Data for Characterization of the Optical Properties of Atlantic Salmon  
(*Salmo salar*) Blood

---

## RESEARCH ARTICLE

# Data for characterization of the optical properties of Atlantic salmon (*Salmo salar*) blood

Eirik Svendsen<sup>1,2</sup>  | Lise L. Randeberg<sup>3</sup> | Martin Føre<sup>1</sup> | Bengt Finstad<sup>4</sup> | Rolf Erik Olsen<sup>4</sup> | Nina Bloecher<sup>2</sup> | Jo Arve Alfredsén<sup>1</sup>

<sup>1</sup>Department of Engineering Cybernetics, Norwegian University of Science and Technology, Trondheim, Norway

<sup>2</sup>Department for Aquaculture, SINTEF Ocean AS, Trondheim, Norway

<sup>3</sup>Department of Electronic Systems, Norwegian University of Science and Technology, Trondheim, Norway

<sup>4</sup>Department of Biology, Norwegian University of Science and Technology, Trondheim, Norway

## Correspondence

Eirik Svendsen, Department of Engineering Cybernetics, Norwegian University of Science and Technology, Trondheim, 7034, Norway.  
Email: [eirik.svendsen@sintef.no](mailto:eirik.svendsen@sintef.no)

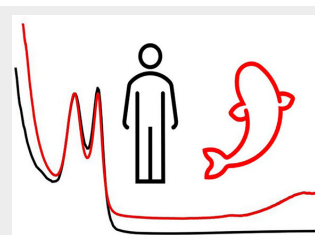
## Funding information

Norges Forskningsråd; SINTEF Ocean AS; Research Council of Norway, Grant/Award Number: 280864

## Abstract

Photoplethysmography is a recent addition to physio-logging in Atlantic salmon which can be used for pulse oximetry provided that the properties for light propagation in salmon tissues are known.

In this work, optical properties of three constituents of Atlantic salmon blood have been characterized using a photo spectrometer in the VIS–NIR range (450–920 nm). Furthermore, Atlantic salmon blood cell size has been measured using a Coulter counter as part of light scattering property evaluations. Results indicate that plasma contributes little to scattering and absorption for wavelengths typically used in pulse oximetry as opposed to blood cells which are highly scattering. Extinction spectra for oxygenated and deoxygenated hemoglobin indicate that Atlantic salmon hemoglobin is similar to that in humans. Pulse oximetry sensors originally intended for human applications may thus be used to estimate blood oxygenation levels for this species.



## KEYWORDS

blood cells, extinction, hemoglobin, photoplethysmography, plasma, scattering, spectral analysis

## 1 | INTRODUCTION

The advent of miniaturized sensors for measurement of physiological signals has enabled wearable devices for use in, for example, patient monitoring [1], sports performance tracking [2] and animal monitoring [3]. Such devices have found their use in fishes as they can contribute to improved understanding of behavioral and physiological responses [4]. This is particularly relevant for Atlantic salmon (*Salmo salar*) as it is an important

species in aquaculture with 2.7 million tonnes live weight produced worldwide in 2020 [5].

Salmon husbandry entails a broad range of interrelated operations (e.g., feeding, crowding, pumping) with convoluted effects on (fish) stress level, welfare and mortality rates [6, 7]. For ethical and economic reasons such effects must be minimized. However, our current understanding of the behavioral and physiological responses of salmon to aquaculture operations is limited. Relevant physiological data must therefore be collected from

This is an open access article under the terms of the [Creative Commons Attribution](https://creativecommons.org/licenses/by/4.0/) License, which permits use, distribution and reproduction in any medium, provided the original work is properly cited.

© 2023 The Authors. *Journal of Biophotonics* published by Wiley-VCH GmbH.

individuals in different contexts so physiological tolerances can be better understood. Such extended knowledge can then be used to further refine and tailor Atlantic salmon husbandry operations to minimize stress, thus improving animal welfare [8, 9].

Measuring individual-level physiological data is commonly done using intraperitoneal implants [4]. The selection of parameters possible to acquire with this technique was recently expanded to include photoplethysmography (PPG) [10]. This facilitates more robust heart rate measurements [11] and, potentially, pulse oximetry (PO) for blood oxygen saturation ( $SpO_2$ ) estimation—an interesting parameter to monitor in environments with variations in dissolved oxygen [12, 13]. Successful  $SpO_2$  estimation, however, depends on knowledge of parameters determining light propagation in tissues [14]. While a large body of such data on mammalian tissues is available in literature (e.g., [15]), this is not the case for Atlantic salmon and fishes in general. In the context of PO, blood is a particularly important (fluid) tissue since knowledge of blood absorption and scattering characteristics largely determine the optical path length crucial for  $SpO_2$  estimation [14, 16]. The purpose of this work was therefore to obtain data for characterization of the optical properties of Atlantic salmon blood in the visible to near-infrared (VIS–NIR) wavelength range, and to identify suitable procedures for obtaining such data. This will support future analysis of PPG data obtained from this species using any pulse oximeter with the aim to estimate  $SpO_2$ .

To this end, blood was sampled from 10 fish in total. Five blood samples were used to extract plasma, hemoglobin and blood cells. The VIS–NIR spectra were then recorded for plasma and oxygenated and deoxygenated hemoglobin and blood cell solutions. The remaining five blood samples were used to measure cell sizes using a Coulter counter to support optical scattering evaluations.

## 2 | MATERIALS AND METHODS

### 2.1 | Ethics statement

During blood sampling all individuals were in surgical anesthesia (level 3 [17]). Blood sampling was approved under experiment animal permit 26 085 issued by the animal ethics committee of the Norwegian Food Safety Authority.

### 2.2 | Experiment animals

Atlantic salmon post smolt were held in an indoor tank ( $2 \times 2 \times 1.6$  m) (SINTEF Ocean AS, Trondheim, Norway) supplied with  $9^\circ\text{C}$  filtered seawater (30 L per min) from

70 m depth. The tank was equipped with a Sterner Oxy-guard oxygenation system maintaining oxygen saturation  $\geq 85\%$ , and a water circulation pump (EMAUX Super-Power) to maintain a current speed of 1 body length (BL) per at the tank periphery and 24 h lighting to stimulate growth. The fish were fed commercial feed (Skretting, 2 mm) at 2% of the tank biomass distributed across 12 feedings per 24 h using automatic feeders. In total, 10 fish ( $181 \pm 56.5$  g,  $264 \pm 25$  mm,  $1.26 \pm 0.09$  Fulton's condition factor [18]) were used for two main samplings: Spectral measurements (5 fish) and cell size measurements for light scattering evaluations (5 fish).

### 2.3 | Blood sampling

For blood sampling, a  $1.10 \times 38$  mm (19G  $\times$  1.5") needle was mounted on a 3 ml syringe. 5000 IU heparin was pulled into the syringe to coat and lubricate the inner walls. The syringe was then emptied by pushing the syringe's plunger to the hub. A random fish was captured from the holding tank using a knotless dip net and immediately transferred to a tub containing 70 mg/L Benzoak Vet knock-out anesthetic. When the fish was judged to have reached surgical anesthesia (level 3 [17]), it was placed ventral side up on a holding tray for blood sampling. Blood was sampled from the caudal vein/artery of the fish by inserting the needle in parallel with the sagittal plane posterior from the anal fin (i.e., the anterior region of the caudal peduncle). With the needle in place,  $\geq 2$  ml blood was drawn into the syringe. After removing the needle, the blood was transferred to a 6 ml Vacutainer tube coated with 1.8 mg per K2EDTA. The sample was then transferred to an 2 ml Eppendorf tube (or equally divided between two) for immediate processing in a room with a temperature of  $15^\circ\text{C}$ .

### 2.4 | Blood processing

#### 2.4.1 | Plasma extraction

To obtain plasma, whole blood was centrifuged in its Eppendorf tube using a Hettich EBA 3S centrifuge (Hettich GmbH & Co. KG, Tuttlingen, Germany) at 1500 RPM / 195 g for 10 min. After centrifuging, the supernatant (plasma) was removed for spectral measurements using a pipette.

#### 2.4.2 | Blood cell extraction

To obtain blood cell samples, the packed cell volume remaining after plasma removal was washed by adding

1 ml Phosphate Buffered Saline (PBS) (137 mmol) to the packed cell volume (PCV) in the Eppendorf tube after plasma extraction. The mix was then centrifuged at 1500 RPM/195 g for 1 min. The supernatant was removed using a pipette and discarded. This procedure was repeated twice. The relatively gentle centrifuging compared with other protocols (e.g., [19]) was necessary because previous attempts showed that applying greater force to the samples resulted in increased hemolysis and a PCV which did not dissolve in PBS during cell washing. This also excluded the use of plasma separator Vacutainers which requires powerful centrifuging for the cells to pass through the separating gel. 25  $\mu$ l of the PCV remaining after the second wash were then pipetted into a test tube containing 50 ml PBS and carefully agitated for mixing to obtain a 1:2000 ratio. This sample was divided into equal parts and 25 ml PBS added to obtain two times 25 ml samples in a 1:4000 ratio.

### 2.4.3 | Hemoglobin extraction

Hemoglobin was extracted from blood cells by pipetting 50  $\mu$ l of the PCV after washing into a test tube containing 50 ml deionized water resulting in a ratio of 1:250. The tube was then capped, agitated to promote hemolysis and finally divided equally between two test tubes for further processing and analysis.

### 2.4.4 | Sample oxygenation and deoxygenation

Samples (1:4000 blood cells+PBS or 1:250 hemoglobin +deionized water) were oxygenated or deoxygenated via gassing using industrial oxygen (purity  $\geq 99\%$ ) or instrument nitrogen (purity  $\geq 99.9\%$ ), respectively. Gassing was achieved using closed test tubes with gas tight penetrations. A  $0.5 \times 25$  mm (25G  $\times$  1") needle was inserted through the cap and glued in place for pressure relief (Figure 1). All samples were gassed for  $\geq 20$  min since shorter gassing times resulted in large differences in the measured spectra.

## 2.5 | Spectral measurements

### 2.5.1 | Sensing equipment

Spectral data were collected using a Flame FLAME-T-VIS-NIR-ES (350–1000 nm) spectrometer and a 360–2000 nm HL-2000-LL tungsten-halogen light source. The spectrometer and light source were connected to a SQUARE ONE cuvette holder via a QP200-2-VIS-NIR fiber

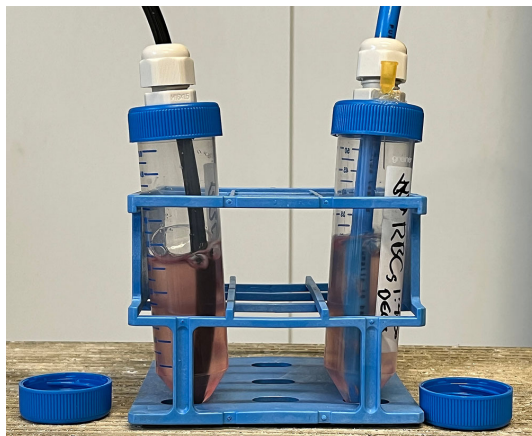


**FIGURE 1** Sample gassing set up. Note that the sample volume in the left test tube is lower compared with the right because a sample had been removed from the tube before the image was taken.

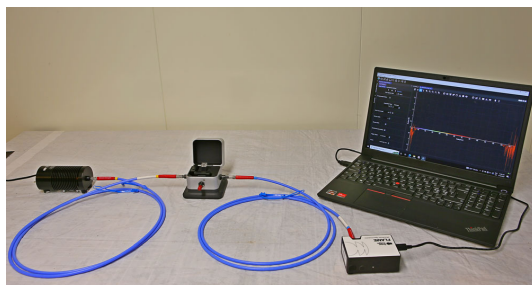


**FIGURE 2** Sensing equipment. From left to right: Light source, cuvette holder, spectrometer, and laptop.

(200  $\mu$ m core diameter) on the source side, and a QP50-2-VIS-NIR fiber (50  $\mu$ m core diameter) on the detector side. All equipment from Ocean Insight, Duiven, The Netherlands. The light source was allowed a  $\geq 30$  min warm-up time for it to reach thermal equilibrium with the environment to minimize drift. The spectrometer was controlled using OceanView (v2.0.7) by OceanInsight (Ocean Insight, Duiven, The Netherlands) running on a Leonovo laptop. All samples were measured using a CVS-Q-10 quartz cuvette with a 10 mm path length and a 1.4 ml maximum sample volume. The set-up is shown in Figure 2.

By adding a sample to the cuvette, this set up allows measurement of the sample's extinction, that is, its combined absorption and scattering spectrum [20]. Before each spectral measurement, the cuvette was flushed with PBS and its outside wiped with 96% ethanol using a

non-lint cloth. The spectrometer was then zeroed/reset by measuring the white and dark references using the cuvette filled with PBS.

By adding individual blood constituents to the cuvette, knowledge on the optical properties could be obtained. Spectra were measured for five undiluted plasma samples, oxygenated and de-oxygenated 1:4000 washed blood cells+PBS samples and oxygenated and deoxygenated 1:250 hemoglobin+deionized water samples, respectively. A measurement was defined as the average of 200 scans acquired using 750  $\mu$ s integration time, with a boxcar width of 10. Both electric dark and non-linearity corrections were enabled.

For the purpose of visual comparison, all samples were photographed using a tripod-mounted Canon EOS-1D X, 18.1 megapixel full-frame DSLR camera with a Canon 70–200 f/2.8 L IS II USM lens. The lens was set to 200 mm and the aperture to f/2.8 to maximize background separation. All images were captured against an even, white background and included a calibrated 18 gray reflectance standard for color and intensity corrections. Color and intensity corrections were done as post-processing using GNU Image Manipulation Program (GIMP) V2.10. Following color and intensity corrections, the cuvette was cut from the image. All sample images are given in Data S1.

## 2.6 | Cell size measurement and whole blood scattering coefficient

To estimate a value for the whole blood scattering parameter,  $\mu_s$ , published values for blood cell prevalence and volume for Atlantic salmon blood were compiled (Table 2). Using the average of the compiled data, values for particle concentration per  $\mu\text{m}^3$  and spherical-equivalent diameters in  $\mu\text{m}$  were calculated. The particle concentration was found by dividing the average number of blood cells per L by  $10^{15}$  which is the number of  $\mu\text{l}^3$  per L. The spherical-equivalent diameter,  $D_{\text{cell}}$ , was found by using the average blood cell volume,  $V_{\text{cell}}$  inserted into the expression for sphere volume and solving for the radius,  $r_{\text{cell}}$ , so

$$D_{\text{cell}} = 2 \cdot r_{\text{cell}} = 2 \cdot \left( \sqrt[3]{\frac{3V_{\text{cell}}}{4\pi}} \right). \quad (1)$$

With these values,  $\mu_s$  was calculated for 660, 880, and 940 nm using Prah's Mie scattering calculator [21]. These are wavelengths commonly used in pulse oximetry and are therefore of particular interest to facilitate this sensing technique for Atlantic salmon.

Measurements in the five last blood samples were obtained by subjecting the samples to the same procedure of plasma removal and cell washing as described above. The resulting samples were then diluted in PBS in a 1:800000 ratio before their spherical equivalent sizes were measured using a Coulter counter (Multisizer 4, Beckman Coulter, South Kraemer Boulevard, Brea, California 92821-6232) with a 100  $\mu\text{m}$  aperture. Each measurement was the average of three runs on the same sample (i.e., fish) by the Coulter counter. The resulting cell sizes were compared with those computed from published data to assess that these were similar.

## 3 | RESULTS AND DISCUSSION

### 3.1 | Spectral measurements

The measured plasma extinction spectra are shown in Figure 3.

The plasma samples were clear to the naked eye but with slight differences in hue (see Data S1). The average plasma extinction spectrum showed two small peaks at 540 and 576 nm typically associated with oxyhemoglobin, thus indicating its presence in the samples and possibly explaining the differences seen in sample color.

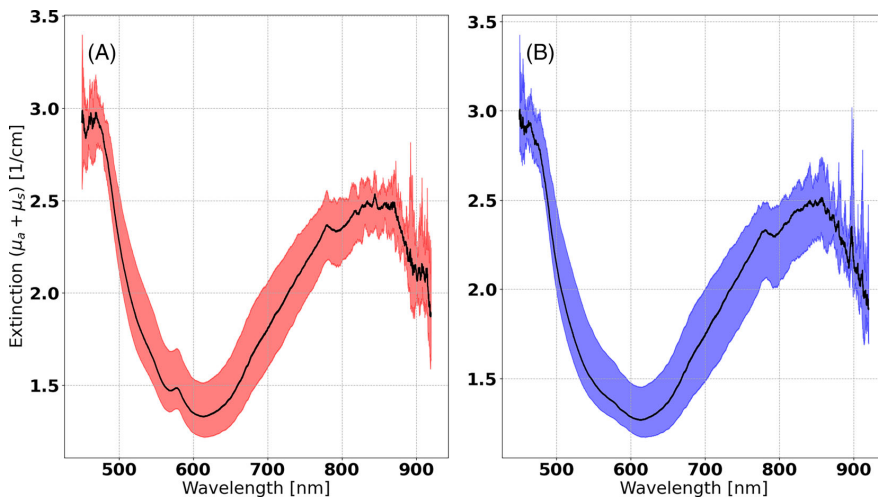
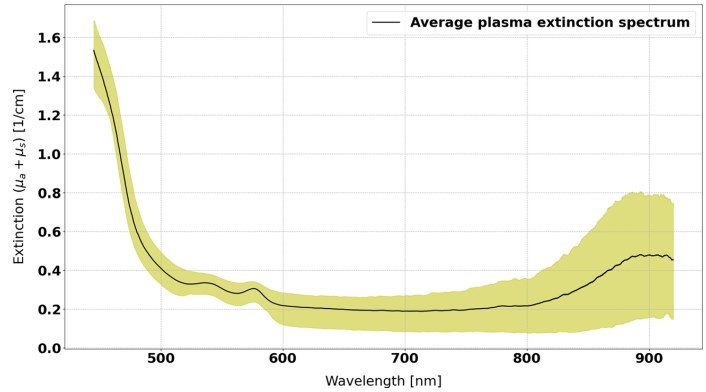
The plasma spectra showed low extinction between 500 and 820 nm and increasing extinction outside this range. This is similar to spectra reported for human blood [22], and may be caused by plasma protein scatterers in the low end of the spectrum and increasing absorption by water in the higher end. Because PO use wavelengths where plasma extinction is low, special considerations for plasma effects are likely unnecessary when estimating  $SpO_2$ .

Washed blood cell extinction spectra are presented in Figures 4 and 5.

The blood cell extinction spectra are similar in morphology compared with those reported for human blood cells [23] within the measured wavelength range. As seen in Figure 5, deoxygenated blood cells display slightly lower extinction values below 840 nm.

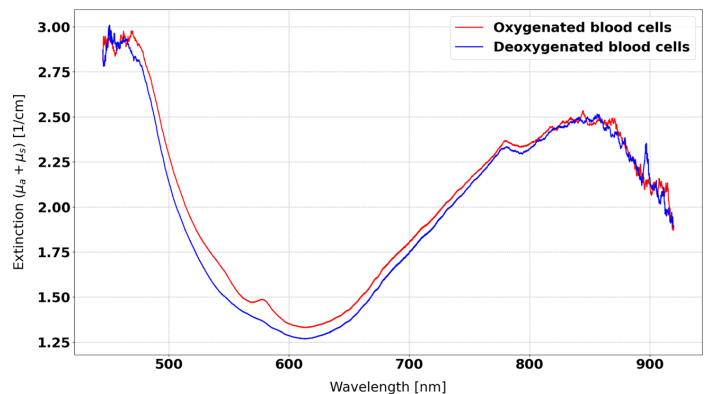
The averaged extinction spectrum for oxygenated blood cells had two peaks at 540 and 576 nm, respectively, which are associated with oxyhemoglobin. The absence of these peaks in the spectrum for deoxygenated blood cells indicates that the gassing approach was effective. The noise in the far ends of the measured range can be attributed to the HL-2000-LL tungsten-halogen light source being weaker for these wavelengths, thus reducing the signal to noise ratio. Also note that the measured extinction for the blood cell dilution is higher compared

**FIGURE 3** Extinction spectra for undiluted plasma. The black line illustrates the average for all samples, while the colored background illustrates the min-max range within which individual plasma spectra were distributed.



**FIGURE 4** Extinction spectra for (A) oxygenated and (B) deoxygenated blood cells in a 1:4000 PBS dilution. The solid black lines are the mean of all measured samples, while the colored backgrounds illustrate the min-max range within which individual spectra were distributed.

**FIGURE 5** Comparison of blood cell extinction spectra in a 1:4000 PBS dilution. The solid red line is the mean of all measured samples of oxygenated blood cells while the solid blue line is the mean of all measured samples of deoxygenated blood cells.





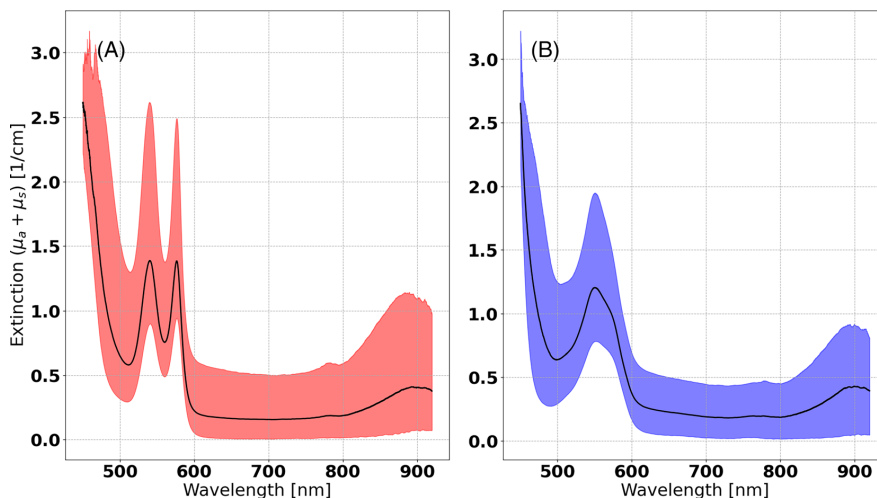


**FIGURE 6** Extinction spectra using 1:250 deionized water dilutions for (a) oxyhemoglobin with spectral peaks at 540 and 576 nm and (b) deoxyhemoglobin with a spectral peak at 550 nm. The solid black lines are the mean values, while the colored backgrounds illustrate the min-max range within which individual spectra were distributed.

with plasma (Figure 3 vs. Figure 4). This indicates that Atlantic salmon blood cells are highly scattering.

Oxyhemoglobin and hemoglobin extinction spectra were expected to be dominated by absorption. The extinction spectrum for the former showed two distinct spectral peaks at 540 and 576 nm (Figure 6A), while the extinction spectrum for the latter showed a spectral peak at 550 nm (Figure 6B).

The averaged hemoglobin spectrum exhibited the expected morphology up to 850 nm. Beyond this wavelength, an unexpected isosbestic point was identified. This can be explained by the properties of the HL-2000-LL tungsten-halogen light source which is weak in the far ends of the measured wavelength range. The resulting reduction in signal to noise ratio will therefore affect accuracy in these regions if extinction is low. This effect was minimized by using an appropriate sample concentration (1:4000 for blood cells and 1:250 for hemoglobin), high averaging (200 samples) and integration time (750  $\mu$ s). It is, however, generally difficult to achieve 0% and 100% oxygenation levels. The samples may therefore have been close to, but not completely at, these levels. Furthermore, any remaining cells and scatterers in the samples would also have introduced a scattering component in the measurement adding to the effect (Figure 7).

Sample transfer was achieved by pipetting directly from the gassing test tube into the measurement cuvette. Apart from the opening at the tip, the pipette was completely closed. Transfer of the sample to the cuvette

and spectral measurement was achieved within a matter of seconds. Although this method momentarily exposed the samples to air after transfer to the cuvette, consistent results were obtained using 200 samples and 750  $\mu$ s for averaging and integration time, respectively. The method was, thus, considered sufficiently robust for the purpose of this work. Future attempts at such measurements may consider using a completely closed sample transfer system, for example, by integrating a sampling tube in the gassing system.

The measured spectra and published spectra for human hemoglobin [24] were scaled to the value of their first spectral peak (540 nm for Atlantic salmon and human oxyhemoglobin, 550 nm for Atlantic salmon hemoglobin and 555 nm for human hemoglobin, respectively) and plotted for comparison (Figure 8).

Atlantic salmon hemoglobin spectra presented in Figure 8 show a morphology similar to human hemoglobin. Although the spectra for salmon oxyhemoglobin and deoxyhemoglobin were expected to be dominated by absorption some degree of scattering must be expected. Since the human oxyhemoglobin and hemoglobin spectra are considered to be reference absorption spectra they are virtually unaffected by scattering, thus leading to differences in morphology. It is also noted that the oxyhemoglobin spectrum (Figure 8A) has a small peak at 757 nm. This peak is typical for hemoglobin which indicates that the samples were not fully oxygenated, adding to the divergence from the (human) reference.



**FIGURE 7** Comparison of average oxyhemoglobin (red) and deoxyhemoglobin spectra (blue) in a 1:250 deionized water dilution. The blue dots denote the isosbestic points (i.e., crossings).

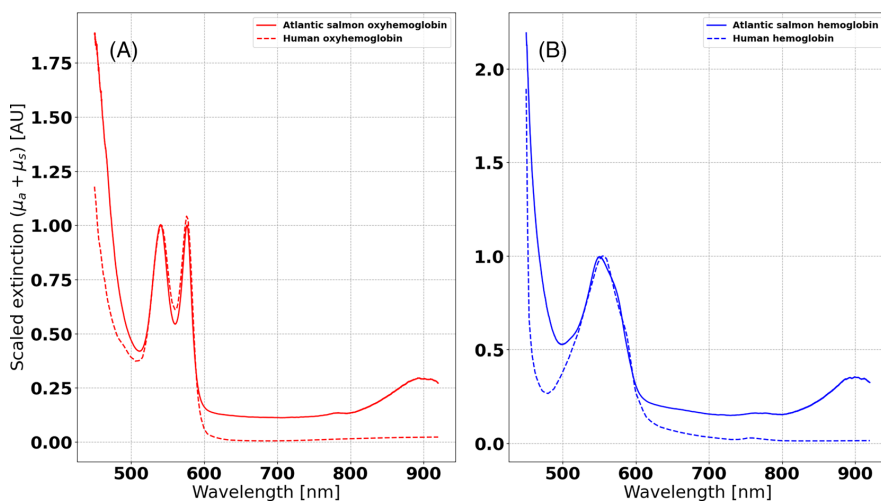
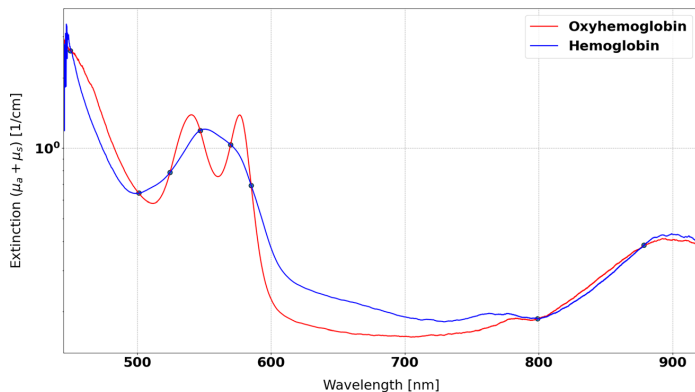


**FIGURE 8** Comparison of measured Atlantic salmon and human scaled oxyhemoglobin (A) and hemoglobin (B) spectra. Due to the scaling, values along the y-axis are given in arbitrary units (AU).

Using the hemoglobin extinction spectra, a list of points with equal extinction (i.e., isosbestic points) can be compiled and compared with reference values for human hemoglobin [24].

Table 1 shows that the isosbestic points for Atlantic salmon hemoglobin are very close to those reported for human hemoglobin. The differences may be introduced by residual scatterers in the samples. Note also that the abovementioned unexpected isosbestic point at 879 does not have a counterpart in human blood.

The Coulter counter measurements (Figure 9) show two distinct peaks for spherical equivalent diameters of 7.2 and 8.84  $\mu\text{m}$  indicating that the washed cell samples contained two dominating cell populations.

Since washing mainly removes plasma, the remaining PCV must be expected to include multiple cell types

typically found in Atlantic salmon blood, such as erythrocytes, reticulocytes, white blood cells (e.g., neutrophils, monocytes, and lymphocytes) and platelets (thrombocytes). Out of these, erythrocytes were expected to dominate in size and number ( $\approx 1 \times 10^{12} \cdot \text{L}^{-1}$ ) [25, 26] followed by reticulocytes (smaller, immature erythrocytes) constituting  $\approx 15\%$  of all blood cells [26, 27]. This mix of cell sizes and prevalence is a likely contributor for the two peaks seen in Figure 9. Another potential impact is that Coulter counter size estimates depend on a range of factors such as particle shape and lateral position when passing through the counter's aperture. Thus, due to the oblate shape of Atlantic salmon blood cells, their orientation as they pass through the aperture will affect the size estimate. The two most extreme orientations “flat” and “on edge” may therefore contribute to separate the

measurement into two distinct peaks [28] as seen in the results. To reduce this effect, the Coulter counter aperture was  $\approx 10$  times larger than the largest expected particle size as recommended for such measurements. Nevertheless, the combination of this effect and the mix of cell sizes is considered a likely explanation for this result.

The peak for the largest particle size (8.84  $\mu\text{m}$ ) from the Coulter counter results was assumed to represent the spherical equivalent blood cell diameter. This value was compared with published values to evaluate the blood sample quality and assess other unmeasured parameters (Table 2).

The spherical equivalent cell diameter obtained from the Coulter counter measurements were consistent with published values, indicating that the blood samples used in this work were representative for Atlantic salmon blood. This also indicates that all fish used for blood sampling in this work were in good health.

Since the cell sizes in Table 2 are orders of magnitude larger than the wavelengths used in the spectral measurements, Mie scattering is dominant [20]. In Mie scattering,

scattering efficiency increases with the fourth power of the particle size [16] which means that the largest particles contribute more to scattering than smaller particles. The peak for the cell population with the largest diameter was therefore used to calculate  $\mu_s$ .

Mie scattering calculations depend on the refractive index of both the medium (i.e., plasma) and the spheres (i.e., the blood cells) [20]. To the best of the authors knowledge, no published values for refractive indices for Atlantic salmon blood have been published. It was therefore assumed that Atlantic salmon blood has refractive indices similar to those published for human blood [31, 32]. Using the average values in Table 2 and these refractive indices as input to the Mie calculator [21] for selected wavelengths used in pulse oximetry, we obtain the scattering parameter values in Table 3.

The values for  $\mu_s$  obtained using these methods are larger than those published for human blood [33]. This was expected and is consistent with Mie scattering theory because Atlantic salmon blood cells are larger compared with those in humans.

TABLE 1 Isosbestic points for Atlantic salmon compared with human hemoglobin.

Atlantic salmon hemoglobin	Human hemoglobin
450	452
501	500
525	529
547	545
570	570
585	584
799	797
879	–

TABLE 2 Overview of literature values listing cell density as cells per, cell volume as mean corpuscular volume (MCV,  $\mu\text{m}^3$ ), and cell diameter ( $D$ ) calculated using Equation (1), as well as the average of those values compared with the result from this study.

$C$ (cells/ $\mu\text{l}$ )	MCV ( $\mu\text{m}^3$ )	$D$ ( $\mu\text{m}$ )	References
$0.97 \cdot 10^{-3}$	485	9.75	[25]
$0.97 \cdot 10^{-3}$	369	8.90	[29]
$0.83 \cdot 10^{-3}$	489	9.77	[30]
$1.25 \cdot 10^{-3}$	366	8.87	[26]
$1.29 \cdot 10^{-3}$	324	8.52	[27]
–	362	8.84	Coulter counter
$1.01 \cdot 10^{-3}$	399	9.23	Average

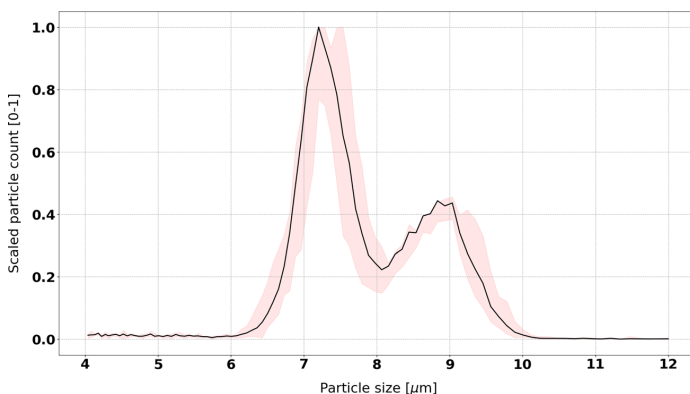


FIGURE 9 Coulter counter results of measured cell size. The solid black line shows the average of all measurements, while the colored background illustrates the min-max range of the measurements.

TABLE 3 Estimated scattering coefficient,  $\mu_s$ , for Atlantic salmon whole blood for selected wavelengths used in pulse oximetry.

$\lambda$ (nm)	$\mu_s$ (cm <sup>-1</sup> )
660	1887
880	2207
940	2170



FIGURE 10 Example of plasma sample with hemolysis typically observed after vacutainer blood sampling (A) compared with plasma obtained using syringes (B).

### 3.2 | Sampling challenges

The blood sampling and processing methods described in Materials and methods are the final result of multiple attempts to measure optical properties of Atlantic salmon blood because preceding attempts presented several challenges which had to be overcome.

Two main methods for blood sampling were compared: Using syringes and Vacutainers. The latter is attractive due to the ease of sampling and the wide selection of available anti-coagulant coatings as well as plasma

separator gels. Processing of samples obtained using Vacutainers, however, consistently resulted in various degrees of hemolysis evident in the form of red-tinted plasma as shown in Figure 10.

Consequently, it was decided to use heparinized syringes and 19G needles. Even then, oxygen peaks were present in measured plasma absorption spectra (Figure 3) indicating some hemolysis taking place during sampling.

Hemolysis of blood cell dilutions also occurred during gassing if bubbling was too vigorous. The latter was seen when attempting to improve gas distribution in samples using an air stone (sinter) even at the lowest gas pressure available equipment would allow. This was likely caused by turbulence in the gap between the air stone and the test tube wall resulting in shear forces excessive for cell integrity. Bubbling was, thus, changed to using gas tubing directly in the samples (Figure 1).

During earlier tests, sample deoxygenation was attempted using sodium dithionite. Dosing was according to [34] without achieving consistent results. Samples were either not deoxygenated within the expected time frame or rapidly started to form methemoglobin [35]. Future attempts to deoxygenate dilutions of salmon blood constituents should therefore be preceded by a systematic study on how to obtain consistent and reliable deoxygenation using sodium dithionite.

Some of the measured hemoglobin solutions contained impurities (see Data S1). The light passes through the sample slightly below middle height of the cuvette. Because all samples were clear/homogeneous to the naked eye in this area, such contamination is considered to have had limited effect on the results. Nevertheless, future attempts at measuring the optical properties of salmon blood may consider filtering the hemoglobin samples using, for example, a nylon mesh before gassing and measurement.

Sample coagulation was also a challenge. Despite using heparin in vessels during blood collection, samples would (partially) coagulate before centrifuging if left unprocessed on the rocker for more than approximately 30 min. Additionally, samples obtained using only heparin coagulated rapidly when adding deionized water to obtain the hemoglobin solution. These events may be explained by the onset of the coagulation cascade. At some point the amount of heparin present in the sample can no longer block fibrin formation during hemolysis and the sample coagulates. The addition of K2EDTA to the samples prevented these issues, likely by blocking calcium. In the future, sodium citrate may be tested as an alternative directly in the syringe since it acts as both an anti-coagulant and a calcium blocker if an acceptable mixing ratio can be identified.

## 4 | CONCLUSION

This work presents data describing the optical properties of Atlantic salmon blood between 450 and 920 nm. This wavelength range is relevant for pulse oximetry sensors which typically use wavelengths around 660, 880, and 940 nm.

The results indicate that plasma contributes little to scattering and absorption, which hemoglobin absorption is similar to that in humans and that blood cells have strong scattering properties. Furthermore, a novel sampling procedure had to be established to obtain these measurements, as no suitable methods for such sampling on fish blood existed. This method can be used and further refined for future measurements of blood from salmon and other fishes, and is as such a contribution to the toolbox available for science.

In the context of pulse oximetry, the low plasma absorbance indicates that plasma will not require special compensation when aspiring to sample  $SpO_2$ . Furthermore, the isosbestic points for hemoglobin absorbance imply that published values for molar extinction coefficients for human hemoglobin and oxyhemoglobin [24] can be used, thus supporting that pulse oximeters originally intended for human applications can be used for similar purposes in Atlantic salmon. However, scattering results show that Atlantic salmon blood is highly scattering, thus implying that PPGs obtained by a pulse oximeter must be compensated. This can be achieved using the scattering parameters in Table 3 as part input to the pulse oximeters  $SpO_2$  estimation algorithm. Accurate  $SpO_2$  estimation may increase understanding of the physiological responses and tolerances of Atlantic salmon via scientific trials using raceways or swim tunnels where water quality can be controlled and stress levels accurately quantified. Using such knowledge,  $SpO_2$  estimation in Atlantic salmon farming may, thus, facilitate adaptation of production methods for stress reduction and improved animal welfare.

## ACKNOWLEDGMENT

This work was carried out as part of the SalmonInsight project funded by the Research Council of Norway (project number 280864) and through in-kind provided by SINTEF Ocean AS.

## CONFLICT OF INTEREST STATEMENT

The authors declare no conflict of interest.

## DATA AVAILABILITY STATEMENT

The data supporting the findings of this study are available from the corresponding author upon reasonable request.

## ORCID

Eirik Svendsen  <https://orcid.org/0000-0003-1038-6560>

## REFERENCES

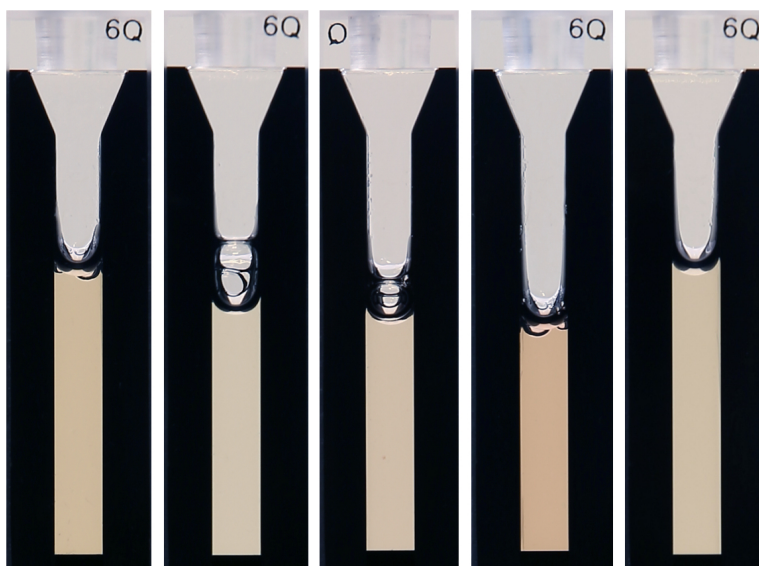
- [1] J.-W. Jeong, W. Lee, Y.-J. Kim, *Sensors* **2021**, 22, 104.
- [2] E. A. Thomson, K. Nuss, A. Comstock, S. Reinwald, S. Blake, R. E. Pimentel, B. L. Tracy, K. Li, *J Sports Sci* **2019**, 37, 1411.
- [3] H. J. Williams, J. Ryan Shipley, C. Rutz, M. Martin Wikelski, L. A. H. Wilkes, *Philos Trans Roy Soc B* **2021**, 376, 20200230.
- [4] E. B. Thorstad, A. H. Rikardsen, A. Alp, F. Økland, *Turk J Fish Aquat Sci* **2013**, 13, 881.
- [5] FAO. Food and Agriculture Organization of the United Nations, Fisheries and Aquaculture Department. **2022** [https://www.fao.org/fishery/statistics-query/en/aquaculture/aquaculture\\_quantity](https://www.fao.org/fishery/statistics-query/en/aquaculture/aquaculture_quantity)
- [6] C. Noble, K. Gismervik, M. H. Iversen, J. Kolarevic, J. Nilsson, L. H. Stien, J. F. Turnbull, *Welfare Indicators for farmed Atlantic salmon: tools for assessing fish welfare*, Nofima, Tromsø, Norway **2018**.
- [7] I. Sommerset, B. B. Jensen, G. Bornø, A. Haukaas, E. Brun, *Fiskehelse rapporten*, Norwegian Veterinary Institute, Ås, Norway **2021**.
- [8] M. Føre, K. Frank, T. Norton, E. Svendsen, J. A. Alfredsen, T. Dempster, H. Eguiraun, W. Watson, A. Stahl, L. M. Sunde, C. Schellewald, K. R. Skoien, M. O. Alver, D. Berckmans, *Biosyst Eng* **2018**, 173, 176.
- [9] M. Føre, K. Frank, T. Dempster, J. A. Alfredsen, E. Høy, *Aquacult Eng* **2017**, 78, 163.
- [10] E. Svendsen, M. Føre, L. L. Randeberg, J. A. Alfredsen, *IEEE Sens* **2021**, 1, 4.
- [11] E. Svendsen, F. Økland, M. Føre, L. L. Randeberg, B. Finstad, R. E. Olsen, J. A. Alfredsen, *Anim Biotelemetry* **2021**, 9, 1.
- [12] M. O. Alver, M. Føre, J. A. Alfredsen, *Aquaculture* **2022**, 548, 737720.
- [13] D. Johansson, K. Ruohonen, A. Kiessling, F. Oppedal, J.-E. Stiansen, M. Kelly, J.-E. Juell, *Aquaculture* **2006**, 254, 594.
- [14] P. A. Kyriacou, J. Allen, *Photoplethysmography: Technology, Signal Analysis and Applications*, Academic Press, London **2021**.
- [15] J. L. Sandell, T. C. Zhu, *J Biophoton* **2011**, 4, 773.
- [16] I. J. Bigio, S. Fantini, *Quantitative biomedical optics: theory, methods, and applications*, Cambridge University Press, Cambridge **2016**.
- [17] S. D. Coyle, R. M. Durborow, J. H. Tidwell, et al., *Anesthetics in Aquaculture*, Vol. 3900, Southern Regional Aquaculture Center Stoneville, Stoneville **2004**.
- [18] W. E. Ricker, *Bull. Fish. Res. Bd. Can.* **1975**, 191, 1.
- [19] M. Iversen, B. Finstad, R. S. McKinley, R. A. Eliassen, K. T. Carlsen, T. Evjen, *Aquaculture* **2005**, 243, 373.
- [20] C. F. Bohren, D. R. Huffman, *Absorption and Scattering of Light by Small Particles*, John Wiley & Sons, New Jersey **1983**.
- [21] S. Prah. Mie scattering calculator. **2018** [https://omlc.org/calc/mie\\_calc.html](https://omlc.org/calc/mie_calc.html)
- [22] M. Meinke, G. Müller, J. Helfmann, M. Friebe, *J Biomed Opt* **2007**, 12, 014024.

- [23] M. Friebel, J. Helfmann, U. Netz, M. Meinke, *J Biomed Opt* **2009**, *14*, 034001.
- [24] S. Prah. Optical Absorption of Hemoglobin. **1999** <https://omlc.org/spectra/hemoglobin/>
- [25] K. Sandnes, Ø. Lie, R. Waagbø, *J Fish Biol* **1988**, *32*, 129.
- [26] K. Hamre, B. Hjeltnes, H. Kryvi, S. Sandberg, M. Lorentzen, Ø. Lie, *Fish Physiol. Biochem.* **1994**, *12*, 421.
- [27] J. Härdig, L. B. Höglund, *Comp Biochem Physiol A Physiol* **1983**, *75*, 35.
- [28] Z. Qin, J. Zhe, G.-X. Wang, *Meas. Sci. Technol.* **2011**, *22*, 045804.
- [29] J. Sadler, R. M. G. Wells, P. M. Pankhurst, N. W. Pankhurst, *Aquaculture* **2000**, *184*, 349.
- [30] H. D. Rodger, R. H. Richards, *J Fish Dis* **1998**, *21*, 101.
- [31] N. Ghosh, P. Buddhiwant, A. Uppal, S. K. Majumder, H. S. Patel, P. K. Gupta, *Appl. Phys. Lett.* **2006**, *88*, 084101.
- [32] S. Liu, Z. Deng, J. Li, J. Wang, N. Huang, R. Cui, Q. Zhang, J. Mei, W. Zhou, C. Zhang, et al., *J Biomed Opt* **2019**, *24*, 035003.
- [33] N. Bosschaart, G. J. Edelman, M. C. G. Aalders, T. G. van Leeuwen, D. J. Faber, *Lasers Med Sci* **2014**, *29*, 453.
- [34] K. Briely-Sabo, A. Bjonnerud, *Proc. Intl. Sot. Mag. Reson. Med* **2000**, *8*, 2025.
- [35] K. Dalziel, J. R. P. O'Brien, *Biochem. J.* **1957**, *67*, 119.

## SUPPORTING INFORMATION

Additional supporting information can be found online in the Supporting Information section at the end of this article.

**How to cite this article:** E. Svendsen, L. L. Randeberg, M. Føre, B. Finstad, R. E. Olsen, N. Bloecher, J. A. Alfreksen, *J. Biophotonics* **2023**, e202300073. <https://doi.org/10.1002/jbio.202300073>

**SUPPLEMENTARY MATERIAL**

**FIGURE 1** Measured plasma samples. Note the slight color variations likely caused by some degree of haemolysis during blood sampling.

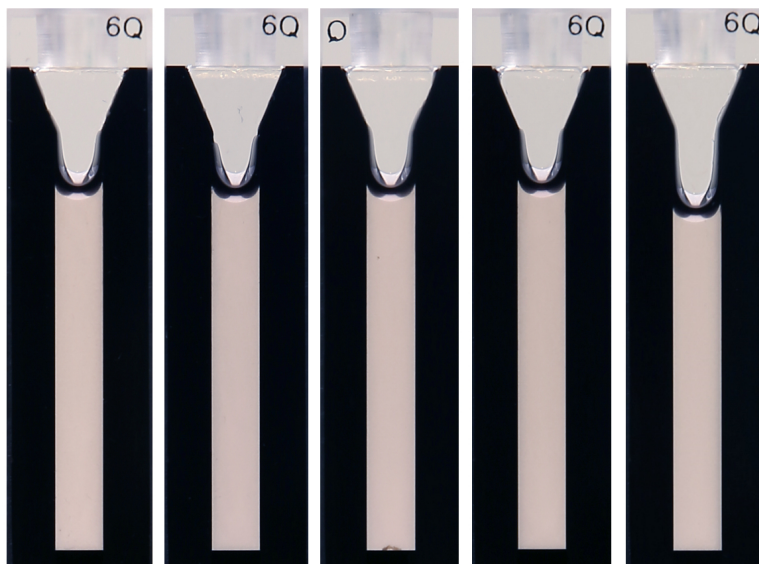


**FIGURE 2** Oxygenated blood cells. Note that color intensity is low due to the high dilution.



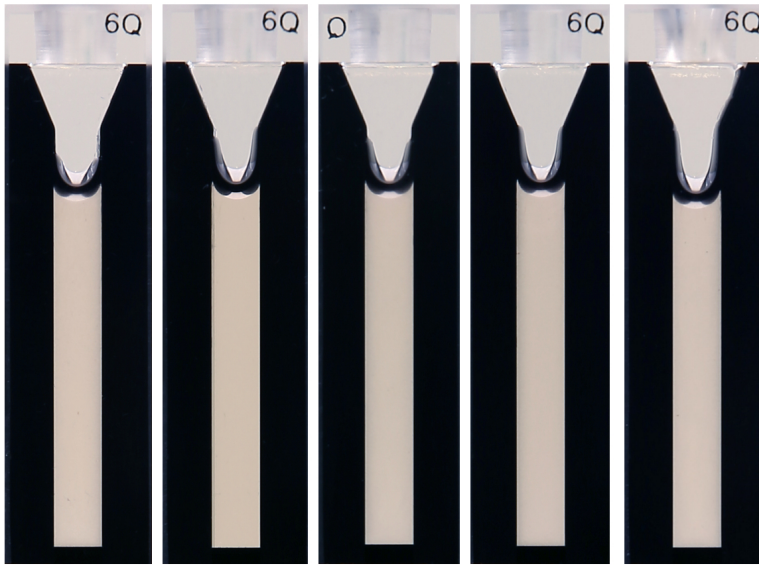


**FIGURE 3** Deoxygenated blood cells. Note that color intensity is low due to the high dilution.

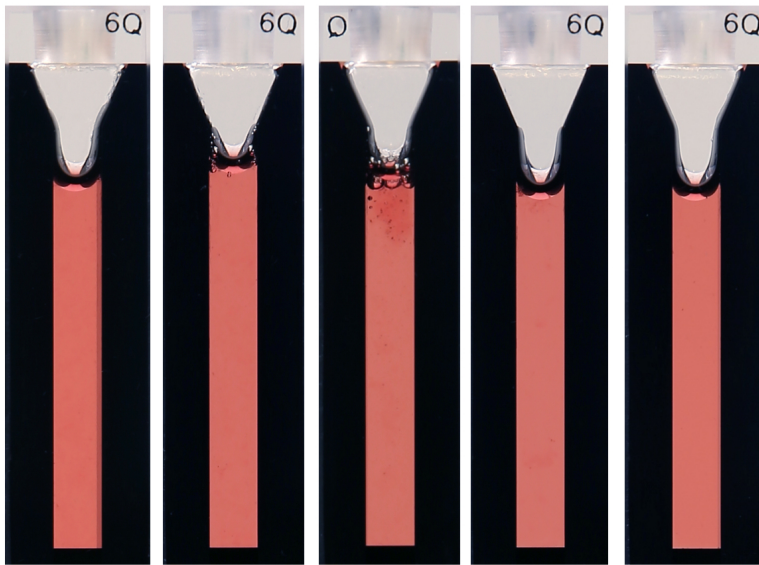


**FIGURE 4** Oxygenated hemoglobin. Note the presence of foreign material at the very top of sample 3 when numbering from the left.

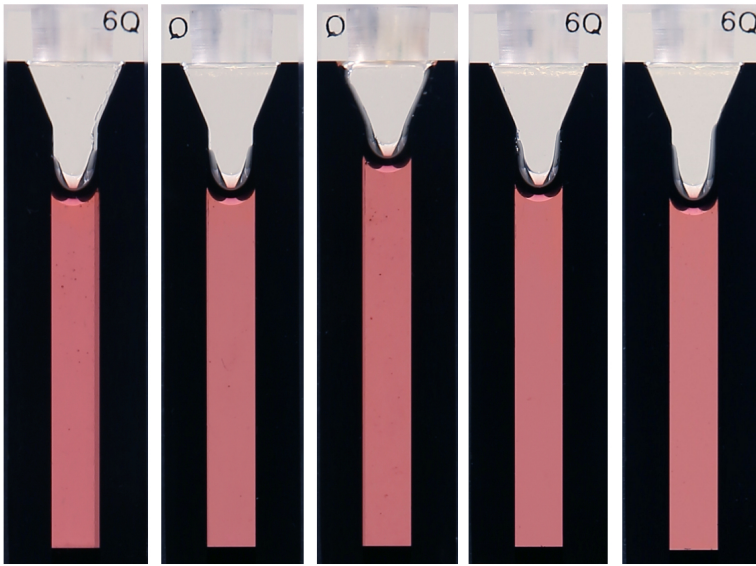


**FIGURE 5** Deoxygenated hemoglobin.





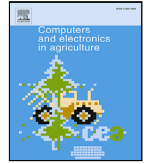
Paper F  
ECG Augmented Pulse  
Oximetry in Atlantic Salmon  
(*Salmo salar*) - a Pilot Study





Contents lists available at ScienceDirect

## Computers and Electronics in Agriculture

journal homepage: [www.elsevier.com/locate/compag](http://www.elsevier.com/locate/compag)

Original papers

ECG augmented pulse oximetry in Atlantic salmon (*Salmo salar*)—A pilot study<sup>☆</sup>E. Svendsen<sup>a,b,\*</sup>, M. Føre<sup>a</sup>, L.L. Randeberg<sup>c</sup>, R.E. Olsen<sup>d</sup>, B. Finstad<sup>d</sup>, M. Remen<sup>b</sup>, N. Bloecher<sup>b</sup>, J.A. Alfredsen<sup>a</sup><sup>a</sup> Department of Engineering Cybernetics, Norwegian University of Science and Technology, O.S. Bragstads plass 2D, Trondheim, 7034, Norway<sup>b</sup> SINTEF Ocean AS, Brattørkaia 17C, Trondheim, 7010, Norway<sup>c</sup> Department of Electronic Systems, Norwegian University of Science and Technology, O.S. Bragstads plass 2B, Trondheim, 7034, Norway<sup>d</sup> Department of Biology, Norwegian University of Science and Technology, Brattørkaia 17B, Trondheim, 7010, Norway

## ARTICLE INFO

## Keywords:

Pulse oximetry  
Light scattering  
Motion artifact  
Electrocardiogram  
Least mean square filtering

## ABSTRACT

Understanding the tolerance limits of fish is crucial for developing aquaculture operations that ensure good animal welfare. However, there exist little data describing the physiological responses in farmed Atlantic salmon, much because the technological tools for taking such measurements have not existed. Recent advances in electronic implants have enabled concurrent measurement of electrocardiogram (ECG) and photoplethysmograms (PPG) in salmon that can be used for robust estimation of HR and oxygen saturation in arterial blood (i.e.,  $SpO_2$ /pulse oximetry) if appropriate strategies for motion artifact and light scattering compensation can be realized. To enable pulse oximetry for farmed Atlantic salmon (and fish in general), two experiments have been conducted. In Experiment 1, PPGs were obtained from salmon induced to swim at two different water currents under normoxic conditions. By using two water currents, the resulting data provided a foundation for developing methods for motion artifact compensation. Data from this experiment were also used to calculate an average light scattering parameter using the modified Beer–Lambert law, under the assumption that  $SpO_2$  was 100% for individual fish. In Experiment 2, fish were placed in a swim tunnel and subjected to hypoxic conditions and corresponding changes in  $SpO_2$  were estimated using the motion artifact and light scattering compensation approaches from Experiment 1.

Results show that the suggested compensation approaches gives  $SpO_2$  estimates within the expected range (95% to 100%) under normoxic conditions. Under hypoxic conditions, changes in  $SpO_2$  that coincide with experiment events were observed, demonstrating that PPGs can be used to quantify such changes. The results from this pilot study therefore extend the selection of physiological parameters feasible to measure using electronic implants for Atlantic salmon. In doing so, the scope for physiological measurements is extended such that an improved understanding of physiological responses and tolerances in Atlantic salmon farming can be acquired, and ultimately be used to improve animal welfare in fish production.

## 1. Introduction

Aquaculture has grown into an important global food-producing industry with Atlantic salmon (*Salmo salar*) being one of the most popular farmed species. In Norway, 1.5 million tonnes were produced for worldwide consumption in 2022 (FDIR, 2023). Salmon production involves a broad range of farming operations (e.g., crowding, pumping, de-lousing and net cleaning) which may have negative impacts on fish health and welfare. Lack of real-time, objective physiological inputs to animal welfare and production control routines is a persistent challenge

in Atlantic salmon farming and is difficult to detect and quantify. Despite extensive use of different sensing technologies (Føre et al., 2017b), current farming practices result in a 17% mortality rate during the sea phase (Sommerset et al., 2023). A part of this may be attributed to limited access to, and knowledge of, the tolerances of the fish in different farming contexts. Research tools that may increase such knowledge are miniaturized, implantable electronic sensing systems commonly referred to as ‘tags’ that can be used to directly measure physiological and behavioral parameters (Thorstad et al., 2013). Typical behavioral parameters possible to measure using existing off-the-shelf tags include

<sup>☆</sup> This work was funded by the Research Council of Norway (RCN) (Project Number 280864) and through in-kind contribution by SINTEF Ocean AS.

\* Corresponding author at: Department of Engineering Cybernetics, Norwegian University of Science and Technology, O.S. Bragstads plass 2D, Trondheim, 7034, Norway.

E-mail addresses: [eirik.svendsen@ntnu.no](mailto:eirik.svendsen@ntnu.no), [eirik.svendsen@sintef.no](mailto:eirik.svendsen@sintef.no) (E. Svendsen).

<https://doi.org/10.1016/j.compag.2023.108081>

Received 24 March 2023; Received in revised form 10 July 2023; Accepted 17 July 2023

Available online 29 July 2023

0168-1699/© 2023 The Author(s). Published by Elsevier B.V. This is an open access article under the CC BY license (<http://creativecommons.org/licenses/by/4.0/>).

activity and swimming depth (Føre et al., 2011), and, more recently, the position of individual fish (Baktoft et al., 2017; Hassan et al., 2019), while physiological parameters obtainable in full scale salmon farming are currently limited to heart rate (HR) (Brijs et al., 2018).

To expand the selection of physiological measurements for farmed Atlantic salmon, a novel implant has been developed which measures PPGs (Svendsen et al., 2021b), i.e., the pulsatile change in tissue light absorption. The PPGs can be used to make HR estimates more robust (Svendsen et al., 2021c) and in principle, estimate oxygen saturation in arterial blood ( $S_pO_2$ ). This technique is referred to as *pulse oximetry* (PO) (Aoyagi, 2003; Wypych, 2013; Mannheimer, 2007), and successful implementation of PO may increase insight into the fish's physiological response, and by extension, its tolerances. This may be of use in salmon farming where low dissolved oxygen events may occur with negative impacts on the fish (Oppedal et al., 2011; Remen et al., 2013, 2016; Jónsdóttir et al., 2019).

PO is based on the Beer–Lambert law (BLL) and the assumption that arteries expand during heart contraction (systole) and contract during heart relaxation (diastole) (Kyriacou and Allen, 2021). Due to the higher blood perfusion, light absorption in tissues will increase during systole and conversely decrease during diastole creating a pulsatile ‘AC’ component in the PPG. However, motion introduces artifacts (Motion Artifacts, MA) distorting the PPG, thus affecting  $S_pO_2$  accuracy (Chan et al., 2013). Before attempting to estimate  $S_pO_2$  using PPGs, MA must be reduced.

MA reduction is a persistent challenge in PPG signal processing. Common approaches to detect and reduce MA in human PPGs include morphology analysis (Sukor et al., 2011), thresholding of statistical moments (Hanyu and Xiaohui, 2017) and various filtering approaches using synthetic or accelerometer based Refs. Zhang et al. (2014), Casson et al. (2016), Xiong et al. (2016) and Dubey et al. (2018). Based on such references, the PPG can be (re)constructed using variants of principal component analysis (e.g., singular spectrum analysis (SSA) Golyandina et al., 2018). Such methods commonly focus on estimating HR rather than  $S_pO_2$ , potentially causing information crucial for determining  $S_pO_2$  (i.e., the PPG pulse amplitude) to be degraded or lost. Furthermore, several of these approaches assume that MAs are separable from the PPG in the time and/or frequency domain. This may be true for human PPGs during physical exertions such as running. In the case of Atlantic salmon, co-inspection of PPG and inertial motion unit (IMU) data from free swimming fish suggest that MAs are generally oscillatory in nature and also appear within a frequency range close to the HR of the fish, meaning that conventional methods of MA reduction may remove too much of the PPG information required for  $S_pO_2$  estimation. This implies the need for an alternative approach. Considering that the pulsatile components in PPG are linked with the HR of the fish, a potential approach could be to extract the components of the PPG signal that share frequency properties with the HR and use these to estimate  $S_pO_2$ , as this would effectively remove all components arising due to other phenomena, including MAs.

Furthermore, the BLL precludes that light travels in a non-scattering homogeneous medium. This is not the case for biological tissues. Using BLL, thus, requires that such effects are compensated. In humans, this is achieved empirically using reference oximeters by obtaining a baseline for comparison when human volunteers breathe a desaturated gas mixture. To the best of our knowledge, no reference oximeter for fishes exists, thus, excluding reference based empirical mapping. An alternative approach is to use the modified BLL (MBLL) which includes a scattering compensation term. This term can be calculated if  $S_pO_2$  is known or can be reasonably assumed. In this study, initial steps towards realizing PO in Atlantic salmon, are taken by conducting two experiments to derive a viable MA compensation approach and identify an average scattering compensation parameter that give credible results when combined. The purpose of Experiment 1 was, thus, to obtain PPG data under normoxic conditions that could be used to identify

an average scattering correction parameter and develop an MA reduction/filtering approach and verify that its application results in an  $S_pO_2$  estimate within the expected range (i.e., 95% to 100%), while the purpose of Experiment 2 was to apply the processing methods and average scattering correction parameter from Experiment 1 to evaluate if the PO implant responded to changes in  $S_pO_2$ .

## 2. Materials and methods

### 2.1. Ethical statement

The experiments were approved by the Norwegian Food Safety Administration under animal experiment permits 27 675 (Experiment 1) and 24 907 (Experiment 2). Data were obtained from 13 fish in total. After the experiments, all fish were euthanized using methods compliant with Appendix C in the Norwegian research animal regulations (FOR-2015-06-18-761, 2015).

### 2.2. Experiment animals

Atlantic salmon were held in an indoor tank ( $2 \times 2 \times 1.6$  m) with a flow through sea water supply (30 l per min,  $8.2^\circ\text{C}$  average temperature during the experiment period) from a 70 m deep intake in the Trondheimsfjord. The fish were fed in abundance using 5 mm pellets (EWOS HP 500 50 A 500) using 24 h lighting to facilitate growth. The tank was equipped with a water circulation pump (EMAUX Super-Power) with a tangential outlet to provide a water current of  $\approx 1$  body length per s ( $BLs^{-1}$ ) at the tank periphery. A Sterner Oxyguard oxygenation system ensured water oxygen saturation  $\geq 90\%$ .

### 2.3. Pulse oximetry tag

The PO tag (Svendsen et al., 2021b) used in both experiments included a biosensor module (MAX86150, Maxim Integrated) measuring PPG at two wavelengths,  $\lambda_1 = 660$  nm and  $\lambda_2 = 880$  nm. The biosensor module also measured ECG via electrodes embedded in the implant's encapsulation. An inertial motion unit (IMU) measuring acceleration and rotation in three dimensions was also part of the implant design and were logged concurrently with PPG and ECG for activity evaluations. The implant was cylindrical in shape and measured 13 mm in diameter, 47 mm in length and weighing 9.4 g (in air)/6 g (in water) making it suitable for use in fish  $\geq 600$  g.

### 2.4. Experiment 1

Experiment 1 was conducted in an indoor tank that was identical to the holding tank and used the same water supply. The tank was covered by a thin, white tarpaulin taut over a pyramidal framework to shield the experiment animals from visual disturbances. Water oxygen saturation was maintained at  $90 \pm 0.62\%$  ( $10.7 \pm 0.07$  mg  $L^{-1}$ ) by a Sterner Oxyguard oxygenation system through the experiment. A water circulation pump (EMAUX Super-Power) was used to control water current speed at the tank periphery.

The experiment took place over 2 days. On day 1 between 12:20 and 15:00, PO tags were surgically implanted into the peritoneal cavity of five Atlantic salmon (fork length  $53.5 \pm 1.3$  cm, weight  $2426 \pm 55.7$  g, Foulton's K-factor  $1.6 \pm 0.1$ ) captured randomly from their holding tank using a knotless dip net. Surgery was identical to the procedure described in literature for a similar tag type (Svendsen et al., 2021a; Føre et al., 2021), with an additional step of suturing a colored bead to the anterior root of the dorsal fin for visual identification purposes. After surgery each fish was placed in a wake-up tank with circulating sea water. After regaining consciousness, the fish was transferred to the experiment tank for habituation/recovery for 18 h to 20 h at  $\approx 15$  cm/s current.

On day 2, data collection started automatically and simultaneously for all fish at 09:00. The PO tags were programmed to sample data at 200 Hz in 1 min sampling bursts spaced by 1 min of idle time (i.e., a 1:2 duty cycle), which, given the internal storage space in the tag, allowed an experiment duration of 66 min. The (peripheral) current for the first 30 min was  $\approx 15$  cm/s and thereafter increased to  $\approx 40$  cm/s for the remaining 36 min.

After data collection, the fish were extracted using a knotless dip net and euthanized by an anesthetic overdose (Benzoak vet, 70 mg/L until level 4 anesthesia Coyle et al., 2004 was reached) followed by a blow to the head. The implant was then recovered and data downloaded. Four complete data sets (Fish 1, 3, 4 and 5) were obtained from the experiment. During data download, sampling bursts were concatenated into two continuous steady-state data sets where the first 15 min represented low current speed and the final 15 min represented high current speed. The middle 3 minutes (corresponding to 6 min in real time due to the duty cycling) were omitted to avoid the transient phase between the two speeds. Due to an unknown tag failure, one fish (Fish 2) provided only a partial dataset from the first 12 min of the experiment which after concatenation resulted in a 6 min data set.

## 2.5. Experiment 2

Experiment 2 was conducted using a Blazka swim respirometer (116 cm length X 24 cm diameter, 551 volume) (Blazka et al., 1960) equipped with a temperature compensated dissolved oxygen sensor (NEOFOX, Ocean Insight, Duiven, The Netherlands).

Eight random fish (fork length  $46.4 \pm 1.1$  cm, weight  $1367 \pm 130.0$  g, Fulton's K-factor  $1.4 \pm 0.1$ ) were captured from their holding tank using a knotless dip net and subsequently underwent the same protocol for surgically implanting the tags as described for Experiment 1. Each fish was implanted with a PO tag programmed with a 65 min start delay and a sampling frequency of 200 Hz. The tags were not set up with duty cycling and thus provided continuous data sets of 33 min. After surgery, the fish was placed inside the swim tunnel for wake-up. Swimming speed (i.e., water speed) inside the swim tunnel was set to  $\approx 0$  BLs<sup>-1</sup> during this period.

During the wake-up period for each individual fish, 30 l sea water were deoxygenated by vigorous bubbling with instrument nitrogen (purity  $\geq 99.9\%$ ) for  $\geq 20$  min. After the fish had woken from anesthesia, swimming speed was increased to 0.5 BLs<sup>-1</sup> where it was kept for the remainder of the experiment. The tunnel remained connected to the same sea water supply as the holding tank until the logger started (i.e., about 65 min post tagging). The water supply was closed 3 min after logging had started, and the deoxygenated water pumped into the swim tunnel, thus abruptly reducing the dissolved oxygen in the tunnel to hypoxic levels. For the next 25 min, no water was replaced in the swim tunnel, effectually keeping the conditions hypoxic with fish respiration leading to a gradual decrease in the DO level from  $\approx 5.5$  mg L<sup>-1</sup> to 3.8 mg L<sup>-1</sup>. Five min before the experiment ended (i.e., 25 min after logging started), the valve to the water supply was reopened and fresh sea water exchange was resumed until logging was concluded at 33 min. Experiment 2 therefore consisted of three periods: Pre-hypoxia (3 min), hypoxia (25 min) and post-hypoxia (5 min).

Using this procedure, data were obtained for one control fish under normoxic conditions and seven test fish exposed to hypoxic conditions. The experiments for the control fish and test fish 2, 4, 5, 6, and 7 resulted in complete 33 min data sets. The experiment for Fish 3 resulted in a partial data set due to tag failure after 29 min. Although the experiment for Fish 1 resulted in a full 33 min data set, water circulation in the swim tunnel was restored  $\approx 3$  min later than dictated by the general procedure because of a valve issue during the trial for this fish. Thus the period of hypoxia was  $\approx 27$  min and the re-oxygenation period  $\approx 1$  min for this fish. It should also be noted that the DO sensor in the tunnel failed during the trial for Fish 7. However, since the test procedure was identical to that of all other fish, the DO profile

in the tunnel was expected to be comparable to that of the other test fish. All individual fish were removed from the swim tunnel after their data logging periods had elapsed and immediately euthanized using the same method as in Experiment 1.

## 2.6. Data processing

To address the  $S_pO_2$  estimation challenge for Atlantic salmon, the proposed processing method is an adaptation of techniques used for human PPGs, and consists of four main steps: Preprocessing, ECG HR estimation, MA reduction and  $S_pO_2$  estimation (Fig. 1).

Preprocessing and HR estimation were applied to entire data series, while the remaining steps applied to 20 s processing windows with 15 s overlap. Details for each step are presented in subsequent sections. All data were processed using Anaconda's Python 3.8 distribution (Anaconda Inc., Austin, Texas, USA).

### 2.6.1. Preprocessing

Preprocessing involved applying a 3rd order Butterworth band-pass filter with passbands 0.2 Hz to 10 Hz for PPG and 5 Hz to 80 Hz for ECG. The cutoff frequencies were determined by considering the signal bandwidth in the frequency domain. PPG for both wavelengths was then scaled to [0, 1] using

$$x_{scaled} = (b - a) \cdot \left( \frac{x_i - x_{min}}{x_{max} - x_{min}} \right) + a, \quad (1)$$

with  $a = 0$  and  $b = 1$  to reduce the likelihood of numerical instability during MA reduction.

### 2.6.2. ECG HR estimation

ECG HR estimation required processing steps to enhance the QRS complex to obtain the HR. ECG signal quality was evaluated by considering which of the categories 'Good', 'Acceptable' or 'Unacceptable' the raw signals fit into. This was similar to evaluations used for human ECGs for this purpose (van der Bijl et al., 2022). Generally, the ECG signals fit into the 'Good' and 'Acceptable' categories with only very few and short instances of 'Unacceptable' during the swim tunnel experiment where the fish exhibited temporary behavior which it would not express in other contexts outside the swim tunnel (e.g., trying to turn inside the tunnel). HR was obtained by applying the slope sum method (SSM) followed by the Teager-Kaiser instantaneous energy operator (TKEO) (Rankawat et al., 2015) to preprocessed ECG data. SSM involved taking the derivative of the ECG and summing only the positive derivative values over a time window matching the duration of the ECG QR slope. In this case, the time window was set to 0.02 s for all ECG data. TKEO involved calculating the instantaneous ECG energy,  $\Psi[x(n)]$ , by applying

$$\Psi[x(n)] = x^2(n) - x(n+1)x(n-1) \quad (2)$$

to the ECG data where  $x(n)$  is the preprocessed ECG value at time  $t = n$ , followed by averaging within a 20 samples wide rolling window. ECG peaks were then detected and peak-to-peak time differencing was finally used to calculate the HR in Hz:

$$HR = \frac{1}{\Delta t}, \quad (3)$$

where  $\Delta t$  is the peak-to-peak time difference. An example of these processing steps is given in Fig. 2.

### 2.6.3. Motion artifact reduction

The MA reduction approach was based on the assumption that perfusion changes with the cardiac cycle (Yoshida et al., 2009; Svendsen et al., 2021c). Because ECG was available and the cardiac cycle correlates with PPG, a synthetic PPG reference was generated using ECG and its amplitude driven by the measured PPG, thus, enabling  $S_pO_2$  estimation. Because PPG signals are oscillatory in nature, a sinusoid

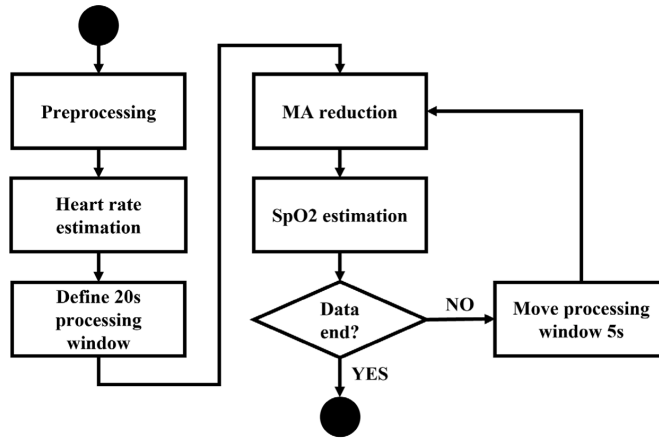


Fig. 1. Data processing main steps.

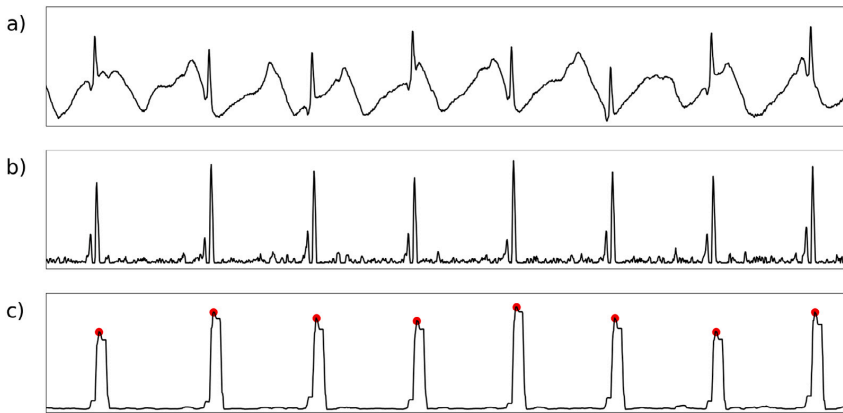


Fig. 2. Processing steps: (a) Raw ECG, (b) ECG after preprocessing and SSM, and (c) ECG after TKEO was applied and peaks detected (indicated with red dots).

matching the average HR was used as the synthetic PPG reference in each processing window. Thus,

$$ref = \sin(2\pi \cdot HR_{avg} \cdot t_s). \tag{4}$$

In Eq. (4),  $HR_{avg}$  is the average ECG HR within a processing window and  $t_s$  the concurrent sampling time for both PPG and ECG.

The least mean squares (LMS) adaptive filter is a well established algorithm used to minimize the mean squared error between the filter's output and its desired response by adjusting its coefficients (Haykin, 2013) (Fig. 3).

The filter's intrinsic properties include independence on the reference phase and amplitude because only the error between the estimate  $y(k)$  and desired  $d(k)$  outputs are used to adjust the coefficients where the two correlate. In vector form, the LMS filter can be described as

$$y(k) = \mathbf{x}^T(k)\mathbf{w}(k), \tag{5}$$

where  $k$  is a discrete time index,  $y(k)$  is the filtered signal,  $\mathbf{w}$  is a vector of adaptive filter weights, and  $\mathbf{x}$  is a vector consisting of the last  $n$

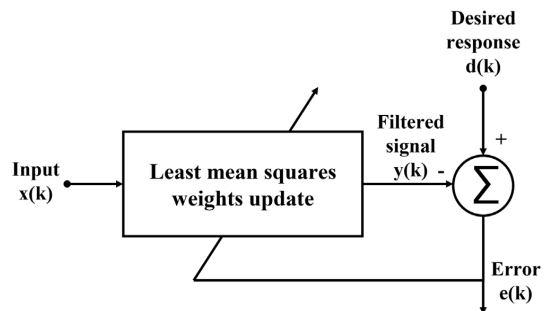


Fig. 3. LMS filter block general schematic.

samples of the input signal, defined by

$$\mathbf{x}(k) = [x(k), \dots, x(k - n - 1)]. \quad (6)$$

The weights,  $\mathbf{w}$ , are updated by

$$\mathbf{w}(k + 1) = \mathbf{w}(k) + \Delta\mathbf{w}(k), \quad (7)$$

and  $\Delta\mathbf{w}(k)$  is

$$\Delta\mathbf{w}(k) = \frac{1}{2} \cdot \frac{\delta e^2(k)}{\delta \mathbf{w}(k)} = \mu \cdot e(k) \cdot \mathbf{x}(k). \quad (8)$$

In Eq. (8), which represents a step in the steepest gradient search for the optimal filter weights,  $\mu$  is the adaptation rate and  $e(k)$  the LMS filter error defined by

$$e(k) = d(k) - y(k). \quad (9)$$

By considering the synthetic reference (Eq. (4)) as noisy in the sense that it lacks the features (i.e., amplitude change) required for  $S_pO_2$  estimation, it was set as the filter's desired output signal,  $d(k)$ , and the measured PPG as the filter input,  $\mathbf{x}(k)$ . Thus, the LMS algorithm imprints changes onto the synthetic PPG reference,  $d(k)$ , such that it correlates with the measurement,  $x(k)$ . Thus, the LMS adaptive filter is a suitable algorithm to drive the synthetic reference amplitude using the measured PPG. Data were processed using a filter width of  $n = 40$  samples and a learning rate  $\mu = 5 \cdot 10^{-4}$ .

#### 2.6.4. Scattering correction parameter

The starting point for deriving the scattering correction parameter,  $\Gamma$ , is the expression for  $S_pO_2$  that was estimated using the modified Beer–Lambert law,

$$A = \sum_i \epsilon_{\lambda} \cdot C_i \cdot DPpF_{\lambda} \cdot d, \quad (10)$$

where  $A$  is absorption,  $\epsilon_{\lambda}$  chromophore  $i$ 's molar extinction coefficient for wavelength  $\lambda$ ,  $DPpF_{\lambda}$  the scattering-dependent differential path length factor for wavelength  $\lambda$ , and  $d$  the PO sensor's source-detector separation distance.  $S_pO_2$  is commonly expressed as the percent fraction of oxyhemoglobin ( $HbO$ ) to total hemoglobin,  $HbT = HbO + Hb$ , where  $Hb$  is deoxygenated hemoglobin, so

$$S_pO_2 = \frac{HbO}{HbO + Hb} \cdot 100\% = \frac{HbO}{HbT} \cdot 100\%. \quad (11)$$

By substituting Eq. (10) for two chromophores (HbO and Hb) into Eq. (11) and taking the ratio of two wavelengths to cancel unknowns, we arrive at an expression for  $S_pO_2$  that also includes  $\Gamma = DPpF_{\lambda_1}/DPpF_{\lambda_2}$ ,

$$S_pO_2 = \frac{\epsilon_{Hb,\lambda_2} \cdot R \cdot \Gamma - \epsilon_{Hb,\lambda_1}}{(\epsilon_{HbO,\lambda_1} - \epsilon_{Hb,\lambda_1}) - R \cdot \Gamma \cdot (\epsilon_{HbO,\lambda_2} - \epsilon_{Hb,\lambda_2})} \cdot 100\%, \quad (12)$$

where  $\epsilon_{HbO,\lambda_1}$ ,  $\epsilon_{HbO,\lambda_2}$ ,  $\epsilon_{Hb,\lambda_1}$  and  $\epsilon_{Hb,\lambda_2}$ , are molar extinction coefficients that need to be set to proper values, and  $R$  is the modulation ratio,

$$R = \frac{\max_{\lambda_1} - \min_{\lambda_1}}{\max_{\lambda_2} - \min_{\lambda_2}}, \quad (13)$$

for PPGs normalized by their DC components (Nitzan and Taitelbaum, 2008; Kyriacou and Allen, 2021). Under the assumption that  $S_pO_2$  never exceeds 100% for individual fish, Eq. (12) can be solved for  $\Gamma$  resulting in

$$\Gamma = \frac{\alpha \epsilon_{Hb,\lambda_1} + (\epsilon_{HbO,\lambda_1} - \epsilon_{Hb,\lambda_1})}{R_{\min}(\epsilon_{HbO,\lambda_2} - \epsilon_{Hb,\lambda_2}) + \alpha \epsilon_{Hb,\lambda_2}}, \quad (14)$$

where  $R_{\min}$  is the smallest modulation ratio (Eq. (13)) in a data set and  $\alpha$  is  $100/S_pO_2$ . Eq. (14) was solved for  $S_pO_2 = 100\%$  for each data set (i.e., fish) from Experiment 1. The average of all correction parameters,  $\Gamma_{avg}$ , was then used during subsequent  $S_pO_2$  estimations.

#### 2.6.5. $S_pO_2$ Estimation

Because Atlantic salmon hemoglobin has absorption characteristics similar to human hemoglobin (Svendsen et al., 2023), the molar extinction coefficients needed in Eq. (12) were set to  $\epsilon_{HbO,\lambda_1} = 319.6$ ,  $\epsilon_{HbO,\lambda_2} = 1154.0$ ,  $\epsilon_{Hb,\lambda_1} = 3226.56$  and  $\epsilon_{Hb,\lambda_2} = 726.44$ , respectively (Prah, 1998). When solving Eq. (12), the average modulation ratio within a 20 s processing window was used for  $R$  and  $\Gamma_{avg}$  obtained using Eq. (14) for  $\Gamma$ . Finally, the  $S_pO_2$  results were smoothed using a 3rd order Butterworth low pass filter with a cutoff frequency of 0.02 Hz. The initial 30 s of data after filtering were omitted due to the filter's settling time.

#### 2.6.6. Result interpretations

For Experiment 1 it was hypothesized that  $S_pO_2$  estimated using  $\Gamma_{avg}$  would remain within the expected range of 95% to 100% for both water current speeds. The data were tested for normality by using quantile–quantile (Q–Q) analysis (Ghasemi and Zahediasl, 2012). For each data set, outliers were removed by calculating the z-score of each value relative to the sample mean and standard deviation. Data points with a z-score greater than  $\pm 3$  were labeled as outliers and removed. The mean and 95% confidence intervals for each data set were then calculated and evaluated with respect to the expected range.

For Experiment 2 it was hypothesized that the relative  $S_pO_2$  difference during hypoxia would be greater compared to pre and post hypoxia periods because each fish had to adapt to the changing conditions. Because physiological response depends on the (physiological) state of each individual and, in this case, residual effects expected from anesthesia and surgery, data was not assumed to be normally distributed in any of the experiment periods. This assumption was supported by Q–Q analysis where sample quantiles did not align well with the theoretical quantiles for a normal distribution. For Experiment 2, the relative  $S_pO_2$  differences and medians were therefore calculated separately for each period and compared.

### 3. Results

The results show that PPG for 660 nm and 880 nm could be successfully measured. Both the long term trend (i.e., baseline) and the high frequency variations caused by blood circulation were visible (Fig. 4).

All data sets from both experiments featured typical PPG traits such as saliency, baseline wandering, hyperperfusion events and MA (Figs. 5 and 6).

The measured PPGs could be divided into three categories: 'salient', 'MA corrupted' and 'bad' (Fig. 6). In general, the measured PPGs were in the 'salient' and 'MA corrupted' categories with sporadic instances of the 'bad' category. PPGs in the 'bad' category were coincident with high activity events such as burst swimming in Experiment 1 and flight responses in Experiment 2. The LMS algorithm successfully tracked 'salient' PPGs and reconstructed signals for 'MA corrupted' signals. In the case of 'bad' PPGs no clear pulsatile component concurrent with HR was present. Thus, the correlation with the synthetic reference was too low for successful filtering by the LMS algorithm.

#### 3.1. Experiment 1

The MA compensated data from Experiment 1 allowed an estimation of the average scattering compensation parameter using Eq. (14) for low ( $\Gamma_{avg,low} = 0.33$ ) and high ( $\Gamma_{avg,high} = 0.37$ ) water currents, resulting in an average scattering correction parameter of  $\Gamma_{avg} = (\Gamma_{avg,low} + \Gamma_{avg,high})/2 = 0.35$  (Table 1).

Using  $\Gamma_{avg}$  in Eq. (12) for all data obtained from Experiment 1 resulted in average  $S_pO_2$  values of  $96.98 \pm 0.08$  and  $96.44 \pm 0.09$  calculated for low and high water current speeds, respectively. Both means and confidence intervals were within the expected  $S_pO_2$  range of 95% to 100% for both water currents (Table 2).

The average relative  $S_pO_2$  differences (max–min) for low and high water current were 2.42% and 2.87%, respectively (Table 2).

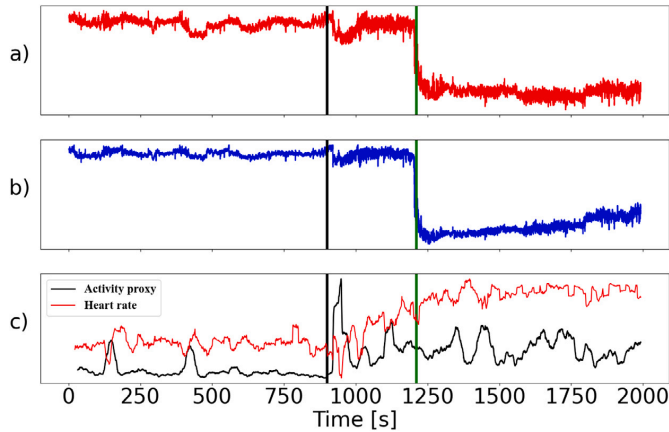


Fig. 4. Raw PPG data from one exemplary fish for (a) 660 nm and (b) 880 nm from Experiment 1. An acceleration based activity proxy (black) and HR (red) are shown in (c). The black vertical line denotes the time when the water current speed was increased, and the green vertical line indicates a hyperperfusion event (i.e., increased perfusion). Note the increase in amplitude after water current speed was increased which coincided with the higher activity levels seen in (c).

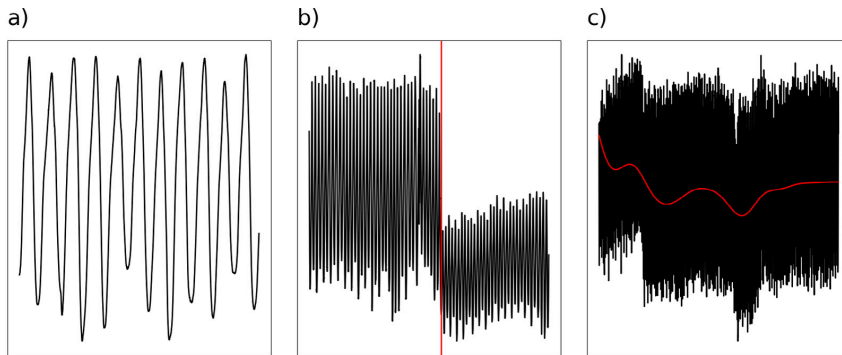


Fig. 5. Examples of typical PPG traits such as saliency (a), hyperperfusion event (b), indicated by the vertical red line and baseline wandering (c) identified in the measured data from Fish 2 in Experiment 2.

**Table 1**  
Individual and average scattering compensation parameter  $\Gamma$  at high and low current speed, respectively, from Experiment 1.

	Fish 1	Fish 2	Fish 3	Fish 4	Fish 5	Average
Low speed	0.31	0.34	0.31	0.35	0.36	0.33
High speed	0.33	-	0.38	0.41	0.41	0.37

### 3.2. Experiment 2

Using the MA compensation approach and the average scattering coefficient obtained in Experiment 1 ( $\Gamma_{avg}$ ), a median  $SpO_2$  of 100.70%, and a min-max variation of 4.53% was calculated for the entire data set for the control fish. For the test fish, the average median  $SpO_2$  before, during, and after hypoxia was 97.18% for the pre hypoxia period, 97.27% for the hypoxia period and 97.43% for the post hypoxia period (Table 3). The corresponding average relative  $SpO_2$  differences (max-min) were 2.41% pre hypoxia, 4.75% during hypoxia, and 2.25% post hypoxia (Table 4).

All test fish had a larger relative difference in  $SpO_2$  during the hypoxia period compared to the pre and post hypoxia periods. This indicates that the PPG was affected by changes in dissolved oxygen, manifesting as observable changes in the  $SpO_2$  estimate. Test fish 1–6

were able to maintain a median  $SpO_2$  value within the expected  $SpO_2$  range at all times. For fish 7, the same applied to the pre hypoxia and hypoxia periods, while the  $SpO_2$  estimate just exceeded 100% for the post hypoxia period. The average relative change for the test fish was 0.22% higher during the hypoxia period compared to the relative change calculated for the control fish but with individual differences up to 2.6%. Additional plots and evaluations for each fish from Experiment 2 are given in Appendix.

### 4. Discussion

In this pilot study for PO in Atlantic salmon, PPG and ECG data were successfully collected under normoxic and hypoxic conditions. Using these data, a viable MA compensation approach was derived and an average scattering compensation parameter calculated. Based on these results, PPGs measured under normoxic conditions resulted in an  $SpO_2$  estimate within the expected range, while PPGs measured under hypoxic conditions showed that the PO sensor responded to changes in  $SpO_2$ . The experiments can thus be considered successful.

The relative  $SpO_2$  difference from Experiment 1 were greater for high compared to low water currents which may indicate greater impact from MA for high compared to low water current. This is supported by both activity proxies and video material for the experiment which



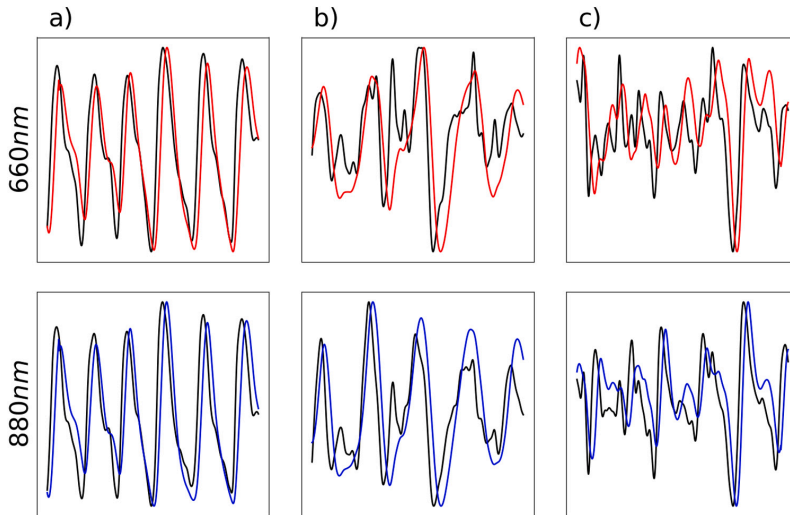


Fig. 6. Examples of (a) a salient PPG, (b) a MA corrupted PPG, and (c) a bad PPG. In all plots the black line depicts the preprocessed PPG, while the colored line depicts the LMS filtered (i.e. MA compensated) PPG.

Table 2

Absolute  $SPO_2 \pm 95\%$  confidence interval and relative differences ( $\Delta SPO_2$ ) for all fish at high and low current speeds, for all fish at high and low current speeds. Due to tag failure, low speed data duration for Fish 2 was 6 min. High speed data was not available for Fish 2.

	Fish 1	Fish 2	Fish 3	Fish 4	Fish 5	Average
Low speed	96.56 $\pm$ 0.08	97.23 $\pm$ 0.06	97.43 $\pm$ 0.07	97.00 $\pm$ 0.04	96.68 $\pm$ 0.15	96.98 $\pm$ 0.08
High speed	96.34 $\pm$ 0.09	–	97.17 $\pm$ 0.09	96.94 $\pm$ 0.02	95.32 $\pm$ 0.14	96.44 $\pm$ 0.09
Low speed $\Delta SPO_2$	2.41	0.63	3.13	1.30	4.64	2.42
High speed $\Delta SPO_2$	2.91	–	2.53	1.43	4.60	2.87

Table 3

Median and average values for the pre hypoxia, hypoxia and post hypoxia periods.

	Fish 1	Fish 2	Fish 3	Fish 4	Fish 5	Fish 6	Fish 7	Average
Pre hypoxia median	95.17	96.15	97.77	96.06	97.36	98.68	99.25	97.18
Hypoxia median	94.96	96.88	97.94	95.75	99.24	99.24	99.91	97.27
Post hypoxia median	95.41	97.10	97.95	96.73	97.18	97.18	100.47	97.43

Table 4

Relative differences in estimated  $SPO_2$  between the pre hypoxia, hypoxia and post hypoxia periods for the fish subjected to hypoxic conditions.

	Fish 1	Fish 2	Fish 3	Fish 4	Fish 5	Fish 6	Fish 7	Average
Pre hypoxia	5.10	1.84	1.07	2.69	2.20	2.01	1.97	2.41
Hypoxia	6.66	4.58	3.04	5.26	7.15	3.47	3.08	4.75
Post hypoxia	2.87	1.97	0.72	2.39	3.54	3.19	1.04	2.25

document intermittent swimming bursts after water current speed was increased and the fish had to re-establish their positions in the tank (Fig. 4(c)). The absolute values, however, were all within the expected range of 95% to 100% (Table 2). It is thus considered likely that the methods used to estimate  $SPO_2$  gave reasonable results.

For Experiment 2 the estimated  $SPO_2$  consistently showed greater variation during hypoxia period compared to the pre and post hypoxia periods (Table 3). This was as expected since the fish had to adapt to the hypoxic conditions through behavioral and physiological adjustments to maintain median levels. Because the combined time for surgery and recovery was limited to 65 min for the swim tunnel, the control for Experiment 2 was included to get an impression of whether or not the

$SPO_2$  estimate resulted in expected values. The relative difference and median for the control indicate that the fish recovered sufficiently for the technology test in this pilot study.

During Experiment 1, data were collected from five Atlantic salmon under normoxic conditions with the aim to find an average scattering compensation parameter and an MA compensation approach using an LMS filter with a synthetic PPG reference constructed using ECGs collected intraperitoneally. This is considered valid because PPG correlates with the cardiac cycle (Yoshida et al., 2009; Svendsen et al., 2021c). Intraperitoneal ECG collection is the most common way to obtain HR from free swimming fish, and the measured ECGs were generally of ‘Good’ and ‘Acceptable’ signal quality. Short instances of ‘Unacceptable’ signal quality were recorded when the fish exhibited behavior which it would not express outside a swim tunnel. The effect of these instances were mitigated by HR averaging within a processing window.

For Experiment 1 it was assumed that  $SPO_2$  for all individuals would be 100% due to the normoxic conditions. This assumption is supported by e.g., Steinhilber et al. (2008) and Clark et al. (2008) who reported that species comparable to Atlantic salmon (Sockeye Salmon (*Oncorhynchus nerka*) and Chinook salmon (*Oncorhynchus tshawytscha*)), have  $PaO_2$  at rest of 97 Torr and 90 Torr, respectively which corresponds to  $\approx 100\%$   $SPO_2$  (Madan, 2017). Using the MA compensated PPGs and  $\Gamma_{avg}$  in Eq. (12), the resulting  $SPO_2$  estimates for the fish in Experiment 1 were within the expected range of 95% to 100%.

Although the implantation procedure and tag placement were similar for all fish, individual differences in anatomy and tissue composition within the sensing volume mean an average value for scattering compensation ( $\Gamma_{avg} = 0.35$ ) introduces an inaccuracy when calculating  $SPO_2$  using Eq. (12) which may result in values exceeding 100%. This effect is similar to that arising from empirical mapping procedures in human PO. Note, however, that values in Table 1 are quite similar for

low and high speeds. This indicates that PPG sensing conditions were comparable between individuals. The calculated values for  $T$  were, however, consistently higher for high compared to low water speed. One possible explanation for this could be that the increased swimming speed resulted in increased blood pressure and tissue perfusion, thus affecting sensing conditions (e.g., light back scattering). This is supported by increased PPG amplitude (associated with blood pressure) and a decrease in PPG mean (associated with increased perfusion) observed in raw data for all fish in Experiment 1 (Fig. 4). PPG decreases when perfusion increases due to greater light scattering and absorption, thus, reducing the amount of light reaching the photo detector. These elements indicate that the PO measured a PPG (as opposed to pure MA noise), and that the MA compensation approach and the average scattering compensation parameter were valid and could be used for  $S_pO_2$  estimation.

In Experiment 2, Atlantic salmon were implanted with the aim to see if the PO sensor would respond to changes in  $S_pO_2$  using the methods and results from Experiment 1. To this end, individual implanted fish were consecutively placed in a swim tunnel and subjected to hypoxic conditions (down to  $3.8 \text{ mg L}^{-1}$ ). At such levels, hypoxic responses have been observed previously in Atlantic Salmon (Vikeså et al., 2017; Remen et al., 2016) suggesting that reduced arterial  $S_pO_2$  may be observed (Farrell and Richards, 2009). Thus,  $S_pO_2$  was expected to vary between individuals during the hypoxia period as observed.

The data processing methods were inspired by approaches for MA detection and removal in human PPGs using synthetic Refs. Lim et al. (2018) and Shin et al. (2021). These approaches rely on widely accepted PPG morphology. Although the measured PPGs generally show typical PPG traits such as saliency, hyperperfusion events, and baseline wandering (Fig. 5) (Park et al., 2022), accurate knowledge of fish PPGs is currently limited. Such variations may be caused by anatomical differences and circulatory function. For instance, Atlantic salmon has a secondary, low pressure, circulatory system (Bone and Moore, 2008). Any difference in pulse transit time (PTT) for arterial blood between the two circulatory systems can for the same cardiac cycle change the PPG shape because the (arterial) blood arrives in the sensing volume at different times.

The MA reduction method was successful in most situations when the PPG signal was not extremely distorted and had a clear pulsatile component. However, the variability between cases yielding valid PPG signals (e.g., Fig. 6(a) vs. (b)) seems to be much higher compared to valid human PPGs, implying a greater variation in PPG morphology may have to be accepted for fish compared to humans when estimating both HR and  $S_pO_2$ . It is likely that this approach will not be equally effective when the pulsatile component is not equally clear. For example, the data shown in Fig. 6(c) were obtained during Experiment 1 where a fish showed momentary intensive burst swimming. This implies that the filtering/MA reduction approach cannot be expected to work well in all instances where the fish exhibits abrupt changes in movement. Thus, the LMS approach may be limited to MAs that are not so large that they effectually override any pulsatile components in the signal, and thus remove the ability to correlate this with the reference. However, in such cases it can be expected that the MAs are distinct from the PPG in the time/frequency domains and can then be compensated for by constructing a suitable MA reference using the 9-axis inertial motion unit which is part of the PO tag. Such an approach, combining both the synthetic PPG reference presented in this study with conventional acceleration based approaches, should be a subject in future work.

The  $S_pO_2$  processing method required that an accurate HR estimate could be obtained using ECG for a valid synthetic reference. Although ECG was susceptible to motion (though less than PPG), SSM and TKEO are methods suited to enhance peaks in noisy signals (Rankawat et al., 2015) and generally performed well for the purposes of this pilot study, as seen in Fig. 2. In some cases in Experiment 2, motion affected ECG in a way that made peak detection challenging. Such periods

may have been caused by abrupt changes in movement momentarily changing the ECG sensing conditions. They were, however, of limited duration and their effects were alleviated by averaging. The synthetic reference consisted of a sinusoid with a frequency matching the average HR within a processing window (lasting 20 s with a 15 s overlap with the previous window). These values were chosen because a window  $< 20$  s increased the likelihood of numerical instability in the LMS filter and generally resulted in increased noise, likely due to reduced averaging effect in the  $S_pO_2$  estimate. Similarly, a window  $> 20$  s reduced performance of the LMS filter because HR is likely to change over time. The average HR may thus not correlate sufficiently with the PPG using longer windows. The overlap of 15 s was chosen to minimize this effect. Additionally, the 15 s overlap was motivated by the lowest expected HR of 15 BPM for Atlantic Salmon (Lucas, 1994) and comparable species (Brijs et al., 2019), i.e., one heart beat every 4 s. To allow for some margin for new data to be included within the processing window and to obtain a reasonable data resolution, the overlap was set to 15 s, thus giving one  $S_pO_2$  estimate every 5 s.

Because the  $S_pO_2$  estimate is driven by the modulation ratio (Eq. (13)) the reference did not have to be an exact morphological PPG duplicate as long as its amplitude was driven by correlation with the measured PPG in the LMS filter. Since perfusion is concurrent with the cardiac cycle, a sinusoid with a frequency matching the HR was considered a feasible choice. Note, however, that this approach could also be a source of error if the HR changes considerably within a processing window. In such instances the difference between the average HR used for the synthetic reference and the instantaneous HR will affect the correlation between the measured signal and the reference used by the LMS filter, thus reducing its performance. Future implementations may employ more sophisticated approaches such as template matching to address this challenge if an accepted PPG shape for Atlantic salmon becomes available.

Tissue composition and their optical properties within the PPG sampling volume are important when estimating  $S_pO_2$ . Due to individual differences in anatomy it is prudent to consider whether sensor placement could have had an impact on the data. The link between the estimated  $S_pO_2$  values and ambient DO-conditions appeared to be stronger for some fish (e.g., Fish 5 in Experiment 2 (Table 3)) compared to others. An explanation for such differences may be salmon's capabilities compensate for reduced DO through physiological mechanisms that increase their ability to absorb  $O_2$  from the water (e.g., increased gill area and ventilation frequency, increased HR and/or stroke volume), or mechanisms reducing their consumption of  $O_2$  (e.g., reduced activity). This could also explain some of the larger inter-individual variations seen during the hypoxic periods as the above mentioned mechanisms can take some time before being properly activated, and that different individuals could have different tolerance limits at which such mechanisms will be necessary.

While the results show that it is possible to estimate  $S_pO_2$  in free-swimming salmon, they also imply that Atlantic salmon are resilient with respect to temporary hypoxia due to their various coping mechanisms. Exploring the potential effect of such mechanisms and their role in maintaining homeostasis would require further trials, where the fish could be kept at lower DO levels over longer times as this could identify when these mechanisms are no longer sufficient to prevent physiological breakdown. However, conducting such experiments would be both complex and difficult to do properly, as well as being ethically challenging.

## 5. Future work

While the results from this pilot study indicate that  $S_pO_2$  can be estimated for Atlantic salmon, future work aimed at exploring ways to further improve the accuracy and reliability of the estimates could strengthen the potential of this method in monitoring the physiological status of farmed fish. As mentioned, the MA compensation works

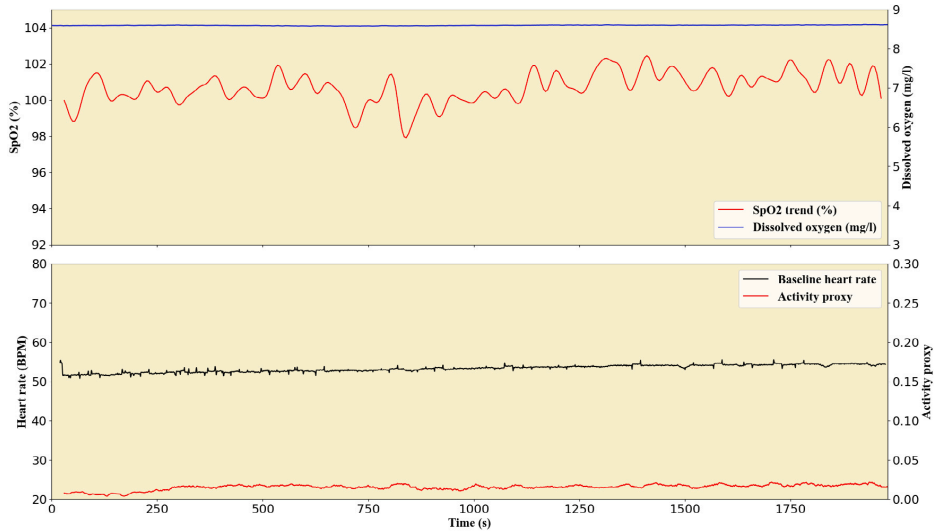


Fig. 7. Experiment 2 - Control.

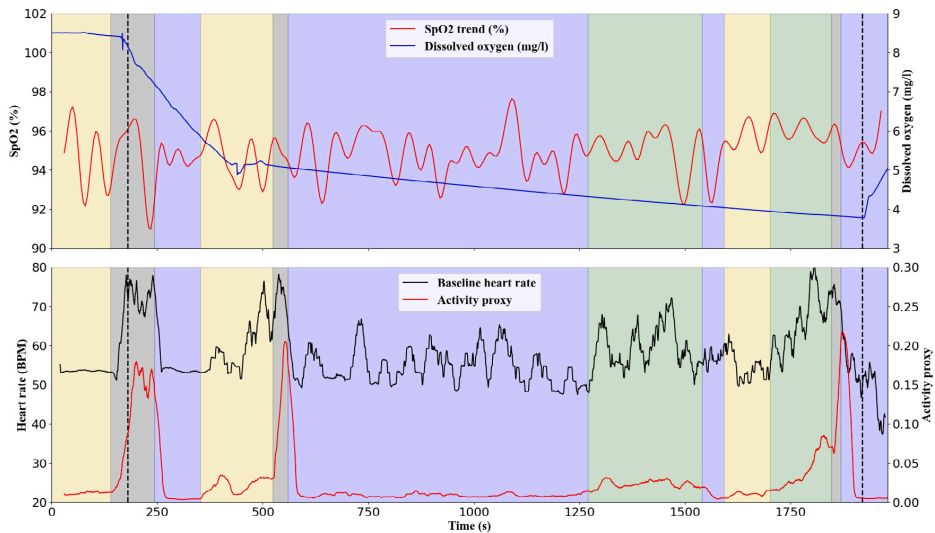


Fig. 8. Results for Fish 1.

for cases where a synthetic reference can be constructed using ECG. Because the PO implant also contains an inertial motion unit, MA compensation could be enhanced by combining the current method with motion data for improved and robust MA compensation and PO in Atlantic salmon.

Although these experiments have proven the concept of using such sensors to monitor fish, it is possible to further strengthen this conclusion by increasing the number of fish to allow sufficient statistical power for evaluations of statistical significance. This would require that authorities allow more effective measures to rapidly and reliably deoxygenate arterial blood (e.g., carbon monoxide exposure).

$SpO_2$  estimation accuracy may further benefit from additional validation studies combining implantation with dorsal aorta (DA) cannulation in controlled raceway/swim tunnel trials. Since DA cannulation

enables blood gas analysis simultaneous with measurements acquired with the implant, this would provide a more accurate  $SpO_2$  baseline for comparison.

The PPGs measured in the experiments show traits (e.g., PPG amplitude and hyperperfusion events) which in humans are associated with changes in cardiac output (CO), the product of stroke volume and HR. It is believed that fishes actively adjust their heart's stroke volume by the Frank-Starling mechanism (Tota et al., 2005). It has also been shown that stress response is associated with HR (Svendsen et al., 2021a). Because the ability to deliver oxygen to tissues depends on CO, it is possible that using HR as a stress indicator alone is inaccurate if the fish simply compensates by adjusting CO. This may offer an explanation the drop in PPG mean without a concurrent increase in HR as seen in Fig. 4 which indicates that the fish increased the stroke volume of its

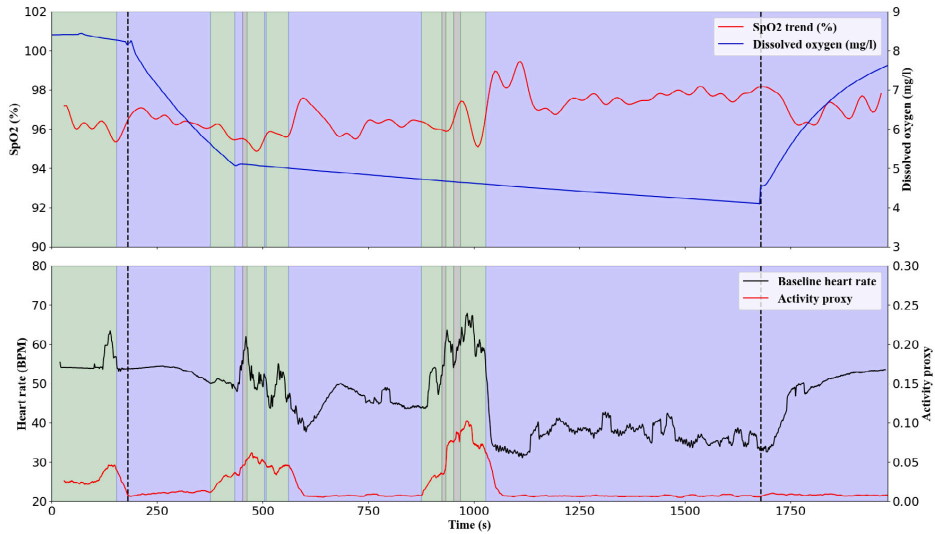


Fig. 9. Results for Fish 2.

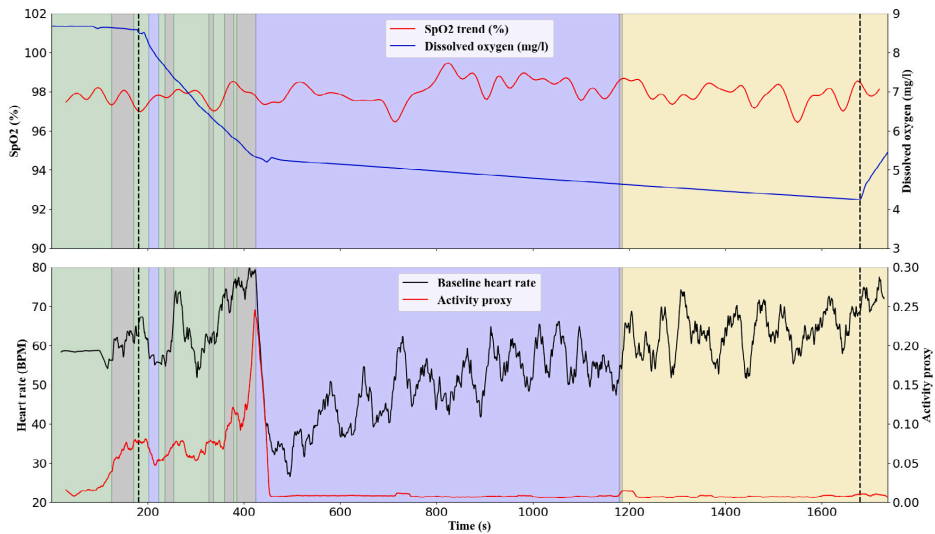


Fig. 10. Results for Fish 3.

heart to increase perfusion. Thus, PPG measurements with appropriate signal processing open the possibility to evaluate stress levels in terms of both HR and CO evaluations.

ECG was also affected by MA, thus challenging the accuracy of the synthetic reference. Combining SSM and TKEO resulted in a powerful tool to enhance the QRS complex in preprocessed ECG signals (Fig. 2), but robustness may in the future be improved by implementing scaling and a more sophisticated peak detection approach after TKEO.

## 6. Conclusion

The results from this pilot study show that PPG from free swimming Atlantic salmon can be collected using an implanted PO tag. Although

PPGs were affected by MA, a filtering approach using a synthetic PPG reference and a LMS filter were successfully derived and used for compensation. Because alternative calibration techniques were unavailable for fish, a light scattering compensation parameter was calculated under the assumption that  $SpO_2$  was 100% for fish under normoxic conditions. Using MA and light scattering compensation, values for  $SpO_2$  within the expected range were calculated for all experiment fish. It is therefore considered that  $SpO_2$  can be an addition to the selection of physiological response parameters possible to measure using implants. If PO implants can be adapted as part of future Atlantic salmon farming (e.g., in the form of sentinel fish Føre et al., 2017a), producers may obtain additional objective data providing insight into the physiological state of the biomass. This can, in turn, contribute to improved animal health and welfare.

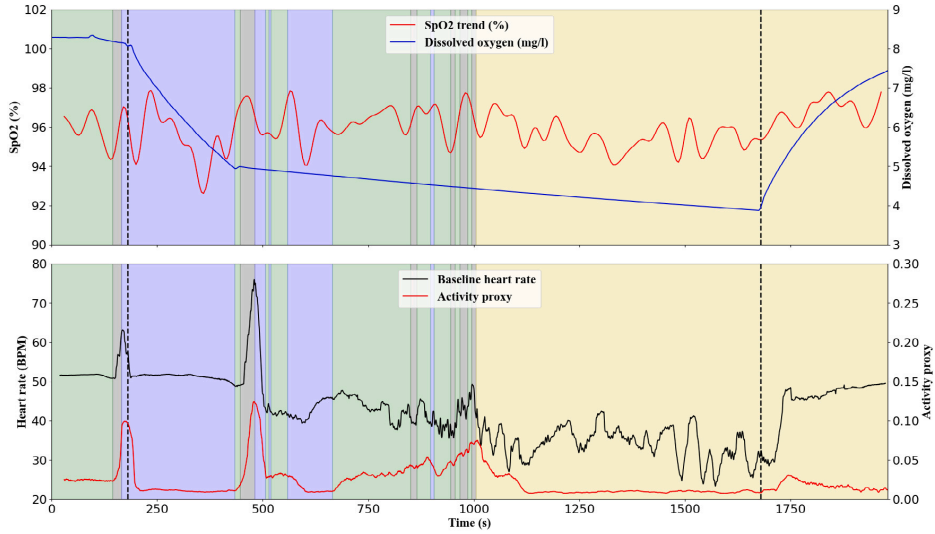


Fig. 11. Results for Fish 4.

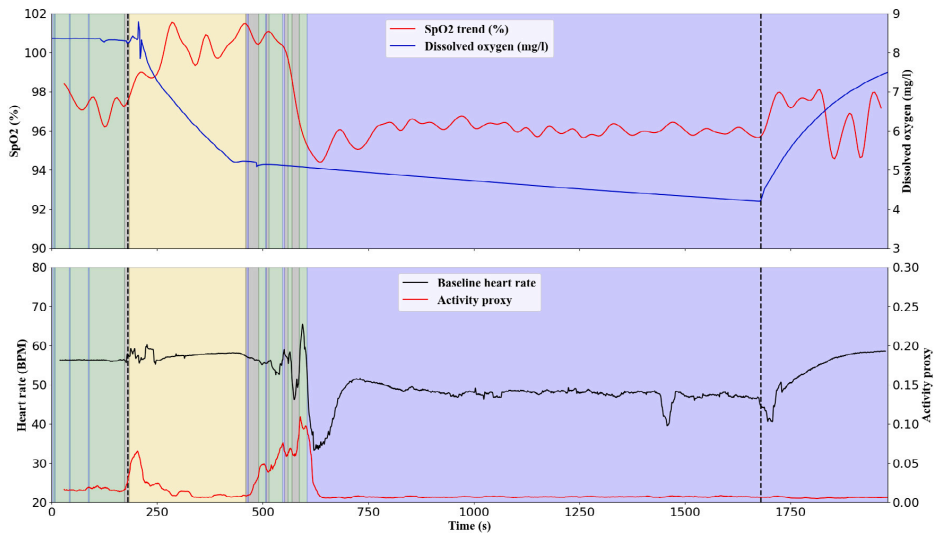


Fig. 12. Results for Fish 5.

#### CRedit authorship contribution statement

E. Svendsen: Method development, Data curation, Writing – original draft. M. Føre: Method development, Writing – original draft. L.L. Randeberg: Method development, Writing – original draft. R.E. Olsen: Writing – original draft. B. Finstad: Writing – original draft. M. Remen: Writing – original draft. N. Bloecher: Writing – original draft. J.A. Alfredsen: Method development, Writing – original draft.

#### Declaration of competing interest

The authors declare that they have no known competing financial interests or personal relationships that could have appeared to influence the work reported in this paper.

#### Data availability

Data will be made available on request.

#### Appendix

In this appendix data from each individual fish used in Experiment 2 are presented and discussed. Because MA is caused by activity, the common activity proxy using the 30 s rolling mean of the acceleration norm commonly found in literature (e.g., Svendsen et al., 2021a) was calculated for co-evaluation with  $SpO_2$  and the baseline HR used for the synthetic PPG reference. In all figures, the colored background denotes different behaviors with green being swimming, yellow being burst and glide (glide period  $\leq 5$  s), blue is station keeping and gray

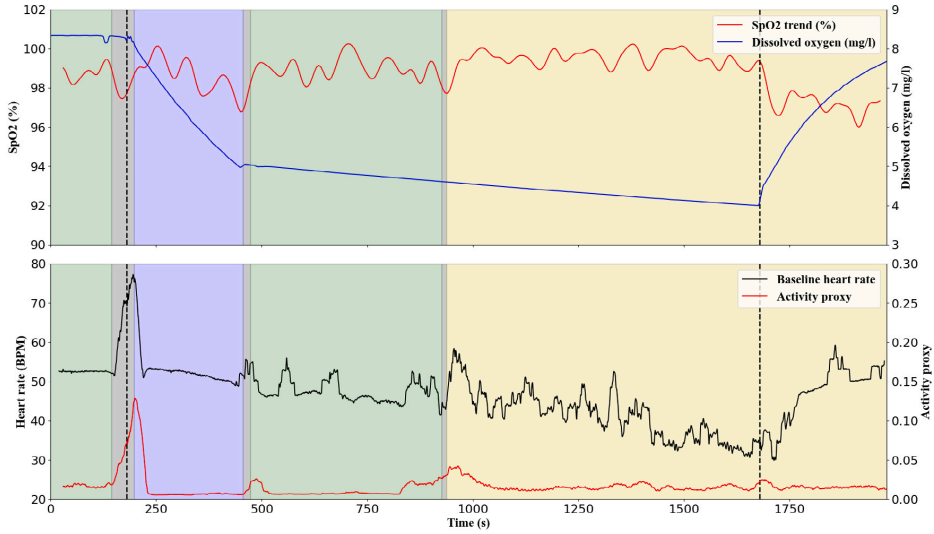


Fig. 13. Results for Fish 6.

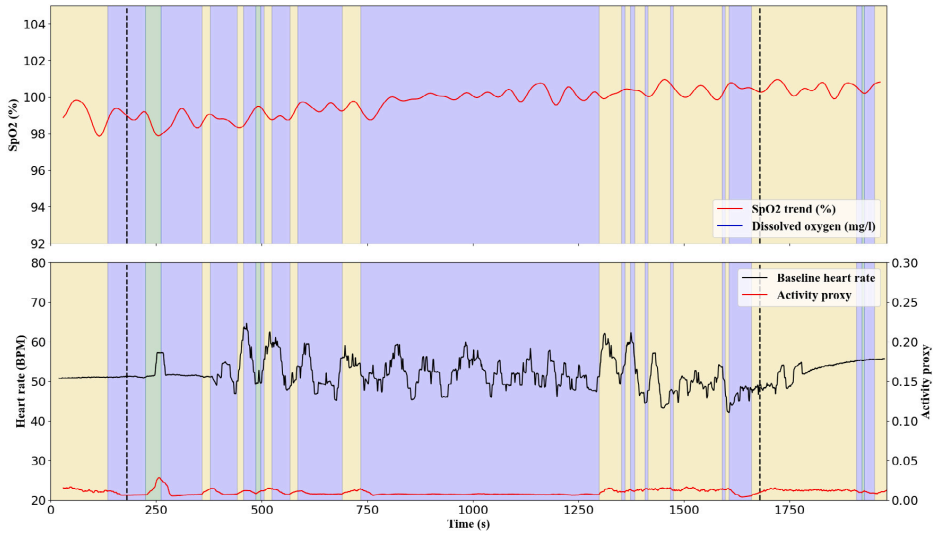


Fig. 14. Results for Fish 7.

is high activity periods with behavior not falling into any of the other categories. In the figures below, the vertical dotted lines, where present, indicate the hypoxia period.

**Control**

The control exhibited the same behavior and stable HR throughout the entire duration of the trial.  $SpO_2$  was stable showing little change as can be expected under normoxic conditions. Note that  $SpO_2$  is high and sometimes more than 100%. This is caused by using an average value for scattering compensation which will introduce an estimation inaccuracy for individuals (see Fig. 7).

**Fish 1**

Measurements for Fish 1 resulted in a complete 33 min data set. Compared to the other fish, the hypoxia period was  $\approx 3$  min longer due to an unforeseen valve issue. Fish 1 was generally able to maintain  $SpO_2$  with the exception of transient reductions during high activity periods. During periods of station keeping the  $SpO_2$  level is restored, likely due to reduced demand (see Fig. 8).

**Fish 2**

Measurements for Fish 2 resulted in a complete 33 min data set. Fish 2 was generally able to maintain  $SpO_2$  throughout the hypoxic period,



with the exception of transients during periods of high activity. The high activity periods are followed by a period of reduced activity during which  $S_pO_2$  is restored or even increased. These results may reflect successful compensation during a period of reduced oxygen availability, e.g. by increasing gill ventilation and perfusion (Perry et al., 2009) (see Fig. 9).

#### Fish 3

Measurements for Fish 3 resulted in a 29 min data set, i.e. 4 min shorter compared to the other data sets to tag failure. Thus, the post hypoxia period was only 1 min for Fish 3. During hypoxia Fish 3 is able to maintain  $S_pO_2$ , also during and following a period of high activity as oxygen is reduced from  $> 8$  mg/l to approximately 5.5 mg/l. This indicates that compensatory responses (e.g. increased gill ventilation and perfusion) successfully upholds oxygen uploading at the gills, also during a period of high activity, possibly as a response to the declining DO. The reduced HR and activity that follows after the activity burst, at low DO, may indicate a post exercise oxygen demand that results in functional hypoxia and bradycardia (reduced HR and increased stroke volume Farrell and Richards, 2009) (see Fig. 10).

#### Fish 4

Measurements for Fish 4 resulted in a complete 33 min data set. Fish 4 was generally able to maintain  $S_pO_2$  with the exception of a transient increase during a period with stable swimming activity when the hypoxia period starts. Fish 4 was quite active during the trial, and together with the maintained  $S_pO_2$ , this may indicate successful compensation during a period with lowered oxygen availability (see Fig. 11).

#### Fish 5

Measurements for Fish 5 resulted in a complete 33 min data set. The results show interesting and distinct  $S_pO_2$  responses. Of note is the first major  $S_pO_2$  drop after a period of increasing activity, when DO declines and reaches approximately 5 mg/l. After this,  $S_pO_2$  remains lower than in the pre-hypoxia and post-hypoxia periods. Coincident with the drop in  $S_pO_2$ , the HR dropped, first to low, then to intermediate levels compared to normoxia. These results may indicate that the individual first responded behaviorally to the declining DO (flight response), after which the post-exercise oxygen demand induced functional hypoxia and bradycardia. With DO levels between 4 and 5 mg/l in the hypoxic period, this individual was not able to successfully re-establish normoxic  $S_pO_2$  and HR before oxygen levels where increased (see Fig. 12).

#### Fish 6

Measurements for Fish 6 resulted in a complete 33 min data set. Fish 6 was generally able to maintain  $S_pO_2$  with exception of a transient increase during a low activity period when the hypoxia period starts. Fish 6 was quite active during the trial. Combined with  $S_pO_2$  results, this may indicate successful compensation during the hypoxic period (see Fig. 13).

#### Fish 7

Measurements for Fish 7 resulted in a complete 33 min data set. The DO sensor failed during the trial for Fish 7, thus, DO data are not available for this individual. The procedure for this fish was, however, identical to the other fish, so it was expected that the DO profile for Fish 7 was comparable to the other fish. Fish 7 was generally able to maintain and even increase  $S_pO_2$  during the trial. Fish 7 was not very active during the trial. This could indicate that oxygen availability and oxygen uptake was sufficient to fulfill the oxygen demand, possibly through compensatory responses such as increased ventilatory effort (see Fig. 14).

## References

- Aoyagi, T., 2003. Pulse oximetry: its invention, theory, and future. *J. Anesth.* 17 (4), 259–266.
- Baktoft, H., Gjelland, K.Ø., Økland, F., Thygesen, U.H., 2017. Positioning of aquatic animals based on time-of-arrival and random walk models using YAPS (Yet Another Positioning Solver). *Sci. Rep.* 7 (1).
- Blazka, P., Volf, M., Cepela, M., 1960. A new type of respirometer for the determination of the metabolism of fish in an active state. *Physiol. Bohemoslov.* 9 (6), 553–558.
- Bone, Q., Moore, R., 2008. *Biology of Fishes*. Taylor & Francis.
- Brijs, J., Sandblom, E., Axelsson, M., Sundell, K., Sundh, H., Huyben, D., Broström, R., Kiessling, A., Berg, C., Gräns, A., 2018. The final countdown: Continuous physiological welfare evaluation of farmed fish during common aquaculture practices before and during harvest. *Aquaculture* 495, 903–911.
- Brijs, J., Sandblom, E., Rosengren, M., Sundell, K., Berg, C., Axelsson, M., Gräns, A., 2019. Prospects and pitfalls of using heart rate bio-loggers to assess the welfare of rainbow trout (*Oncorhynchus mykiss*) in aquaculture. *Aquaculture* 509, 188–197.
- Casson, A.J., Galvez, A.V., Jarchi, D., 2016. Gyroscope vs. accelerometer measurements of motion from wrist PPG during physical exercise. *ICT Express* 2 (4), 175–179.
- Chan, E.D., Chan, M.M., Chan, M.M., 2013. Pulse oximetry: understanding its basic principles facilitates appreciation of its limitations. *Respir. Med.* 107 (6), 789–799.
- Clark, T.D., Sandblom, E., Cox, G.K., Hinch, S.G., Farrell, A.P., 2008. Circulatory limits to oxygen supply during an acute temperature increase in the Chinook salmon (*oncorhynchus tshawytscha*). *Am. J. Physiol.-Regul., Integr. Comp. Physiol.* 295 (5), R1631–R1639.
- Coyle, S.D., Durborow, R.M., Tidwell, J.H., et al., 2004. *Anesthetics in Aquaculture*, Vol. 3900. Southern Regional Aquaculture Center Stoneville.
- Dubey, H., Kumaresan, R., Mankodiya, K., 2018. Harmonic sum-based method for heart rate estimation using PPG signals affected with motion artifacts. *J. Ambient Intell. Humaniz. Comput.* 9 (1), 137–150.
- Farrell, A.P., Richards, J.G., 2009. Defining hypoxia: an integrative synthesis of the responses of fish to hypoxia. In: *Fish Physiology*, Vol. 27. Elsevier, pp. 487–503.
- FDIR, 2023. Biomassestatistikk etter fylke. URL: <https://www.fiskeridir.no/Akvakultur/Tall-og-analyse/Biomassestatistikk/Biomassestatistikk-etter-fylke>, Accessed: 09.02.2023.
- FOR-2015-06-18-761, 2015. Forskrift om bruk av dyr I Forsøk. URL: <https://lovdata.no/dokument/SF/forskrift/2015-06-18-761>.
- Føre, M., Alfreðsen, J.A., Gronningsater, A., 2011. Development of two telemetry-based systems for monitoring the feeding behaviour of Atlantic salmon (*Salmo salar* L.) in aquaculture sea-cages. *Comput. Electron. Agric.* 76 (2), 240–251.
- Føre, M., Frank, K., Dempster, T., Alfreðsen, J.A., Høy, E., 2017a. Biomonitoring using tagged sentinel fish and acoustic telemetry in commercial salmon aquaculture: a feasibility study. *Aquacult. Eng.* 78, 163–172.
- Føre, M., Frank, K., Norton, T., Svendsen, E., Alfreðsen, J.A., Dempster, T., Eguiraun, H., Watson, W., Stahl, A., Sunde, L.M., et al., 2017b. Precision fish farming: A new framework to improve production in aquaculture. *Biosystems Engineering*.
- Føre, M., Svendsen, E., Økland, F., Gräns, A., Alfreðsen, J.A., Finstad, B., Hedger, R.D., Uglem, I., 2021. Heart rate and swimming activity as indicators of post-surgical recovery time of Atlantic salmon (*Salmo salar*). *Animal Biotelemetry* 9 (1), 1–13.
- Ghasemi, A., Zahediasl, S., 2012. Normality tests for statistical analysis: a guide for non-statisticians. *Int. J. Endocrinol. Metabol.* 10 (2), 486.
- Golyandina, N., Korobeynikov, A., Zhigljavsky, A., 2018. *Singular Spectrum Analysis with R*. Springer.
- Hanyu, S., Xiaohui, C., 2017. Motion artifact detection and reduction in PPG signals based on statistics analysis. In: 2017 29th Chinese Control and Decision Conference (CCDC). IEEE, pp. 3114–3119.
- Hassan, W., Føre, M., Urke, H.A., Kristensen, T., Ulvund, J.B., Alfreðsen, J.A., 2019. System for real-time positioning and monitoring of fish in commercial marine farms based on acoustic telemetry and internet of fish (IoF). In: The 29th International Ocean and Polar Engineering Conference. ISOPE.
- Haykin, S., 2013. *Adaptive Filter Theory* (5th Edition). Pearson Education India.
- Jónsdóttir, K.E., Hvas, M., Alfreðsen, J.A., Føre, M., Alver, M.O., Bjelland, H.V., Oppedal, F., 2019. Fish welfare based classification method of ocean current speeds at aquaculture sites. *Aquac. Environ. Interact.* 11, 249–261.
- Kyriacou, P.A., Allen, J., 2021. *Photoplethysmography: Technology, Signal Analysis and Applications*. Academic Press.
- Lim, P.K., Ng, S.-C., Lovell, N.H., Yu, Y.P., Tan, M.P., McCombie, D., Lim, E., Redmond, S.J., 2018. Adaptive template matching of photoplethysmogram pulses to detect motion artefact. *Physiol. Meas.* 39 (10), 105005.
- Lucas, M., 1994. Heart rate as an indicator of metabolic rate and activity in adult Atlantic salmon, *Salmo salar*. *J. Fish Biol.* 44 (5), 889–903.
- Madan, A., 2017. Correlation between the levels of  $SpO_2$  and  $PaO_2$ . *Lung India* 34 (3).
- Mannheimer, P.D., 2007. The light-tissue interaction of pulse oximetry. *Anesth. Analg.* 105 (6), S10–S17.
- Nitzan, M., Taitelbaum, H., 2008. The measurement of oxygen saturation in arterial and venous blood. *IEEE Instrum. Meas. Mag.* 11 (3), 9–15.
- Oppedal, F., Dempster, T., Stien, L.H., 2011. Environmental drivers of Atlantic salmon behaviour in sea-cages: A review. *Aquaculture* 311 (1), 1–18.
- Park, J., Seok, H.S., Kim, S.-S., Shin, H., 2022. Photoplethysmogram analysis and applications: An integrative review. *Front. Physiol.* 2511.

- Perry, S., Jonz, M., Gilmour, K., 2009. Oxygen sensing and the hypoxic ventilatory response. In: *Fish Physiology*, Vol. 27. Elsevier, pp. 193–253.
- Prahl, S., 1998. Tabulated molar extinction coefficients for hemoglobin in water. Available at <https://omlc.org/spectra/hemoglobin/summary.html> (Accessed 08.11.2021).
- Rankawat, S.A., Rankawat, M., Dubey, R., 2015. ECG artifacts detection in noncardiovascular signals using Slope Sum Function and Teager Kaiser Energy. In: 2015 International Conference on BioSignal Analysis, Processing and Systems (ICBAPS). IEEE, pp. 6–10.
- Remen, M., Oppedal, F., Imsland, A.K., Olsen, R.E., Torgersen, T., 2013. Hypoxia tolerance thresholds for post-smolt Atlantic salmon: Dependency of temperature and hypoxia acclimation. *Aquaculture* 416–417, 41–47.
- Remen, M., Sievers, M., Torgersen, T., Oppedal, F., 2016. The oxygen threshold for maximal feed intake of Atlantic salmon post-smolts is highly temperature-dependent. *Aquaculture* 464, 582–592.
- Shin, H., Sun, S., Lee, J., Kim, H.C., 2021. Complementary photoplethysmogram synthesis from electrocardiogram using generative adversarial network. *IEEE Access* 9, 70639–70649.
- Sommerset, I., Walde, C., Bang Jensen, B., Wiik-Nielsen, J., Børnø, B., Oliveira, V., Brun, E., 2023. Fiskehelsesrapporten 2022, Veterinærinstituttets rapportserie nr 5a/2023. URL: <https://www.vetinst.no/rapporter-og-publikasjoner/rapporter/2023/fiskehelsesrapporten-2022>, Accessed: 08.02.2023.
- Steinhausen, M., Sandblom, E., Eliason, E., Verhille, C., Farrell, A., 2008. The effect of acute temperature increases on the cardiorespiratory performance of resting and swimming sockeye salmon (*Oncorhynchus nerka*). *J. Exp. Biol.* 211 (24), 3915–3926.
- Sukor, J.A., Redmond, S., Lovell, N., 2011. Signal quality measures for pulse oximetry through waveform morphology analysis. *Physiol. Meas.* 32 (3), 369.
- Svendsen, E., Føre, M., Økland, F., Gråns, A., Hedger, R.D., Alfredsen, J.A., Uglem, I., Rosten, C., Frank, K., Erikson, U., et al., 2021a. Heart rate and swimming activity as stress indicators for Atlantic salmon (*Salmo salar*). *Aquaculture* 531, 735804.
- Svendsen, E., Føre, M., Randeberg, L.L., Alfredsen, J.A., 2021b. Design of a novel biosensor implant for farmed Atlantic salmon (*Salmo salar*). *IEEE Sens.*
- Svendsen, E., Økland, F., Føre, M., Randeberg, L.L., Finstad, B., Olsen, R.E., Alfredsen, J.A., 2021c. Optical measurement of tissue perfusion changes as an alternative to electrocardiography for heart rate monitoring in Atlantic salmon (*Salmo salar*). *Animal Biotelemetry* 9 (1), 1–12.
- Svendsen, E., Randeberg, L.L., Føre, M., Finstad, B., Olsen, R.E., Bloecher, N., Alfredsen, J.A., 2023. Characterization of optical properties of atlantic salmon (*Salmo salar*) blood. *J. Biophotonics* Submitted for review.
- Thorstad, E.B., Rikardsen, A.H., Alp, A., Økland, F., 2013. The use of electronic tags in fish research—an overview of fish telemetry methods. *Turk. J. Fish. Aquat. Sci.* 13 (5), 881–896.
- Tota, B., Amelio, D., Pellegrino, D., Ip, Y., Cerra, M., 2005. NO modulation of myocardial performance in fish hearts. *Comp. Biochem. Physiol. A* 142 (2), 164–177.
- van der Bijl, K., Elgendi, M., Menon, C., 2022. Automatic ECG quality assessment techniques: A systematic review. *Diagnostics* 12 (11), 2578.
- Vikeså, V., Nankervis, L., Hevroy, E.M., 2017. Appetite, metabolism and growth regulation in atlantic salmon (*Salmo salar* L.) exposed to hypoxia at elevated seawater temperature. *Aquacult. Res.* 48 (8), 4086–4101.
- Wypych, G., 2013. Photophysics. In: *Handbook of Material Weathering*. Elsevier, pp. 1–25. <http://dx.doi.org/10.1016/b978-1-895198-62-1.50004-4>.
- Xiong, J., Cai, L., Jiang, D., Song, H., He, X., 2016. Spectral matrix decomposition-based motion artifacts removal in multi-channel PPG sensor signals. *IEEE Access* 4, 3076–3086.
- Yoshida, M., Hirano, R., Shima, T., 2009. Photocardiography: a novel method for monitoring cardiac activity in fish. *Zool. Sci.* 26 (5), 356–361.
- Zhang, Z., Pi, Z., Liu, B., 2014. TROIKA: A general framework for heart rate monitoring using wrist-type photoplethysmographic signals during intensive physical exercise. *IEEE Trans. Biomed. Eng.* 62 (2), 522–531.



ISBN 978-82-326-7378-0 (printed ver.)  
ISBN 978-82-326-7377-3 (electronic ver.)  
ISSN 1503-8181 (printed ver.)  
ISSN 2703-8084 (online ver.)



**NTNU**

Norwegian University of  
Science and Technology